

**NUMERICAL MODELLING OF THE  
UNDRAINED VERTICAL BEARING  
CAPACITY OF SHALLOW FOUNDATIONS**

by

**VAN NGUYEN QUOC**

A Thesis submitted for the Degree of

Master of Philosophy

at the University of Southern Queensland

October 2008

---

**Certification of Dissertation**

*I certify that the ideas, results and analyses, conclusions reported in this dissertation are entirely my own effort, except where otherwise acknowledged. I also certify that the work is original and has not been previously submitted for any other award or higher degree to any other University or Institute.*

*VAN NGUYEN QUOC, Candidate*

*Date*

**Endorsement**

*Dr RICHARD SIMON MERIFIELD, Supervisor*

*Date*

---

## **ABSTRACT**

The bearing capacity of foundations is a fundamental problem in geotechnical engineering. For all structures placed on a soil foundation, geotechnical engineers must ensure that the soil has sufficient load carrying capacity so that the foundation does not collapse or become unstable under any conceivable loading. The ultimate bearing capacity is the magnitude of bearing pressure at which the supporting ground is expected to fail in shear, i.e. a collapse will take place.

During the last fifty years various researchers have proposed approximate techniques to estimate the short term undrained bearing capacity of foundations. The majority of existing theories are not entirely rigorous and contain many underlying assumptions. As a consequence, current design practices include a great deal of empiricism. Throughout recent decades, there has also been a dramatic expansion in numerical techniques and analyses, however, very few rigorous numerical analyses have been performed to determine the ultimate bearing capacity of undrained soils.

In this study, finite element analysis has been used to analyse a range of bearing capacity problems in undrained soil. The numerical models account for a range of variables including footing size, shape, embedment depth, soil layering and undrained bearing capacity of footings on slopes.

By using the powerful ability of computers a comprehensive set of solutions have been obtained therefore reducing the uncertainties apparent in previous solutions.

---

## **ACKNOWLEDGMENTS**

I gratefully acknowledge the Research Scholarship from Vietnamese Government and officers of The Committee on Overseas Training Projects, Ministry of Education and Training of Vietnam.

I would like to express my deepest appreciation to Dr Richard Simon Merifield, Prof Thanh Tran–Cong, Dr Amar Khennane and Assoc Prof David Buttsworth for their effective guidance. Without their continuing dedication and encouragement this dissertation would not have been possible.

Finally, I am indebted to my family, my parents, my wife Huong and my son Viet for much support and encouragement over the years of my studies.

---

## PREFACE

The research work presented in this thesis was conducted in the Faculty of Engineering and Surveying at the University of Southern Queensland from August 2004 to August 2006. This work was performed under the supervision of Dr Richard Simon Merifield. During the term of the candidature, the following paper was published:

1. Merifield R. S. and Nguyen V. Q. (2006). “Two and three–dimensional bearing capacity solutions for footings on two–layered clays.” *Geomechanics and Geoengineering*, Taylor and Francis, 1(2) , pp.151–162.

---

## NOTATION

All variables used in this thesis are defined as they are introduced into the text. For convenience, frequently used variables are described below. The general convention adopted is that vector and matrix variables are shown in bold print while scalar variables are shown in italic.

$A$	area of footing.
$B$	footing width.
$C_1, C_2$	constant coefficients.
$c$	soil cohesion.
$c'$	drained soil cohesion.
$c_u, s_u$	undrained soil cohesion.
$c_1, c_1'$	horizontal shear strengths at the top of the first and second layer respectively;
$c_2, c_2'$	vertical shear strengths at the top of the first and second layer respectively;
$c_{u1}, C_t$	undrained soil cohesion of top layer.
$c_{u2}, C_b$	undrained soil cohesion of bottom layer.
$c_0$	cohesive strength on the surface
$D$	problem dimensionality, diameter of circular footing, the embedded depth of footing.
$D_f$	footing depth.
$D_e$	distance from footing to the crest of slope.
$d/b$	ratio between thickness of the top layer and the width of footing.
$E$	total number of elements in finite element mesh, Youngs Modulus.
$E_u$	undrained Youngs modulus.
$F_{cs}, F_{qs}, F_{\gamma s}, s_c, s_s$	shape factors.

---

---

$F_{cd}, F_{qd}, F_{\gamma d}, d_c$	depth factors.
$F_{ci}, F_{qi}, F_{\gamma i}$	inclination correction factors.
$F, F_S, F_R$	dimensionless factor of footing/soil interaction, that for smooth, rough case.
$\mathbf{g}, g_i$	vector/components of prescribed body force, gravity.
$H$	slope height, top layer thickness.
$K$	relative shear strengths between horizontal and vertical direction.
$L$	length of rectangular footing, distance from the edge of slope to footing.
$N_c, N_q, N_\gamma, N_{c\phi}, N_{c\phi}, N_{cq}, N_{\gamma q}$	bearing capacity factors.
$N$	total number of nodes in finite element mesh, stability number.
$N_f$	stability number.
$N_{ms}, N_{mc}, N_{mr}$	modified bearing capacity factors of strip, circular and rectangular footing.
$N_s$	slope stability factor.
$N_c^*$	modified bearing capacity factor.
$n$	relative shear strengths between the top of first layer and the top of the second layer.
$Q_n$	net footing capacity.
$Q_u$	ultimate footing capacity.
$q_u, q_f, q_{ult}$	ultimate bearing capacity/pressure of the footing.
$\mathbf{q}, q_i$	vector/components of optimisable surface traction.
$q_{bL}^{net}/s_u$	ratio of net bearing capacity to undrained shear strength.
$q$	uniform pressure, surcharge.
$R$	radius of circular footing.
$s_1, s_2$	characteristic lines.
$u_j, \dot{u}_j$	displacement/velocity components.

---

$ur_j, \dot{ur}_j$	rotational displacement/velocity components.
$u_{if}, \dot{u}_{if}$	displacement/velocity components of footing.
$\tau_f$	soil shear strength.
$\alpha$	parameter of hyperbolic approximation of Mohr–Coulomb yield criterion.
$\gamma$	unit weight of soil.
$\delta$	footing displacement, soil footing interface roughness/friction.
$\rho$	change in soil cohesion with depth $dc_u/dz$ .
$\xi_{cs}$	empirical shape factor.
$\sigma_{ij}$	stress tensor.
$\sigma_i$	principal stresses.
$\phi$	internal friction angle of soil.
$\phi'$	drained friction angle of soil.
$\phi_u$	undrained friction angle of soil.
$\nu$	Poissons ratio.

---

---

<b>ABSTRACT</b> .....	<b>ii</b>
<b>ACKNOWLEDGMENTS</b> .....	<b>iii</b>
<b>PREFACE</b> .....	<b>iv</b>
<b>NOTATION</b> .....	<b>v</b>
<b>1. INTRODUCTION</b> .....	<b>1</b>
1.1 BACKGROUND .....	2
1.2 BEARING CAPACITY OF FOUNDATIONS .....	4
1.3 THESIS OUTLINE .....	8
<b>2. HISTORICAL REVIEW</b> .....	<b>10</b>
2.1 INTRODUCTION .....	11
2.2 PREVIOUS EXPERIMENTAL INVESTIGATIONS .....	12
2.2.1 Undrained bearing capacity of surface footings .....	12
2.2.2 Undrained bearing capacity of embedded footings .....	18
2.2.3 Undrained bearing capacity of footings near slopes .....	20
2.3 PREVIOUS THEORETICAL ANALYSES .....	22
2.3.1 Undrained bearing capacity of surface footings .....	23
2.3.2 Undrained bearing capacity of embedded footings .....	30
2.3.3 Undrained bearing capacity of footings near slopes .....	38
2.4 SUMMARY .....	42
<b>3. UNDRAINED BEARING CAPACITY OF SURFACE FOOTINGS ON LAYERED SOILS</b> .....	<b>44</b>
3.1 INTRODUCTION .....	45
3.2 PROBLEM DEFINITION .....	45
3.3 FINITE ELEMENT MODELLING DETAILS .....	47
3.4 ABAQUS FINITE ELEMENT ANALYSIS (FEA) RESULTS .....	51
3.4.1 Footing on homogeneous clay .....	51
3.4.2 Footing on layered clay .....	52
3.4.3 2-D Strip footing on layered clay .....	62
3.4.4 3-D square and circular footings on layered clay .....	62
3.4.5 Effect of footing roughness .....	69
3.5 CONCLUSION .....	69
<b>4. UNDRAINED BEARING CAPACITY OF EMBEDDED FOOTINGS ...</b>	<b>71</b>
4.1 INTRODUCTION .....	72
4.2 PROBLEM DEFINITION .....	72

---

---

4.3	FINITE ELEMENT MODELLING DETAILS .....	73
4.4	ABAQUS FINITE ELEMENT ANALYSIS RESULTS .....	81
4.4.1	Shape factors .....	102
4.4.2	Bearing capacity and depth factor for strip footings .....	105
4.4.2	Bearing capacity and depth factor for square footings .....	107
4.4.3	Bearing capacity and depth factor for circular footings .....	108
4.4.4	Bearing capacity and depth factor for rectangular footings .....	109
4.5	CONCLUSIONS .....	129
<b>5.</b>	<b>UNDRAINED BEARING CAPACITY OF FOOTINGS NEAR SLOPES .</b>	<b>131</b>
5.1	INTRODUCTION .....	132
5.2	PROBLEM DEFINITION .....	132
5.3	FINITE ELEMENT MODELLING DETAILS .....	135
5.4	ABAQUS FINITE ELEMENT ANALYSIS RESULTS .....	138
5.4.1	Effect of ratio L/B .....	166
5.4.2	Effect of the footing roughness .....	167
5.4.3	Effect of slope angle .....	167
5.4.4	Comparison of this study with Narita and Yamaguchi (1990) & Kusakabe (1981)	168
5.5	CONCLUSION .....	168
<b>6.</b>	<b>CONCLUDING REMARKS .....</b>	<b>170</b>
6.1	INTRODUCTION .....	171
6.2	UNDRAINED BEARING CAPACITY OF SURFACE FOOTINGS ON LAYERED SOILS	171
6.3	UNDRAINED BEARING CAPACITY OF EMBEDDED FOOTINGS .....	172
6.4	UNDRAINED BEARING CAPACITY OF FOOTINGS NEAR SLOPES .....	172
	REFERENCES .....	174

---

**CHAPTER 1**  
**INTRODUCTION**

---

## 1.1 BACKGROUND

All onground engineering structures require soil foundation systems to support the associated structural loads and transfer these loads to the underlying soil. Therefore, it is essential that checks are made to ensure the underlying soil has sufficient bearing strength such that collapse does not occur. The capacity of a foundation to carry a given load is referred to as the ultimate bearing capacity.

In addition to providing adequate load capacity, a routine foundation design process must include provision for limiting settlement or other movement to tolerable limits.

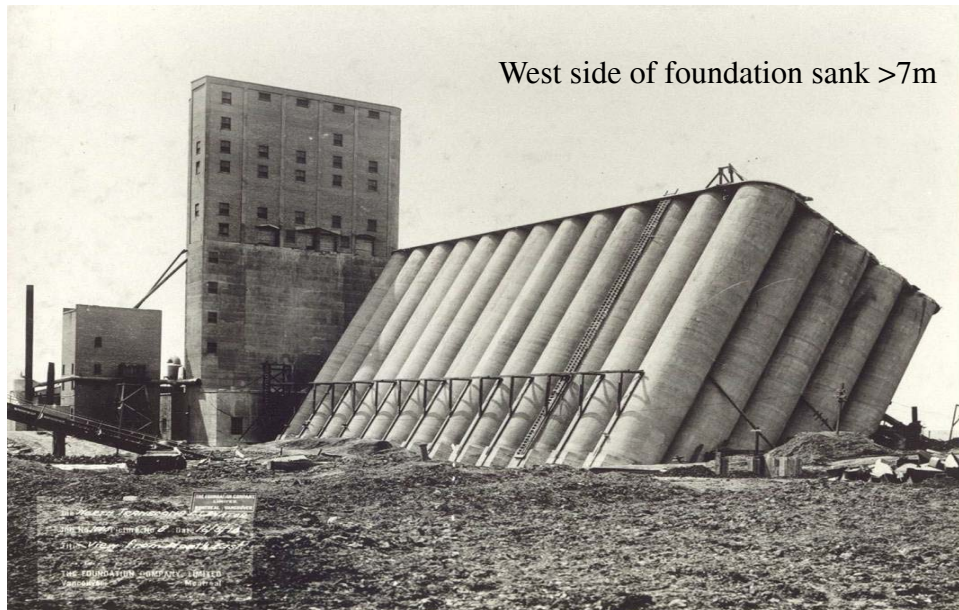
Two well known cases of bearing capacity failure can be seen in Transcosna Grain Elevator, Canada Oct. 18, 1913 and Nigata, Japan, 1964 (Figure 1.1).

Factors that affect the bearing capacity of foundations include the soil properties, footing geometry and the interaction between them. In the past, research into the undrained bearing capacity of footings has been limited as the interaction of these factors makes the solution of this problem much more complex. However, the recent advancements in numerical methods such as finite element method and the rapid increase in computing power mean that more rigorous solutions to both two dimensional and three dimensional bearing capacity problems can be found.

The aim of this thesis is to provide comprehensive numerical solutions to three common bearing capacity problems, namely undrained bearing capacity of surface footings on layered soils, of embedded footings, and of footings on slopes.

The purpose of this chapter is to provide an introduction to the topic of bearing capacity and an overview of the thesis. In this context, the common types of bearing capacity failure modes and standard definitions will be presented.

---



Source: Adapted from Day (2001)

(a) Transcosna Grain Elevator, Canada Oct. 18, 1913



Source: [http://www.ngdc.noaa.gov/seg/hazard/slideset/1/1\\_slides.html](http://www.ngdc.noaa.gov/seg/hazard/slideset/1/1_slides.html)

(b) Niigata, Japan, 1964

**Figure 1.1** Two well known cases of bearing capacity failure

---

## 1.2 BEARING CAPACITY OF FOUNDATIONS

In order to facilitate the discussion in the later chapters, a number of definitions which will be used in this thesis are presented below.

*Bearing capacity* is the ability of a soil to safely carry the pressure placed on it from any engineered structure without undergoing a shear failure with accompanying large settlements. Applying a bearing pressure which is safe with respect to failure does not ensure that settlement of the foundation will be within acceptable limits. Therefore, settlement analysis should generally be performed since most structures are sensitive to excessive settlement (Merifield (2005)).

*Ultimate bearing capacity* is the intensity of bearing pressure at which the supporting ground is expected to fail in shear, i.e. a collapse will take place (Whitlow (1995)).

The loads carried by structures include a dead load (overall weight of the structure itself) and a live load (loads that are not permanently imposed on the structure). Live loads may include those caused by wind, snow, water flow (on bridges), people, animals and movable furniture (in buildings), vehicles (on the road, highway and bridges), etc. Every combination of some or all these loads will affect the soil foundation and therefore must be considered. However, in this thesis the loads and combination of loads are not studied as these typically are the responsibility of the structural engineer, not the geotechnical engineer.

The collapse and failure modes for shallow foundations can be divided into three common types, namely general shear failure, local shear failure and punching shear failure.

The description of the failure modes presented below is summarized from a number of sources including Merifield (2005), Whitlow (1995), and Liu & Evett (1998).

**General Shear:** Figure 1.2(a) illustrates a right side rotation shear failure along a well defined and continuous slip path which will result in bulging of the soil adjacent to the foundation. A wedge under the footing goes down, and the soil is pushed to the side laterally and up. Surcharge above and outside the footing helps hold the block of soil down.

Most bearing capacity failures occur in general shear under stress controlled conditions and lead to tilting and sudden catastrophic type movement. For example, dense sands and

---

saturated clays loaded rapidly are practically incompressible and may fail in general shear. After failure, a small increase in stress causes large additional settlement of the footing. The bulging of surface soil may be evident on the side of the foundation undergoing a shear failure. In relatively rare cases, some radial tension cracks may be present.

Shear failure has been found to occur more frequently under shallow foundations supporting silos, tanks, and towers than under conventional buildings. Shear failure usually occurs on only one side, because soils are not homogeneous and the load is often not symmetric.

**Local shear:** Figure 1.2 (b) is a punching-type failure, and is more likely to occur in loose sands, silty sands, and weak clays. Local shear failure is characterised by a slip path that is not well defined except immediately beneath the foundation. Failure is not catastrophic and tilting may be insignificant. Applied loads can continue to increase on the foundation soil following local shear failure.

**Punching Shear:** Figure 1.2(c) illustrates punching shear failure. Slip lines do not develop and little or no bulging occurs at the ground surface. Vertical movement associated with increased loads causes compression of the soil immediately beneath the foundation. Vertical settlement may occur suddenly as a series of small movements without visible collapse or significant tilting. Punching failure is often associated with deep foundation elements, particularly in loose sands.

### ***Factors affecting the ultimate bearing capacity***

The principal factors that influence ultimate bearing capacities are type and strength of soil, foundation geometry, soil weight in the shear zone, and surcharge. Structural rigidity, and the contact stress distribution do not greatly influence bearing capacity. Bearing capacity analysis assumes a uniform contact pressure between the foundation and the underlying soil.

---

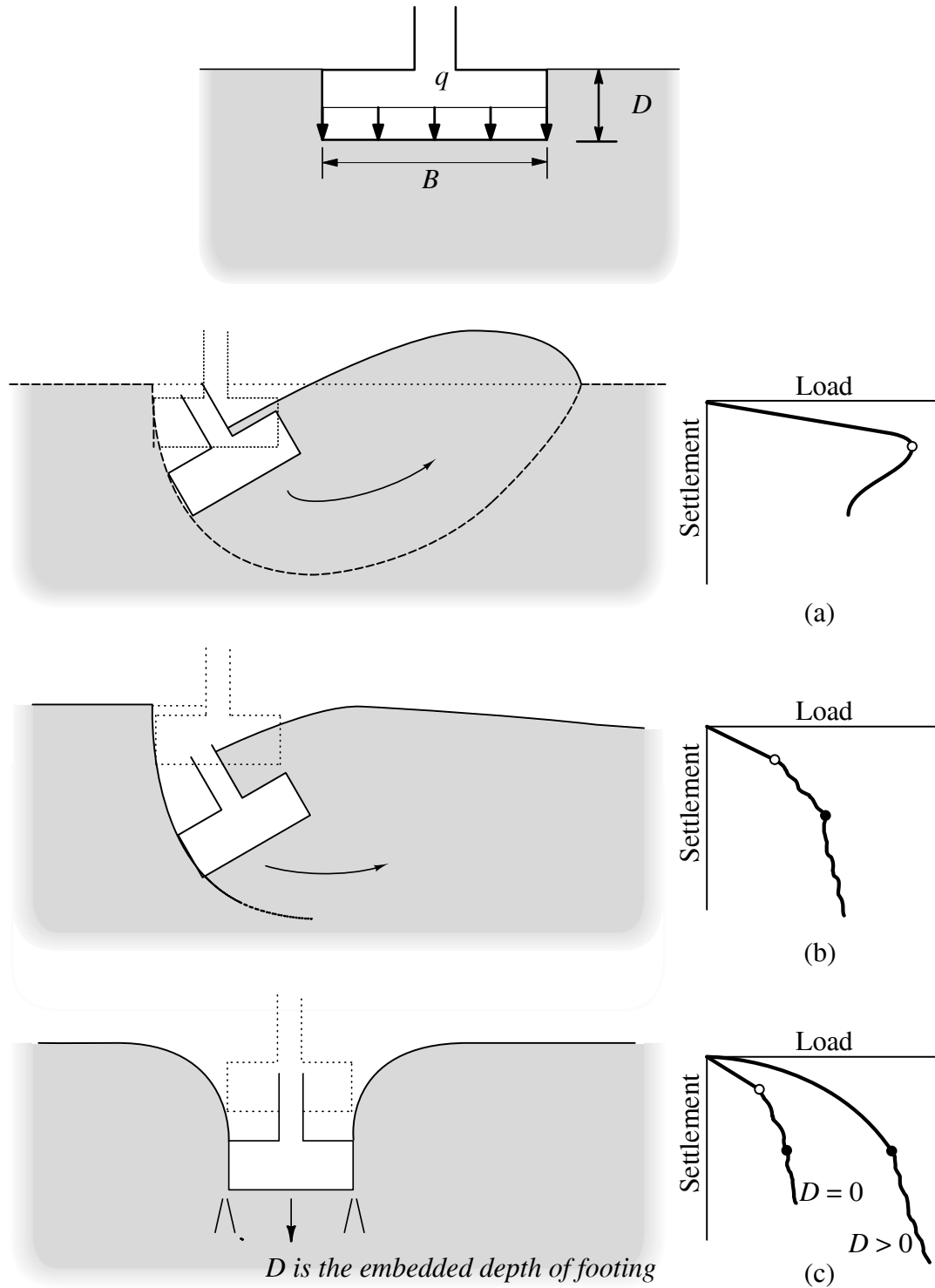


**Figure 1.2** Typical failure modes and load–displacement curves for:

(a) general shear failure; (b) local shear failure; (c) punching shear failure. The circles indicate various interpretations of failure. (Adapted from Coduto 2001, Vesic 1968, Merifield 2005).

**Soil Strength.** Many sedimentary soil deposits have an inherent anisotropic structure due to their common natural deposition in horizontal layers. Other soil deposits such as saprolites may also exhibit anisotropic properties. The undrained strength of cohesive soil and friction angle of cohesionless soil will be influenced by the direction of the major principal stress relative to the direction of deposition.

Using strength parameters determined when the major principal stress is applied in the direction of deposition, the bearing capacity is calculated for each case as follows:

(1) *Cohesive Soil.* The bearing capacity of a cohesive soil is proportional to the undrained soil cohesion  $c_u$  if the effective friction angle  $\phi = 0^\circ$ .

(2) *Cohesionless Soil.* The bearing capacity of a cohesionless soil  $\phi'$  and mixed  $c' - \phi'$  soils increases nonlinearly with increases in the effective friction angle.

**Foundation Width.** The foundation width influences the ultimate bearing capacity in cohesionless soil. Foundation width also influences settlement, which is important in determining the design loads. The theory of elasticity shows that for an ideal soil whose properties do not change with stress level, the settlement is proportional to the foundation width.

(1) *Cohesive Soil.* The ultimate “short term” bearing capacity of a cohesive soil of infinite depth and constant shear strength is independent of the foundation width.

(2) *Cohesionless Soil.* The ultimate bearing capacity of a footing placed at the surface of a cohesionless soil where soil shear strength largely depends on internal friction is directly proportional to the width of the bearing area.

**Foundation Depth.** The bearing capacity, particularly that of a cohesionless soil, increases with foundation depth if the soil is uniform. The bearing capacity is reduced if the foundation is carried down to a weak stratum.

(1) The bearing capacity of larger footings with a slip path that intersects a rigid stratum will be greater than that of a smaller footing with a slip path that does not intersect a deeper rigid stratum.

---

---

(2) Foundations placed at depths where the structural weight equals the weight of displaced soil usually assure adequate bearing capacity and only recompression settlement. Exceptions include structures supported by underconsolidated soil and collapsible soil subject to wetting.

**Soil Weight and Surcharge.** Subsurface and surcharge soil weights contribute to bearing capacity. The depth to the water table influences the subsurface and surcharge soil weights. Water table depth can vary significantly with time.

### 1.3 THESIS OUTLINE

The purpose of the thesis is to provide a comprehensive set of solutions for undrained bearing capacity of foundations. For continuous strip footings ( $L/B = \infty$ ), a condition of plane strain can be assumed, and therefore such a problem can be modelled in two dimensions.

As footings are typically square, circular, or rectangular in shape, the plane strain assumption may not apply. For these cases, a three-dimensional study of bearing capacity should be performed to determine the effect of footing shape.

As an overview, the research presented in this thesis will focus on three main problems:

- (1) Undrained bearing capacity of surface footings on layered soils;
- (2) Undrained bearing capacity of embedded footings;
- (3) Undrained bearing capacity of footings near slopes;

The structure of thesis reflects the three main topics listed above. It is organized as follows:

Chapter 2 presents a basic historical review of the bearing capacity of foundations. Each topic contains previous experimental investigations and theoretical/numerical analyses.

Chapter 3 presents the results obtained for the undrained bearing capacity of surface footings on layered clays. Both two-dimensional strip footing and three-dimensional square and circular footing problems will be discussed. The results will be compared to previous studies. In addition, the effects of smooth or rough footing/soil interaction will be also discussed.

---

Chapter 4 focuses on undrained bearing capacity of embedded footings. The soil is homogeneous, but the footing is placed at some depth from the surface of the soil. Similarly to chapter 3, both two- and three-dimensional configurations will be considered.

Chapter 5 describes the modelling of the undrained bearing capacity of footings near slopes. The model is non-symmetric but in plane strain conditions and can be modelled in two-dimensions.

Chapter 6 concludes the thesis, providing a summary of this study and some recommendations for further work.

---

**CHAPTER 2**  
**HISTORICAL REVIEW**

---

## 2.1 INTRODUCTION

The purpose of this chapter is to summarise previous work on the topic of undrained bearing capacity of foundations. Particular emphasis will be placed on discussing those works that are most relevant to the problems analysed in this thesis.

The determination of the bearing capacity of foundations has been developed through both experimental investigations and numerical/theoretical analyses. In this chapter, previous research results in these two areas are reviewed.

The bearing capacity of foundations has been investigated for many years. Prandtl (1920) pioneered research into bearing capacity and showed theoretically that a wedge of material becomes trapped below a rigid plate when it is subjected to concentric vertical loads. Terzaghi (1943) applied Prandtl's theory to a strip footing on soil with the assumption that the soil is semi-infinite, homogeneous, isotropic, weightless and rigid-plastic. Terzaghi (1943) presented a bearing capacity theory with equations for calculating the ultimate bearing capacity of surface footings. These results are still in use today.

The majority of past research has been experimentally based and that is why current design practices are mostly empirical. Some experimentalists have proposed correlations which satisfy certain demands of geotechnical engineering. However, in some cases, as the models become more complex (for example when extended to multi-layered soil, arbitrary shape footings, etc), deficiencies in the empirical approach become apparent. In these cases, design practice involves the treatment of the complex problem as a simpler one with the use of large safety factors to account for uncertainties.

The rapid advancement of numerical methods can be applied to calculate the bearing capacity of foundations, which provides civil engineers with a clear understanding of foundation problems; we now have the opportunity to solve very complex geotechnical engineering problems. Among these numerical/theoretical methods are the upper-bound and lower-bound methods of limit analysis, finite difference method, boundary element method, and finite element method. Researchers routinely use these methods to solve very complex problems including the ultimate bearing capacity of foundations. Fortunately, computer and software technologies have been developing rapidly such that numerical/theoretical analyses can be used to solve large problems in a short period of time.

---

---

In addition, visualisation techniques can display the process and results of the numerical/theoretical analyses. Importantly, most of the results from numerical/theoretical analyses can be considered as rigorous.

## **2.2 PREVIOUS EXPERIMENTAL INVESTIGATIONS**

The undrained bearing capacity problem has been researched widely since the first important discoveries made by Prandtl (1920). The essential role and behaviour of undrained bearing capacity of foundations has been steadily developing since this time. Over the last two decades, the property of clay and bearing capacity of clay soil has been investigated. Most concepts and design guidelines for the undrained bearing capacity of foundations in use at the moment are based on experimental investigations. These investigations were typically performed with scale models in a laboratory with very few full-scale field tests undertaken. Scale model testing has been used more often because full-scale testing of bearing capacity is costly, time consuming and in most cases impractical. The precision and depth of the subscale measurement capability of geotechnical laboratory equipment have been improved in recent decades.

As an overview, this section outlines briefly the important contributions of experimentalists into the three topics:

- (1) Undrained bearing capacity of surface footings on layered soils
- (2) Undrained bearing capacity of embedded footings
- (3) Undrained bearing capacity of footings near slopes

### **2.2.1 Undrained bearing capacity of surface footings**

This subsection describes the experimental investigations reported by Terzaghi (1943), Meyerhof (1951), deBeer (1970) and Vesic (1973), Brown and Meyerhof (1969), and Das and Dallo (1984).

An early approximate solution to bearing capacity was defined as a general shear failure by Terzaghi (1943). The Terzaghi model is applicable to level strip footings placed on or near a level ground surface where foundation depth  $D$  is less than the minimum width  $B$ . The solutions are based on the Limit Equilibrium Method. Assumptions include the use of

---

a surface footing on soil at plastic equilibrium, and a failure surface similar to the one shown on Figure 1.2(a). Shear resistance of the soil above the base of an embedded foundation is not included in the solution. Figure 2.1 illustrates the failure mechanism assumed by Terzaghi (1943).

Referring to Figure 2.1, the total ultimate bearing capacity can be expressed as:

$$q_u = cN_c + qN_q + \frac{1}{2}\gamma BN_\gamma \quad (2.1)$$

where:  $c$  = soil cohesion

$\gamma$  = soil unit weight below the base of the footing

$q$  = soil surcharge at the base level of the footing =  $\gamma D$

$N_c, N_q, N_\gamma$  are bearing capacity factors.

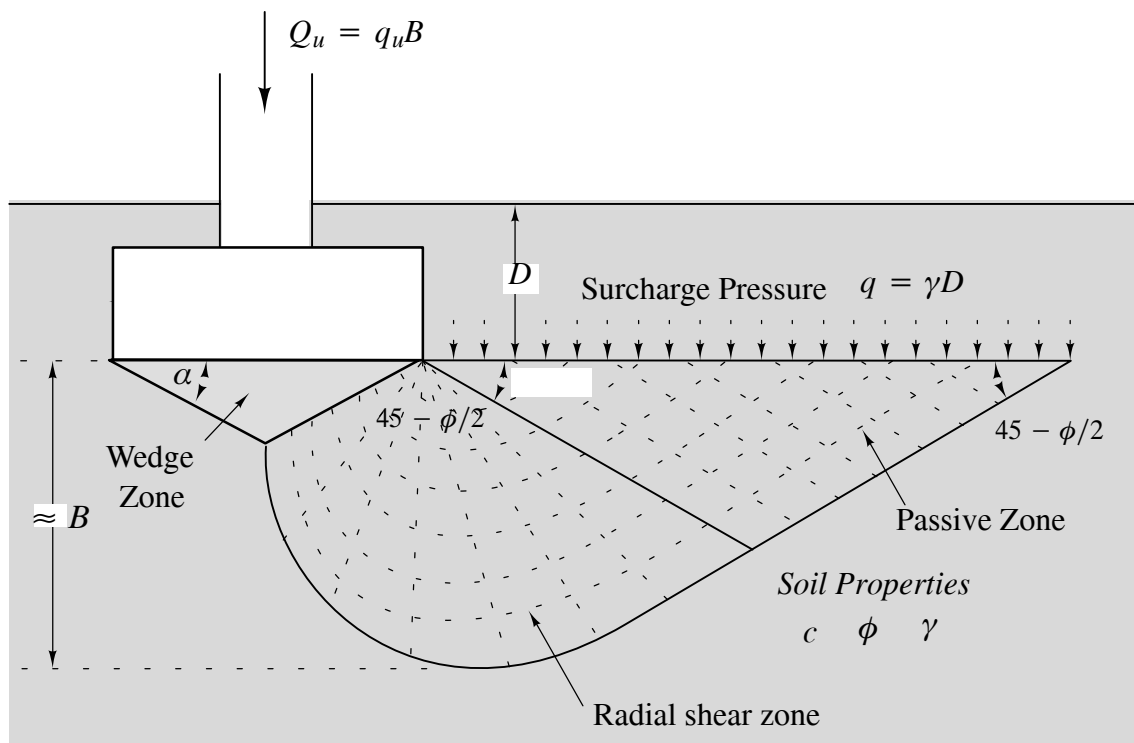


**Figure 2.1** Geometry of failure surface from Terzaghi's bearing capacity theory (Adapted from Coduto 2001)

Since the founding works of Terzaghi (1943), geotechnical engineers around the world have considered this as the base-line analysis of the ultimate bearing capacity of foundations. Equation (2.1) was an approximate solution which uses the superposition technique to combine the effects of cohesion, surcharge and soil weight.

Meyerhof (1951) suggested a general bearing capacity theory with consideration for correction factors for eccentricity, load inclination, and foundation depth. Not only the soil below the foundation, but also the influence of the shear strength of soil above the base of the foundation was investigated.

According to Meyerhof (1951), the ultimate bearing capacity  $q_u$  is written as:

$$q_u = cN_cF_{cs}F_{cd}F_{ci} + qN_qF_{qs}F_{qd}F_{qi} + \frac{1}{2}\gamma BN_\gamma F_{\gamma s}F_{\gamma d}F_{\gamma i} \quad (2.2)$$

where:  $c$ ,  $q$ ,  $\gamma$ ,  $B$ ,  $N_c$ ,  $N_q$ ,  $N_\gamma$  are defined in (2.1)

$F_{cs}, F_{qs}, F_{\gamma s}$  are shape factors

$F_{cd}, F_{qd}, F_{\gamma d}$  are depth factors

$F_{ci}, F_{qi}, F_{\gamma i}$  are inclination correction factors

Undrained bearing capacity of a surface footing can be deduced from equation (2.2) by considering the soil as clay with shear strength and without internal frictional angle, and expressed as:

$$q_u = cN_cF_{cs} \quad (2.3)$$

For a strip footing on homogeneous clay, the undrained bearing capacity factor is  $N_c = \pi + 2 = 5.14$ , an exact solution, first found by Prandtl, 1920. Studies on square, rectangular and circular footings on homogeneous clay can be found in the works of deBeer (1970) and Vesic (1973). They performed a range of tests and suggested the shape factors in order to calculate the bearing capacity of rectangular, circular and square footings on homogeneous soil. These shape factors are shown in the Table 2.1.

Shape of footing	$F_{cs}$	$F_{qs}$	$F_{\gamma s}$
Strip	1.0	1.0	1.0
Rectangular	$1 + \left(\frac{B}{L}\right)\left(\frac{N_q}{N_c}\right)$	$1 + \left(\frac{B}{L}\right)\tan\phi$	$1 - 0.4\left(\frac{B}{L}\right)$
Circular	$1 + \left(\frac{N_q}{N_c}\right)$	$1 + \tan\phi$	0.6

Source: Adapted from Whitlow (1995)

**Table 2.1** Shape factors of deBeer (1970) and Vesic (1973)

While performing experimental investigations on the bearing capacity of shallow foundations on a strong sand layer underlain by soft clay, Das and Dallo (1984) also researched the homogeneous clay model in the laboratory. In these tests, the three types of footing, namely strip footing ( $L/B = \infty$ ), square footing ( $L/B = 1$ ), and rectangular footing ( $L/B = 2$  and  $3$ ) were investigated. Clay was packed into a wooden box having inside dimensions of 24 in. x 24 in. x 30 in. high (0.61m x 0.61m x 0.76m) and model footings were made of 3/8 in. (9.53mm) aluminium plates. After compacting the clay into the test box, the average vane shear strength of compacted clay was  $251\text{lb/ft}^2$  ( $12.02\text{KN/m}^2$ ). The results are in the form of an ultimate bearing capacity  $q_u$ , so the bearing capacity factor can be back calculated as:

$$N_c = \frac{q_u}{F_{cs}} \quad (2.4)$$

For strip footings  $N_c = 4.8$  which is smaller than Prandtl's exact solution  $N_c = 5.14$ . The reasons for that were explained by two major factors, namely inaccurate measurement of  $c_u$  and local shear failure in the soft clay layer under testing. Other results are  $N_c = 5.71$  for  $L/B = 1$ ,  $N_c = 5.39$  for  $L/B = 2$  and  $N_c = 5.11$  for  $L/B = 3$ . With these results, a chart for bearing capacity of strip footings and rectangular footings for a range of  $L/B$  varying from 0 to 1 was proposed.

However, a foundation usually consists of more than two layers. Brown and Meyerhof (1969) made a significant contribution to the theory of the bearing capacity of layered clays. They used a scale model consisting of two layers of different strength clays of varying thickness. The experiments were carried out in terms of total stresses. For the strong over weak clay layer case, failure occurs as the footing punches through the top layer with full development of bearing capacity of the lower layer. For the weak layer over strong layer case, failure occurs mainly by squeezing of the soft layer between the footing and stiffer lower layer, with some interaction between the layers as the strength ratio approaches unity. However, there were some limitations of the study. Firstly, all the studies were carried out in terms of undrained shear strength of clay, using total stresses or  $\phi = 0$  analyses. Secondly, the studies were confined to surface loadings using rigid strip and circular footings with rough bases. Thirdly, only one type of clay was used.

Brown and Meyerhof (1969) also performed tests on strip and circular footing on homogeneous clay. From the strip footing test results, the bearing capacity factor,  $N_c$ , was calculated as 5.14, while from the circular footing tests the bearing capacity factor,  $N_c$  was calculated as 6.05. In addition, the general load–settlement behaviour and failure zones were observed. The typical load–settlement curves have the form of local shear failure similar to the curve shown in Figure 1.2b.

For the case of footings on strong clay overlying weak clay, the bearing capacity factor was found to be a function of only the ratio of the top layer thickness to the footing width or diameter,  $H/B$  or  $H/2R$  which varied from 0.5 to 3.0. One limitation of this study is that the shear strength of the top layer ( $C_t$ ) was four times the shear strength of the bottom layer ( $C_b$ ) for all the tests. The point of failure was clearly visible at an average penetration of 16% of the footing width for strip footings, and 7% of the footing diameter for circular footing tests. Brown and Meyerhof (1969) produced equations for the modified bearing capacity factors for strip and circular footings as  $N_{ms}$  and  $N_{mc}$  respectively. They were a function of the variables  $H/B$  or  $H/2R$  and  $C_b/C_t$ .

$$q_f = C_t N_{ms} \text{ for strip footing} \quad (2.5)$$

$$q_f = C_t N_{mc} \text{ for circular footing} \quad (2.6)$$

$$N_{ms} = 1.5 \frac{H}{B} + 5.14 \frac{C_b}{C_t} \leq 5.14 \quad (2.7)$$

$$N_{mc} = 3.0 \frac{H}{2R} + 6.05 \frac{C_b}{C_t} \leq 6.05 \quad (2.8)$$

For the cases of footings on weak clay over strong clay, the test configurations were similar to the cases of footings on strong clay overlying weak clay. Again, the point of failure was noticed. At the point of failure, average penetrations for the complete series of strip and circular footing tests were 6% and 3% of the footing width respectively. In these cases, Brown and Meyerhof (1969) also proposed an equation for estimating the modified bearing capacity factors  $N_{ms}$  and  $N_{mc}$ , but both of these modified bearing capacity factors were independent of the ratio of shear strength between the two layers:

$$N_{ms} = 4.14 + 0.5 \frac{B}{H} \quad (2.9)$$

$$N_{mc} = 5.05 + 0.33 \frac{2R}{H} \quad (2.10)$$

For rectangular footings, Brown and Meyerhof (1969) proposed an equation for the modified bearing capacity by modifying the equations for strip and circular footings and including the ratio of width to length of the rectangular footing:

$$N_{mr} = N_{mc} \frac{B}{L} + N_{ms} \left(1 - \frac{B}{L}\right) \quad (2.11)$$

where  $N_{mc}$  and  $N_{ms}$  are obtained from their figures for modified bearing capacity factors.

Equation (2.11) can be used for both cases of strong over weak and weak over strong clay layers. The equations (2.5) to (2.11) are being used in practice.

Layered soils are very common in geotechnical engineering, and still constitute a huge problem for researchers throughout the world. Meyerhof (1974), Meyerhof and Hanna (1978), Das and Dallo (1984), Michalowski and Shi (1995) tested the model of sand over clay layers.

Meyerhof (1974) investigated a model of both dense sand over weak clay, and loose sand on stiff clay. He found that the ultimate bearing capacity of footings on sand layers overlying clay can be expressed by a punching shear coefficient for the case of dense sand on weak clay, and by a modified bearing capacity coefficient or an empirical interaction relationship for the case of loose sand on stiff clay. The theory of bearing capacity, and Meyerhof's (1974) test also showed that the influence of the sand layer thickness beneath the footing depends mainly on the bearing capacity ratio of the clay to the sand, the friction angle of the sand, and the shape and depth of the foundation. For stiff sand overlying weak clay model, this result can be seen as a development of punching theory. Following this idea, and the result of Brown and Meyerhof (1969), a division between full, partial punching and general shear failure have been found by Merifield et al (1999) for strip footing, and Merifield and Nguyen (2006) for strip, square and circular footing by finite element analyses. This division is discussed in the Section 3.4.4 and Figure 3.9.

Das and Dallo (1984) studied the bearing capacity of strip, square and rectangular footings by experimenting with sand over clay. However, the properties of the layered sand/clay were the same in all tests. The thickness of the top layer and the shape of the footing were

changed. The model test results were compared with the theory of bearing capacity. In general the experimental and theoretical results are quite close to each other. In the tests for square footings, only the cases of ratio  $H/B$  of 1/3 to 1.95 were investigated. For rectangular footings where  $L/B = 2$  Das and Dallo (1984) studied only  $H/B=1/3$  to 2.5. And for  $L/B = 3$  only  $H/B$  ratios of 0.5 to 2.9 were investigated. For strip footings ratios of  $H/B = 1$  to 3.57 were studied.

Indeed, it is very difficult to test all the different layered configurations with varying soil properties. The alternative is to construct numerical models, and run a virtual simulation.

### 2.2.2 Undrained bearing capacity of embedded footings

This subsection describes the experimental investigations and formulas of undrained bearing capacity of embedded footings reported by Terzaghi (1943), Meyerhof (1951), and Skempton (1951).

Most foundation structures use embedded footings because they have a higher bearing capacity than surface footings, all other things being equal. This can be seen in equation (2.1) by Terzaghi (1943) or equation (2.2) by Meyerhof (1951), where the bearing capacity factors  $N_c$  of embedded footings is larger than that of surface footings.

For undrained bearing capacity of foundations embedded in clay, where shape and depth factors are considered, equation (2.2) becomes:

$$q_u = F_{cs} F_{cd} c_u N_c + \gamma D N_q \quad (2.12)$$

where:  $F_{cs}$  = the shape factor;

$F_{cd}$  = the depth factor;

$c_u$  = the undrained strength of the soil;

$\gamma D N_q$  = the surcharge.

The Terzaghi bearing capacity factors ( $N_c, N_q, N_\gamma$ ) are functions of the soil angle of internal friction ( $\phi$ ). For a strip footing on undrained soil,  $\phi = 0$ ,  $N_c = 2 + \pi$ ,  $N_q = 1$ .

However, there is some uncertainty regarding the values of depth and shape factors  $F_{cs}$  and  $F_{cd}$  for square, circular and rectangular footings. Meyerhof (1951) proposed the following shape and depth factor for undrained soil ( $\phi=0$ ):

$$F_{cs} = 1 + 0.2\left(\frac{B}{L}\right) \quad (2.13)$$

$$F_{cd} = 1 + 0.2\left(\frac{D_f}{B}\right) \quad (2.14)$$

Skempton (1951) also suggested that for undrained clay, the basic form of Terzaghi's equation should be used but the bearing capacity factor  $N_c$  should be modified to include the effects of depth and shape as follows:

$$N_c = 5.14\left(1 + 0.2\frac{B}{L}\right)\left[1 + \sqrt{\left(0.053\frac{D}{B}\right)}\right] \quad (2.15)$$

$$= 5.14F_{cs}F_{cd}$$

with maximum values when  $D/B \geq 4.0$  as follows:

when  $B/L = 0$ ,  $N_c = 7.5$  (i.e. strip footing);

when  $B/L = 1.0$ ,  $N_c = 9.0$  (i.e. square or circular footing).

These values can be found from Figure 2.2.

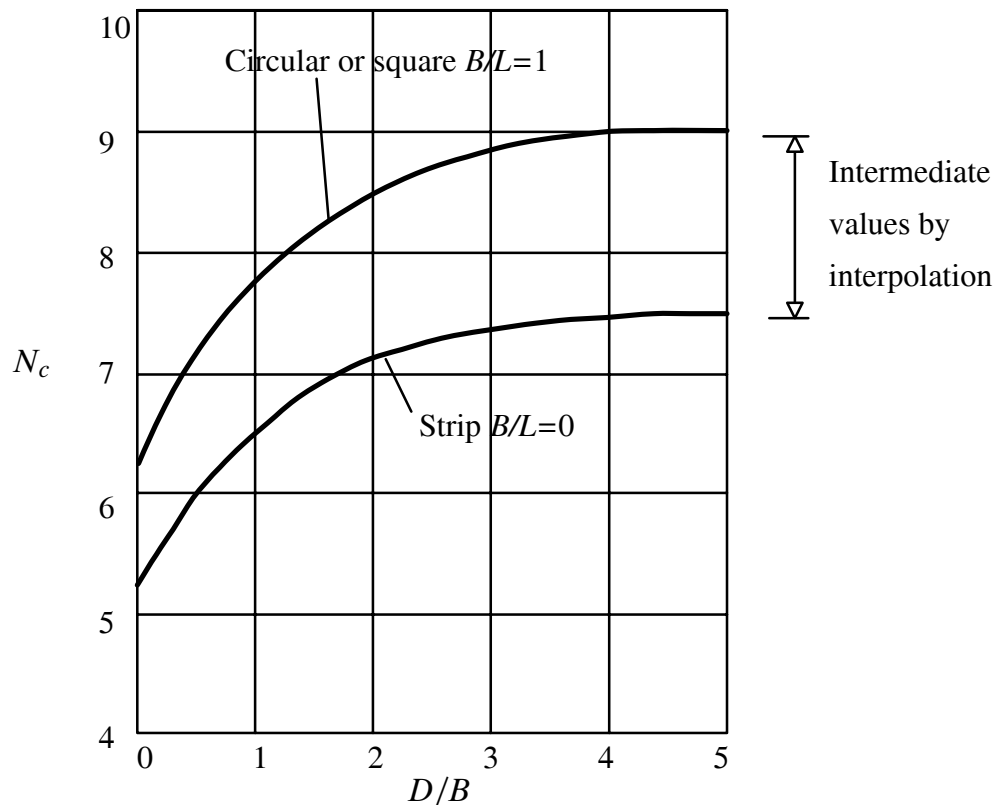


**Figure 2.2** Skempton's bearing capacity factor  $N_c$  for undrained conditions

Equation (2.15) and chart in Figure 2.2 are being used widely in practice.

### 2.2.3 Undrained bearing capacity of footings near slopes

Footings or foundations are sometimes placed on slopes, adjacent to slopes or near a proposed excavation. Several civil engineering examples include embankment roads, highways, railway foundations and abutments of bridges. However, experimental investigations to ascertain the effect of placing a footing near a slope are very limited. This subsection describes the experimental investigations of footings on slopes reported by Liu and Evett (1998).

Liu and Evett's (1998) study on the bearing capacity of footings on slopes was presented for both cohesive and cohesionless soil (Figure 2.3). The results include cases for both footings on slopes, and footings at the top of slopes. If the footings are near or on slopes, their bearing capacity will be less than if they were on level ground. The ultimate bearing capacity for strip footings on slopes can be determined from the following equation:

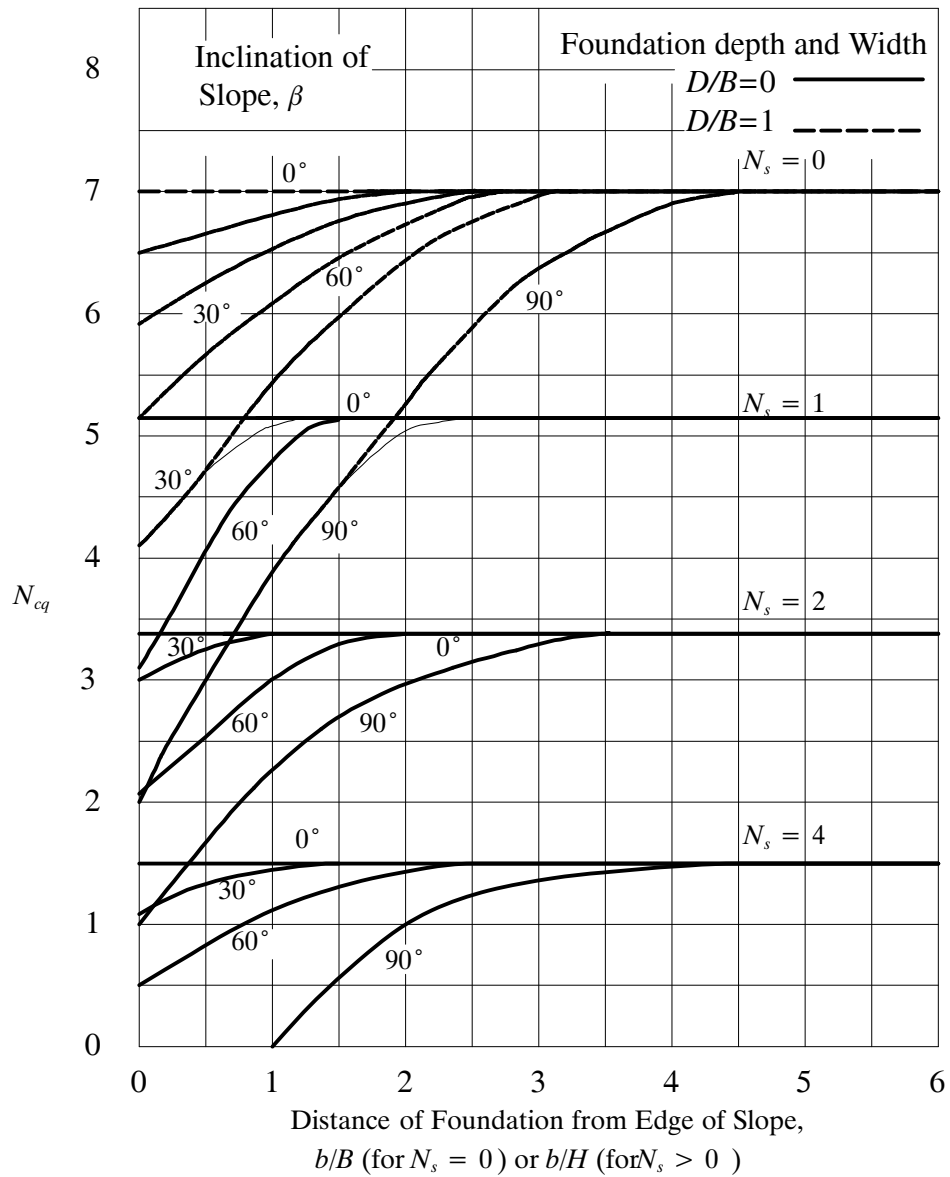
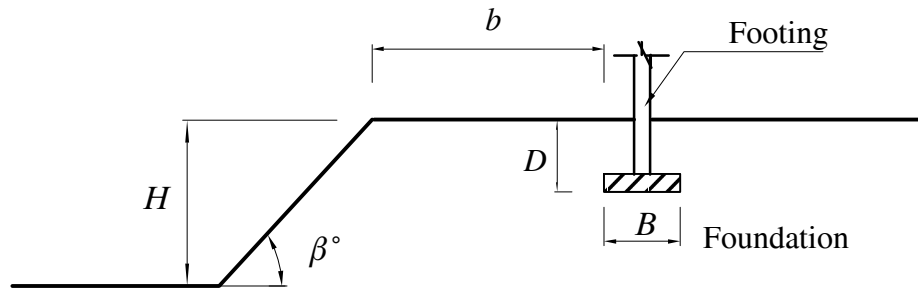
$$q_{ult} = cN_{cq} + \frac{1}{2}\gamma BN_{\gamma q} \quad (2.16)$$

For cohesive soil, (2.16) reduces to:

$$q_{ult} = cN_{cq} \quad (2.17)$$

where  $N_{cq}$  are bearing capacity factors for footings on slopes and can be determined from charts in Figure 2.3 of Liu and Evett (1998).

However, these results only apply to the two cases of  $D/B=0$  and 1, and slope stability factors of  $N_s=0$  to 5 for  $D/B=0$ , and  $N_s=0$  for  $D/B=1$  and slope angles of  $30^\circ$ ,  $60^\circ$  and  $90^\circ$ . For circular and square footings on slopes, it was assumed that the ratio of their bearing capacities on slopes to their bearing capacities on level ground are in the same proportions as the ratio of bearing capacities of continuous footings on slopes to the bearing capacities of continuous footings on level ground. Hence, their ultimate bearing capacities can be evaluated by first computing  $q_{ult}$  by equation (2.16) (i.e., as if the given footing on a slope were a continuous footing), which is then multiplied by the ratio of  $q_{ult}$  computed from the Terzaghi's equations (2.19) or (2.20) (as if the given circular or square footing were on level ground) to  $q_{ult}$  determined from Terzaghi's equation (2.18) (as if the given continuous footing was on level ground). This may be expressed in the equation (2.21).



$$N_s = \frac{\gamma H}{c} = \text{Slope stability factor;}$$

$\gamma$  = Unit weight of soil

$c$  = Cohesion

**Figure 2.3** Bearing capacity for footings on top of slopes

$$q_{ult} = cN_c + \gamma D_f N_q + 0.5\gamma B N_\gamma \text{ for continuous footings (width B)} \quad (2.18)$$

$$q_{ult} = 1.2cN_c + \gamma D_f N_q + 0.6\gamma B N_\gamma \text{ for circular footings (radius R)} \quad (2.19)$$

$$q_{ult} = 1.2cN_c + \gamma D_f N_q + 0.4\gamma B N_\gamma \text{ for square footings (width B)} \quad (2.20)$$

$$(q_{ult})_{ci \text{ or } s \text{ footing on slope}} = (q_{ult})_{co \text{ footing on slope}} \left[ \frac{(q_{ult})_{ci \text{ or } s \text{ footing on level ground}}}{(q_{ult})_{co \text{ footing on level ground}}} \right] \quad (2.21)$$

Note: “*ci*, *co* or *s*” footing denotes either circular, continuous or square footing.

These results have been used in practice in many countries throughout the world.

### 2.3 PREVIOUS THEORETICAL ANALYSES

As well as the experimental investigations already discussed, numerically and theoretical analyses have also contributed significantly to the understanding of the bearing capacity of foundations. With the powerful ability of computers many complex models of soil foundations have been analysed in a short period of time. This is particularly the case for undrained bearing capacity of footings in cohesive soils.

Nowadays, the trend of research is to validate numerical/theoretical solutions with experimental investigations. Laboratory experimental investigations are often difficult to perform, costly, and time consuming making it very hard to obtain a comprehensive set of results. It can also be difficult to extend from laboratory research to full scale problems with variable parameters such as geometry, material properties and environmental effects. The cost and time required for performing laboratory tests on each and every field problem is very prohibitive. In order to avoid this problem, research can be directed toward numerical/theoretical models to first discover the fundamentals of a particular problem.

Existing numerical analyses generally assume a condition of plane strain for the case of undrained bearing capacity of strip footings, and axi-symmetry for the case of undrained bearing capacity of circular footings. There have been, however, some three-dimensional solutions for square, rectangular and circular footing problems such as Salgado et al. (2004), Michalowski et al. (1995) and Merifield and Nguyen (2006).

This section presents a brief historical review of numerical and theoretical analyses for the three problems in the thesis, namely undrained bearing capacity of surface footings on

layered soils, undrained bearing capacity of embedded footings undrained bearing capacity of footings on slopes.

### 2.3.1 Undrained bearing capacity of surface footings

Prandtl (1920) developed a plastic equilibrium theory which provided a method for the determination of the ultimate bearing capacity of strip footing on the surface of a soil having both cohesion and internal friction. Prandtl's result for the bearing capacity factor of strip footings on homogeneous clay is  $N_c = 2 + \pi = 5.14$ . This can be considered as an exact solution.

Using the limit equilibrium method, Terzaghi (1943) proposed the well-known equations (2.1) for the bearing capacity of foundations. Over the past 60 years, many investigators have proposed to modify and extend Terzaghi's method for calculating the bearing capacity of foundations for more complex models.

This subsection describes the numerical investigations in undrained bearing capacity of surface footings on the layered soil reported by Reddy and Srinivasan (1967), Davis and Booker (1973), Griffiths (1982), Merifield et al. (1999) and Salgado et al. (2004).

Reddy and Srinivasan (1967) investigated the bearing capacity of strip footings on layered clay foundations. In this investigation, they made four basic assumptions, namely that the potential surface of failure is cylindrical, the coefficient of anisotropy is the same at all points in the foundation medium, the soil in each layer is either homogeneous with respect to shear strength or in a given direction the shear strength in each layer varies linearly with depth and for soil at failure,  $\phi = 0$  analysis is valid. Reddy and Srinivasan (1967) considered the shear strength to vary with horizontal or vertical directions or with depth. The moment equilibrium equation about the centre of potential failure surface must be satisfied.

Reddy and Srinivasan (1967) considered a range of relative shear strengths between horizontal and vertical direction  $K = c_2/c_1$  and between the top of first layer and the top of the second layer  $n$ ,  $n = c'_1/c_1 - 1 = c'_2/c_2 - 1$ ,

where  $c_1, c'_1$  = horizontal shear strengths at the top of the first and second layer respectively;

$c_2, c'_2$  = vertical shear strengths at the top of the first and second layer respectively;

In practice, the value of  $K$  is found to be between about 0.8 and 2.0. The values for  $n$  and the corresponding  $c'_1/c_1$  are in Table 2.2.

$n$	-1.0	-0.8	-0.6	-0.4	-0.2	0	0.2	0.4	0.6	0.8	1.0
$c'_1/c_1$	0	0.2	0.4	0.6	0.8	1.0	1.2	1.4	1.6	1.8	2

**Table 2.2** Values for  $n$  and corresponding  $c'_1/c_1$

Note that  $n > 0$  (or  $c'_1/c_1 = c'_2/c_2 > 1$ ) corresponds to the common case of soft layer over weak layer, while  $n < 0$  (or  $c'_1/c_1 = c'_2/c_2 < 1$ ) corresponds to the reverse.

There were two cases of layered clays in this investigation. For the first case, the strength was assumed constant with depth in each layer. For the second case, the strengths vary linearly with depth in each layer. Both cases used limiting equilibrium of the mass above the potential surface of rupture, the total disturbing moment about O (centre of the cylindrical mentioned in basic assumption) will be equal to the total resisting moment about the same point. Solving the equilibrium moment equations Reddy and Srinivasan (1967) obtained the bearing capacity of a footing on layered clay  $q/c_2$ , denoted  $N_c$ .

Another parameter affecting the bearing capacity factors of layered clay soil mentioned in the study of Reddy and Srinivasan (1967) is the thickness of the top layer which has been expressed by the ratio between thickness of the top layer and the width of footing  $d/b$ . In this investigation for  $K$  of 0.8, 1.0, 1.2, 1.4, 1.6, 1.8 and 2.0 Reddy and Srinivasan (1967) considered:

- (1)  $d/b=0, 0.2, 0.4, 0.6, 0.8$  and 1 for the weak layer over strong layer cases, and
- (2)  $d/b=0, 0.5, 1.0, 1.5, 2.0$  and 3.0 for the strong layer over weak layer cases.

All of the bearing capacity of factors  $N_c$  for each case were presented graphically.

The case for  $K=1, c'_1/c_1 = 1$  corresponds to isotropic and homogeneous clay, the bearing capacity of factor  $N_c$  was estimated as 5.60 (higher than the exact solution of Prandtl (1920),  $N_c = 5.14$ ). For values of  $K$  larger than 1, the value of the ultimate bearing capacity for the anisotropic medium is considerably smaller than that for the isotropic medium considering the vertical shear strength to be the same for the two cases. For values

of  $K$  less than 1, the value of the ultimate bearing capacity for the anisotropic medium is larger than that for the isotropic medium, the vertical shear strength being considered the same in the two cases. For the range of anisotropy considered, the ultimate bearing capacity could be reduced by about 30% or increased by approximately 15% of the ultimate bearing capacity for the isotropic case.

Davis and Booker (1973) also investigated the effect of increasing the strengths with depth on the bearing capacity of clays. By means of the theory of plasticity, their results showed that the rate of increase of cohesion with depth plays the same role as density plays in the bearing capacity of homogeneous cohesive–frictional soils. Davis and Booker (1973) considered four cases of non–homogeneous shear strength in the vertical direction  $c = c(z)$ , a function of depth  $z$ . The soil is assumed purely cohesive and isotropic in the horizontal direction. Theoretically, they started from an equation of the characteristic lines  $s_1$  and  $s_2$  Figure 2.4, and then the variation in stress state along characteristic lines to determine the failure.

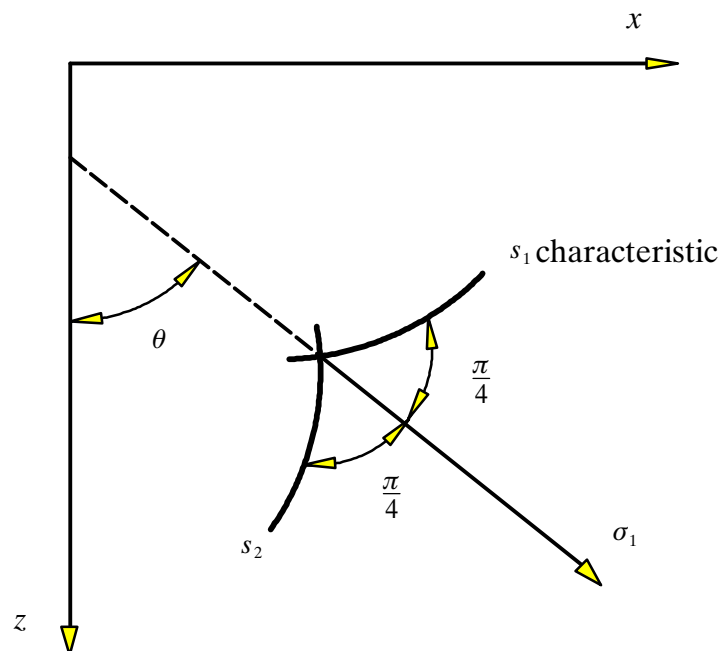


**Figure 2.4** Stress characteristics

The stress field and velocity field were obtained to determine the point at which failure starts. However, in order to solve a system of partial differential equations, a suitable numerical technique must be used. There were two types of interaction between the

footings and the soils investigated in this study, i.e. smooth footings and rough footings. Both of these cases have the same form of equation for bearing capacity, but with different dimensionless factor  $F$ , i.e.  $F = F_S$  corresponds to smooth footings while  $F = F_R$  corresponds to rough footings (Figure 2.5).

$$\frac{Q}{B} = F \left[ (2 + \pi)c_0 + \rho \frac{B}{4} \right] \quad (2.22)$$

where  $c_0$  = cohesive strength on the surface;

$\rho$  = the rate of increase of cohesion with depth.

The ratio  $F_R/F_S$  showed that roughness increases the bearing capacity by a maximum of 16% and causes no increase at the two limits  $c_0 = 0$  and  $\rho = 0$ .

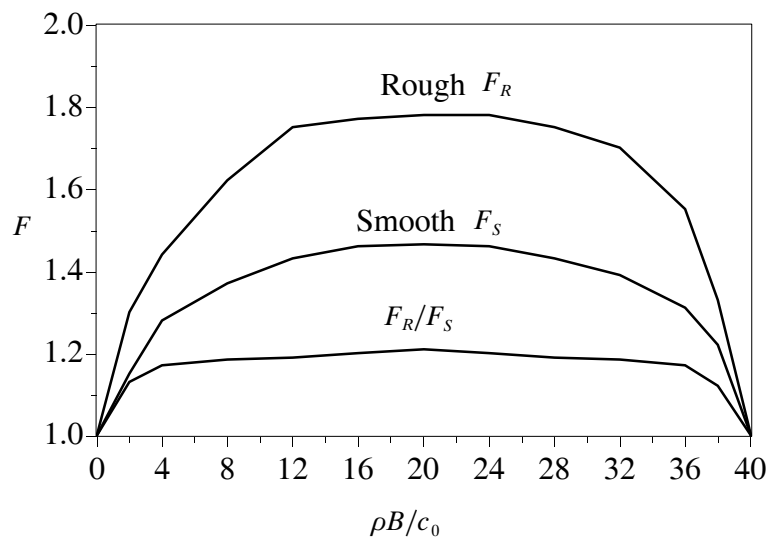


**Figure 2.5** Correction factors  $F$  for both rough and smooth footings

The effect of a stiff surface layer, application to embankments and comparison with slip circular solutions were also investigated.

Griffiths (1982) used the finite element method to study the bearing capacity of footings on cohesive soil whose strength varies linearly with depth, and the case of two layers of different strength but within each layer the strength is constant. Griffiths (1982) considered both rough and smooth footings. In all cases, the bearing pressure mobilised by a given vertical displacement was obtained by averaging the vertical stress component occurring in the first row of integrating points below the displaced nodes. Griffiths (1982) used

eight–node quadrilateral isoparametric elements with reduced (2–point) Gaussian quadrature in both the stiffness and relaxation phases of the calculation. Results of homogeneous soils were compared to the solutions of Terzaghi (1943) and Prandtl (1920) for the bearing capacity factors  $N_c, N_q$  and  $N_\gamma$ . For clay ( $\phi = 0$ ), Griffith's (1982) bearing capacity factor  $N_c$  was the same as the results of Terzaghi (1943) and Prandtl (1920). For soil where  $0 < \phi < 35^\circ$ , the value of  $N_c$  from Griffiths (1982) for smooth footings was lower than that of Terzaghi (1943) and larger than that of Prandtl (1920). For rough footings the value of  $N_c$  from Griffiths (1982) was close to that of Prandtl (1920).

The non–homogeneous two–layer clay system assumed by Griffiths (1982) consisted of a top and bottom layer with strengths designated as  $C_t$  and  $C_b$  respectively. Both weak over strong and strong over weak systems were studied as the ratio  $C_b/C_t$  varied from 0.2 to 2. The ultimate bearing capacity is a function of  $H/B$  (ratio between thickness of the top layer and the width of footing) and  $C_b/C_t$ . Griffiths (1982) also compared his result (by finite element method) with the results of Button (1953) who assumed a simple circular mechanism of failure based upon the upper bound theorem, and the experimental results of Brown and Meyerhof (1969). With the advantages of the finite element method, Griffiths (1982) investigated a wide range of problems and determined the bearing capacity and an adequate stress field at failure, and the ultimate bearing capacity  $Q_{ult}$  can be obtained:

$$Q_{ult} = C_t N_{c_t} \quad (2.23)$$

where  $N_{c_t}$  is bearing capacity factor which can be compared to results of Button (1953) and Brown and Meyerhof (1969) (Figure 2.6). Griffiths (1982) chose a particular case of  $H/B=0.5$  for comparison the finite element results with Button (1953) and Brown and Meyerhof (1969) for a range of  $C_b/C_t$  ratio in Figure 2.6. Generally good agreement was found for other  $H/B$  ratios.

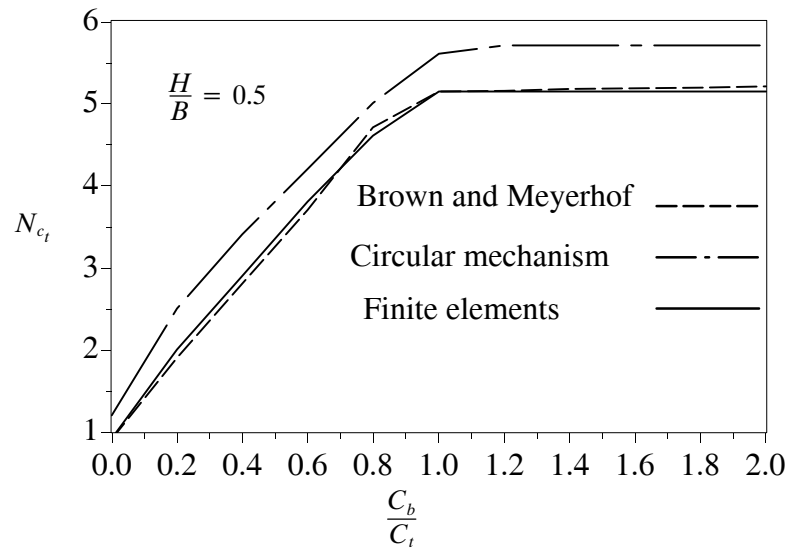


**Figure 2.6** Correction factors for both rough and smooth footings

Among the rigorous plasticity solutions for the bearing capacity of layered clay is the study of Merifield et al. (1999). He used numerical limit analysis in conjunction with the upper and lower bound limit theorems of classical plasticity to obtain a rigorous solution of undrained bearing capacity of strip footing on two-layered clays. Both methods assume a perfectly plastic soil model with a Tresca yield criterion and generate large linear programming problems.

The two-layered clay system adopted by Merifield et al. (1999), consisted of both strong over weak and weak over strong layers, and was characterised by the ratio of the shear strength of the top layer to that of the bottom layer  $c_{u1}/c_{u2}$ . This ratio was varied from 0.2 to 5, covering most of the practical cases of geotechnical engineering. Another parameter investigated influencing the bearing capacity of footing on two-layered clay systems is the ratio of the thickness of top layer to the footing width  $H/B$ . Most cases of interest were covered by varying  $H/B$  from 0.125 to 2. The bearing capacity of a shallow strip footing on two-layered clay without surcharge was expressed as:

$$q_u = c_{u1} N_c^* \quad (2.24)$$

where  $c_{u1}$  = the shear strength of the top layer and

$N_c^*$  = a modified bearing capacity factor which is a function of both  $H/B$  and  $c_{u1}/c_{u2}$ ; for a homogeneous profile  $N_c^* = N_c$ .

$q_u$  = ultimate bearing capacity of strip footing obtained from elements under footing at the state of failure.

The average of the upper and lower bound solutions for  $N_c^*$  were then compared to the results of the available upper bound solutions of Chen (1975) and results of the semi-empirical solutions of Meyerhof & Hanna (1978). All of them were expressed in both tabular and graphical form.

For homogeneous clay, Merifield et al. (1999) obtained an upper and lower bound estimate of the bearing capacity factor  $N_c^* = 4.94$  and  $5.32$  respectively. The average of the upper and lower bound results produced  $N_c^* = 5.13$  which is close to the exact well-known Prandtl's solution (1920)  $N_c^* = 2 + \pi = 5.14$ . Merifield et al. (1999) compared these results to  $N_c^* = 5.53$  obtained from the upper bound solution of Chen (1975) and  $N_c^* = 5.14$  obtained from the semi-empirical solutions of Meyerhof & Hanna (1978).

Salgado et al. (2004) used lower bound and upper bound limit analysis in two- and three-dimensions for footings in homogeneous clay. In the case of surface footings when  $D/B=0$ , the ratio of net bearing capacity to undrained shear strength,  $q_{bL}^{net}/s_u$  can be expressed as a bearing capacity factor  $N_c$ , as shown in Table 2.3:

Strip footing		Circular footing		Square footing	
Lower bound	Upper bound	Lower bound	Upper bound	Lower bound	Upper bound
5.132	5.203	5.856	6.227	5.523	6.221

**Table 2.3** Bearing capacity factors  $N_c$  of Salgado et al. (2004)

In the case of a footing on a strong over weak clay profile, the results of Merifield et al. (1999) indicated that, there is a complex relationship between general, local and punching shear failure and the ratios  $H/B$  and  $c_{u1}/c_{u2}$ . The limit at which punching shear through the top layer occurs in the model and local shear failure has been established depending on  $H/B$  and  $c_{u1}/c_{u2}$ . Merifield et al. (1999) also showed that the limit  $H/B > 2$  at which failure happens entirely within the top layer, is independent of the ratio  $c_{u1}/c_{u2}$ . Chen (1975) also had a similar limit but Meyerhof and Hanna (1978) had a limit  $H/B \approx 2.5$ .

In the case of a footing on a weak over strong clay profile, Merifield et al. (1999) concluded that the bearing capacity increases as the relative strength of the bottom layer rises for ratios

of  $H/B < 0.5$ . There is also a limiting ratio of  $c_{u1}/c_{u2}$  at which time no further increase in the bearing capacity is achieved as the failure surface becomes fully contained within the top layer. However this limit increases as the top layer thickness rises. For all values of  $H/B > 0.5$ , the failure occurs entirely within the top layer and the bearing capacity is independent of the strength of the bottom layer, and is given by Prandtl solution (1920)

$$N_c^* = 2 + \pi.$$

The effects of soil–footing interface have been investigated by Merifield et al. (1999). For a weak over strong clay system where  $H/B \leq 0.5$ , the effect of footing roughness is important and can lead to a reduction in bearing capacity by as much as 25%. For a weak over strong clay system where  $H/B > 0.5$ , and for strong over weak soil profiles, the bearing capacity is not affected by footing roughness.

The first problem studied in this thesis is the undrained bearing capacity of surface footings on layered soils, which is a further development of the work of Merifield et al. (1999). The scope of investigation ( $H/B$  and  $c_{u1}/c_{u2}$ ) is the same. While Merifield et al. (1999) used the lower and upper bound limit theorems for strip footings in two–dimensions, this project uses the finite element method for strip, square, and circular footings in both two– and three–dimensional space.

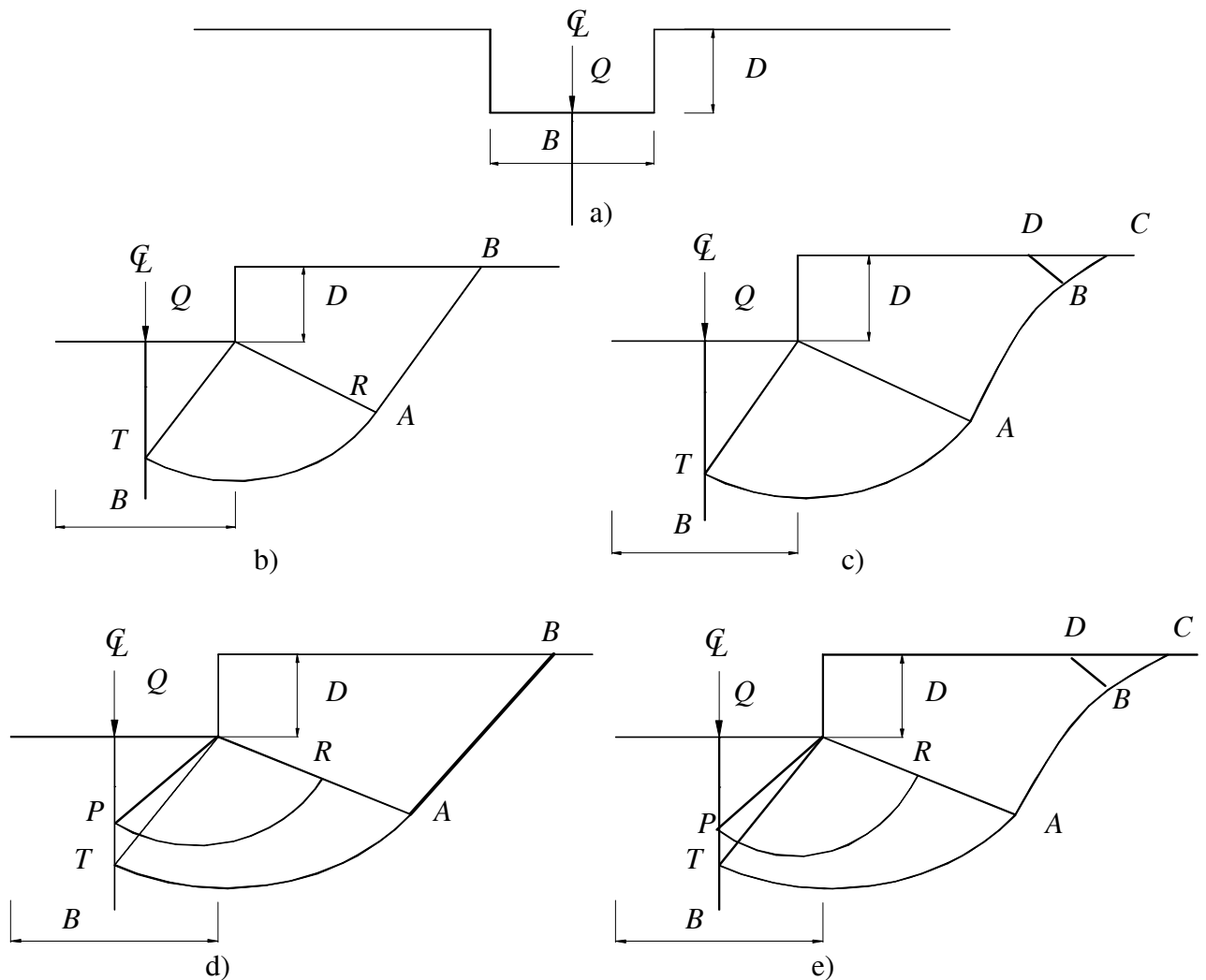
### 2.3.2 Undrained bearing capacity of embedded footings

This subsection describes the numerical investigations of the bearing capacity of embedded footings reported by Hansen (1969), Hu et al. (1998), Salgado et al. (2004), and Edwards et al. (2005).

Hansen (1969) investigated the bearing capacity of a vertically and centrally loaded strip footing placed at a depth  $D$  below a horizontal, unloaded surface in homogeneous clay in the undrained state by the means of the theory of plasticity for ideal rigid–plastic materials (Figure 2.7a). Hansen (1969) also assumed the soil is weightless ( $\gamma = 0$ ), no contact at the vertical soil–footing interface, and shear strength is constant within the soil medium. The scope of the investigations is limited to relatively shallow footings ( $0 \leq D/B \leq 2$ ). First of all, Hansen (1969) proposed one of the simplest possible rupture figures, consisting of a kinematically admissible displacement field, two radial zones with straight radial slip lines and two line ruptures (Figure 2.7b). The bearing capacity was expressed as a ratio of

---

$Q/cB$  as a function of  $D/B$  as curve No.1 on Figure 2.8. Hansen (1969) could calculate the radius  $R$  of radial zone and length of straight line in the failure zone. Applying the lower-bound theorem, two different solutions for bearing capacity in the form of ratio  $Q/cB$  as a function of  $D/B$  were found.



- a) Bearing capacity problem
- b) Rupture figure with simple radial zones
- c) Rupture figure with generalized radial zones
- d) Rupture figure with augmented radial zones
- e) Rupture figure for mathematically correct solution

**Figure 2.7** Bearing capacity problems and solutions

Secondly Hansen (1969) had generalized radial zones which yielded better approximations. The straight line now is replaced by a curve (Figure 2.7c). An

upper-bound solution satisfying all equilibrium conditions, and nowhere exceeded failure conditions is to be found. All the results of the bearing capacity are also expressed as  $Q/cB$  (function of  $D/B$ ) in the same chart for both models (curve No.2 on Figure 2.8).

The third model is simple augmented radial zones because the first model is kinematically admissible but on the unsafe side, mainly because of the strong singularity at the point T on Figure 2.7d. The results of bearing capacity were shown on the curve No.3 on Figure 2.8

The last case is the mathematically correct solution by replacing the simple radial zone with a generalized zone (Figure 2.7e). The bearing capacity is shown as curve No. 4 on Figure 2.8 and it corresponds with equation (2.25) for use in practice.

$$\frac{Q}{cB} = \pi + 2 + 0.533[\sqrt{1 + 1.75D/B} - 1] \quad (2.25)$$

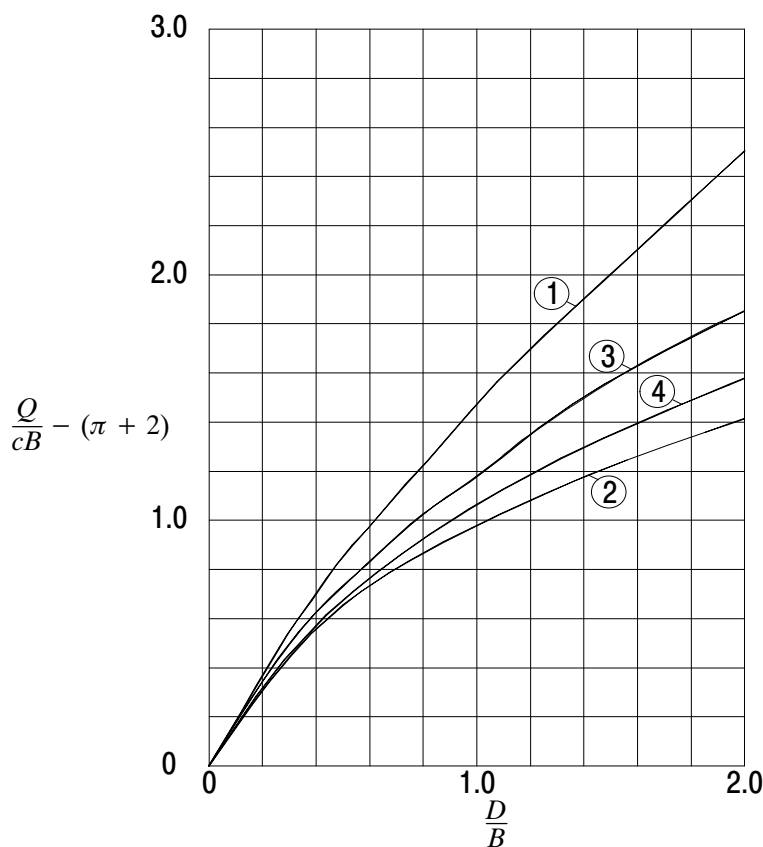


**Figure 2.8** Bearing capacity variation with depth from Hansen (1969)

Salgado et al. (2004) studied the two- and three-dimensional bearing capacity of strip, square, circular and rectangular foundations in clay using finite element limit analysis. The

results of the analyses are used to propose more rigorous values of the shape and depth factors for foundations in clay. The shape and depth factors are determined by computing the bearing capacities of footings of various geometries placed at various embedment depths  $D$  of footings from 0 to 5 times of footing width or diameter. Salgado et al. (2004) used numerical limit analysis formulations based on the lower-bound and upper-bound theorems of plasticity (Hill (1951) and Drucker et al. (1951, 1952)) as a tool for all two and three-dimensional bearing capacity problems. In order to increase the accuracy of computed depth factors for the three-dimensional problems and reduce the computation time, the models have exploited symmetry. Sectors of  $15^\circ$ ,  $45^\circ$  and  $90^\circ$  were adopted for circular, square and rectangular footings respectively. For strip footings, only half of the footing is modelled. In all these cases the boundary conditions can be easily satisfied

In all two and three-dimensional models, Salgado et al. (2004) considered the space vertically above the footings as being filled with soil in an attempt to model the real conditions. However in doing so, they had to assume conditions for the interaction between the top surface of footings and the above soil mass, i.e. perfectly rough with no separation. In order to do that, normal hydrostatic pressure was applied to the top mass of the soil above the footings. The interface between the bottom face of the footings and the soil underneath the footings was assumed rough by prescribing zero tangential velocity for upper bound calculations and specifying no particular shear stresses for lower bound calculations. For strip footing problems, the calculations performed for  $\gamma D/s_u = 1$  and for weightless soil show that the bearing capacity of embedded strip foundations is represented exactly by Terzaghi's bearing capacity equation (2.26) with  $F_{cs} = 1$ :

$$q_{bL,net} = q_{bL} - q_0 = F_{cs} F_{cd} N_c c_u \quad (2.26)$$

where:  $N_c$  = a bearing capacity factor;

$c_u$  = a representative undrained shear strength;

$q_0 = \gamma_m D$  is the surcharge at the footing base level;

$\gamma_m$  is the saturated unit weight of soil;

$D$  = the distance from the ground to the base of the foundation element;

$F_{cs}$  = a shape factor;

$F_{cd}$  = a depth factor;

$q_{bL}$  = limit unit load (referred to as the limit unit base resistance) or bearing capacity of embedment footing;

$q_{bL,net}$  = net limit unit base resistance.

It was clear from the lower bound stress field and upper bound velocity field for both a surface and deep foundation that deeper foundations mobilise larger volumes of soil, dissipate more plastic energy and show mechanisms where the stress rotation becomes less important than for shallow foundations, with a considerable portion of the mechanisms consisting of vertical slippage of the soil parallel to the sides of the foundation. The larger  $D/B$  ratios are, the more work needs to be done by the applied load. In this study, the results for a strip footing on the surface is very close to Prandtl's exact solution (closer for lower bound ( $N_c = 5.13$ )). Salgado et al. (2004) also established depth factors by dividing the average of the lower bound and upper bound bearing capacity  $q_{bL}^{net}$  values at the various ratios of  $D/B$  by that for a surface foundation. For circular, square, rectangular foundations analyses, Salgado et al. (2004) considered both upper- and lower bound solutions and calculated the average values. Shape factors are withdrawn from dividing the  $q_{bL}^{net}$  of circular, square or rectangular footings by the  $q_{bL}^{net}$  of strip footings at the same  $D/B$  value. They concluded that the shape factors are not constant with depth. This is in contrast to the assumption of independence of shape and depth factors implied by traditional expressions.

From the results of limit analysis, Salgado et al. (2004) proposed an equation for depth factor of square, circular and rectangular footings:

$$F_{cd} = 1 + 0.27 \sqrt{\frac{D}{B}} \quad (2.27)$$

They also used the depth factor equation to calculate the shape factors  $s_c$ . And they also built an equation for the shape factor:

$$F_{cs} = 1 + C_1 \frac{B}{L} + C_2 \sqrt{\frac{D}{B}} \quad (2.28)$$

as a function of  $B/L$  and  $D/B$  with constants  $C_1$  and  $C_2$ .

Deep foundations were also investigated and indicated that for  $D/B > 1$ ,  $q_{bL}^{net}/F_{cs} > 9$  while traditionally it has been taken as 9. For example, for  $D/B=5$ ,  $q_{bL}^{net}/F_{cs}$  is at least equal to 11, the value of the lower bound, and possibly as high as 13.7. It is possible that  $q_{bL}^{net}/F_{cs}$  would continue to increase with increasing  $D/B$  beyond  $D/B=5$ . All computations were performed for a rough soil–footing interface. Salgado et al. (2004) concluded that this is not often realized, because the safety factor that is used in current design practice accounts for various sources of uncertainty including those in the analysis, soil properties, load and boundary conditions or construction uncertainties. The results reduce the uncertainties with respect to bearing capacity equation, which can lead to lower safety factors.

The second problem this study addresses is the same as modelled by Salgado et al. (2004) but by a different method. While Salgado et al. used lower–bound and upper–bound theorems of limit analysis, this study uses the displacement finite element method.

Recently, Edwards et al, (2005) carried out investigations about depth factors for undrained bearing capacity, by small–strain finite element analysis of embedded strip and circular foundations using the Imperial College Finite Element Program (ICFEP) (Potts & Zdravkovic, 1999). In their studies, the  $D/B$  ratio was varied from 0 to 4 with every 0.25 as  $D/B \leq 1$ , and every 0.5 as  $1 < D/B \leq 4$ . For both strip and circular footing problems, and because of the symmetry in geometry and loading conditions, only half of the domain was discretized in two–dimensional solutions, using eight–noded quadrilateral elements. The boundary condition adopted was vertical movement only for the embedded footings. The footings/soil interactions have both a rough and smooth interface. The soil was modelled using the Tresca constitutive model, with a constant undrained strength with depth,  $s_u$ , equal to 50 kPa, a Young’s modulus,  $E$ , of 105 kPa and a Poisson’s ratio,  $\mu$ , of 0.499. The soil depth of the model underneath the footing is  $5B$  and the width of the model is  $7.5B$  which is large enough as not to influence the performance of the model. A uniform vertical displacement was applied to the horizontal surface of the footing. From this surface, the total reaction force from soil mass is output as a net bearing force, which is equal to  $F_{cs}F_{cd}N_cC_uA$ .

Edwards et al, (2005) gathered the results and compared them with previous studies. For strip ( $N_c$ ) and circular surface footings they found out  $N_c = 5.18$  ( $F_{cs}N_c$ ) is very close (+0.8%) to the exact  $2 + \pi$  solution of Prandtl 1920.

The result of  $F_{cs}N_c = 6.09$  for circular footing is also close (+0.6%) to the 6.05 solution of Eason & Sheild (1960). The embedded strip footing results were compared to lower bound and upper bound solutions of Salgado et al. (2004), the bearing capacity equation of Skempton (1951) in the same chart of  $d_cN_c$  depending on  $D/B$ . The embedded circular footing results were compared to the solutions of Salgado et al. (2004), Houslby & Martin (2003), Martin (2001) and Skempton (1951) in the same chart of  $F_{cs}F_{cd}N_c$  depending on  $D/B$  (from 0 to 4).

The depth factors of Edwards et al (2005) were obtained by dividing the bearing capacities of footings at depth by that for surface footings. They concluded that the shape factor  $F_{cs}$  is unaffected by depth, while Salgado et al. (2004) concluded that the depth factor derived for strip footing applies to all footing shapes and to use this to determine how the shape factor  $F_{cs}$  varied with depth.

Hu and Randolph (1999) investigated the bearing response of skirted foundation on non-homogeneous soil numerically, analytically and physically with the offshore sediment simulated as a cohesive soil with strength increasing linearly with depth. In the numerical analysis, the  $h$ -adaptive FEM was adopted to provide an optimal mesh, in which a strain-superconvergent patch recovery error estimator and mesh refinement with subdivision concept are used. Hu and Randolph (1999) present two separate studies of circular skirted foundations on non-homogeneous soil, consisting of a bearing-capacity study and a large penetration study. The bearing capacity of the foundation is studied with the degree of non-homogeneity ( $kD/s_{uo}$ ) (where  $k$  =strength gradient,  $D$ =Diameter or width of foundation,  $s_{uo}$ =undrained shear strength at the level of skirt tip) of soil up to 30, different skirt roughness and skirt depth up to five times the foundation diameter (*i.e.*,  $D_f/D = 5$ ) ( $D_f$  = the skirt penetration depth,  $D$ =Diameter or width of foundation) using an  $h$ -adaptive FEM and extended upper-bound method. In small strain analysis, an optimal mesh is first generated using the  $h$ -adaptive refinement strategy, and that mesh is then used for the bearing-capacity analysis. In large strain analysis, the original (refined) mesh is updated periodically through the analysis, using the  $h$ -adaptive refinement strategy

at each stage of remeshing. In all of the FE simulations, the small strain analysis was implemented in the AFENA FE package, which was developed at the Geotechnical Research Centre at the University of Sydney (Carter and Balaam 1990). Soil was modelled as simple-elastic perfect-plastic, taking Poisson's ratio  $\nu = 0.49$ , stiffness ratio  $E/s_u = 500$  ( $E$  is Young's modulus), and friction  $\phi$  and dilation  $\psi$  angles equal to zero. The Tresca yield criterion with associated flow rule was adopted because of the undrained conditions. Hu and Randolph (1999) investigated the bearing capacities of circular foundations with embedment up to  $D_f/D = 5$  for both smooth and rough sides, for a displacement of  $0.3D$  on homogeneous undrained clay. Solution can be seen as:

$$\left(\frac{q_u}{s_u}\right)_{\text{excluding side friction}} = \left(\frac{q_u}{s_u}\right)_{\text{rough side}} - 4\frac{D_f}{D} \quad (2.29)$$

It was apparent that the main difference in the bearing capacity between rough and smooth sides is due to side friction, and that the base capacities of both agree very closely once the skirt depth exceeds  $D_f/D = 1$ . Also, the bearing capacity reaches a constant of  $q_u/s_u = 9.9$  (for a displacement of  $0.3D$ ) when  $D_f/D$  is  $> 2$  (Figure 2.9).

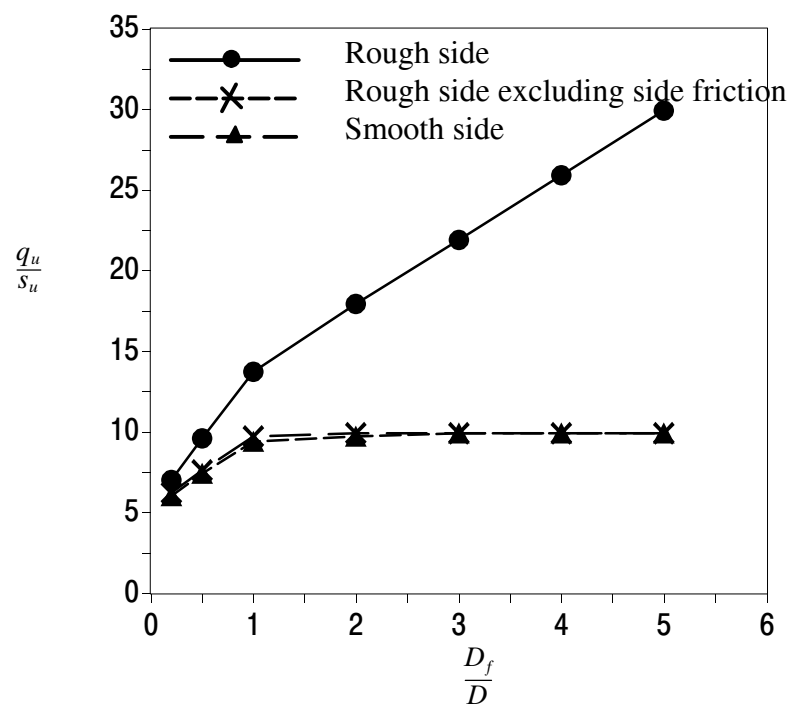


**Figure 2.9** Bearing capacity of circular foundation on homogeneous soil from Hu & Randolph (1999)

### 2.3.3 Undrained bearing capacity of footings near slopes

This subsection describes the numerical investigations of bearing capacity of footings near slopes reported by Saran et al. (1989), Narita and Yamaguchi (1990), and Shiau et al. (2008).

As can be seen in practice, a number of civil engineering structures require the stability of footings placed near an existing slope. Among these are abutments of bridges, foundations of roads and highways on the embankment. The bearing capacity of strip footings on slopes is still an important problem in geotechnical engineering. There are two types of failure modes for a footing on a slope, namely stability of the slope itself and bearing capacity failure of the footing. Using numerical analyses, the problem of bearing capacity of footings on slopes has been studied.

The bearing capacity of footings adjacent to slopes was investigated by Saran et al. (1989). In their studies, analytical solutions have been developed for obtaining the ultimate bearing capacity using limit equilibrium and limit analysis approaches. One-sided rupture/failure on the side of slopes was assumed and partial mobilization was considered on the side of level ground. Saran et al. (1989) mentioned two types of bearing capacity of slopes, namely foundation failure and overall stability of the slopes. The foundation was placed on the edge of the slope and up to three times the footing width away from the slope crest. In addition, embedment ratios ( $D/B$ ) from 0 to 1 were considered. Slope angles of  $5^\circ$ ,  $10^\circ$ ,  $20^\circ$  and  $30^\circ$  were analysed. In the cases of noncohesive soils, Saran et al. (1989) concluded the bearing capacity is always governed by bearing capacity failure, while in cohesive material the stability of the foundation may be dictated by overall slope stability. In the limit equilibrium analysis, assumptions similar to Terzaghi were made regarding the failure mechanism shape, with the only exception being the centre of the logarithmic spiral (Figure 2.1). The bearing capacity expression is then developed by considering the equilibrium of the elastic wedge underneath of footing. The ultimate bearing capacity was obtained using the principle of superposition and expressed by introducing bearing capacity factors. Saran et al. (1989) compared their results with those by Lundgren and Mortenson (1953) and Saran (1969). In the limit analysis study of Saran et al. (1989), some basic assumptions have been made as follows: the soil mass is ideally plastic, the failure mechanism is the same as that adopted in the limit equilibrium analysis, and the associated

flow rule is observed. The bearing capacity equations were obtained theoretically by computations of bearing capacity factors like in limit equilibrium analysis.

The undrained bearing capacity of footings on slopes and seismic bearing capacity of footings on slopes were studied numerically/theoretically by J. Kumar and Kumar (2003), Kumar et al. (2003), and Askari et al (2003). However, the mechanism of bearing capacity is different when lateral accelerations are included.

Narita and Yamaguchi (1990) investigated bearing capacity of strip foundations placed on the level ground on the top of slopes (Figure 2.10). Comparisons are made with other analytical and experimental results to examine applicability of the method to practical problems. It is revealed that the log–spiral analysis somewhat overestimates bearing capacity values as compared to other solutions, the errors involved being around 20% at maximum. Also noticed is a relatively good agreement with experimental results, especially with the model tests on clay ( $\phi = 0$ ), for both the ultimate bearing capacity and shape of sliding surfaces. Narita and Yamaguchi (1990) investigated two types of failures, namely toe and slope failure and base failure. Results of this investigation showed that for purely cohesive  $\phi = 0$  materials where a log–spiral degenerates into a circle, the log–spiral solutions become almost equal to the values obtained using Bishop’s method and are at most 3 ~ 5% larger than the upper bound solutions.

$\beta$	$L/B$	Bearing capacity, kN/m <sup>2</sup>		
		Test	Upper bound	Log–Spiral
30°	0	28.5	21.5	22.5 (1.05)
	0.5	44.4	40.7	42.9 (1.05)
	1.0	34.4	35.3	37.2 (1.05)
45°	0	32.2	20.7	21.4 (1.03)
	0.5	30.8	27.2	28.2 (1.04)
	1.0	38.3	26.5	27.4 (1.03)
60°	0	34.6	27.5	28.0 (1.02)
	0.5	44.8	33.4	34.0 (1.02)
	1.0	30.3	25.3	25.5 (1.01)

( ): ratio to upper bound solution

**Table 2.4** Comparisons with test results for clay (Narita and Yamaguchi (1990))

Narita and Yamaguchi (1990) compared the results with test results for clays as shown in the Table 2.4.

Recently, Shiau et al. (2008) researched the bearing capacity of footings on purely cohesive slopes. In their studies, a rigorous plasticity solution was obtained by using finite element numerical upper and lower bound methods. They also showed that for a footing–on–slope system, ultimate bearing capacity of footings may be governed by either the local foundation failure or global slope failure. Referring to Figure 2.10, the bearing capacity depends on a wide range of dimensionless ratios, namely the slope angle  $\beta^\circ$ ,  $L/B$ ,  $c_u/\gamma B$ ,  $q/\gamma B$  and  $H/B$ ,

where  $B$  = footing width,

$H$  = the slope height and

$L$  = the distance from the edge of the slope to the footing edge,

$\gamma$  = soil unit weight,

$c_u$  = shear strength of soil,

$q/\gamma B$  = slope surcharge.

$$\frac{P}{\gamma B} = f\left(\beta^\circ, \frac{L}{B}, \frac{c_u}{\gamma B}, \frac{q}{\gamma B}, \frac{H}{B}\right) \quad (2.30)$$

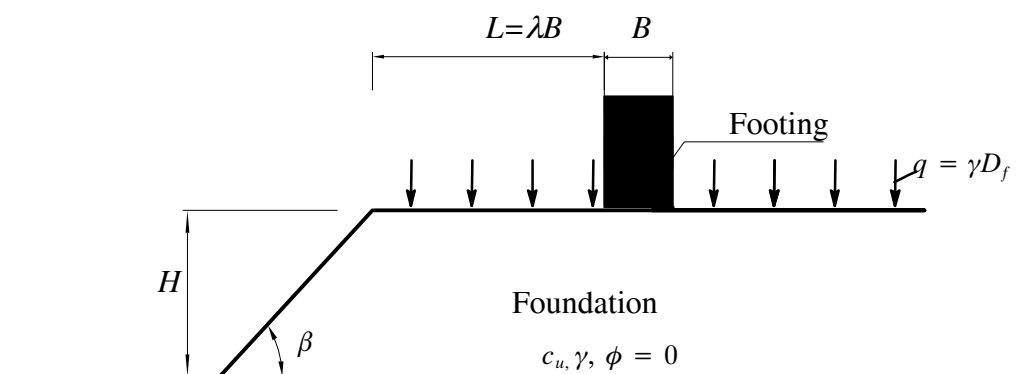


**Figure 2.10** Problems notation of Shiau et al. (2008)

The soil is assumed to be undrained following the Tresca yield criterion with a shear strength  $c_u$  ( $\phi = 0$ ). In the lower bound finite element analysis, the mesh consists of 1585

elements with a total number of 4755 nodes and 2335 discontinuities while in the upper bound finite element analysis, the mesh consists of 2120 elements with a total number of 6360 nodes and 3131 discontinuities. Unlike meshes in the displacement finite element method, lower bound mesh discretisation permits several nodes to share the same coordinates. This extra “degree of freedom”, though increasing the total number of the problem variables, will improve the solution accuracy. The unknown stress field is then sought while maximizing an integral of the normal stresses over some part of the boundary. This integral corresponds to an objective function of a typical mathematical programming problem. Rough and smooth footings for both lower and upper bound analyses were investigated.

The model assumes the soil obeys an associated flow rule and three main parameters are changed, namely  $\beta^\circ$ ,  $L/B$  and  $c_u/\gamma B$  to obtain a wide range of results. The effect of surcharge  $q/\gamma B$ , footing roughness and increasing strength with depth were also investigated.

For weightless slopes, the undrained bearing capacity of strip footings was close to those of Davis and Booker (1973) for vertical cuts. Shiau et al. (2008) showed that for  $L/B \geq 4$ , the vertical cut has no effect on bearing capacity of the footing and the bearing capacity reduces by a factor of 2.5 as the distance ratio  $L/B$  is decreased from four to zero.

For slopes with weight, Shiau’s results showed that the normalised bearing capacity  $p/\gamma B$  from upper bound and lower bounds was found to be within 5% of each other. Their average value is very close to true collapse load which has been bracketed to within  $\pm 2.5\%$ .

The ratio of  $L/B$  was varied from zero to six and  $c_u/\gamma B$  was varied from zero up to ten. All the analyses were performed for a model with  $H/B = 3$ . The results showed that the dimensionless bearing capacity  $p/\gamma B$  decreases linearly with the strength ratio ( $c_u/\gamma B$ ) until becoming non-linear and rapidly approaching zero at a particular value of  $c_u/\gamma B$  where no feasible solution is available from the numerical analysis.

Researching the effect of the slope angle  $\beta^\circ$ , Shiau et al. (2008) indicated that the footing capacity decreases as the slope angle  $\beta^\circ$  increases. The distance from the footings to the crest of the slope  $L$  also influences the ultimate bearing capacity. As  $L/B$  increases from 0, the bearing capacity also increases and tends to reach a constant value at a certain value

of  $L/B$  for all values of  $\beta^\circ$ . Shiau et al. (2008) indicated that the effects of footing roughness can be significant for cases with small values of  $L/B$  and high slope angles  $\beta^\circ$ , an effect up to 30% for  $\beta = 90^\circ$ . By enforcing zero horizontal velocity at the footing–soil interface, the perfectly rough case produces a higher bearing capacity than the perfectly smooth case. This amount is 30% in the case of  $L/B = 0$ ,  $c_u/\gamma B = 5.0$  and  $\beta = 90^\circ$ . In general, footings with perfectly rough bases always produce a higher bearing capacity than those with smooth bases and nearly identical results can be obtained when footings are located outside the slope influence distance. Shiau et al. (2008) found that the existence of surcharge  $q$  on the surface of slope could make the footing capacity either increase or decrease, depending on both  $\beta^\circ$  and  $L/B$ . The effect of increasing strength with depth was also investigated by Shiau et al. (2008). They used soft normally consolidated clays whose undrained strength increased linearly with depth. The rate of change in soil cohesion  $\rho = dc_u/dz$ , to the cohesion at the ground surface,  $\rho B/c_{u0}$  was chosen as 0, 0.5 and 1.0. Shiau et al. (2008) showed that  $H/B=3$  is large enough for local failure mechanisms which can develop without being influenced by the bottom or toe of the slope.

## 2.4 SUMMARY

After researching historical studies about undrained bearing capacity related to the three topics in this thesis, the following points can be drawn:

- A great deal of laboratory testing has been performed to predict the ultimate bearing capacity of foundations. However, the investigations are typically limited in scope. Unfortunately, results obtained from laboratory testing are typically problem specific and are difficult to extend to field problems with different material or geometric parameters.
  - There have been several numerical methods for bearing capacity problems so far. Each problem was solved with certain assumptions and results were compared to laboratory testing. Very few rigorous numerical studies have been undertaken to determine bearing capacity behaviour.
  - A literature review gives us a clear view of previous achievement and some of the weaknesses on this work. This thesis contains elements that examine the previous problem results, but by different methods, and use the power of the computer to solve some the big problems which could not previously be attempted. Using numerical
-

analysis to determine the effects of influent factors to bearing capacity is one part of this investigations. The three topics in this thesis related to previously unsolved problems and can play a significant role in the area of bearing capacity of footings for geotechnical engineering.

---

**CHAPTER 3**

**UNDRAINED BEARING CAPACITY OF**

**SURFACE FOOTINGS ON LAYERED SOILS**

---

### 3.1 INTRODUCTION

In this chapter finite element analysis is used to predict the undrained bearing capacity of strip, square and circular footings resting on layered clays. The soil profile consists of two clay layers having different thicknesses and properties. The results are compared with previous solutions for strip footings on layered clays. The bearing capacity behaviour is discussed and the bearing capacity factors are given for various cases involving a range of layer thicknesses and properties of the two clay soil layers.

The purpose of this study is to produce three-dimensional solutions for square and circular footings on two-layered clays using the finite element method. To do this the commercial software package ABAQUS was used. In addition, two-dimensional analyses for the bearing capacity of strip footings have been performed for verification and comparison purposes. The results are an extension of the solution for strip footings on two-layered clays presented by Merifield et al. (1999).

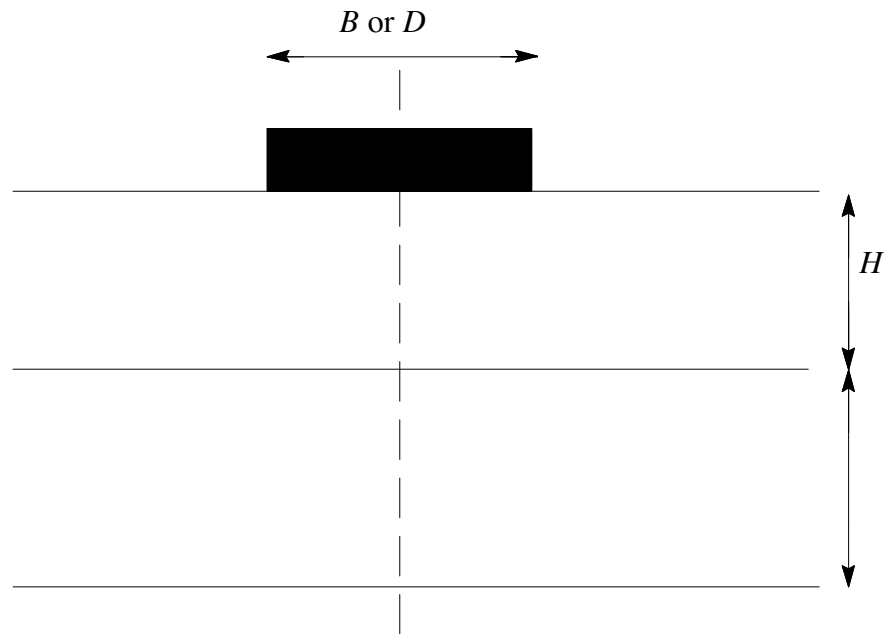
### 3.2 PROBLEM DEFINITION

The two and three-dimensional bearing capacity problem to be considered is illustrated in Figure 3.1. A footing of width  $B$  or diameter  $D$  rests upon an upper layer of clay with undrained shear strength  $c_{u1}$  and thickness  $H$ . This is underlain by a clay layer of undrained shear strength  $c_{u2}$  and infinite depth. Symmetry has been exploited for the three-dimensional analyses and only one quarter of the problem domain has been modelled as shown in Figure 3.1.

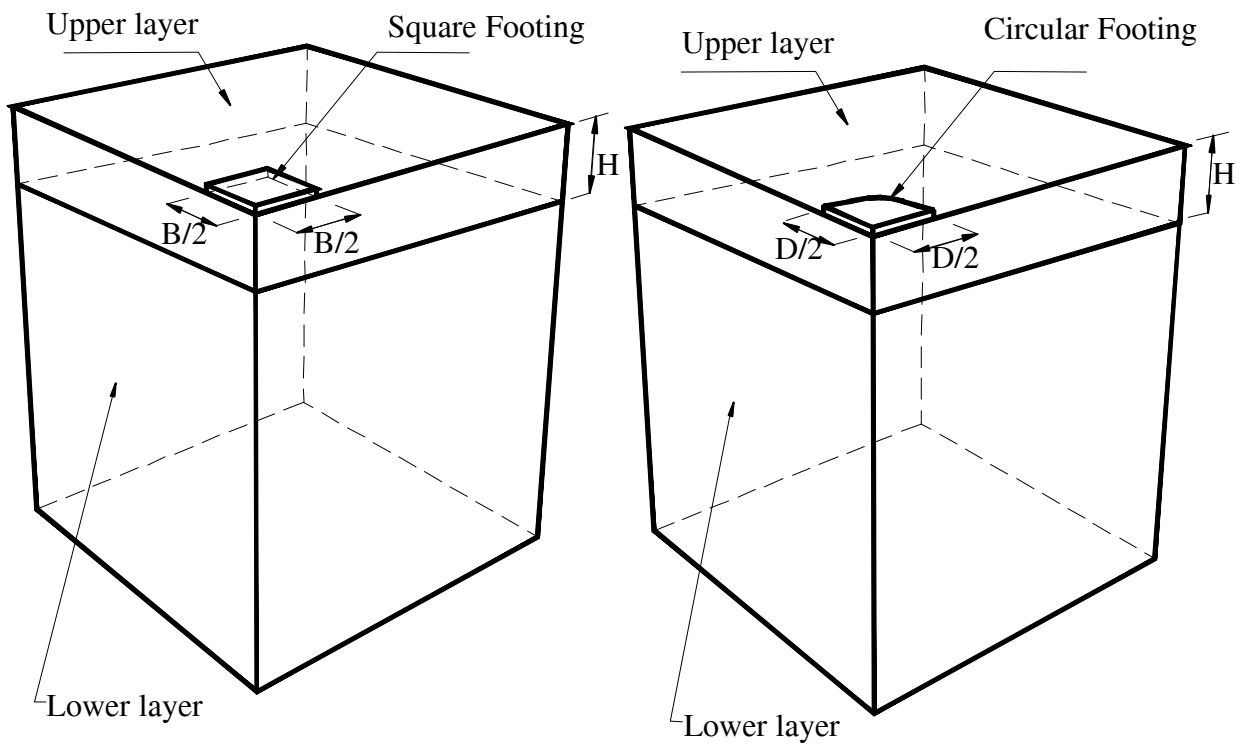
The soil was modelled as an isotropic elasto-perfectly plastic continuum with failure described by the Mohr-Coulomb failure criterion. The elastic behaviour was described by a Poisson's ratio,  $\nu = 0.49$  and a ratio of Young's modulus to shear strength of  $E/c_u = 100 - 500$  depending on whether the soil was soft or stiff.

The bearing capacity solution to this problem will be a function of the two ratios  $H/B$  and  $c_{u1}/c_{u2}$ . Past research by Merifield et al (1999) indicates that a reduction in bearing capacity for a strong over weak clay system may occur up to a depth ratio of  $H/B=2$  for strip footings. In this study solutions have been computed for problems where  $H/B$  ranges from 0.125 to 2 and  $c_{u1}/c_{u2}$  varies from 0.2 to 5. This covers most problems of practical

---



(a) Strip footing



(b) Square footing

(c) Circular footing

**Figure 3.1** Problem Definition

interest. Note that  $c_{u1}/c_{u2} > 1$  corresponds to the common case of a strong clay layer over a weak clay layer, whilst  $c_{u1}/c_{u2} < 1$  corresponds to the reverse.

For the simplest case of a footing on homogeneous clay under undrained conditions including the effect of footing shape without surcharge, equation (2.1) can be re-written as follows:

$$q_u = c_{u1} N_c F_{cs} \quad (3.1)$$

where  $F_{cs}$  = shape factor. Empirically, the shape factor  $F_{cs}$  is given by:

$$F_{cs} = 1 + \left(\frac{B}{L}\right) \left(\frac{N_q}{N_c}\right) \quad (3.2)$$

The shape factor  $F_{cs}$  of Salgado et al (2004) is given as:

$$F_{cs} = 1 + 0.12 \frac{B}{L} \text{ for square, rectangular and circular footings} \quad (3.3)$$

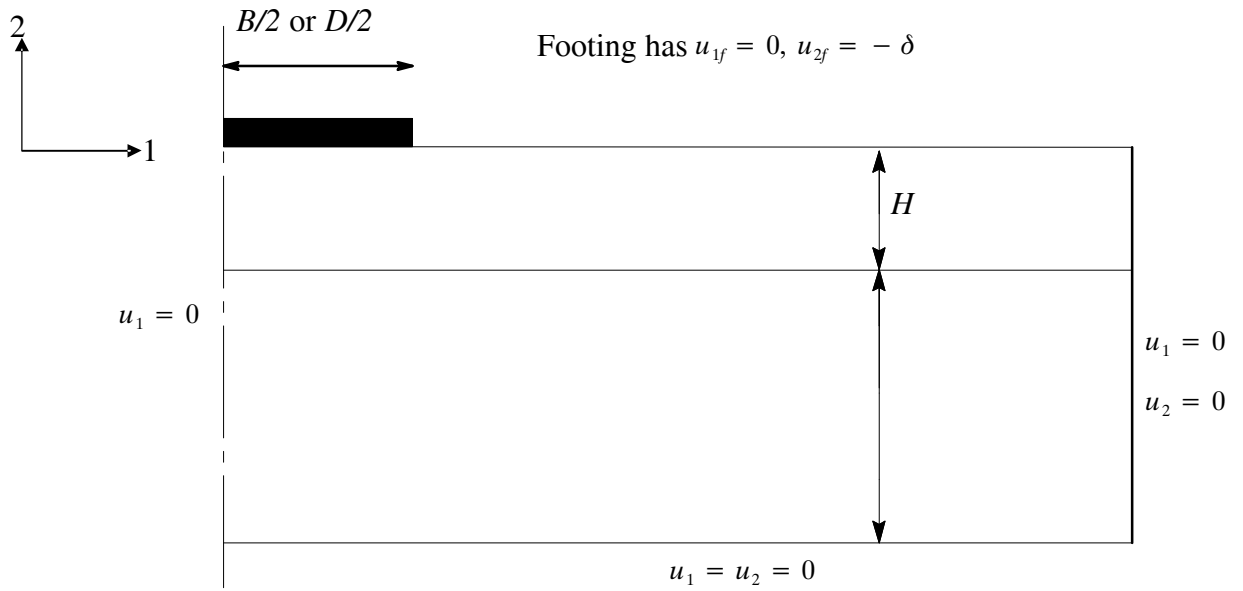
For the case of a layered soil profile, the bearing capacity is given in equation (2.24)

The value of  $N_c^*$  is to be computed using the results from finite element analyses for each ratio of  $H/B$ ,  $c_{u1}/c_{u2}$  and for each footing shape. For a homogeneous profile with  $c_{u1}/c_{u2} = 1$ , the modified bearing capacity factor  $N_c^*$  equals the Prandtl solution of  $(2 + \pi)$ .

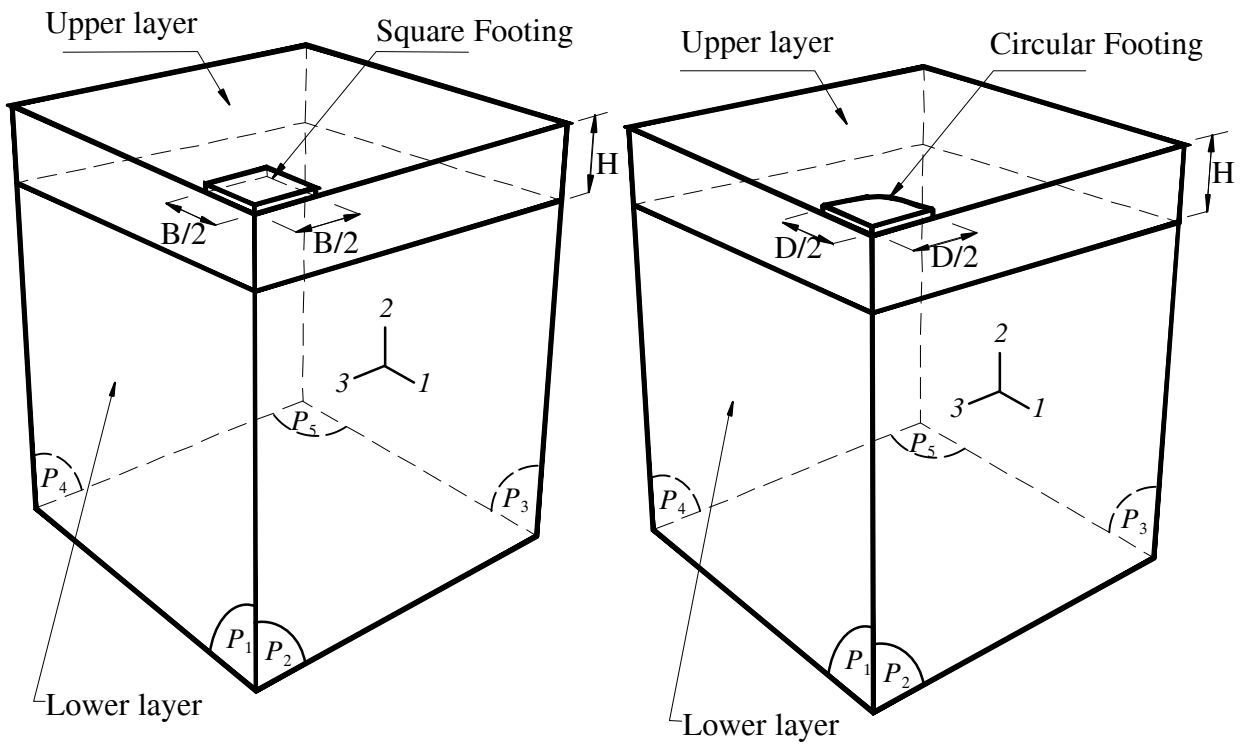
### 3.3 FINITE ELEMENT MODELLING DETAILS

The finite element software ABAQUS was used for solving this problem. For strip, square and circular footing problems, the ABAQUS model consisted of two parts, namely the footing and the soil. This is illustrated in Figure 3.1. Typical boundary conditions are presented in Figure 3.2.

Typical meshes for the problem of strip and three-dimensional footings are shown in Figure 3.3. For the strip footing case, the mesh is as shown in Figure 3.3 (a). The mesh consisted of 6-node modified plane strain triangular elements in Figure 3.4 (a) which were found to provide the best solution convergence. For the three-dimensional case of square and circular footings the 10-node modified quadratic tetrahedron element was adopted for similar reasons (Figure 3.4 (b)). These modified elements are specific to ABAQUS and have been constructed to reduce “node locking” and to have an unambiguous sign of the



(a) Strip footing



Elements in plane  $P_1$  have  $u_3 = ur_1 = ur_2 = 0$

Elements in plane  $P_2$  have  $u_1 = ur_3 = ur_2 = 0$

Elements in planes  $P_3, P_4$  and  $P_5$  have

$$u_1 = u_2 = u_3 = ur_1 = ur_2 = ur_3 = 0$$

Footing has  $u_{1f} = 0, u_{2f} = -\delta, u_{3f} = 0$

(b) Square footing

Elements in plane  $P_1$  have  $u_3 = ur_1 = ur_2 = 0$

Elements in plane  $P_2$  have  $u_1 = ur_3 = ur_2 = 0$

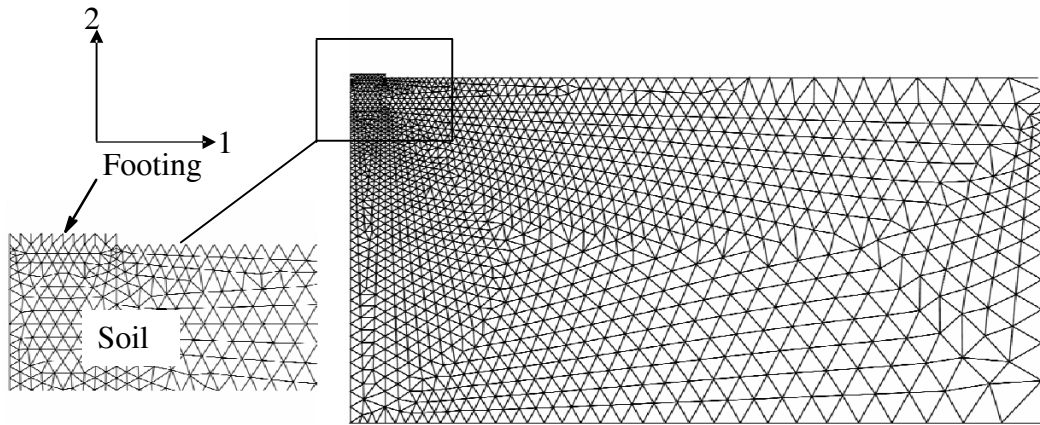
Elements in planes  $P_3, P_4$  and  $P_5$  have

$$u_1 = u_2 = u_3 = ur_1 = ur_2 = ur_3 = 0$$

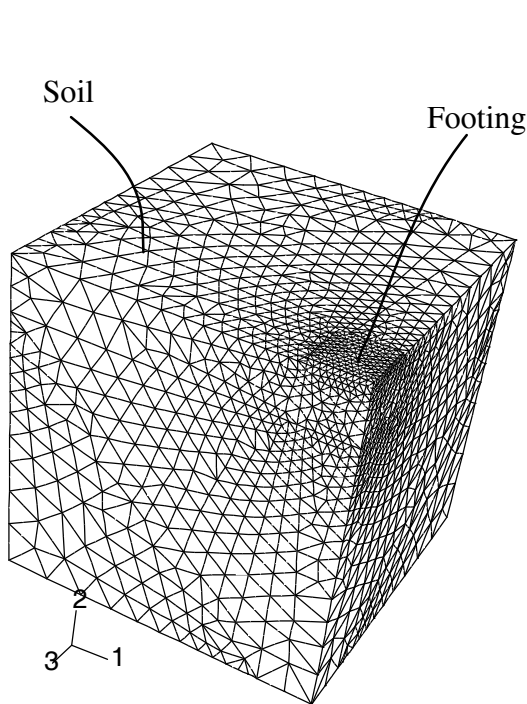
Footing has  $u_{1f} = 0, u_{2f} = -\delta, u_{3f} = 0$

(c) Circular footing

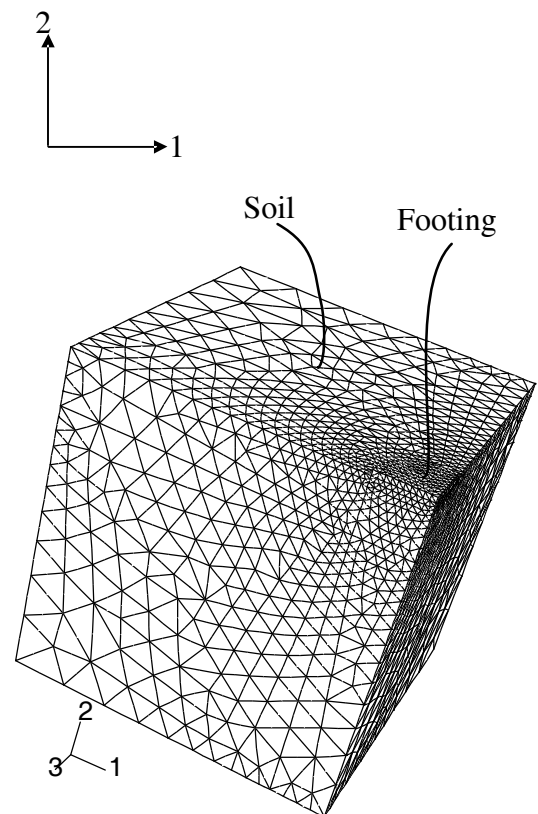
**Figure 3.2** Typical boundary conditions



(a) Strip footing



(b) Square footing



(c) Circular footing

**Figure 3.3** Typical mesh layouts used in the finite element models

contact normal stress that is usually associated with second order elements in contact analyses. The overall mesh dimensions were selected to ensure that the zones of plastic shearing and the observed displacement fields were contained within the model boundaries at all times. The underside of all footings were modelled as perfectly rough by specifying a “tied” contact constraint at the footing/soil interface.

To determine the collapse load of the footing, displacement defined analyses were performed where the footing was considered as being perfectly rigid. That is, a uniform vertical prescribed displacement ( $-\delta$ ) was applied to all those nodes on the footing. The total displacement was applied over a number of substeps and the nodal contact forces along the footing were summed to compute the equivalent bearing capacity.

A distinct advantage of using the finite element method is that it provides the complete load deformation response. This can provide insight into general footing behaviour, particularly in regard to the development of the collapse mechanism and deformation serviceability issues. By observing the load displacement response, a check can be made to ensure that the ultimate bearing capacity has been reached and that overall collapse has in fact occurred (i.e. the load–displacement plot reaches a plateau as shown in Figure 3.5).

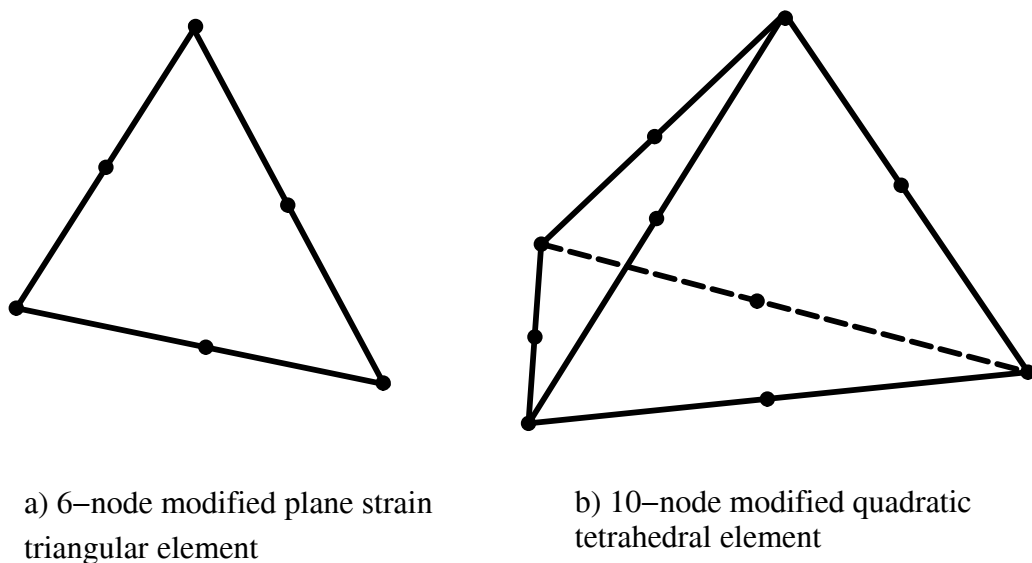


**Figure 3.4** Element types used for FE modelling

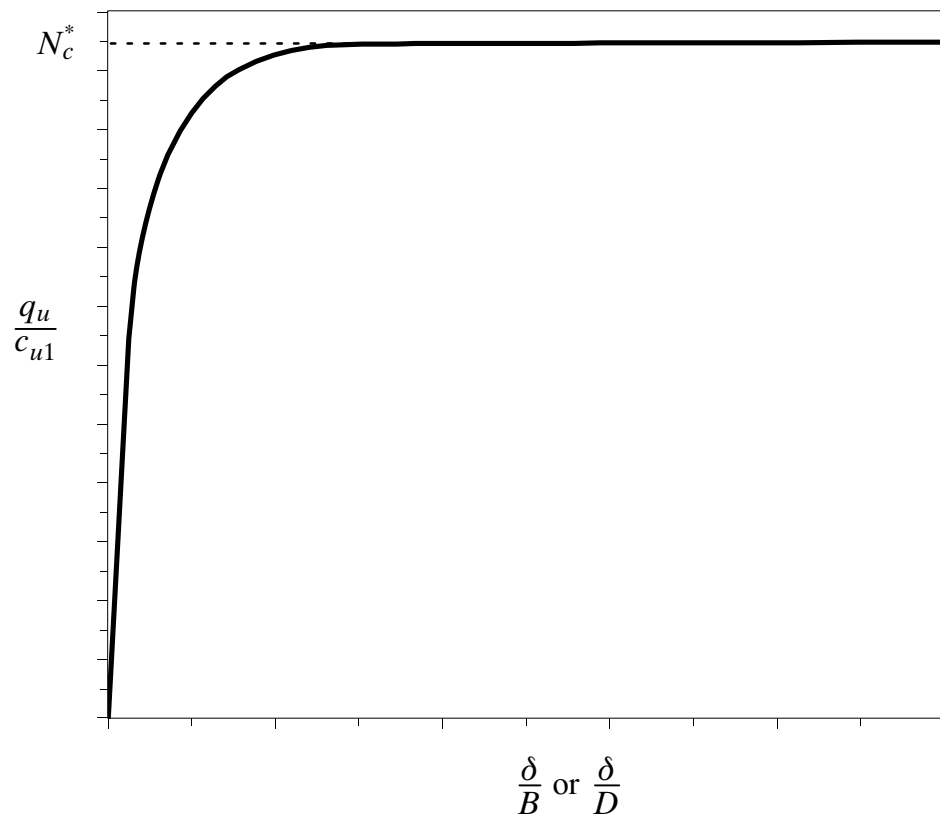


**Figure 3.5** Typical load–displacement curve of footing from Abaqus FE analysis

### 3.4 ABAQUS FINITE ELEMENT ANALYSIS (FEA) RESULTS

#### 3.4.1 Footing on homogeneous clay $c_{u1} = c_{u2}$

As an initial check on the three dimensional finite element model, the bearing capacity factor for the homogeneous case  $N_c$  for square and circular surface footings was calculated and compared to existing published numerical results. This comparison is summarised in Table 3.1. As can be seen, the bearing capacity factors from the current finite element study compare well to that calculated using the widely adopted shape factor in equation (3.2), and the solutions of Salgado et al (2004). The bearing capacity factor for square footings ( $N_c = 5.95$ ) was found to be around 2% below that for circular footings ( $N_c = 6.05$ ). This observation is consistent with the findings of Salgado et al (2004) as shown in Table 3.1. The bearing capacity factor  $N_c$  for strip footings was found to be 5.24, around 2% above the classical Prandtl solution of  $(2 + \pi)$ . Table 3.2 compares Prandtl's (1921) solution for the bearing capacity factor  $N_c$  with those of Griffiths et al. (2002), Merifield

et al. (1999) and Salgado et al. (2004). In general the ABAQUS results compare well with previous estimates of  $N_c$ .

	FEM–ABAQUS		Equation (3.1) Equation (3.2)	Equation (3.1) Equation (3.3)	Salgado et al. 2004			
	Square footing (SQ)	Circular footing (CI)			Square footing		Circular footing	
			Lower bound	Upper bound	Lower bound	Upper bound		
$N_c$	5.95	6.05	6.14	6.168	5.523	6.221	5.856	6.227
Comp ared to SQ	0	-----	+3.19%	+3.66%	-7.18%	+4.55%	-----	-----
Comp ared to CI	-----	0	+1.49%	+1.95%	-----	-----	-3.21%	+2.93%

Note: SQ: Square footings, CI: Circular footing, ---: no need to compare. Compared to SQ(%)= $(N_c - 5.95)/5.95$ , Compared to CI(%)= $(N_c - 6.05)/6.05$

**Table 3.1** Comparison of bearing capacity factors  $N_c$  for square and circular footings

	Prandtl 1921	FEM– ABAQUS	Griffiths et al' 2002	Merifield et al. 1999			Salgado et al. 2004	
				Lower bound	Upper bound	Avera ge	Lower bound	Upper bound
$N_c^*$	5.14	5.24	5.423	4.94	5.32	5.13	5.132	5.203
Compared to Prandtl	0	+1.95%	+5.51%	-3.89%	+3.50%	-0.2%	-0.16%	+1.2%

Note: Positive signifies case when  $N_c > 5.14$ , negative signifies case when  $N_c < 5.14$ , Compared= $(N_c - 5.14)/5.14$ .

**Table 3.2** Comparison of bearing capacity factors  $N_c$  for strip footings

### 3.4.2 Footing on layered clay $c_{u1} \neq c_{u2}$

The bearing capacity factors  $N_c^*$  (equation (2.24)) for the non-homogeneous case ( $c_{u1} \neq c_{u2}$ ) for strip, circular and square footings on two-layered clays are presented in Table 3.3, and shown graphically in Figure 3.6. Also shown in these figures are the bearing capacity factors for strip footings by Merifield et al (1999). Some general observations will be mentioned before discussing the results for strong over weak and soft over strong profiles separately in more detail.

The bearing capacity factor  $N_c^*$  was found to be almost identical for square and circular footings for both the strong over weak and weak over strong layer cases. In all cases the bearing capacity factor for circular footings was around 1–2% above that of a square footing. This is shown clearly in Figure 3.6 where the results for square and circular footings are difficult to distinguish from each other.

As discovered by Merifield et al (1999), all of the analyses herein indicate that a complex relationship exists between the observed modes of shear failure and the ratios  $c_{u1}/c_{u2}$  and  $H/B$ . The modes of failures can best be described as being either “general shear”, “partial punching shear”, or “full punching shear” similar to that described by Merifield et al (1999). Full punching shear (Figure 3.7) is characterised by a vertical separation of the top layer which then effectively acts as a rigid column of soil that punches through to the bottom layer. In this case only a small amount of heaving is observed immediately adjacent to the footing, but significant failure is observed below the upper layer. .

Conversely, only a small vertical separation of the top layer is evident for partial punching shear. General shear failure is as defined by many authors including Terzaghi (1943). In this mode of failure we observe well defined shear planes developing and extending to the surface, and bulging of the soil on both sides of the footing.

When comparing the results for square and circular footings to those for strip footings, in general it was found that the bearing capacity factors  $N_c^*$  for square and circular footings were larger than those for strip footings. This is applicable for both the strong over weak and weak over strong profiles, and was to some extent expected. The only exception to this observation was for the weak over strong profile case where the upper layer is very thin compared to the footing width, namely when  $H/B \leq 0.25$ . This is shown clearly in Figure 3.6(a) where the above trend is reversed and the bearing capacity factors  $N_c^*$  for square and circular footings were smaller than those for strip footings.

Further three dimensional and axi-symmetric analyses with much finer finite element meshes confirmed this observation. However, further investigation is required to properly explain the mechanics of this failure mechanism and the lower than expected collapse load.

---

$H/B$	$c_{u1}/c_{u2}$	Value of bearing capacity factor $N_c^*$			
		Upper Bound (Merifield et al. 1999)	Finite Element Method – ABAQUS		
			Strip Footing	Strip Footing	Square Footing
$H/B=0.125$	0.20	8.55	8.61	7.96	7.95
	0.25	8.55	8.61	7.96	7.95
	0.40	8.55	8.60	7.96	7.95
	0.50	8.55	8.40	7.96	7.89
	0.80	6.36	6.21	6.73	6.85
	1.00	5.32	5.24	5.95	6.05
	1.25	4.52	4.45	5.11	5.27
	1.50	3.93	3.83	4.53	4.66
	2.00	3.09	3.03	3.73	3.85
	2.50	2.61	2.53	3.21	3.32
	4.00	1.82	1.75	2.33	2.41
5.00	1.55	1.48	2.00	2.07	
$H/B=0.25$	0.20	6.52	6.34	6.35	6.36
	0.25	6.52	6.34	6.35	6.36
	0.40	6.52	6.34	6.35	6.36
	0.50	6.52	6.33	6.35	6.36
	0.80	6.25	5.95	6.27	6.34
	1.00	5.32	5.24	5.95	6.05
	1.25	4.6	4.62	5.45	5.59
	1.50	4.08	4.05	5.03	5.17
	2.00	3.34	3.31	4.39	4.51
	2.50	2.88	2.84	3.92	4.02
	4.00	2.12	2.06	3.04	3.13
5.00	1.85	1.71	2.70	2.78	
$H/B=0.375$	0.20	5.84	5.78	6.00	6.10
	0.25	5.84	5.78	6.00	6.10
	0.40	5.84	5.78	6.00	6.10
	0.50	5.84	5.76	6.00	6.10
	0.80	5.84	5.76	6.00	6.10
	1.00	5.32	5.24	5.95	6.05
	1.25	4.78	4.77	5.74	5.88
	1.50	4.28	4.27	5.46	5.60
	2.00	3.65	3.58	4.96	5.10
	2.50	3.2	3.13	4.53	4.68
	4.00	2.42	2.37	3.67	3.80
5.00	2.13	2.07	3.32	3.44	

**Table 3.3** Values of bearing capacity factor  $N_c^*$

$H/B$	$c_{u1}/c_{u2}$	Value of bearing capacity factor $N_c^*$			
		Upper Bound (Merifield et al. 1999)	Finite Element Method –ABAQUS		
			Strip Footing	Strip Footing	Square Footing
$H/B=0.5$	0.20	5.49	5.46	5.96	6.04
	0.25	5.49	5.46	5.96	6.04
	0.40	5.49	5.46	5.96	6.04
	0.50	5.49	5.46	5.96	6.04
	0.80	5.49	5.46	5.96	6.04
	1.00	5.32	5.24	5.95	6.05
	1.25	4.94	4.92	5.94	6.02
	1.50	4.48	4.49	5.82	5.90
	2.00	3.89	3.86	5.46	5.58
	2.50	3.47	3.43	5.08	5.23
	4.00	2.74	2.67	4.22	4.39
5.00	2.44	2.36	3.89	4.03	
$H/B=0.75$	0.20	5.36	5.24	5.95	6.03
	0.25	5.36	5.24	5.95	6.03
	0.40	5.36	5.24	5.95	6.03
	0.50	5.36	5.24	5.95	6.03
	0.80	5.36	5.24	5.95	6.03
	1.00	5.32	5.24	5.95	6.05
	1.25	5.2	5.17	5.98	6.05
	1.50	4.94	4.87	5.98	6.05
	2.00	4.37	4.35	5.96	6.05
	2.50	4.01	3.96	5.91	6.03
	4.00	3.28	3.22	5.24	5.47
5.00	2.98	2.90	4.94	5.15	
$H/B=1.0$	0.20	5.3	5.27	5.93	6.03
	0.25	5.3	5.27	5.93	6.03
	0.40	5.3	5.27	5.93	6.03
	0.50	5.3	5.27	5.93	6.03
	0.80	5.3	5.27	5.93	6.03
	1.00	5.32	5.24	5.95	6.05
	1.25	5.3	5.24	5.94	6.05
	1.50	5.18	5.16	5.94	6.05
	2.00	4.82	4.77	5.93	6.06
	2.50	4.5	4.44	5.93	6.06
	4.00	3.83	3.75	5.86	6.04
5.00	3.54	3.44	5.77	5.94	

**Table 3.3 (continued)** Values of bearing capacity factor  $N_c^*$

$H/B$	$c_{u1}/c_{u2}$	Value of bearing capacity factor $N_c^*$			
		Upper Bound (Merifield et al. 1999)	Finite Element Method –ABAQUS		
		Strip Footing	Strip Footing	Square Footing	Circular Footing
$H/B=1.5$	0.20	5.3	5.25	5.94	6.04
	0.25	5.3	5.25	5.94	6.04
	0.40	5.3	5.25	5.94	6.04
	0.50	5.3	5.25	5.94	6.04
	0.80	5.3	5.25	5.94	6.03
	1.00	5.32	5.24	5.95	6.05
	1.25	5.27	5.24	5.94	6.04
	1.50	5.31	5.24	5.94	6.04
	2.00	5.31	5.23	5.94	6.04
	2.50	5.32	5.19	5.94	6.04
	4.00	4.84	4.67	5.94	6.04
	5.00	4.56	4.40	5.94	6.03
$H/B=2.0$	0.20	5.3	5.24	5.96	6.05
	0.25	5.3	5.24	5.96	6.05
	0.40	5.3	5.24	5.96	6.05
	0.50	5.3	5.24	5.96	6.05
	0.80	5.3	5.24	5.96	6.05
	1.00	5.32	5.24	5.95	6.05
	1.25	5.26	5.21	5.96	6.05
	1.50	5.26	5.21	5.96	6.05
	2.00	5.27	5.21	5.96	6.05
	2.50	5.27	5.21	5.96	6.05
	4.00	5.32	5.21	5.96	6.05
	5.00	5.32	5.13	5.96	6.05

**Table 3.3 (continued)** Values of bearing capacity factor  $N_c^*$

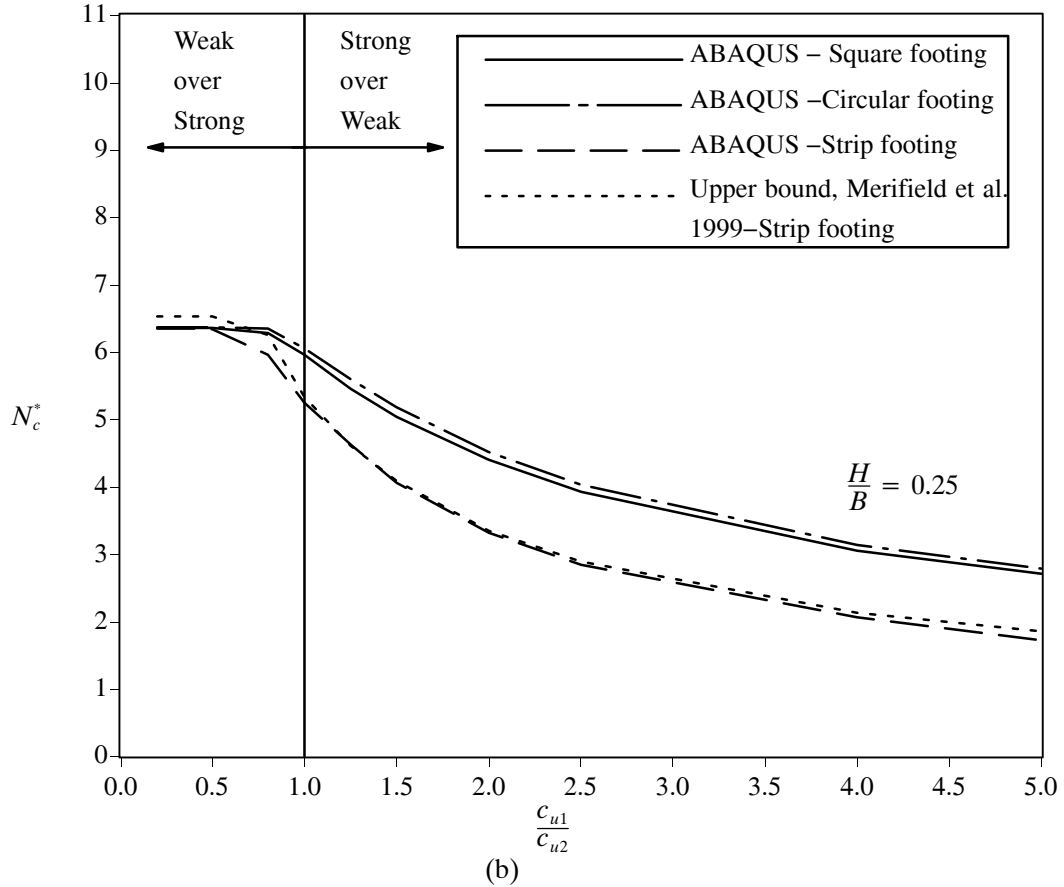
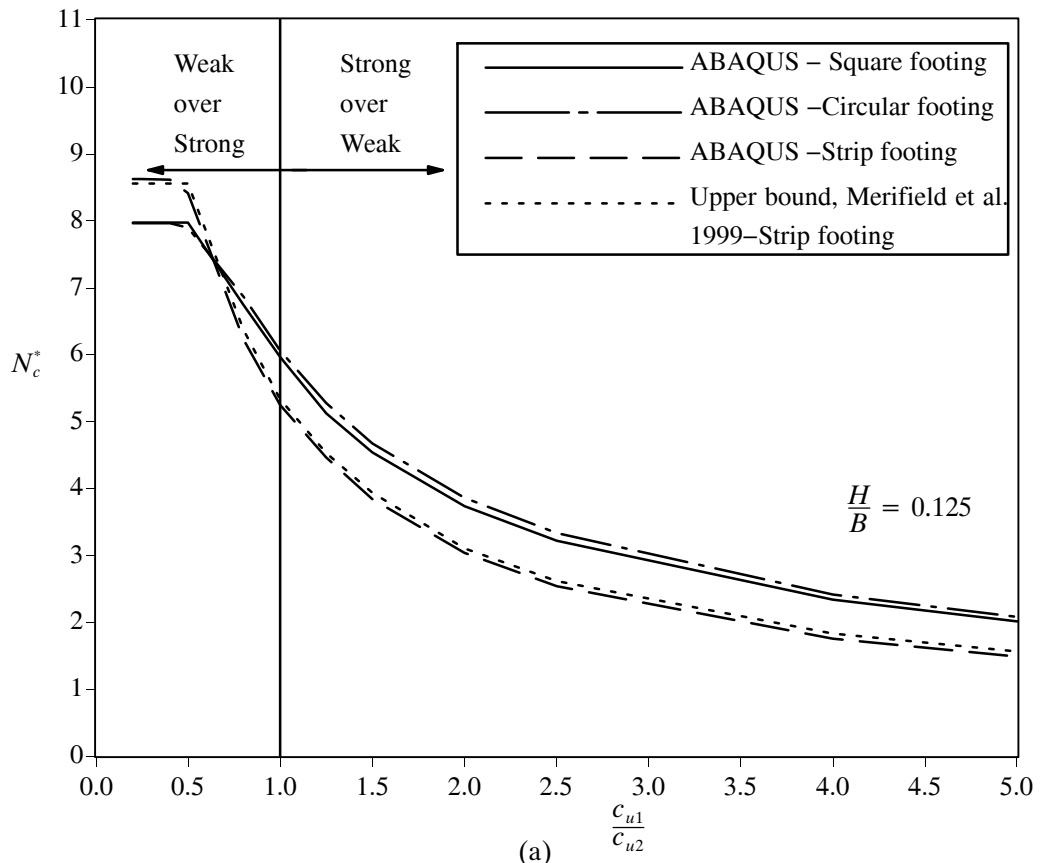


**Figure 3.6** Values of bearing capacity factor  $N_c^*$

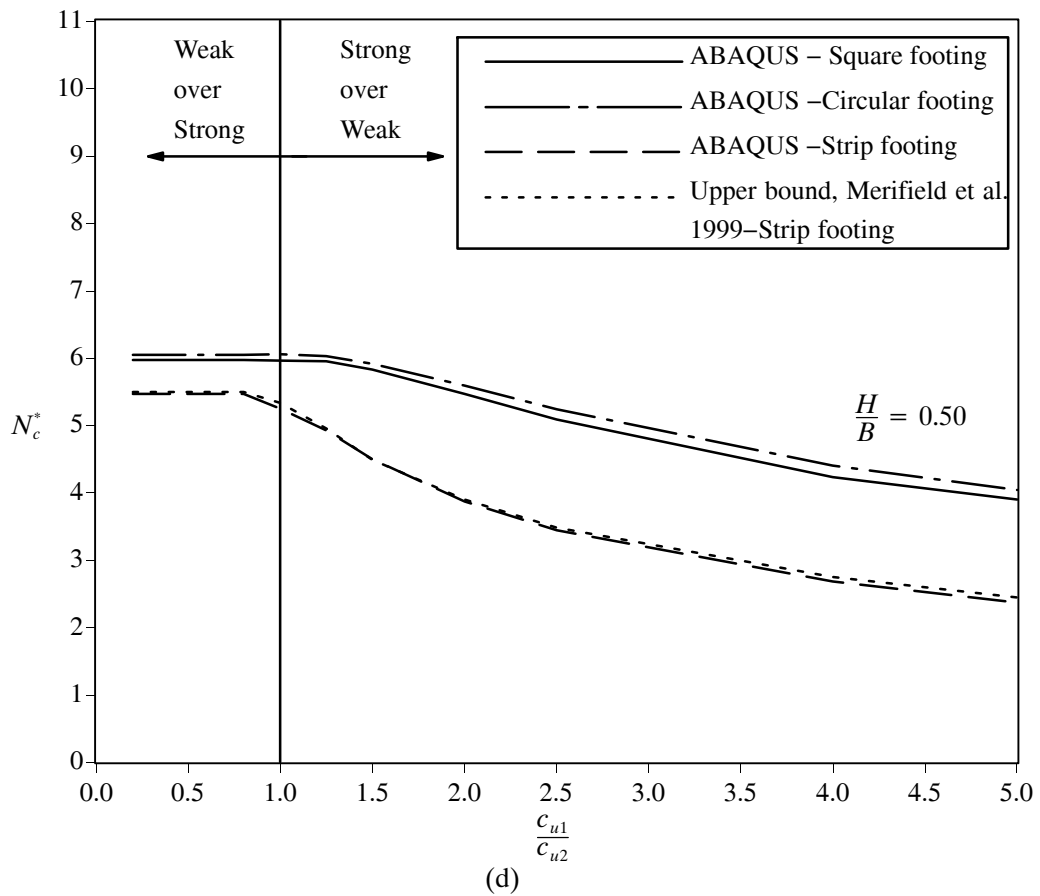
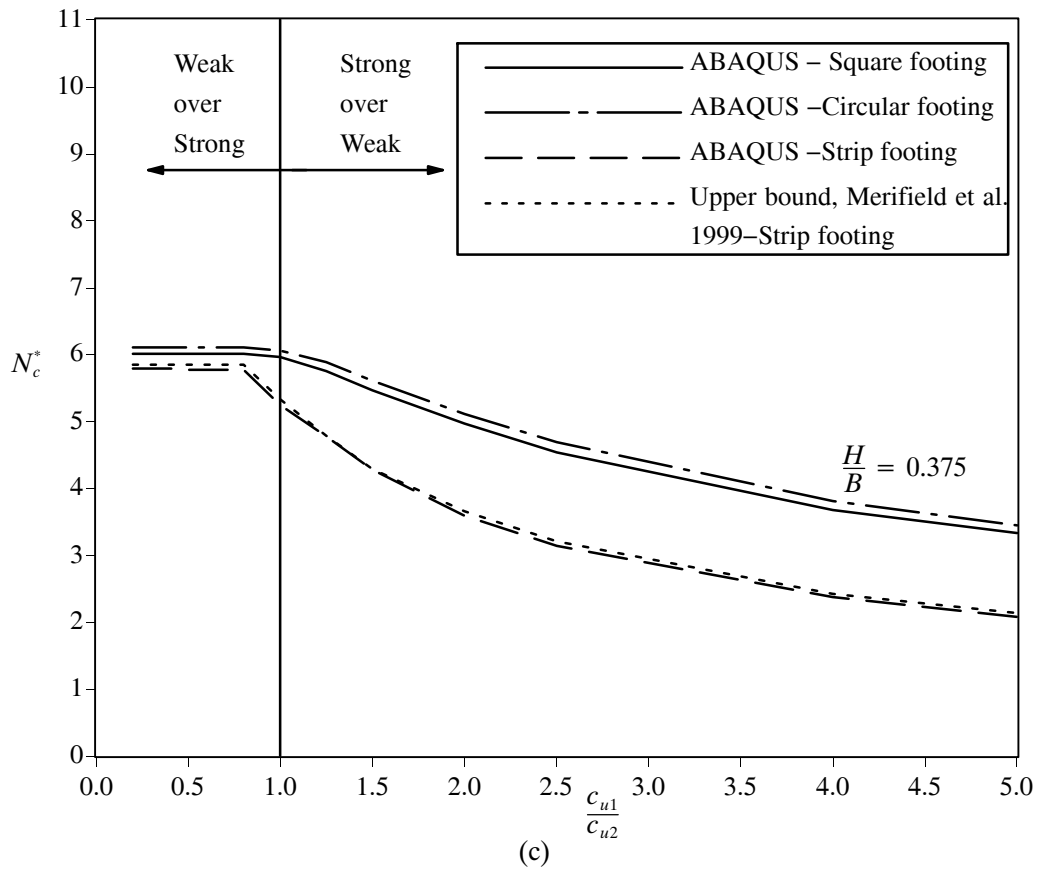


**Figure 3.6 (continued)** Values of bearing capacity factor  $N_c^*$

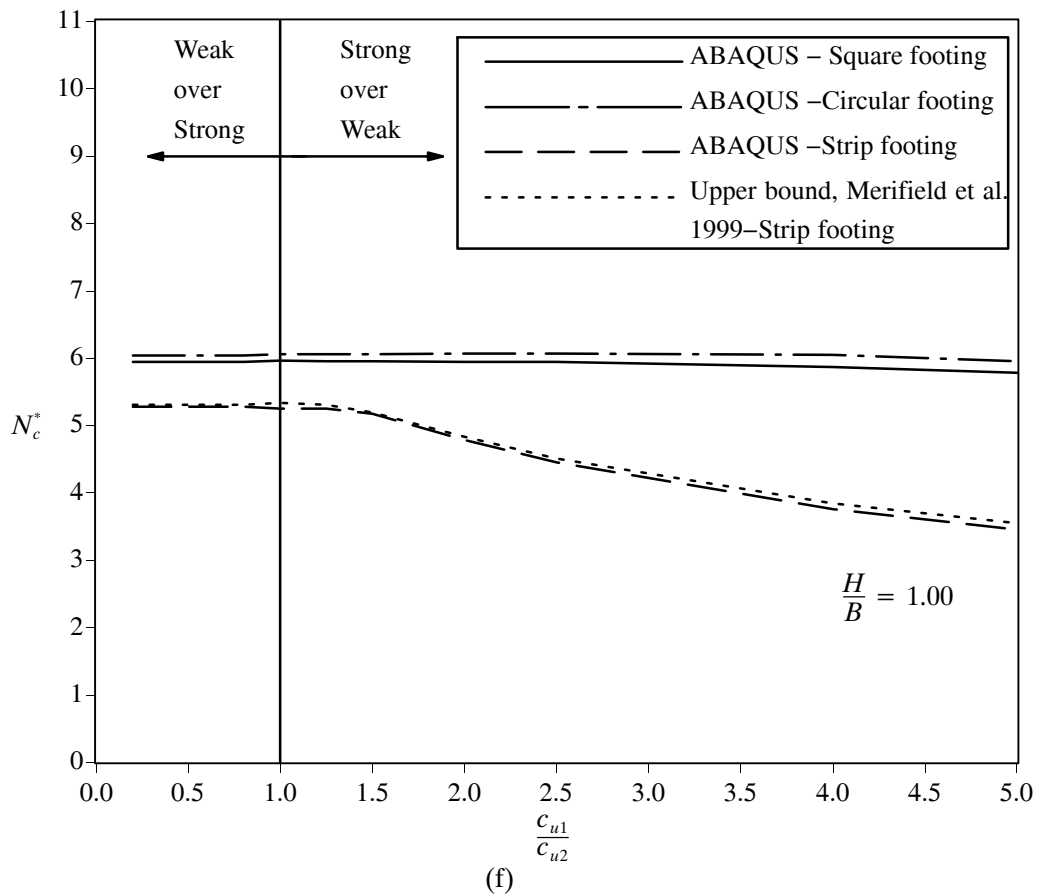
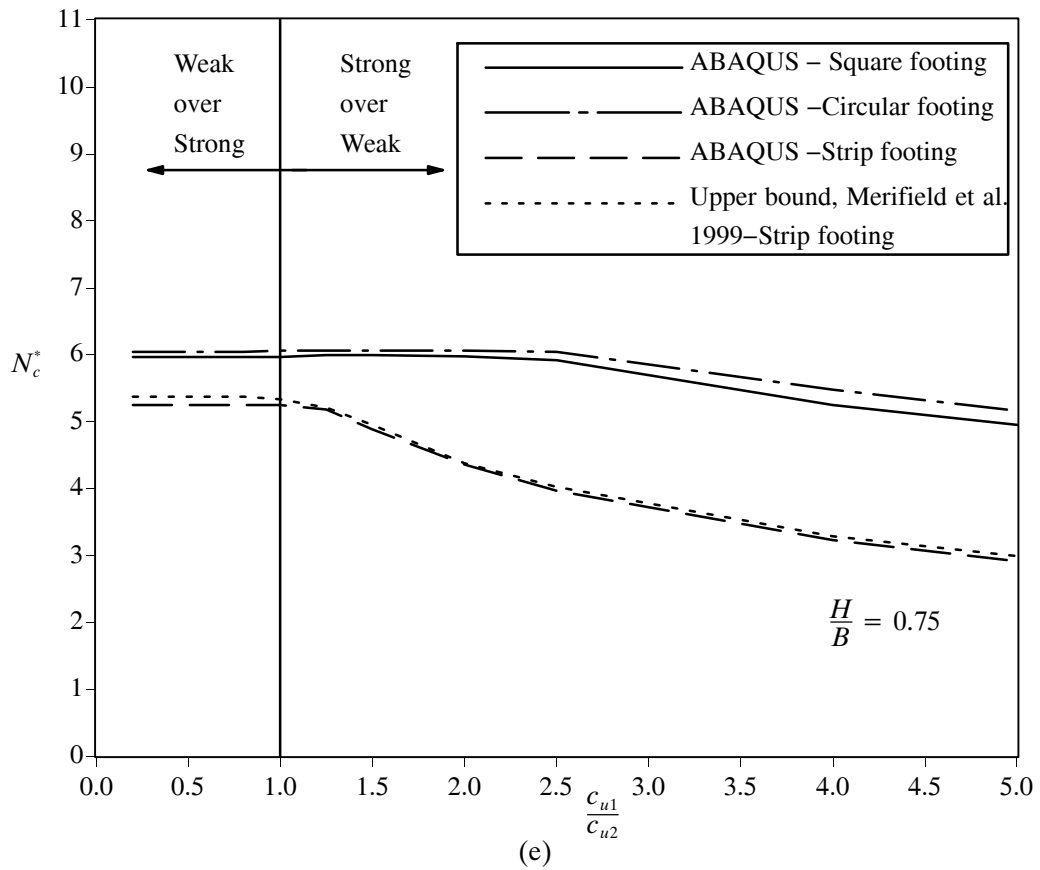


**Figure 3.6 (continued)** Values of bearing capacity factor  $N_c^*$

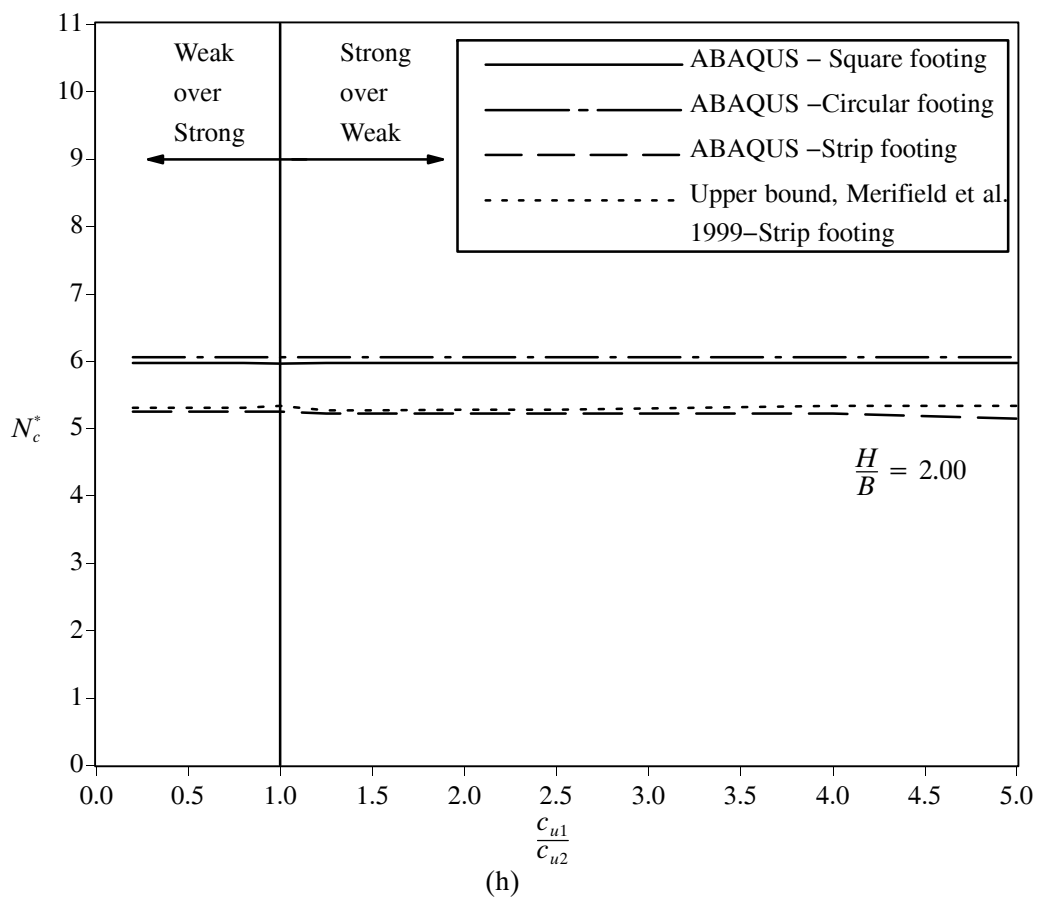
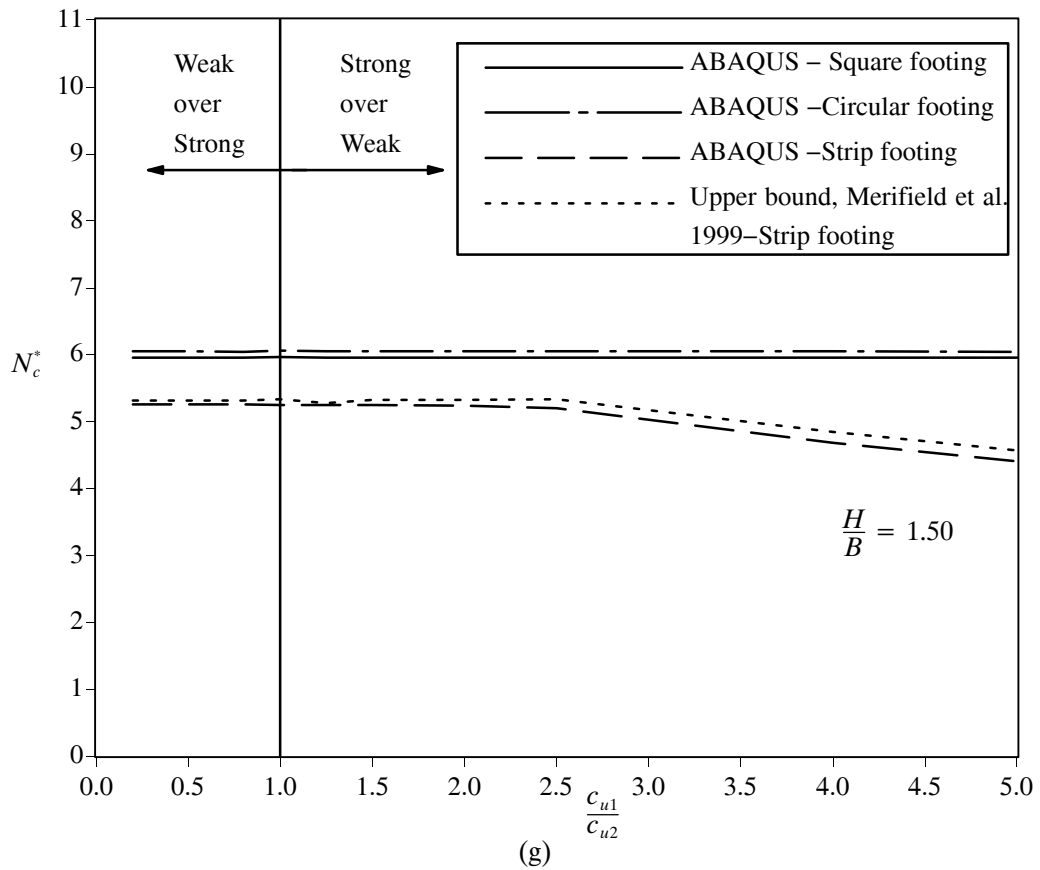


**Figure 3.6 (continued)** Values of bearing capacity factor  $N_c^*$

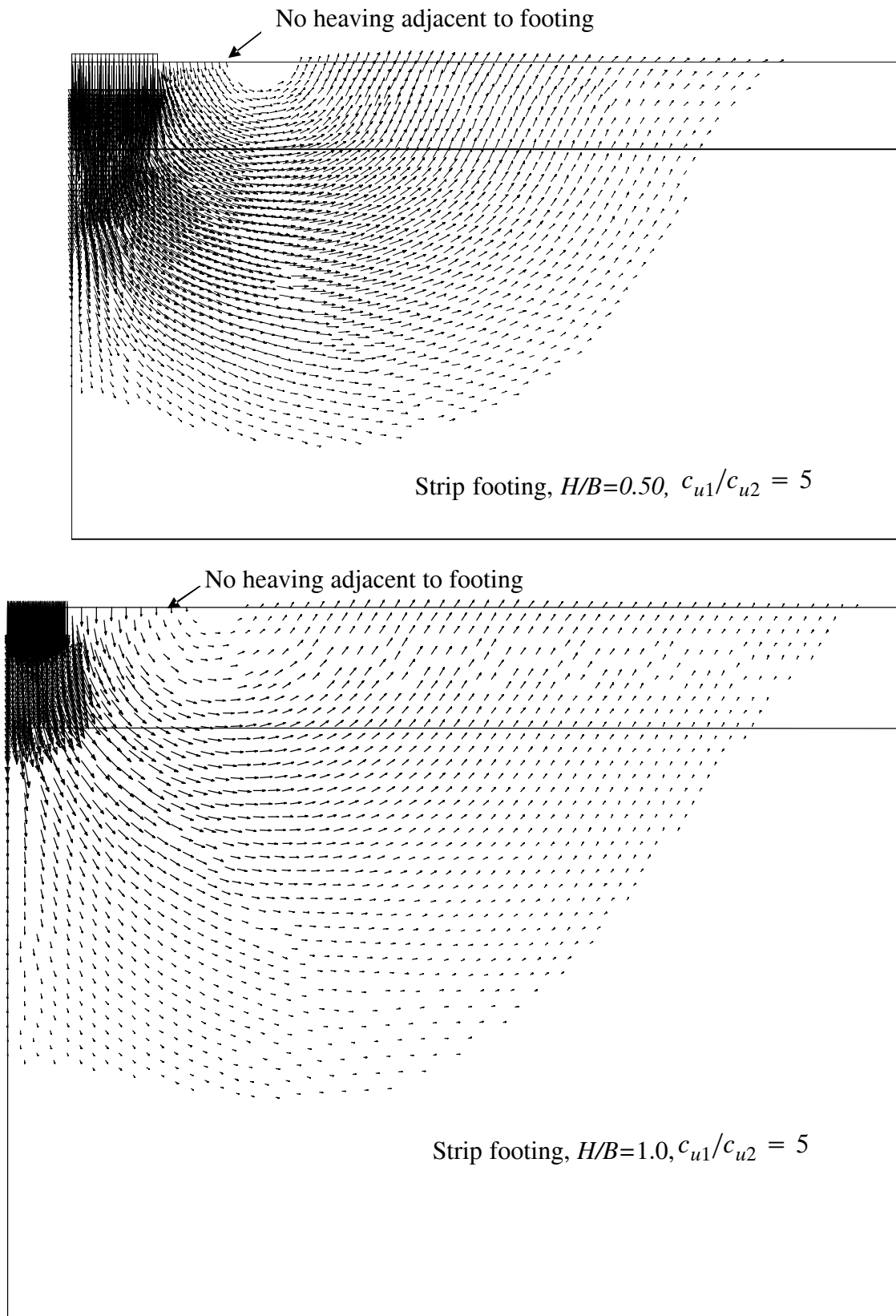


**Figure 3.7** Examples of punching shear failure for strip footings

### 3.4.3 2-D Strip footing on layered clay $c_{u1} \neq c_{u2}$

For strip footings on layered clays, the finite element bearing capacity factors compare well to the upper bound solutions presented by Merifield et al (1999). In general, the displacement finite element solution presented here is within  $\pm 2\%$  of Merifield's solution (see Figure 3.6).

For the strong over weak case where a moderately strong crust exists ( $1 \leq c_{u1}/c_{u2} \leq 2.5$ ), failure is generally caused by partial punching shear. As the depth of the top crust approaches the footing width  $B$ , upward deformations within the bottom layer become restricted causing an increase in the extent of plastic failure. As the top crust becomes very strong compared to the bottom layer ( $c_{u1}/c_{u2} > 2.5$ ) full punching shear through the top layer occurs. The very strong top layer then serves to greatly restrict both lateral and vertical movement of the soil contained in the weak layer below (see Figure 3.7). This results in the formation of a deep zone of plastic shearing within the bottom layer.

The results indicate that a reduction in bearing capacity for a strong over weak clay system occurs up to a depth ratio of  $H/B \approx 1.5 - 2$ . This lower limit is applicable for soil profiles where  $c_{u1}/c_{u2} < 2.5$ , but for profiles that have a very strong top crust with  $c_{u1}/c_{u2} > 2.5$ , punching failure through the top layer is likely to occur up to depth ratio of  $H/B = 2$ . For ratios of  $H/B > 2$ , failure is contained entirely within the top layer and is independent of the ratio  $c_{u1}/c_{u2}$ . These observations are consistent with those predicted by Merifield et al (1999).

For the weak over strong case, the finite element results indicate that for ratios of  $H/B \leq 0.5$ , the bearing capacity increases as the relative strength of the bottom layer rises. At a limiting ratio of  $c_{u1}/c_{u2}$ , no further increase in bearing capacity is achieved as the general shear failure mechanism becomes fully contained within the top layer. For all values of  $H/B > 0.5$ , the solutions indicate that failure occurs entirely within the top layer and the bearing capacity is independent of the strength of the bottom layer.

### 3.4.4 3-D square and circular footings on layered clay

*Square and circular footings on weak clay overlying strong clay  $c_{u1}/c_{u2} < 1$*

For thin upper layers where  $H/B \leq 0.375$ ,  $N_c^*$  increases as the ratio of  $c_{u1}/c_{u2}$  decreases. That is, as the thin top layer becomes weaker and weaker compared to the underlying strong layer, the contribution made by the underlying layer to the ultimate bearing capacity increases. For very thin upper layers ( $H/B = 0.125$ ), the increase in the bearing capacity factor  $N_c^*$  above that for the homogeneous case is significant, as shown in Figure 3.6 (a). This can be explained by observing the failure mechanisms, such as that shown in Figure 3.8(a). The displacement vector diagram indicates that, although much of the failure is contained in the weak upper layer, failure still occurs well into the strong underlying layer.

For upper layer thicknesses where  $H/B > 0.375$ , the stronger underlying layer does not contribute greatly to the ultimate bearing capacity regardless of the ratio of  $c_{u1}/c_{u2}$ . As a consequence no further increase in bearing capacity is achieved as the failure surface becomes fully contained within the top layer. The failure mechanisms shown in Figure 3.8 (d – l) confirm this. The bearing capacity factor is equal to that found for the homogeneous case and is shown as a horizontal line in Figure 3.6. This observation is similar to that found by Merifield et al (1999) for strip footings where for  $H/B > 0.5$ , the limit analysis solutions indicated that failure occurs entirely within the top layer and the bearing capacity is independent of the strength of the bottom layer.

***Square and circular footings on strong clay overlying weak clay  $c_{u1}/c_{u2} > 1$***

In general it was observed that for a given ratio of  $H/B < 1$ , the bearing capacity factor  $N_c^*$  was found to decrease in a nonlinear manner as the ratio of  $c_{u1}/c_{u2}$  increases (Figure 3.6). This indicates the failure mechanism must penetrate into the underlying weaker layer which in turn has the effect of reducing the ultimate bearing capacity. This is confirmed by the displacement velocity plots shown in Figure 3.8(b),(c) and Figure 3.8(e),(f). In these figures large displacements and zones of failure are seen to occur in the underlying weak layer.

As previously mentioned, the ABAQUS finite element results for strip footings and the limit analysis results of Merifield et al (1999) indicate that a reduction in bearing capacity for a strong over weak clay system occurs up to a depth ratio of  $H/B \leq 2$ . This limiting ratio of  $H/B$  is greater than that observed for circular and square footings (i.e.  $H/B \leq 1$ ).

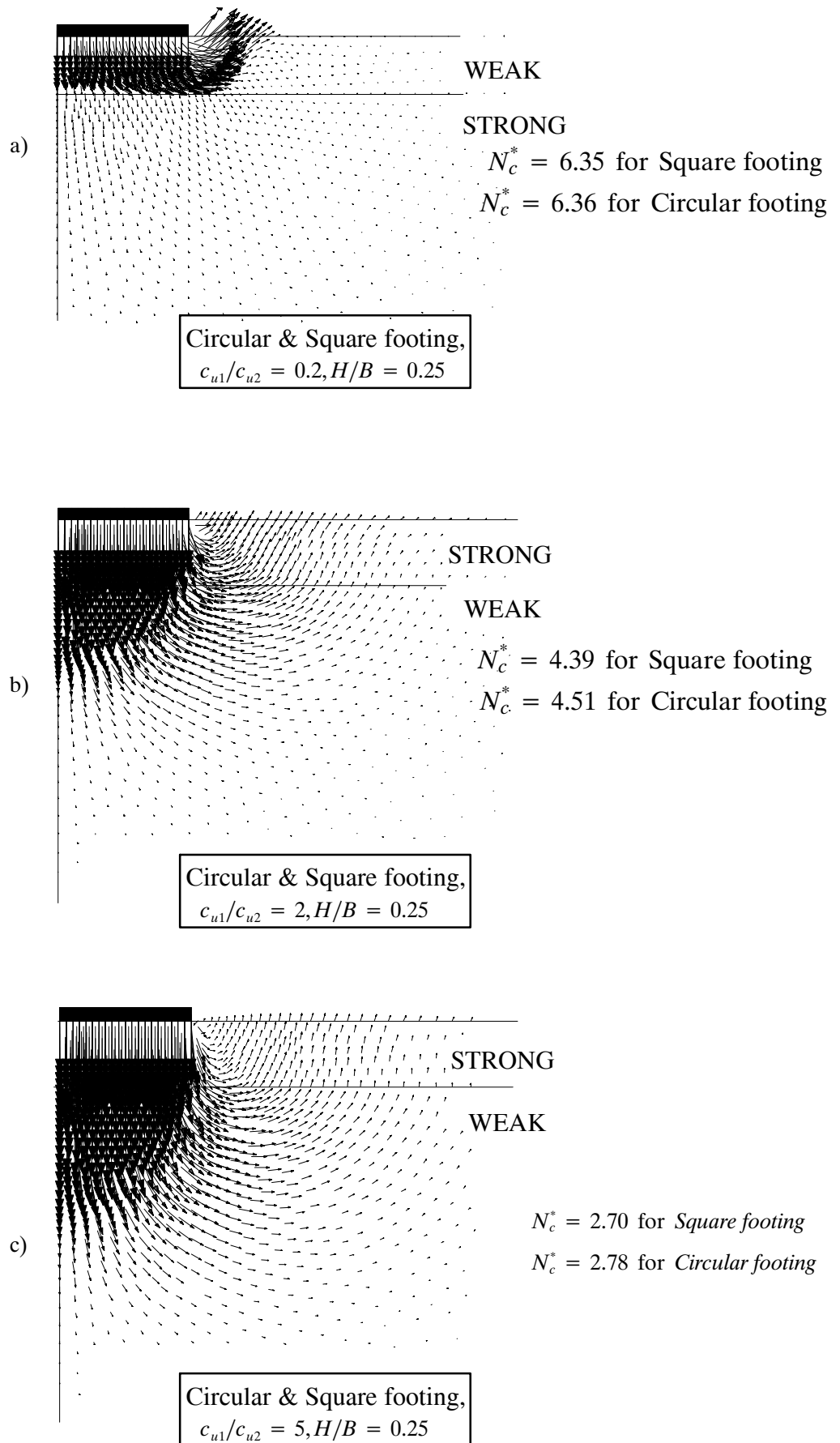


**Figure 3.8** Displacement vectors for square and circular footing on layered clay

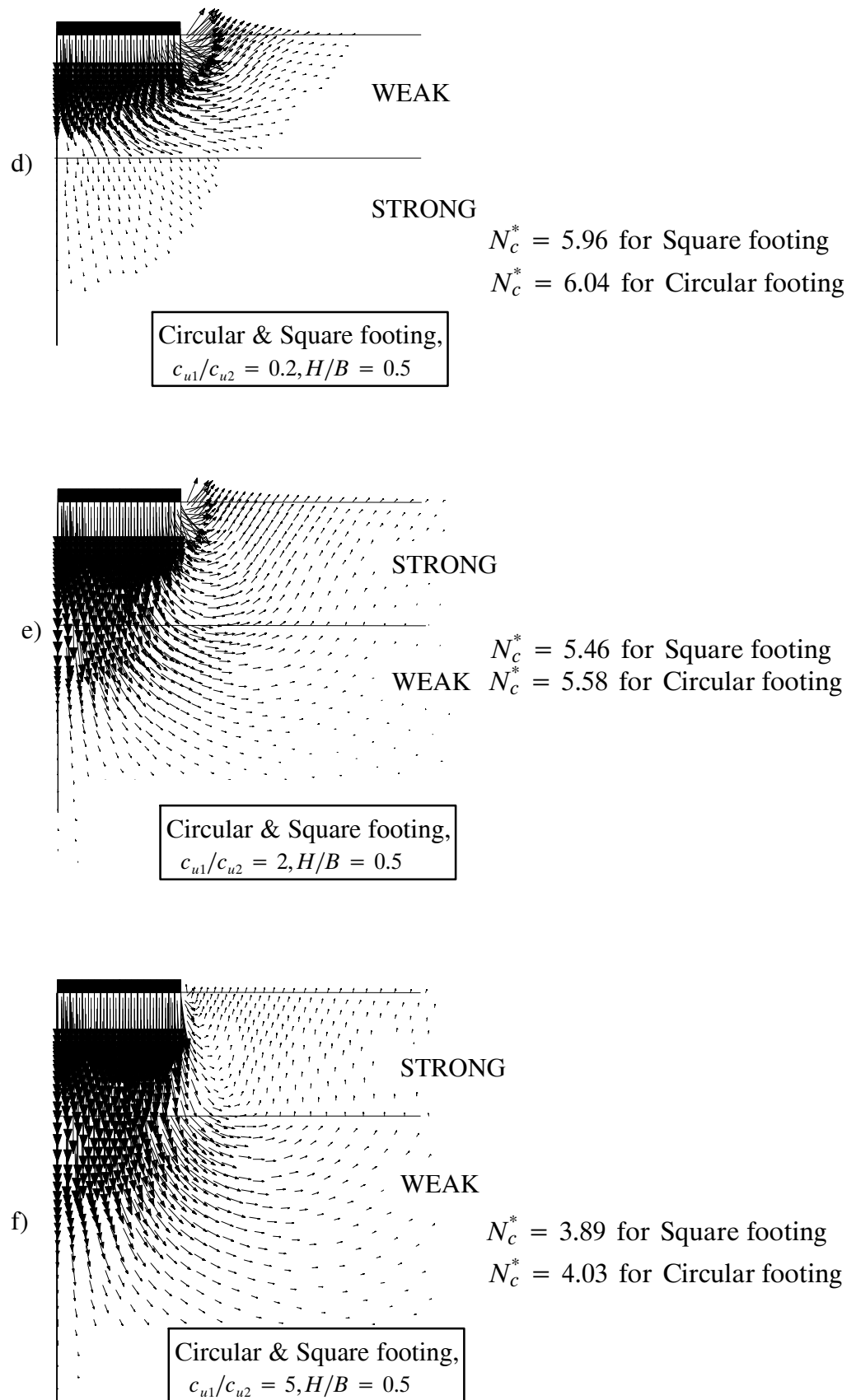


Figure 3.8 cont'd Displacement vectors for square & circular footing on layered clay

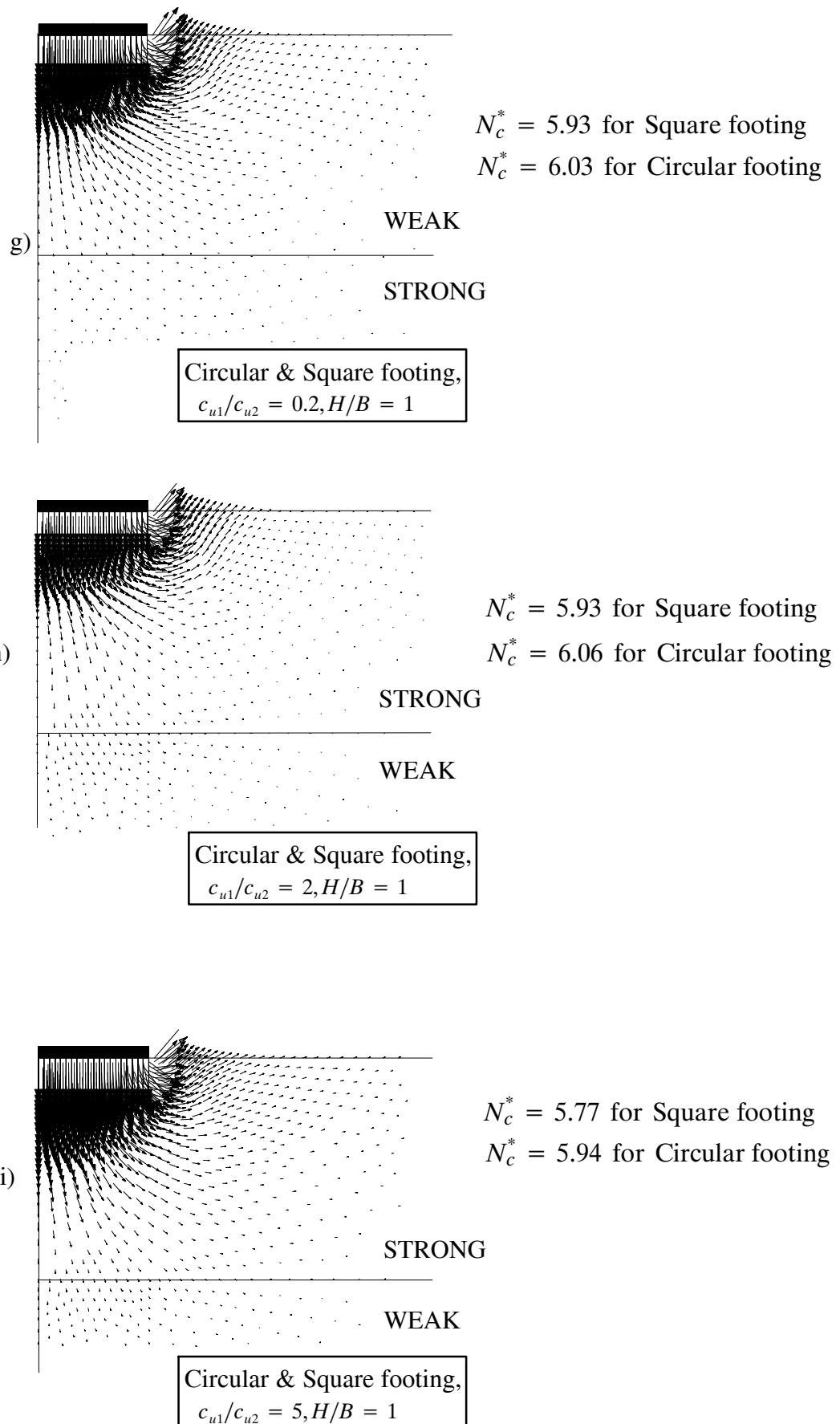
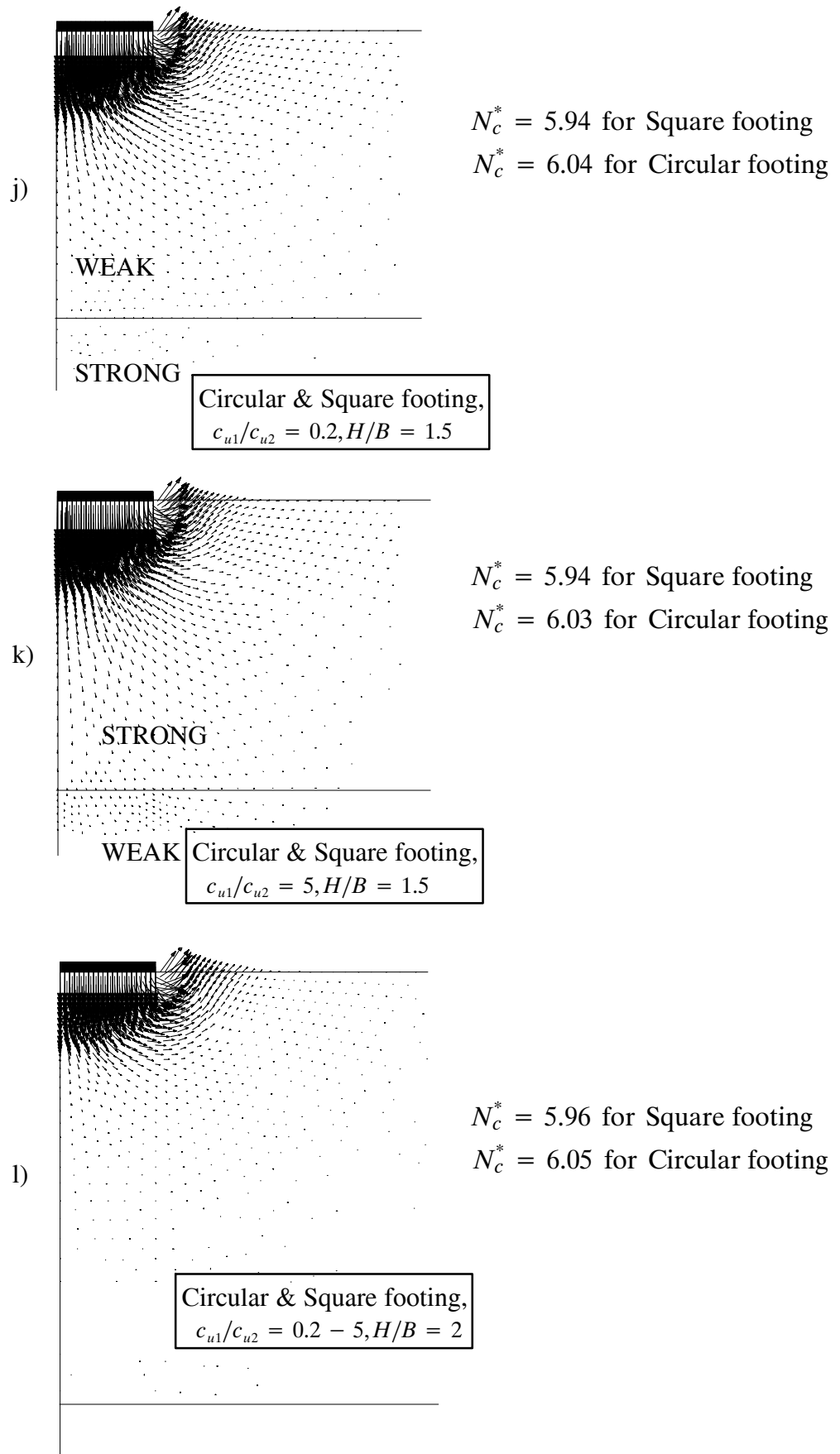


Figure 3.8 cont'd Displacement vectors for square & circular footing on layered clay



**Figure 3.8 cont'd** Displacement vectors for square & circular footing on layered clay

This behavioural difference is most obvious in Figure 3.6(e) where the bearing capacity factor  $N_c^*$  for a strip footing is well below that of a circular or square footing on the same layered profile.

Punching shear failure is a common mechanism observed in the case of strong over weak profiles. Full punching shear failure was generally observed when  $c_{u1}/c_{u2} \geq 2.5$ . For these cases, the top layer acts as rigid column of soil that pushes through the top layer into the underlying weak soil and a significant zone of failure is therefore apparent in the lower layer. Full punching shear failure is highlighted in Figure 3.8(c) and Figure 3.8(f). Based on the observed displacement vectors and stress contours, some guidance is provided in Figure 3.9 as a means of distinguishing the likely mode of failure for circular and square footings on a strong over weak profile. A division between full, partial punching and general shear failure depending on both ratio  $H/B$  and  $c_{u1}/c_{u2}$  is provided in Figure 3.9.

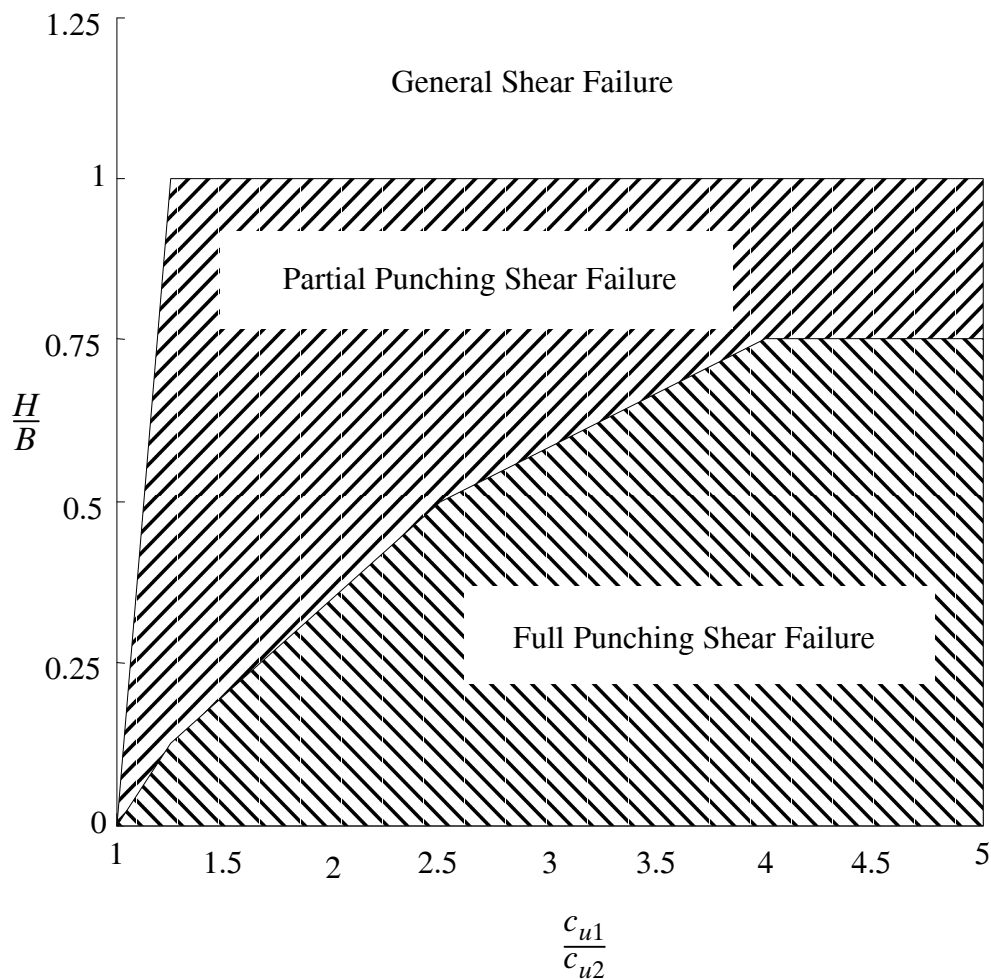


**Figure 3.9** Division between full, partial punching and general shear failure

### 3.4.5 Effect of footing roughness

The results of analyses with a perfectly smooth footing/soil interface indicate that for a strong over weak clay profile the soil/footing interface strength has little or no effect on the calculated bearing capacity. For strip footings the reduction in the bearing capacity was  $< 4\%$  whilst for square and circular footings the reduction was less than  $1\%$ . Similarly for a weak over strong clay system where  $H/B > 0.5$ , the bearing capacity does not vary greatly with footing roughness (i.e.  $< 4\%$  for all footing shapes). This agrees with the conclusions made by Merifield et al (1999).

For square, circular and strip footings on a weak over strong clay system where  $H/B \leq 0.5$ , a perfectly smooth soil/footing interface serves to reduce the bearing capacity by up to  $26\%$ . The greatest reduction occurs when  $H/B = 0.125$  and falls quickly to around  $6\%$  for  $H/B = 0.5$ .

## 3.5 CONCLUSION

The bearing capacity of strip, square and circular footings on two-layered clays using the finite element method has been investigated. The results obtained have been presented in terms of a modified bearing capacity factor  $N_c^*$  in both graphical and tabular form to facilitate their use in solving practical design problems.

The following conclusions can be made based on the finite element results:

- For homogeneous soil profiles, the finite element bearing capacity and shape factors for square and circular footings compare well to previously reported finite element and numerical limit analysis solutions.
- For strip footings on layered clays, the finite element bearing capacity factors compare well to the numerical upper bound limit analysis solutions presented by Merifield et al (1999). In general, the finite element solution presented here are within  $\pm 2\%$  of solution of Merifield et al (1999).
- For a weak over strong clay system where the ratio of  $H/B > 0.375$ , the stronger underlying layer does not contribute greatly to the ultimate bearing capacity regardless of the ratio of  $c_{u1}/c_{u2}$ . As a consequence no further increase in bearing capacity is achieved as the failure surface becomes fully contained within the top layer. When

$H/B \leq 0.375$  the bearing capacity factor  $N_c^*$  increases as the ratio of  $c_{u1}/c_{u2}$  decreases. For very thin upper layers ( $H/B \leq 0.125$ ), the increase in the bearing capacity factor  $N_c^*$  above that for the homogeneous case is significant.

- For both square and circular footings, a reduction in bearing capacity for a strong over weak clay system occurs up to a depth ratio of  $H/B < 1$ . For depth ratios of  $H/B \geq 1$ , failure is likely to be fully contained within the top layer and the bearing capacity factors for square ( $N_c^* = 5.95$ ) and circular footings ( $N_c^* = 6.05$ ) on a homogeneous profile can be used.
-

**CHAPTER 4**

**UNDRAINED BEARING CAPACITY OF**

**EMBEDDED FOOTINGS**

---

## 4.1 INTRODUCTION

Undrained bearing capacity of embedded footings is an important issue when estimating bearing capacity. In this chapter the ultimate undrained bearing capacity of embedded footings is investigated. Consideration has been given to the effect of embedded footing depth for strip, square, circular and selected rectangular footings. The bulk of the results are for cases where: (i) rough interfaces exist between the footings and soil; (ii) the footing has the same shape from the toe to the ground surface; and (iii) no friction operates between the side of the footing and the soil.

To begin with, the problem of undrained bearing capacity of embedded footings is defined in terms of soil strength and problem geometry. A number of numerical solutions for the embedment capacity are then presented which are based on finite element methods. These calculations are compared with the numerical limit analysis results of Salgado et al (2004) in a subsequent section of this chapter.

## 4.2 PROBLEM DEFINITION

A general layout of the problems to be analysed is shown in Figure 4.1 and Figure 4.2.

The system includes a footing and a soil foundation. The footing is placed at an embedment depth  $D$  from the surface. The clay soil foundation has an undrained shear strength  $c_u$  and infinite depth. The geometry of each type of footing is characterised as follows:

- Strip footing has width  $B$ ;
- Square footing has side length  $L$ ;
- Rectangular footing has width  $B$  and length  $L$ ; and
- Circular footing has diameter  $B$ .

In this thesis, equation (2.2) is used to obtain modified bearing capacity factors for a soil without unit weight. For purely cohesive clay ( $\phi_u = 0$ ), equation (2.2) therefore reduces to:

$$q_u = \frac{Q_u}{A} = c_u N_c F_{cs} F_{cd} \quad (4.1)$$

The purpose of this study is to propose bearing capacity, shape, and depth factors for strip, square, circular and rectangular footings at some depth in clay using the finite element method. Once again, the commercial software package ABAQUS was used.

Symmetry has been exploited for the problems. Only one quarter of the problem domain has been modelled for three-dimensional analyses and one half for two-dimensional analyses (Figure 4.1 and Figure 4.2).

The soil was modelled as an isotropic elasto-perfectly plastic continuum with failure described by the Mohr-Coulomb yield criterion. The elastic behaviour was described by a Poisson's ratio  $\nu = 0.48$ , and a ratio of Young's modulus to shear strength of  $E/c_u = 500$ . The soil is treated as weightless. The interactions between the soil and the bottom of the footings are characterized as rough.

For this problem the undrained bearing capacity of embedded footings will be a function of the ratio  $D/B$  and/or  $D/L$ .

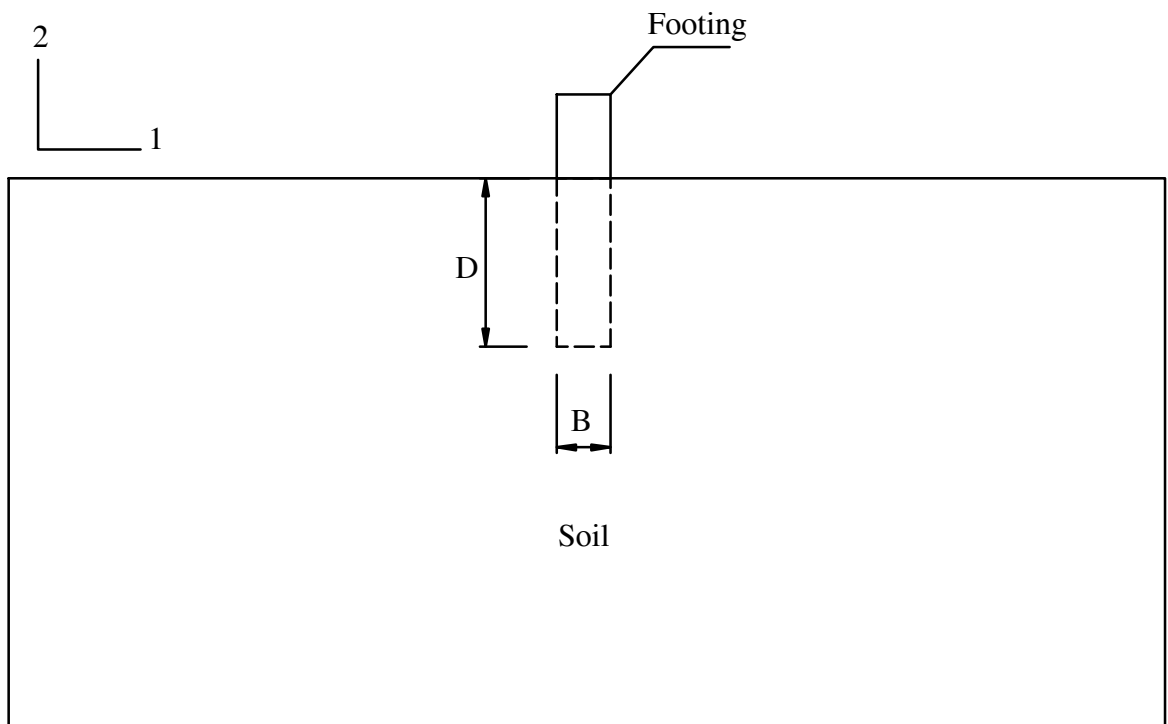
In this thesis, solutions have been computed for problems where  $D/B$  ranges from 0 to 5. In the rectangular case, the additional parameter  $B/L$  varies from 0.2 to 0.5. These ranges cover most problems of practical interest.

The output of the ABAQUS analyses is the total reaction  $Q_u$  force on the footing from which the ultimate bearing capacity  $q_u$  can be calculated. In addition, the depth factor  $F_{cd}$  and shape factors  $F_{cs}$  is obtained via equation (4.1).

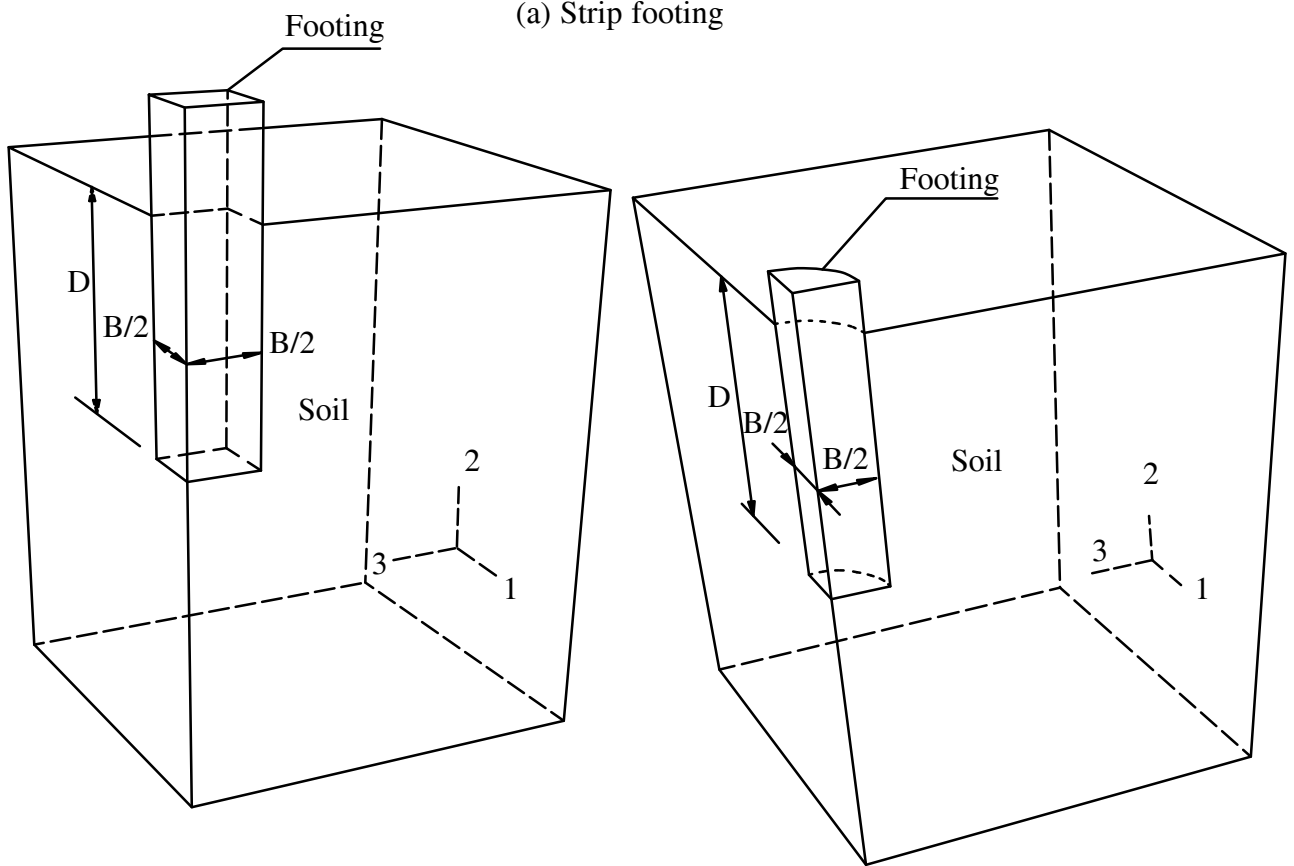
### 4.3 FINITE ELEMENT MODELLING DETAILS

The ABAQUS model consisted of two parts, namely the footing and the soil. This is illustrated in Figure 4.1 and Figure 4.2. At the interface between the footing and the soil, the elements representing the footing and those representing the soil have the same topology. The applied boundary conditions are presented in Figure 4.3 and Figure 4.4.

Typical meshes for the problem of the two-dimensional strip, and the three-dimensional square and circular footings are shown in Figure 4.5, those of the three-dimensional rectangular footing are presented in Figure 4.6. For the strip footing case, the mesh (Figure 4.5(a)) consisted of 8-node plane strain quadrilateral, hybrid, linear pressure, reduced integration elements (CPE8RH) as shown in Figure 4.7(a) because this element was found to provide the best solution convergence. For the three-dimensional case of square, rectangular and circular footings, the 10-node modified quadratic tetrahedron element (C3D10M) was adopted for similar reasons Figure 4.7(b).



(a) Strip footing



(b) Square footing

(c) Circular footing

**Figure 4.1** Problem definition for strip, square and circular footings

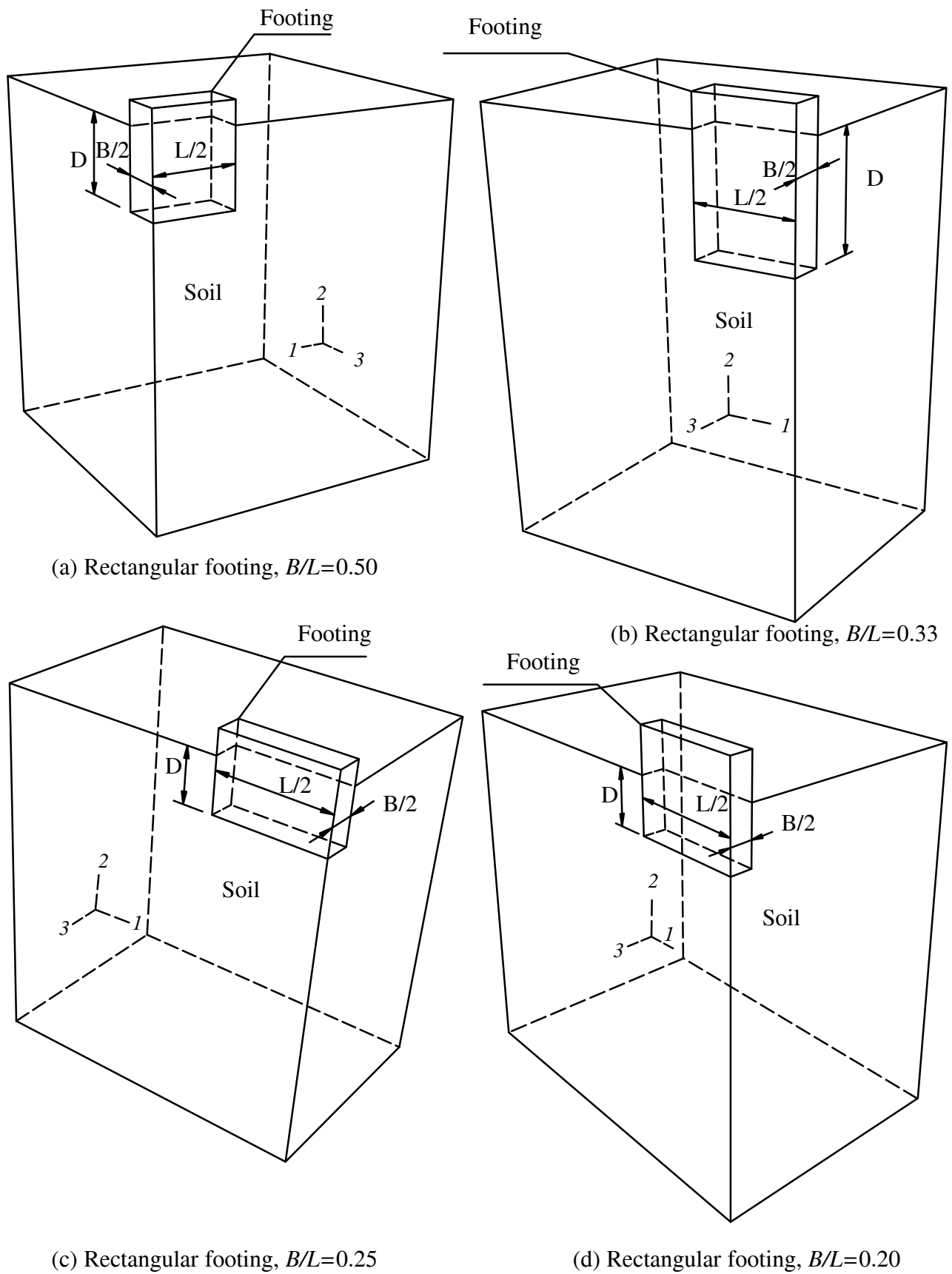
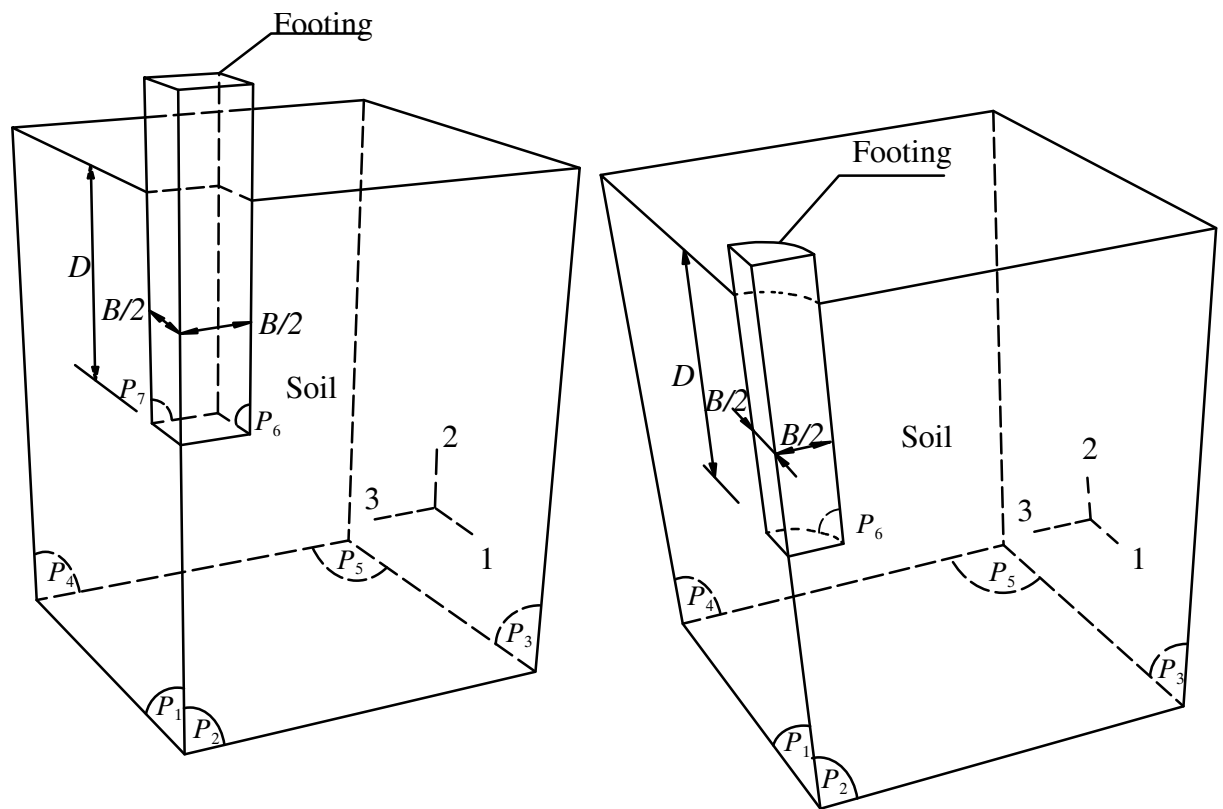
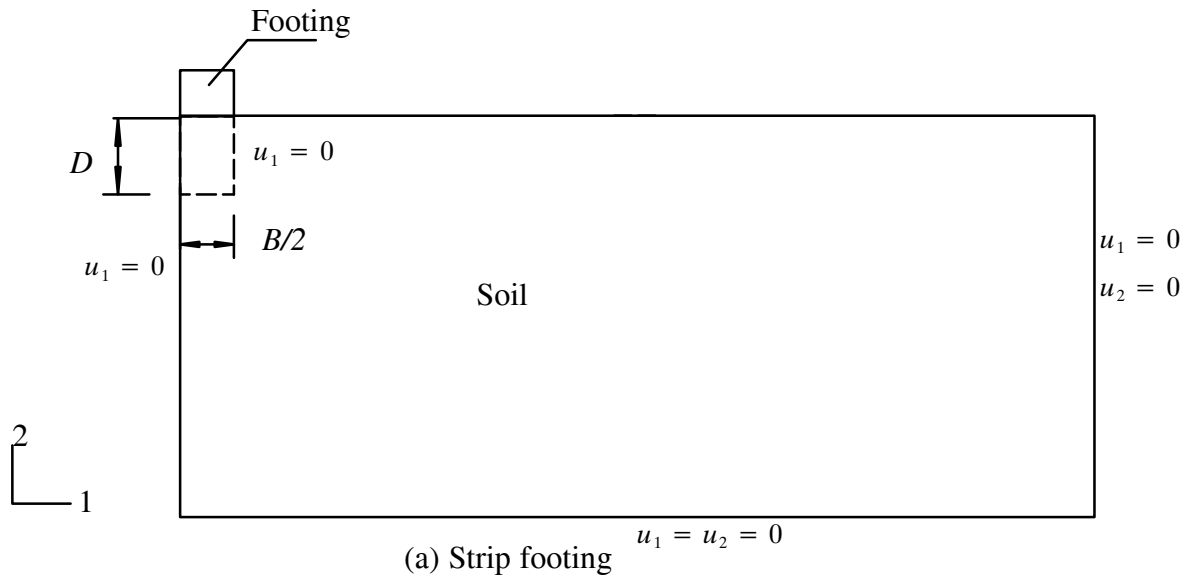


**Figure 4.2** Problem definition for rectangular footings



Elements in planes  $P_1$  and  $P_6$  have  $u_3 = ur_1 = ur_2 = 0$   
 Elements in planes  $P_2$  and  $P_7$  have  $u_1 = ur_2 = ur_3 = 0$   
 Elements in planes  $P_3, P_4$  and  $P_5$  have :  
 $u_1 = u_2 = u_3 = ur_1 = ur_2 = ur_3 = 0$   
 Footing has  $u_{1f} = 0, u_{2f} = -\delta, u_{3f} = 0$

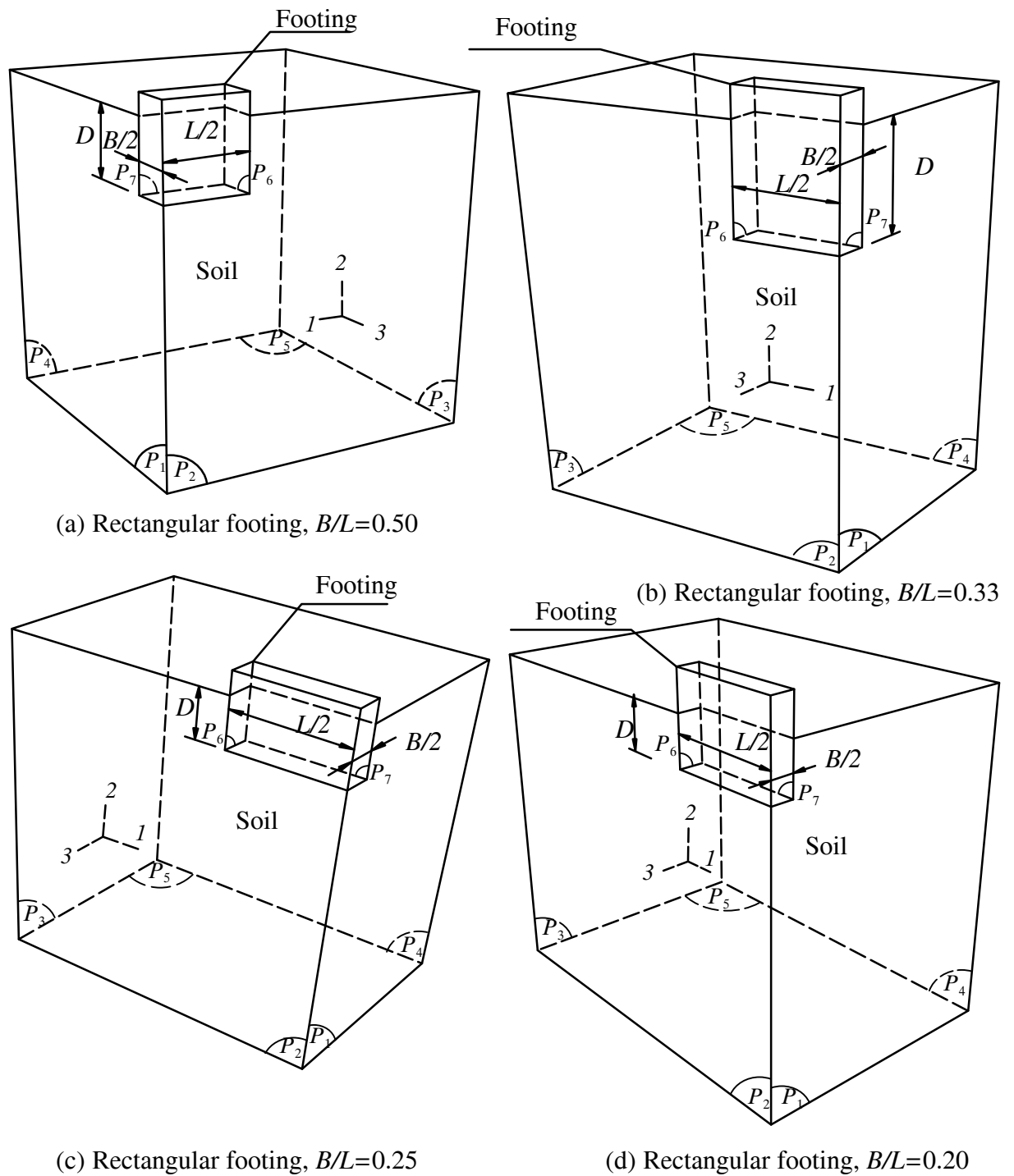
(b) Square footing

Elements in planes  $P_1$  have  $u_3 = ur_1 = ur_2 = 0$   
 Elements in planes  $P_2$  have  $u_1 = ur_2 = ur_3 = 0$   
 Elements in planes  $P_3, P_4$  and  $P_5$  have :  
 $u_1 = u_2 = u_3 = ur_1 = ur_2 = ur_3 = 0$   
 Footing has  $u_{1f} = 0, u_{2f} = -\delta, u_{3f} = 0$   
 Interface of footing sides and soil  $P_6$  just has

vertical displacement only

(c) Circular footing

**Figure 4.3** Typical boundary conditions for strip, square, and circular footings



*Elements in planes  $P_1$  and  $P_6$  have  $u_3 = ur_1 = ur_2 = 0$*

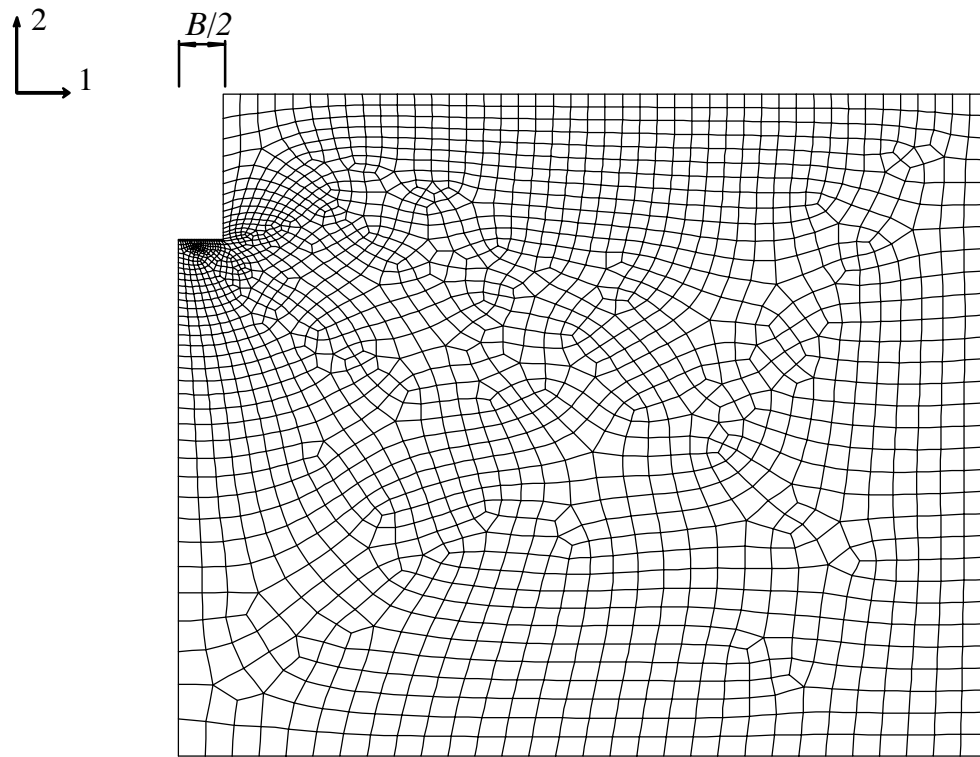
*Elements in planes  $P_2$  and  $P_7$  have  $u_1 = ur_2 = ur_3 = 0$*

*Elements in planes  $P_3, P_4$  and  $P_5$  have :*

$$u_1 = u_2 = u_3 = ur_1 = ur_2 = ur_3 = 0$$

*Footing has  $u_{1f} = 0, u_{2f} = -\delta, u_{3f} = 0$*

**Figure 4.4** Typical boundary conditions for rectangular footings



(a) Strip footing

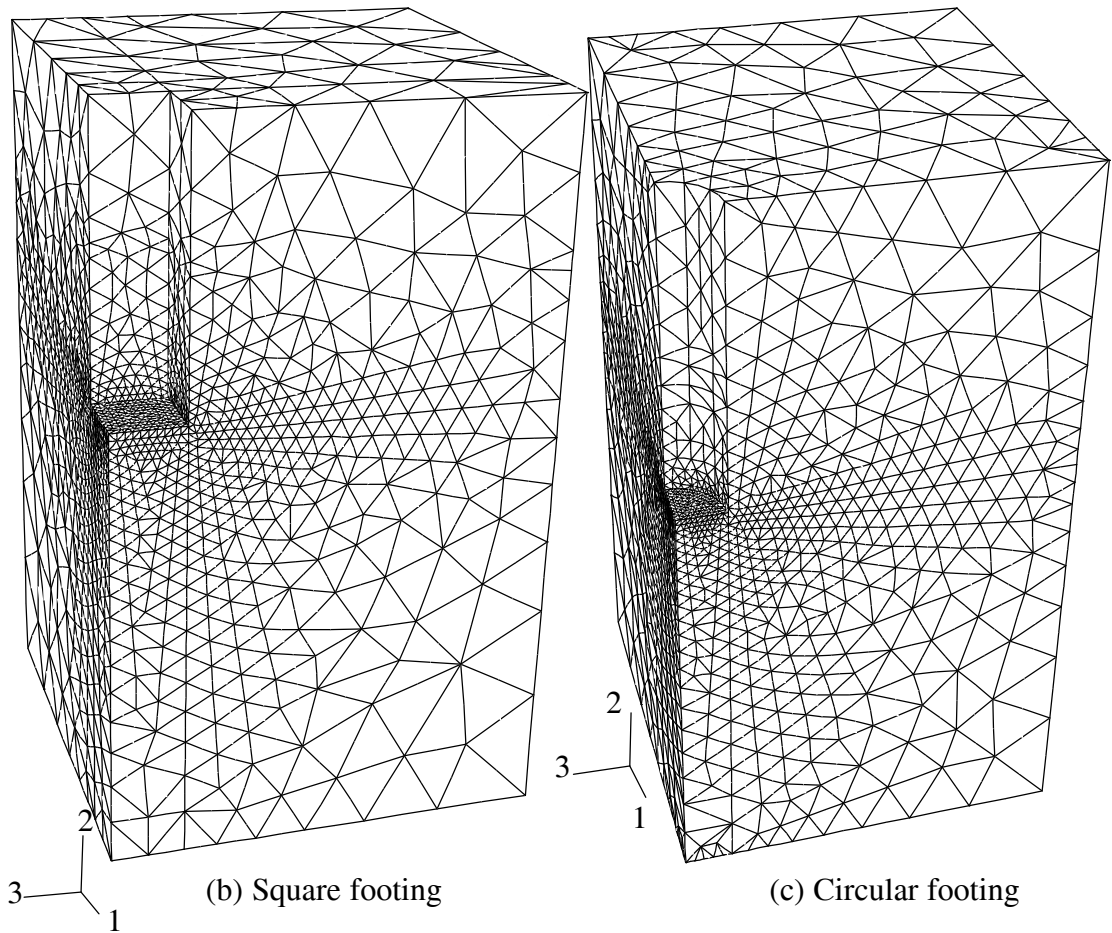


**Figure 4.5** Typical meshing of the finite element models for strip, square, and circular footings

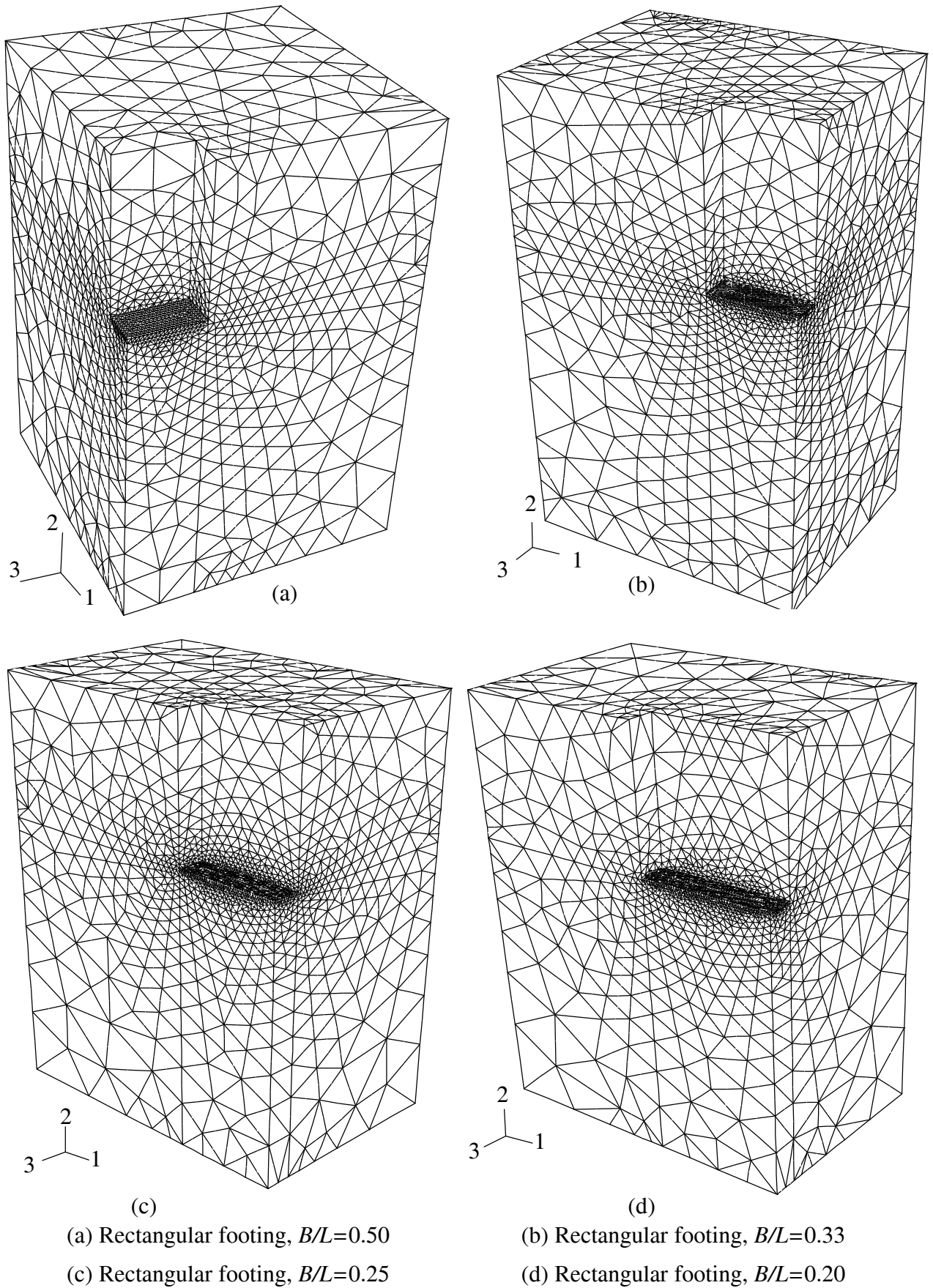
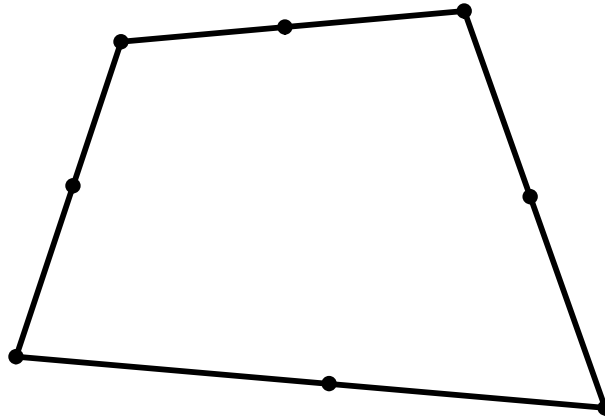
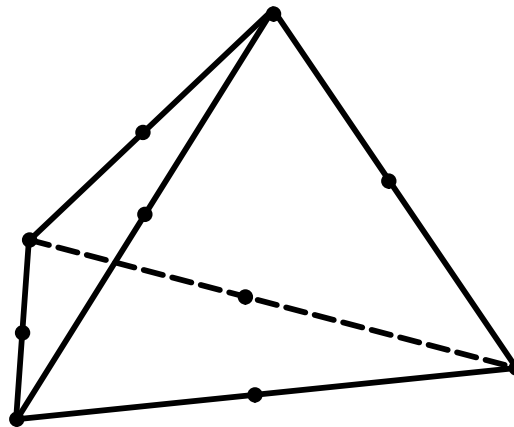


**Figure 4.6** Typical meshing of finite element models of rectangular footings



(a) 8–node plane strain quadrilateral, hybrid, linear pressure, reduced integration element for strip footing problems (CPE8RH)



b) 10–node modified quadratic tetrahedron element for square, circular and rectangular footing problems (C3D10M)

**Figure 4.7** Element types used in the ABAQUS FE models.

The overall mesh dimensions were selected to ensure that the zones of plastic shearing and the observed displacement fields were contained within the model boundaries at all times. The underside of all footings was modelled as perfectly rough by specifying a “tied” contact constraint at the footing/soil interface.

To determine the collapse load of the footing, displacement defined analyses were performed where the footing was considered as being perfectly rigid. That is, a uniform vertical prescribed displacement ( $-\delta$ ) was applied to all those nodes on the footing. The total displacement was applied over a number of substeps and the nodal contact forces along the footing were summed to compute the equivalent bearing capacity. The number

of displacement increments is automatically determined by ABAQUS, within initial, minimum, and maximum values prescribed by users.

#### 4.4 ABAQUS FINITE ELEMENT ANALYSIS RESULTS

In this section the numerical results obtained for the bearing capacity of embedded footings in undrained clay are presented. These results are compared with results of previous numerical and laboratory investigations.

The load–displacement behaviour of embedded footings is presented in Figure 4.8 to Figure 4.11 in terms of the dimensionless parameters  $\delta E_u/Bc_u$ , where  $\delta$  is the displacement of the footing.

The plateaus shown in Figure 4.8 to Figure 4.11 indicate that collapse is clearly defined for each embedment ratio  $D/B$  and footing shape.

For footings at relatively small embedment ratios ( $D/B \leq 0.6$ ) collapse is very clearly defined because the load–displacement plot reaches a plateau at low displacements. The failure mechanism zone can be seen in displacement vectors and contours in Figure 4.22 to Figure 4.25. For deeper footings ( $D/B > 0.6$ ) the displacements at collapse are very large. For example, referring to Figure 4.9 for load–displacement behaviour of embedded square footings, the displacements  $\delta$  at the collapse vary from  $0.3B$  for  $D/B=0.2$  to  $1.5B$  for  $D/B=2$ .

The plateaus shown in Figure 4.8 to Figure 4.11 also indicate that, for the same footing depth at collapse, the value of the displacements of footing  $\delta E_u/Bc_u$  increases as the footing shape changes from strip, circular, square, rectangular  $B/L=0.5$ ,  $B/L=0.33$ ,  $B/L=0.25$  and  $B/L=0.2$ . For example, for  $D/B = 0.6$ , at the collapse,  $\delta E_u/Bc_u=65.5$ ,  $67.32$ ,  $80.23$ ,  $95.44$ ,  $104.09$  and  $132.12$  as footing shape changes from strip, circular, square, rectangular  $B/L=0.5$ ,  $B/L=0.33$ ,  $L=0.25$  and  $B/L=0.2$ .

A summary of all the ABAQUS results is presented in Table 4.1 and Table 4.2. Also shown in this table are the result of lower and upper bound limit analysis of Salgado et al 2004 and those of Skempton (1951) as shown in equation (2.15).

D/B	Strip footing				Square footing				Circular footing			
	AB	LB	UB	SK	AB	LB	UB	SK	AB	LB	UB	SK
0	5.24	5.132	5.203	5.14	5.95	5.523	6.227	6.168	6.048	5.856	6.227	6.168
0.01	5.25	5.164	5.259	5.258	6.211	5.61	6.503	6.31	6.265	5.962	6.503	6.31
0.05	5.48	5.293	5.384	5.405	6.659	5.886	6.84	6.486	6.851	6.295	6.84	6.486
0.1	5.67	5.448	5.548	5.514	7.063	6.171	7.14	6.617	7.324	6.491	7.14	6.617
0.2	5.86	5.696	5.806	5.669	7.539	6.59	7.523	6.803	7.843	6.897	7.523	6.803
0.4	6.27	6.029	6.133	5.888	8.123	7.194	8.104	7.066	8.334	7.303	8.104	7.066
0.6	6.53	6.24	6.341	6.057	8.548	7.671	8.608	7.268	8.774	7.866	8.608	7.268
0.8	6.771	6.411	6.509	6.198	8.921	8.068	9.034	7.438	9.183	8.37	9.034	7.438
1	6.871	6.526	6.657	6.323	9.271	8.429	9.429	7.588	9.574	8.771	9.429	7.588
2	7.52	7.13	7.227	6.813	10.607	9.752	11.008	8.176	11.001	9.973	11.008	8.176
3	7.931	7.547	7.652	7.19	12.108	10.532	12.14	8.627	12.081	10.686	12.14	8.627
4	8.166	7.885	7.994	7.5	13.075	10.941	13.03	9	12.978	10.954	13.03	9
5	8.498	8.168	8.284	7.5	13.848	11.206	13.743	9	13.7	10.998	13.743	9

*Note: AB is results of ABAQUS in this study*

*LB is lower bound and UB is upper bound result of Salgado et al (2004)*

*SK is the results of Skempton (1951) in equation (2.15)*

**Table 4.1** Normalised undrained bearing capacity for embedded strip, square and circular footings ( $q_u/c_u$ ), compared to result of Salgado et al (2004) and Skempton (1951) in equation (2.15)

D/B	Rectangular footing, B/L=0.5				Rectangular footing, B/L=0.33				Rectangular footing, B/L=0.25				Rectangular footing, B/L=0.2			
	AB	LB	UB	SK	AB	LB	UB	SK	AB	LB	UB	SK	AB	LB	UB	SK
0	5.73	5.359	6.022	5.654	5.613	5.256	5.886	5.479	5.54	5.201	5.82	5.397	5.513	5.169	5.776	5.346
0.01	5.822	5.424	6.249	5.784	5.669	5.311	6.085	5.605	5.572	5.253	6.006	5.521	5.572	5.218	5.949	5.469
0.05	6.186	5.64	6.503	5.945	5.983	5.503	6.3	5.761	5.92	5.43	6.203	5.675	5.839	5.389	6.126	5.621
0.1	6.596	5.86	6.756	6.066	6.154	5.697	6.533	5.878	6.122	5.614	6.413	5.79	6.136	5.565	6.321	5.735
0.2	6.947	6.197	7.116	6.236	6.63	5.997	6.867	6.043	6.523	5.895	6.731	5.953	6.529	5.836	6.637	5.896
0.4	7.448	6.68	7.574	6.477	7.112	6.408	7.271	6.277	6.965	6.272	7.113	6.183	6.95	6.19	7.003	6.124
0.6	7.835	7.082	7.993	6.662	7.417	6.74	7.608	6.456	7.239	6.567	7.412	6.359	7.209	6.465	7.299	6.299
0.8	8.185	7.427	8.377	6.818	7.709	7.03	7.936	6.607	7.485	6.717	7.705	6.508	7.421	6.695	7.57	6.446
1	8.482	7.729	8.724	6.956	7.994	7.297	8.24	6.741	7.726	7.048	7.976	6.639	7.619	6.904	7.819	6.576
2	9.692	8.968	10.055	7.495	9.131	8.447	9.476	7.263	8.719	8.109	9.086	7.154	8.525	7.86	8.835	7.086
3	10.593	9.86	11.076	7.909	9.987	9.296	10.473	7.664	9.545	8.92	10.026	7.549	9.309	8.607	9.696	7.477
4	11.38	10.513	11.878	8.257	10.698	10.018	11.242	8.002	10.259	9.594	10.769	7.882	9.961	9.249	10.403	7.807
5	12.043	10.88	12.545	8.565	11.347	10.464	11.887	8.3	10.894	10.117	11.408	8.175	10.581	9.796	11.03	8.097

*Note: AB is results of ABAQUS in this study*

*LB is lower bound and UB is upper bound result of Salgado et al (2004)*

*SK is the results of Skempton (1951) in equation (2.15)*

**Table 4.2** Normalised undrained bearing capacity for embedded rectangular footings ( $q_u/c_u$ ), compared to result of Salgado et al (2004) and Skempton (1951) in equation (2.15)

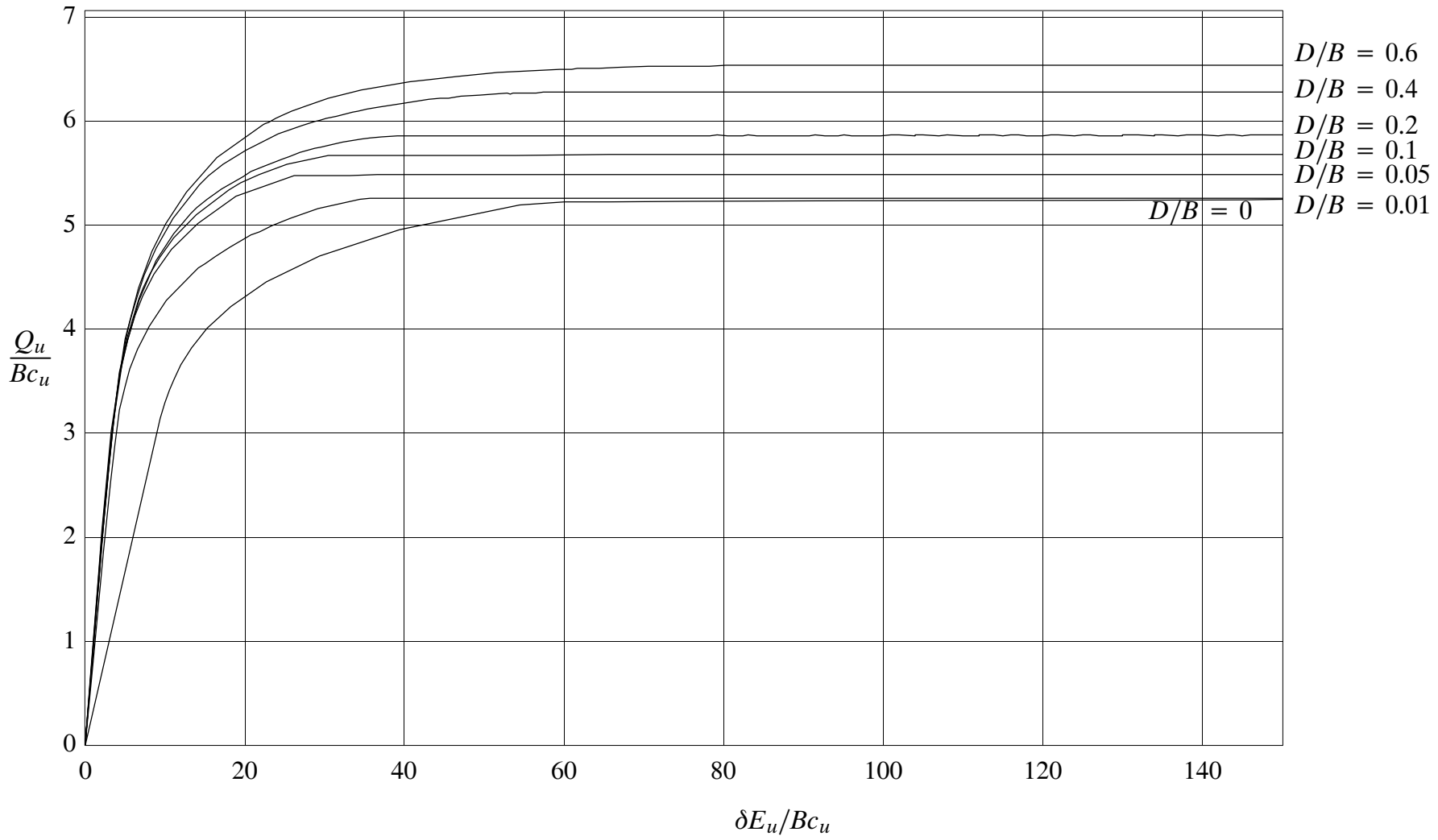


**Figure 4.8** Load–displacement behaviour of embedded strip footing for  $0 \leq D/B \leq 0.6$

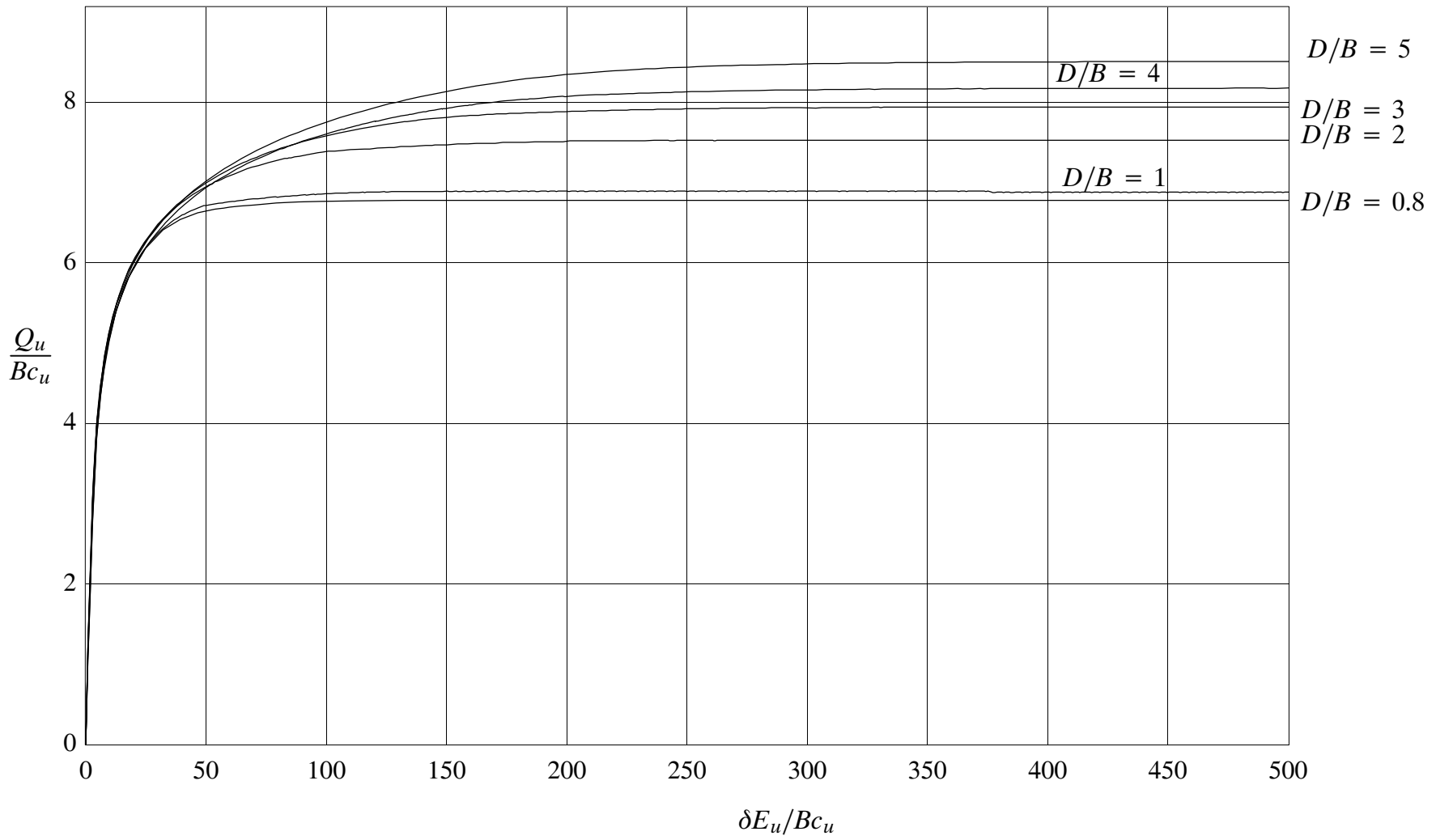


**Figure 4.8 (continued)** Load–displacement behaviour of embedded strip footing for  $0.8 \leq D/B \leq 5$

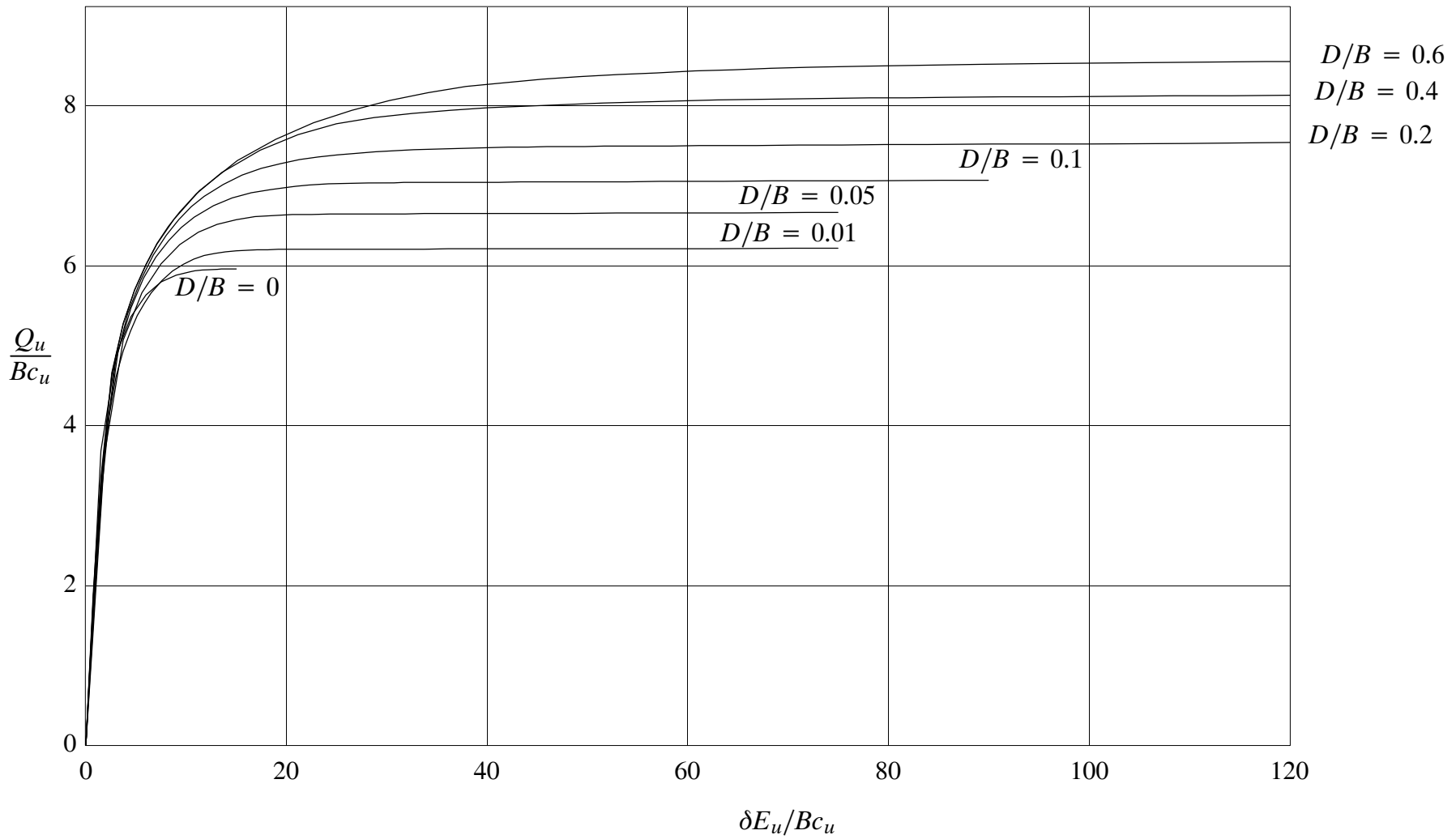


**Figure 4.9** Load–displacement behaviour of embedded square footing for  $0 \leq D/B \leq 0.6$

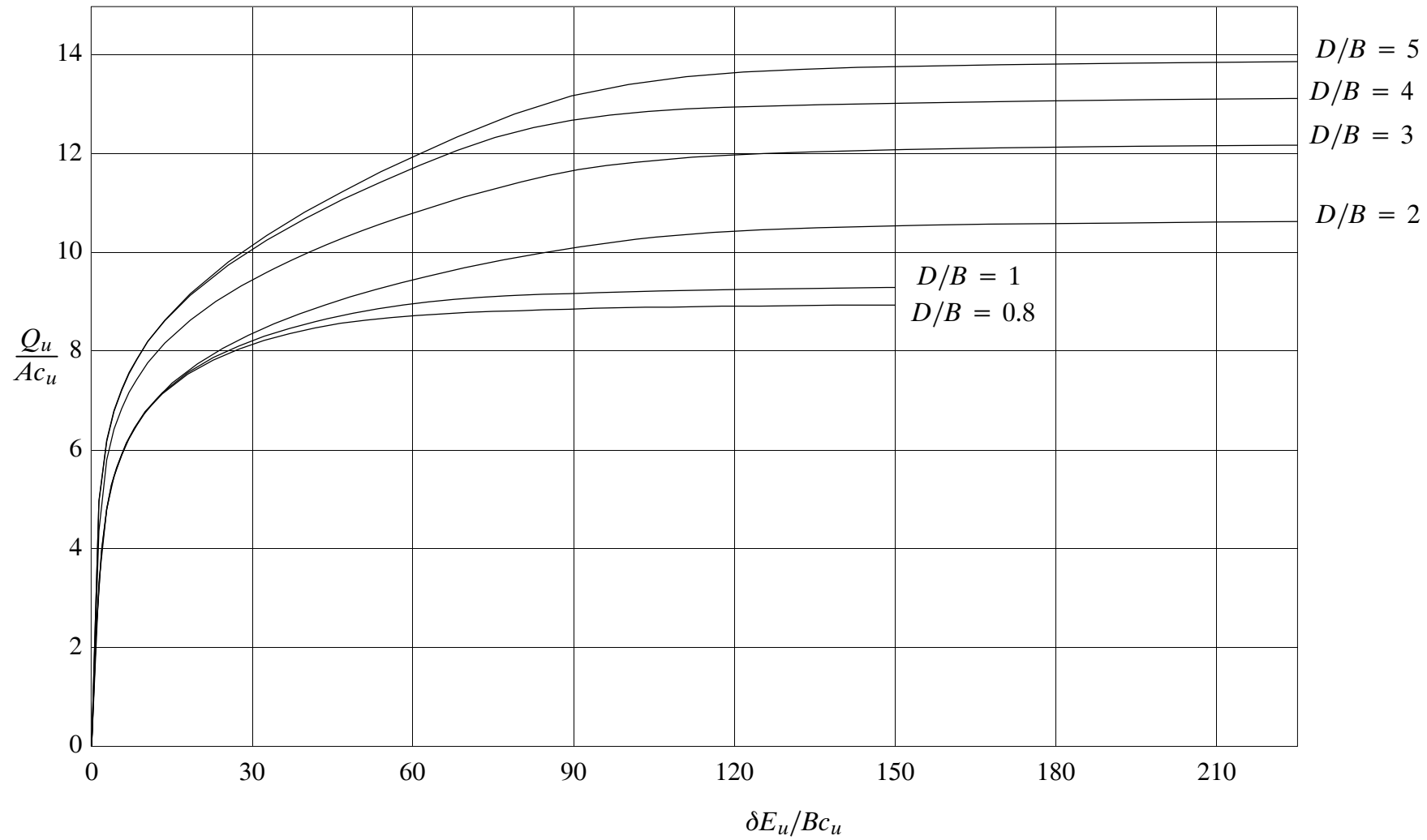


**Figure 4.9 (continued)** Load–displacement behaviour of embedded square footing for  $0.8 \leq D/B \leq 5$

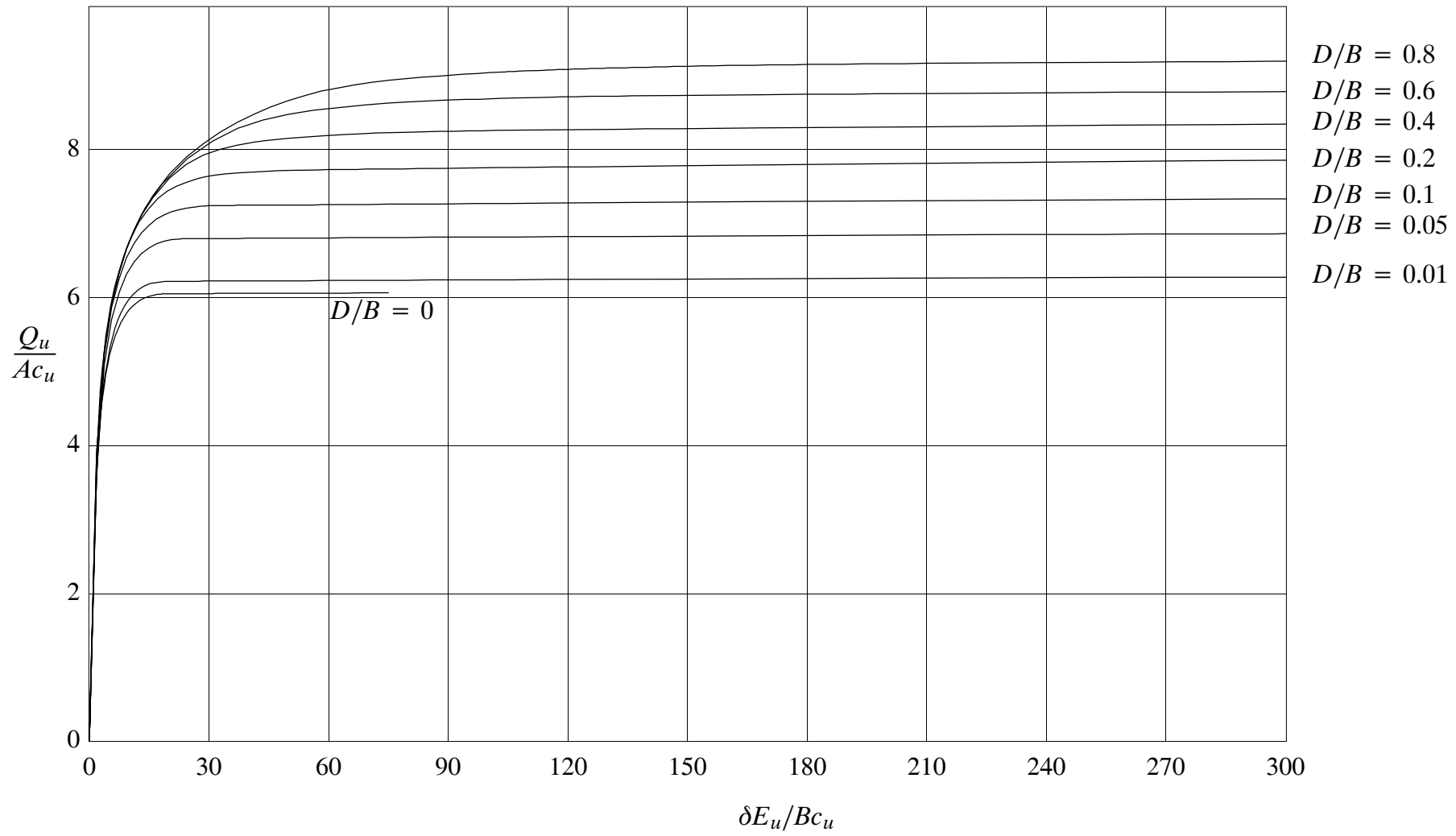


**Figure 4.10** Load–displacement behaviour of embedded circular footing for  $0 \leq D/B \leq 0.8$

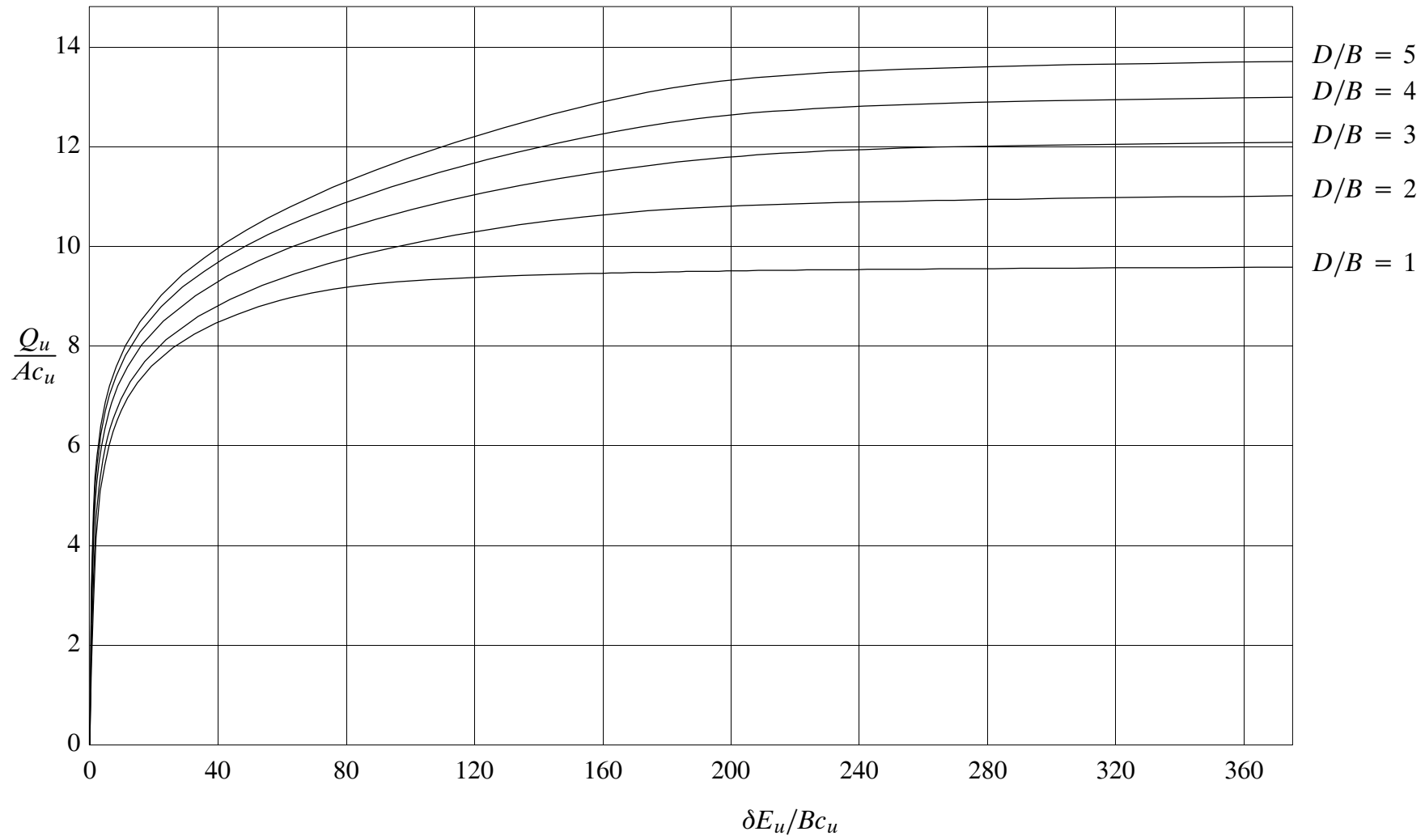


**Figure 4.10 (continued)** Load–displacement behaviour of embedded circular footing for  $1 \leq D/B \leq 5$

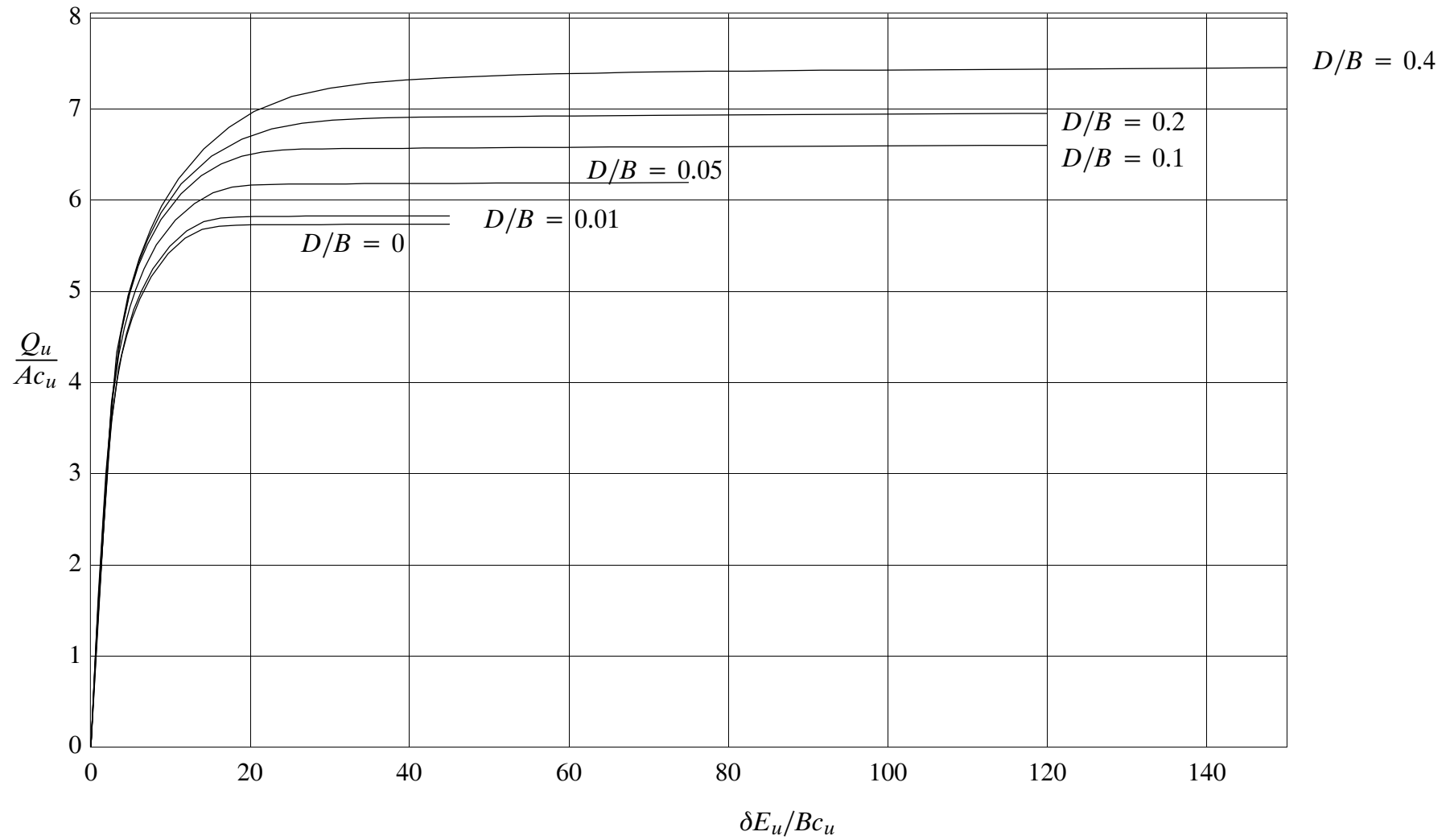


**Figure 4.11** Load–displacement behaviour of embedded rectangular footing for  $B/L = 0.5$  and  $0 \leq D/B \leq 0.4$

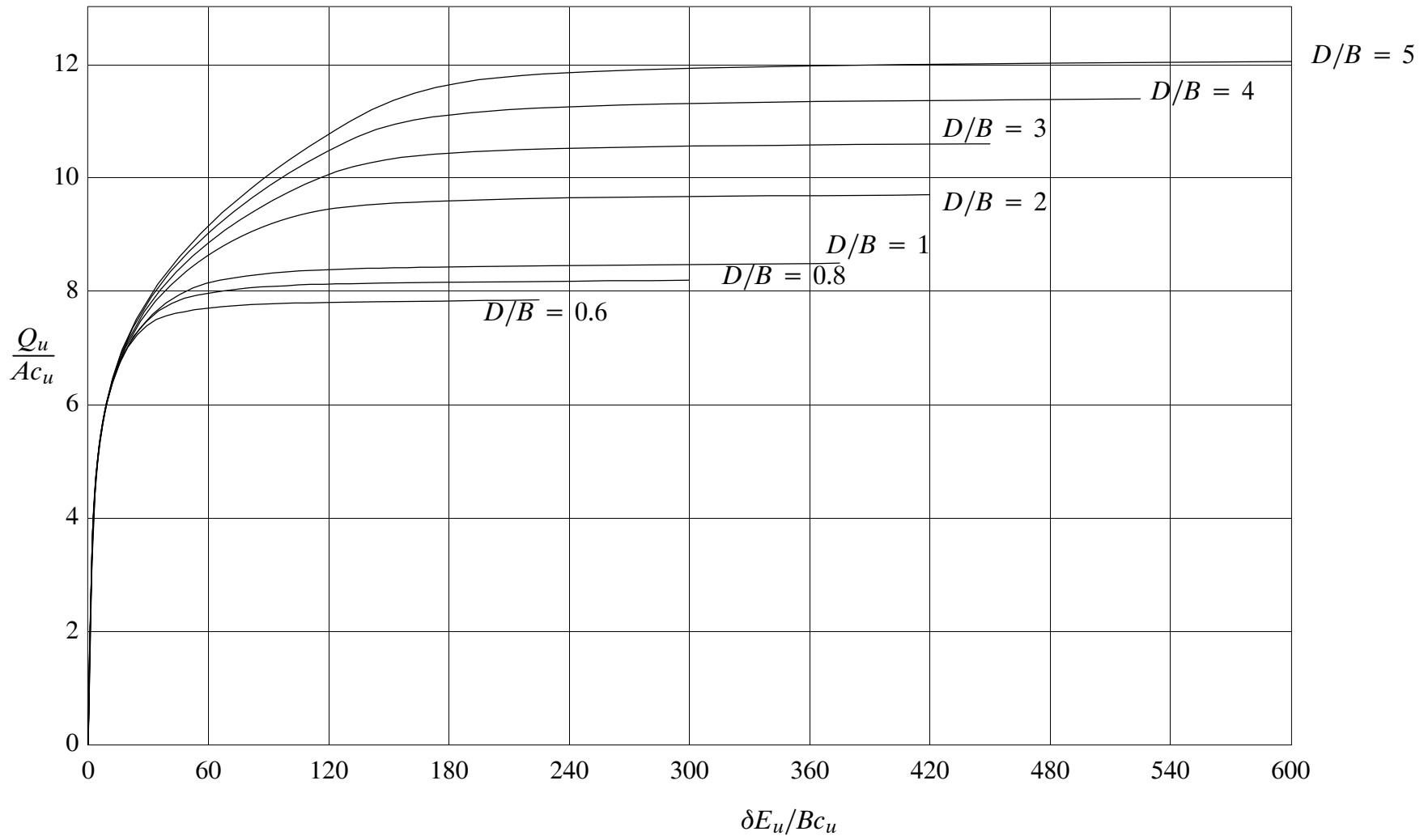


**Figure 4.11 (continued)** Load–displacement behaviour of embedded rectangular footing for  $B/L = 0.5$  and  $0.6 \leq D/B \leq 5$

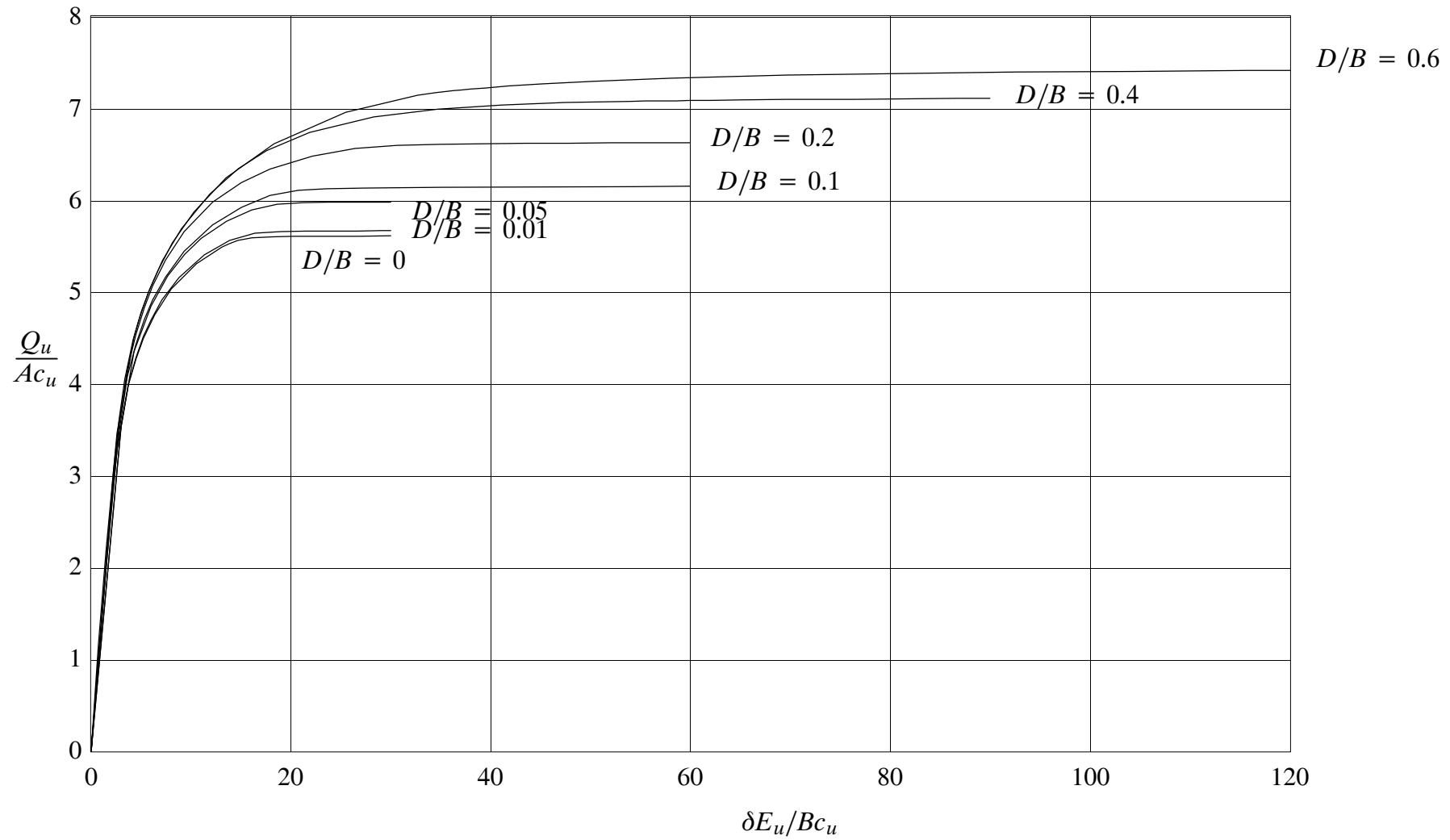


**Figure 4.11 (continued)** Load–displacement behaviour of embedded rectangular footing for  $B/L = 0.33$  and  $0 \leq D/B \leq 0.6$

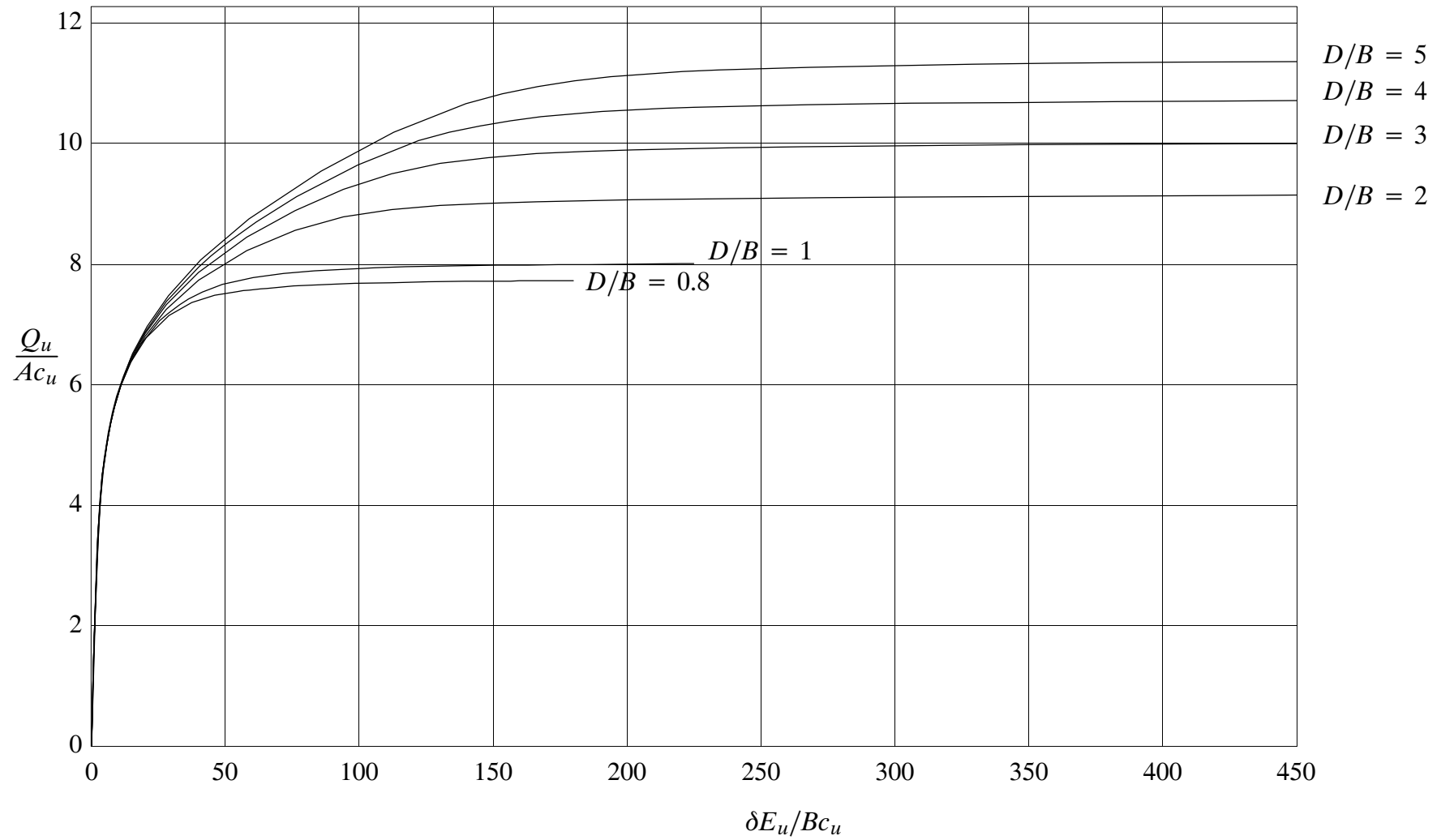


**Figure 4.11 (continued)** Load–displacement behaviour of embedded rectangular footing for  $B/L = 0.33$  and  $0.8 \leq D/B \leq 5$

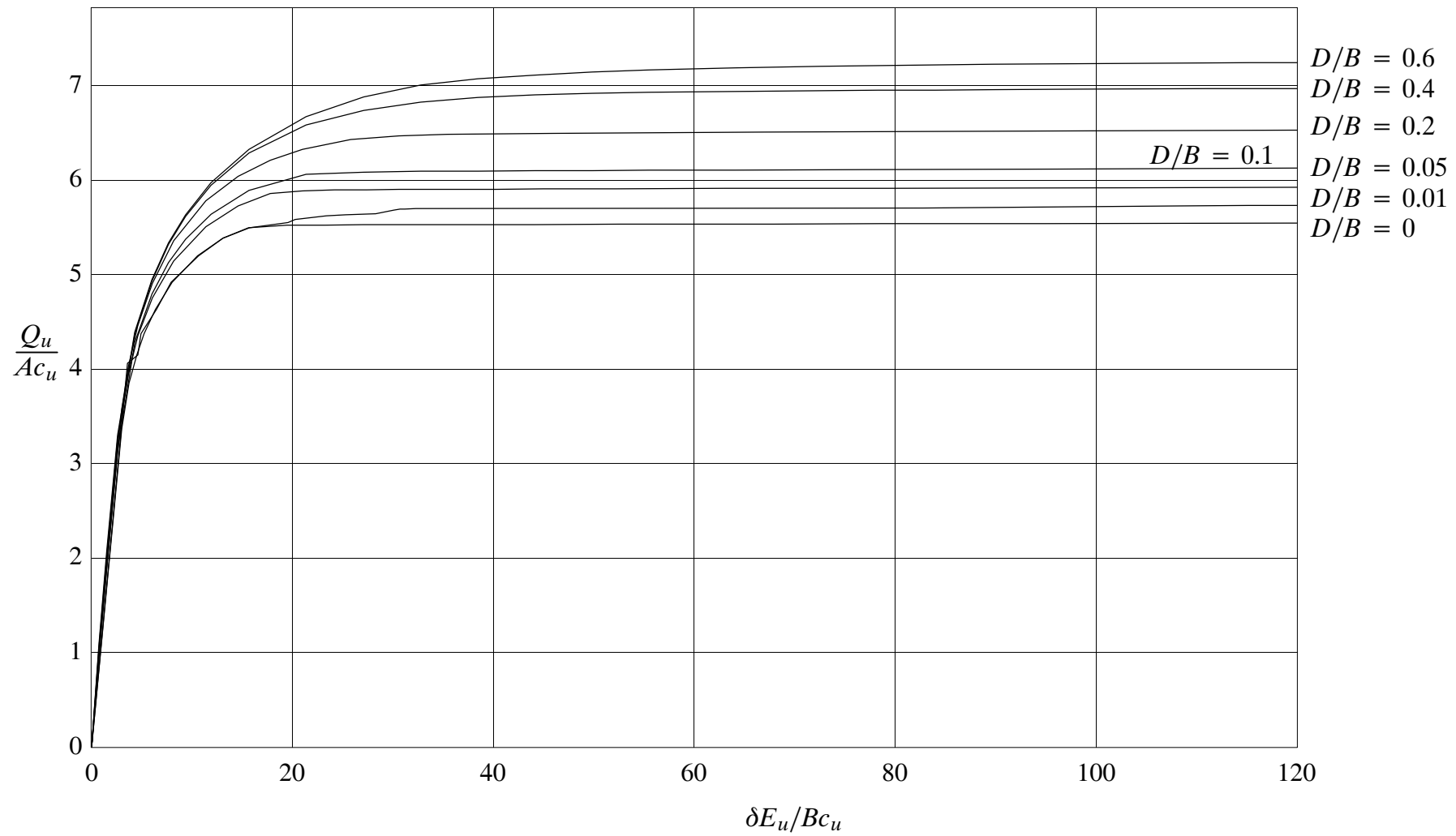


**Figure 4.11 (continued)** Load–displacement behaviour of embedded rectangular footing for  $B/L = 0.25$  and  $0 \leq D/B \leq 0.6$

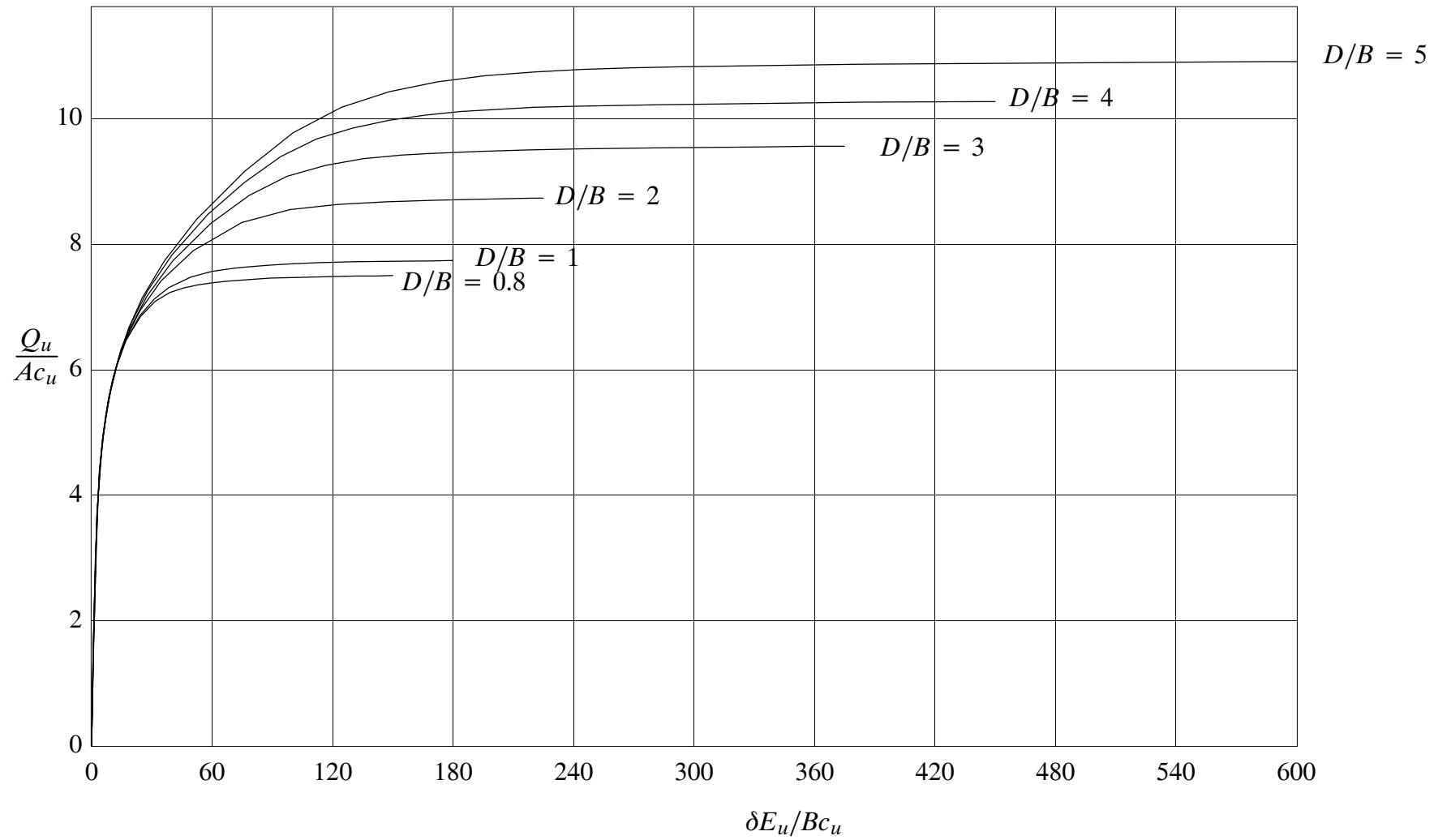


**Figure 4.11 (continued)** Load–displacement behaviour of embedded rectangular footing for  $B/L = 0.25$  and  $0.8 \leq D/B \leq 5$

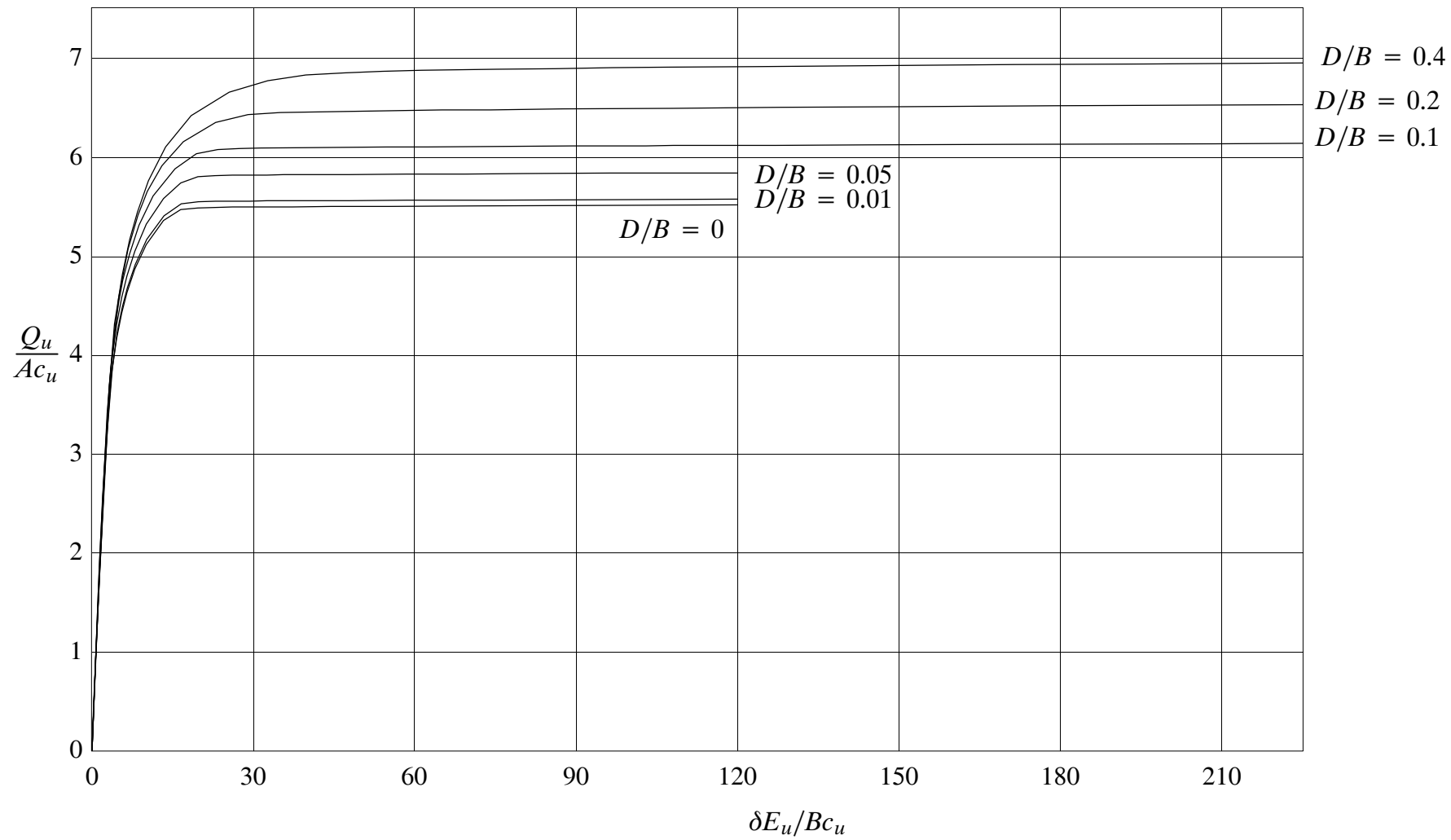


**Figure 4.11 (continued)** Load–displacement behaviour of embedded rectangular footing for  $B/L = 0.2$  and  $0 \leq D/B \leq 0.4$

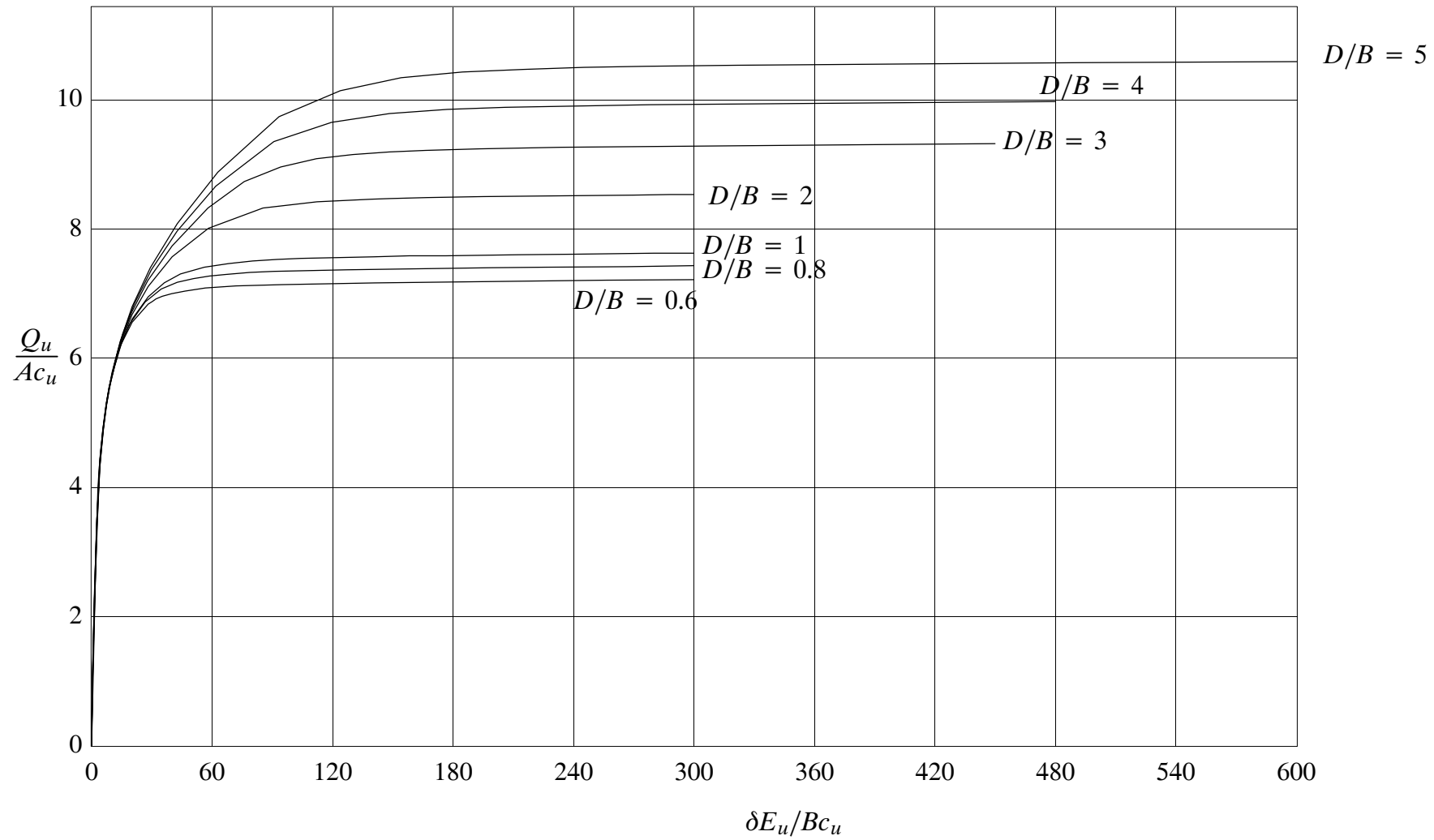


**Figure 4.11 (continued)** Load–displacement behaviour of embedded rectangular footing for  $B/L = 0.2$  and  $0.6 \leq D/B \leq 5$

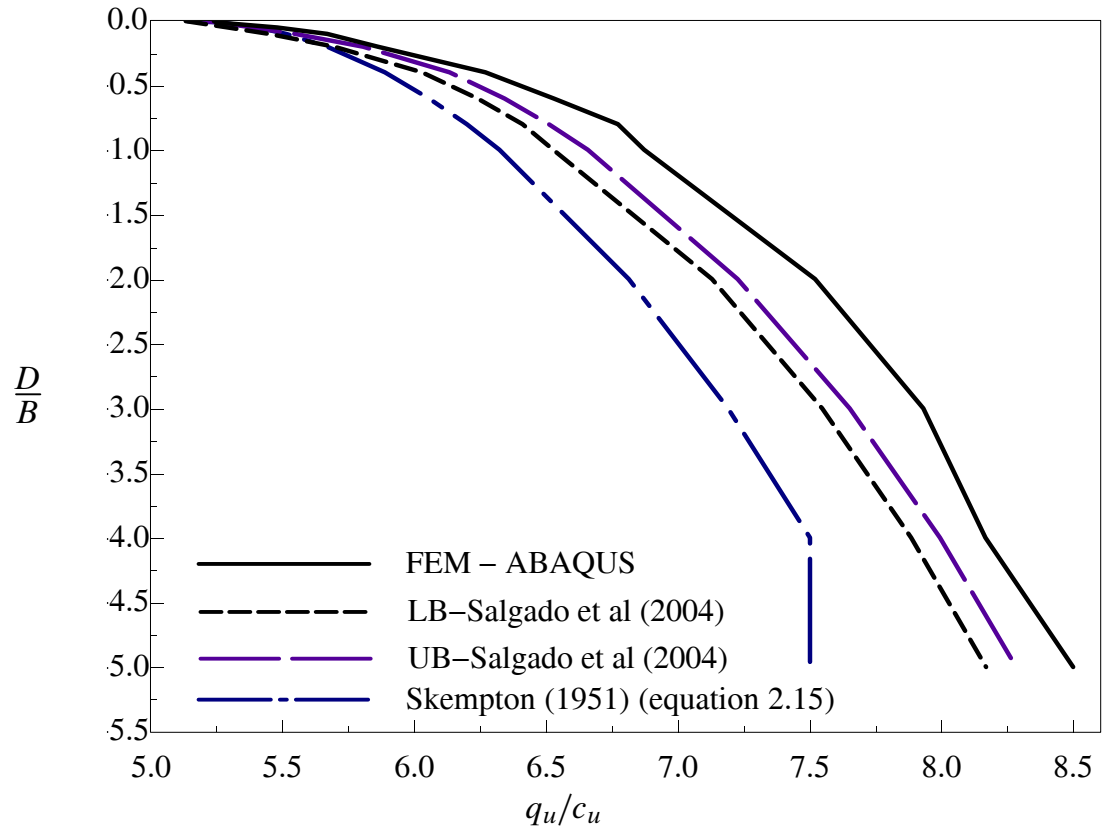


**Figure 4.12** Normalised bearing capacity of embedded strip footings

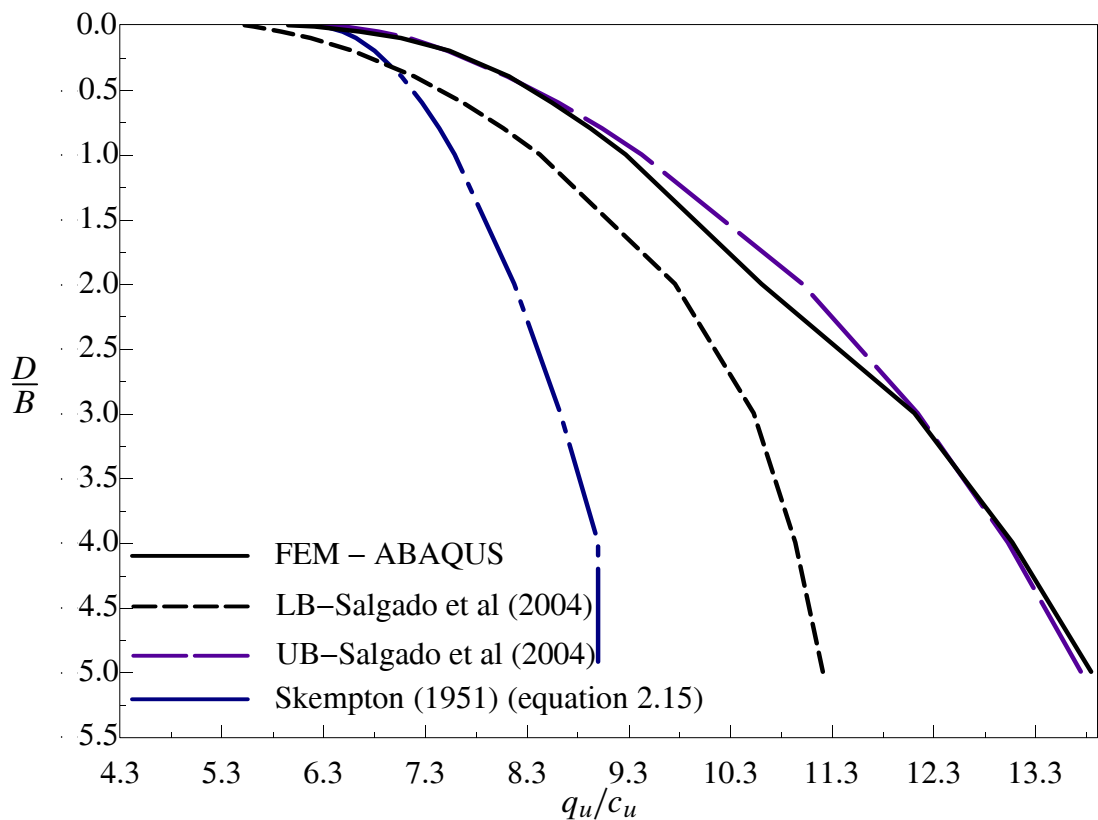


**Figure 4.13** Normalised bearing capacity of embedded square footings

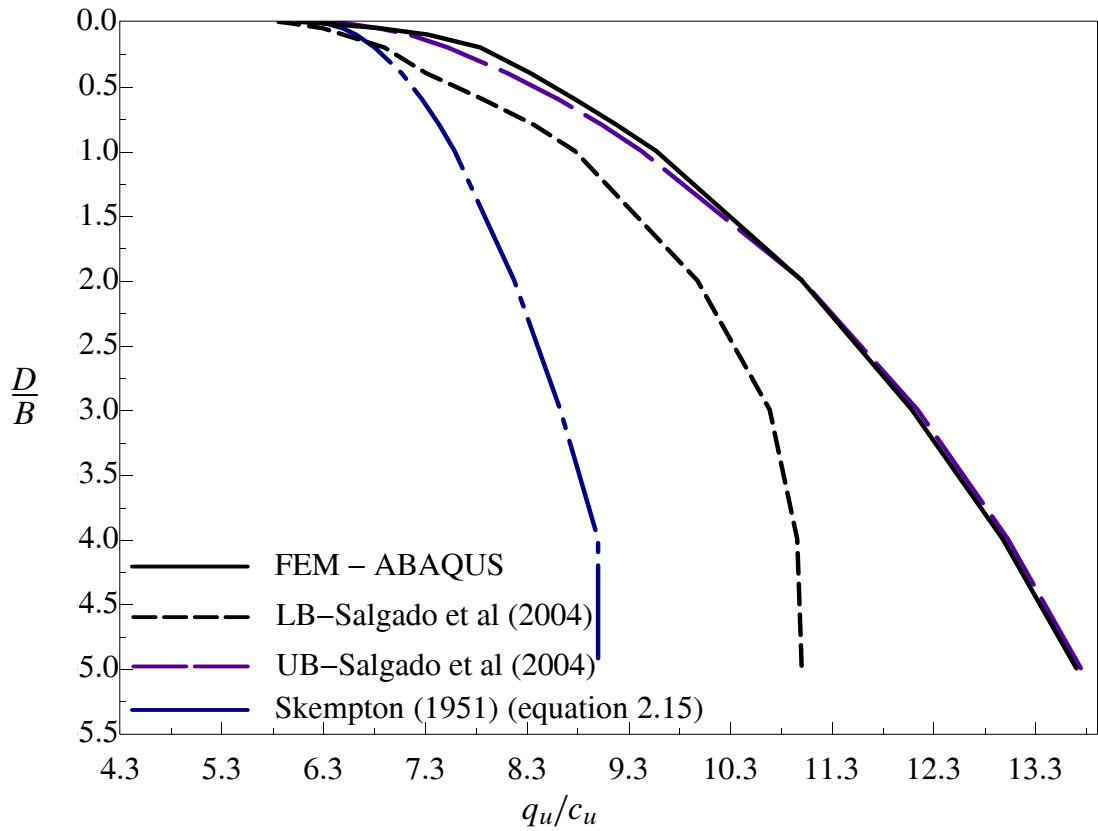


**Figure 4.14** Normalised bearing capacity of embedded circular footings

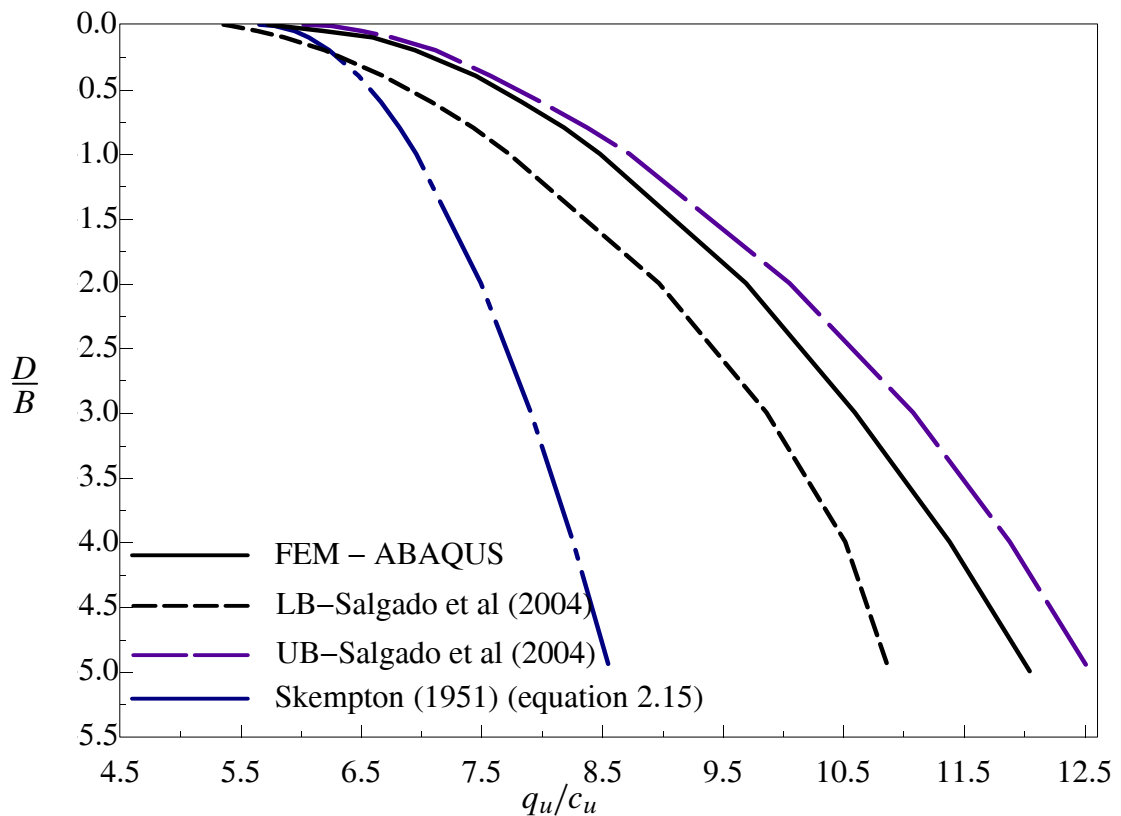


**Figure 4.15** Normalised bearing capacity of embedded rectangular footing for  $B/L=0.5$

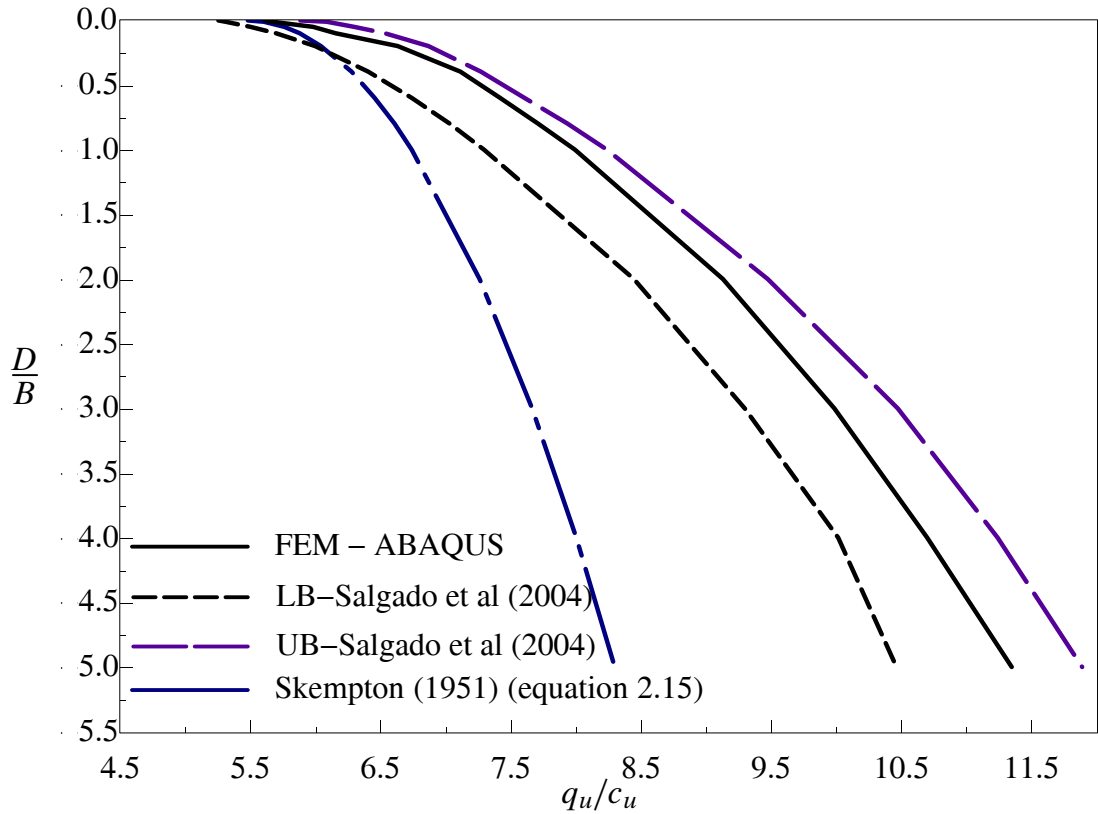


**Figure 4.16** Normalised bearing capacity of embedded rectangular footing for  $B/L=0.33$

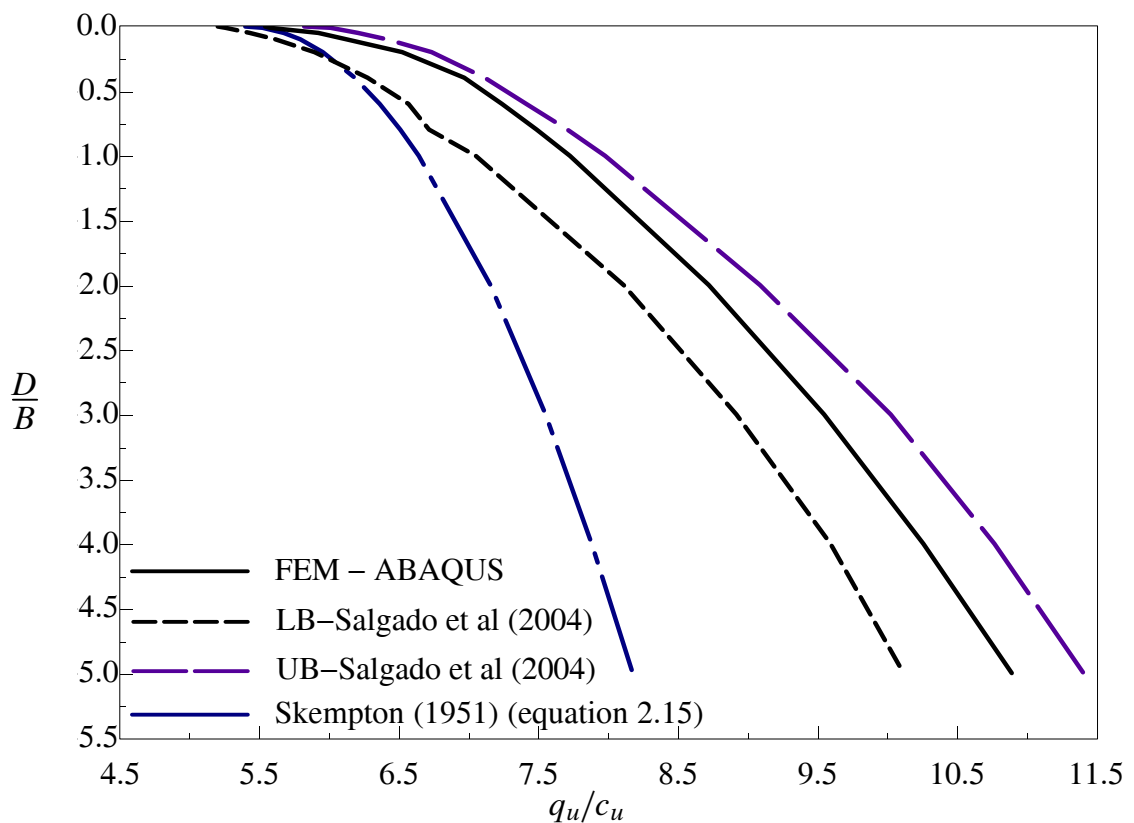


**Figure 4.17** Normalised bearing capacity of embedded rectangular footing for  $B/L=0.25$

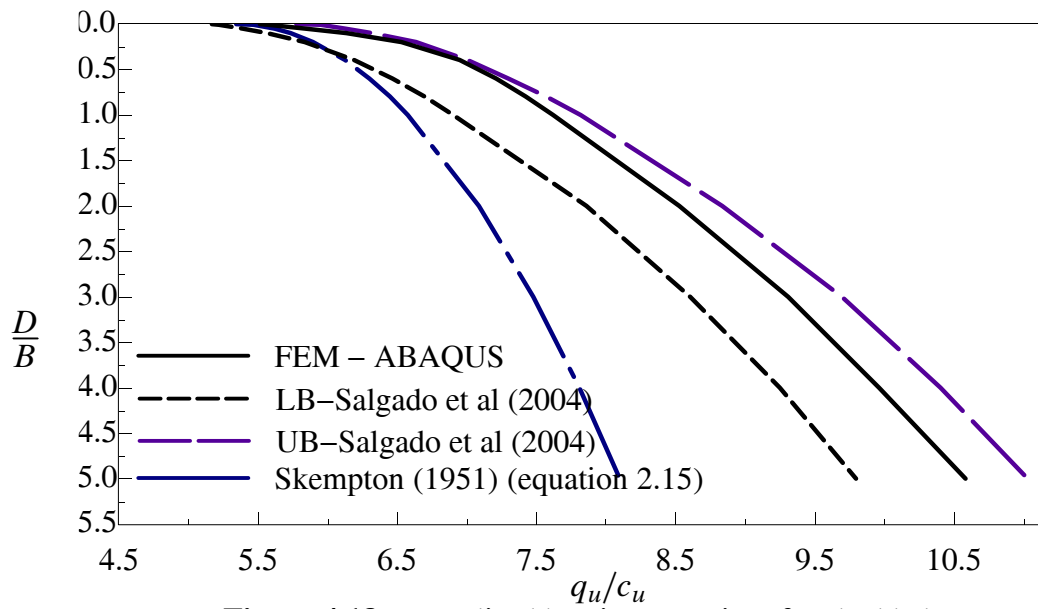


**Figure 4.18** Normalised bearing capacity of embedded rectangular footing for  $B/L=0.20$

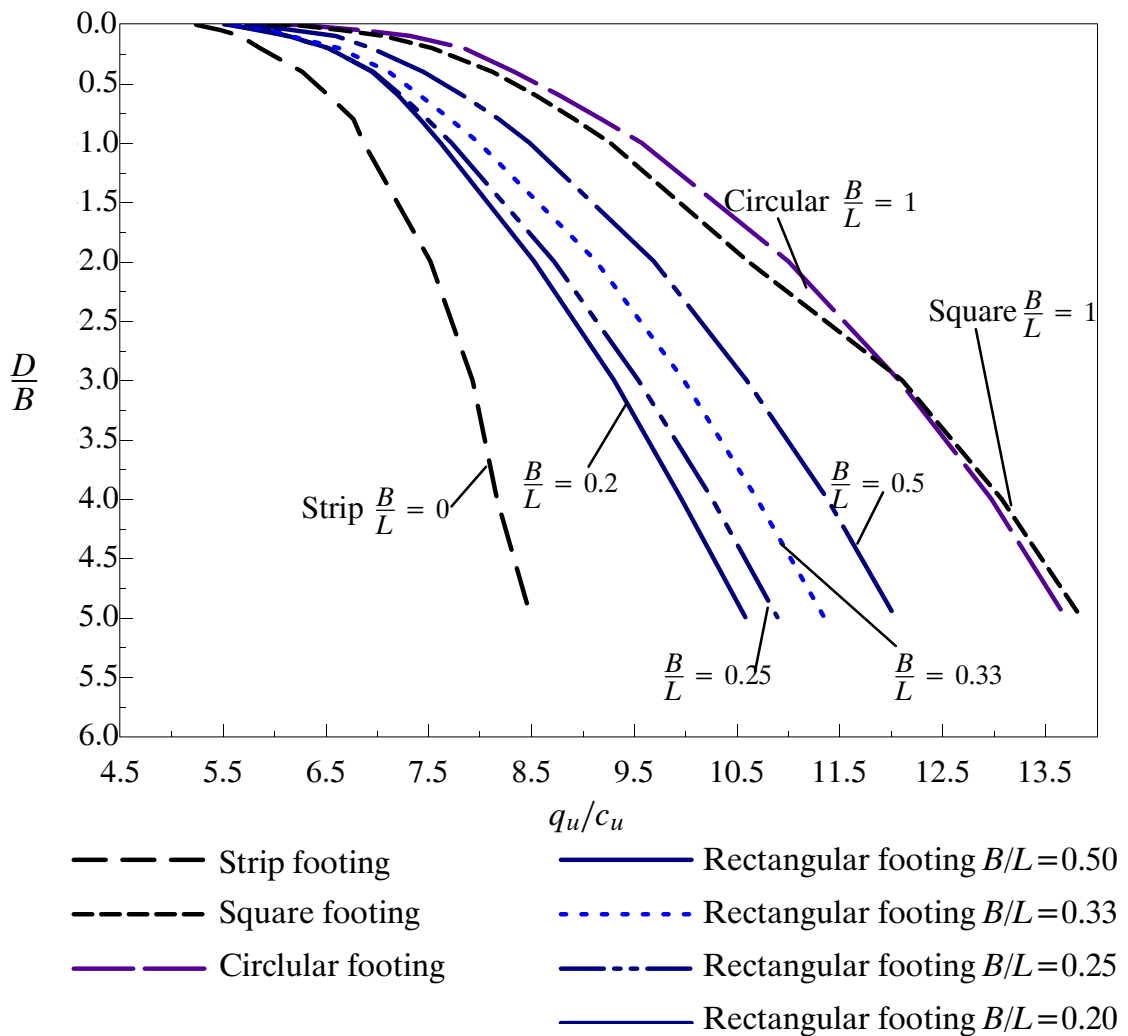


**Figure 4.19** Normalised bearing capacity of embedded footings

It is clear seen from Table 4.1 and Table 4.2 that deeper foundations mobilise larger volumes of soil and dissipate more plastic energy, therefore the larger bearing capacities are at larger  $D/B$  ratios.

For the same value of  $D/B$ , the bearing capacity increases as the ratio of  $B/L$  rises from 0 (for strip footings) to 1 (for square or circular footings). At the same depth, if  $D/B \leq 3$ , the bearing capacity of circular footings is larger than of square footings by about 2–4% and if  $D/B > 3$  bearing capacity of circular footings is smaller than those of square footings by about 1–3%.

The equation (4.1) assumes implicitly that shape factors  $F_{cs}$  and depth factors  $F_{cd}$  are independent from each other. The shape factors will be a equation of  $B/L$  and be calculated by bearing capacity of surface footings ( $D/B = 0$ ) for strip, square, circular and rectangular footings. These shape factors do not depend on the footing depths.

The depth factors  $F_{cd}$  are equations of both parameters  $B/L$  and  $D/B$  and calculated from (4.1) when the shape factors have been determined beforehand.

#### 4.4.1 Shape factors

Shape factors  $F_{cs}$  can be calculated using the values of undrained bearing capacity for embedded footings  $q_u/c_u$  in Table 4.1 and Table 4.2 in conjunction with equation (4.1).

The shape factor  $F_{cs}$  is determined by dividing the bearing capacity factor  $N_c$  for any surface footing by  $N_c$  for strip surface footing.

- For strip footings, shape factor  $F_{cs}=1$ .
- For a square footing, shape factor is determined as:

$$F_{cs} = \frac{N_c^{[square - surface - footing]}}{N_c^{[strip - surface - footing]}} = \frac{5.95}{5.24} = 1.136 \quad (4.2)$$

where  $N_c^{[square - surface - footing]}$  is the bearing capacity factor of a square surface footing, from Table 4.1,  $N_c^{[square - surface - footing]} = 5.95$ .

$N_c^{[strip - surface - footing]}$  is the bearing capacity factor of a surface strip footing, from Table 4.1,  $N_c^{[strip - surface - footing]} = 5.24$ .

– For a circular footing, shape factor is determined as:

$$F_{cs} = \frac{N_c^{[circular - surface - footing]}}{N_c^{[strip - surface - footing]}} = \frac{6.05}{5.24} = 1.155 \quad (4.3)$$

where  $N_c^{[circular - surface - footing]}$  is the bearing capacity factor of a circular surface footing,

$$N_c^{[circular - surface - footing]} = 6.05 \text{ (Table 4.1).}$$

$N_c^{[strip - surface - footing]}$  is the bearing capacity factor of a surface strip footing,

$$N_c^{[strip - surface - footing]} = 5.24 \text{ (Table 4.1).}$$

– For a rectangular footing, shape factor is determined as:

$$F_{cs} = \frac{N_c^{[rectangular - surface - footing]}}{N_c^{[strip - surface - footing]}} \quad (4.4)$$

where  $N_c^{[rectangular - surface - footing]}$  is the bearing capacity factor of a circular surface

footing,  $N_c^{[rectangular - surface - footing]}$  (Table 4.2).

$N_c^{[strip - surface - footing]}$  is the bearing capacity factor of a surface strip footing,

$$N_c^{[strip - surface - footing]} = 5.24 \text{ (Table 4.1).}$$

$$F_{cs} = \frac{5.73}{5.24} = 1.094 \text{ for rectangular footing } B/L = 0.5;$$

$$F_{cs} = \frac{5.613}{5.24} = 1.071 \text{ for rectangular footing } B/L = 0.33;$$

$$F_{cs} = \frac{5.54}{5.24} = 1.057 \text{ for rectangular footing } B/L = 0.25;$$

$$F_{cs} = \frac{5.513}{5.24} = 1.052 \text{ for rectangular footing } B/L = 0.2;$$

All of these values of shape factors  $F_{cs}$  are summarized in Table 4.3.

Footing types	$B/L$	$F_{cs}$
Circular footing	1	1.155
Square footing	1	1.136
Rectangular footing	0.50	1.094
	0.33	1.071
	0.25	1.057
	0.20	1.052
Strip footing	0	1.000

**Table 4.3** Shape factors for various footing geometries

For surface footings the shape factor  $F_{cs}$  can be extracted as a function of the ratio of footing dimensions  $B/L$ . In the present work,  $B/L = 0.5, 0.33, 0.25$  and  $0.2$  which covers most of the practical cases of rectangular footings,  $B/L=0$  for strip footings and  $B/L=1$  for square and circular footings.

The shape factor  $F_{cs}$  increases as the ratio of relative dimensions of footing  $B/L$  rises from 0 (for strip footing) to 1 (for square and circular footing). However, when  $B/L \leq 0.2$ , the shape factor  $F_{cs}$  increases rapidly and when  $B/L > 0.2$ , this increase is slower as the ratio  $B/L$  increases. The shape factor  $F_{cs}$  of circular footing is higher than that of square footing.

For  $0 \leq B/L \leq 1$ , the values of the shape factor  $F_{cs}$  in Table 4.3 can be approximated by the following equation:

$$F_{cs} = 1 + 0.136 \left( \frac{B}{L} \right)^{0.56} \quad \text{for } 0 \leq B/L \leq 1 \quad (4.5)$$

Equation (4.5) provides estimates of the shape factors to within  $\pm 0.5\%$  of the finite element solutions (ABAQUS) and therefore can be used with confidence to solve practical design problems.

The shape factors of ABAQUS in Table 4.3, estimated equation (4.5), and equation (2.13) of Meyerhof (1951) are presented in Figure 4.20.

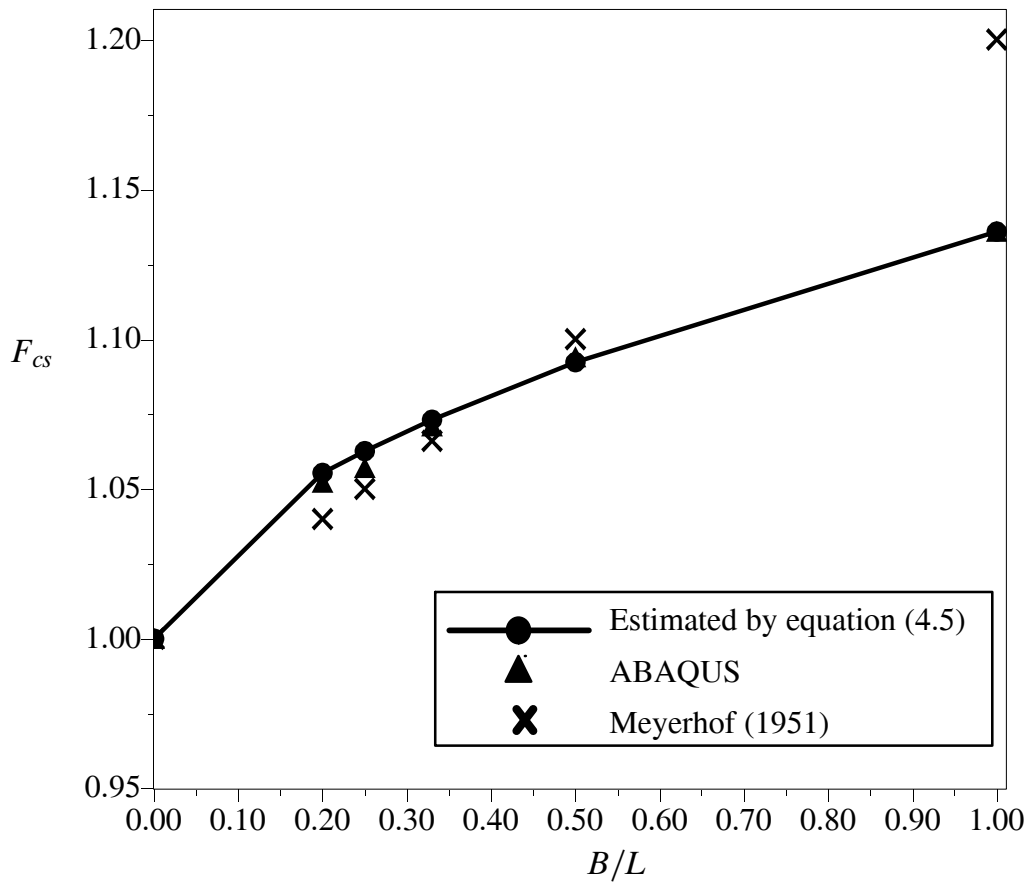


**Figure 4.20** Comparison of the shape factors  $F_{cs}$

In the equation (4.1), the shape factor  $F_{cs}$  is assumed to be a function of  $B/L$  only and not the embedment depth  $D/B$ . This shape factor  $F_{cs}$  will be used when calculating the depth factor  $F_{cd}$ . Therefore equation (4.5) can be used to determine shape factors  $F_{cs}$  for both surface footings and embedded footings.

#### 4.4.2 Bearing capacity and depth factor for strip footings

The bearing capacity factors  $N_c$  from the current finite element study compare well to that calculated using the widely adopted depth factor in the empirical equation (2.15) of Skempton (1951), and the numerical solutions of Salgado et al (2004). They all increase gradually as value of  $D/B$  rises. The results of this study were found to be around 4.2 and 6.4% above that for the upper and lower bound work of Salgado et al (2004), and around 11% above the Skempton (1951) solutions. For example, at the same value of  $D/B=3.0$ , the value of bearing capacity factors  $N_c$  from ABAQUS, upper bound, lower bound and Skempton solutions are 7.931, 7.652, 7.547 and 7.19 respectively.

In the solutions of Skempton (1951), the bearing capacity factor  $N_c$  reaches a maximum value of 7.5 when  $D/B \geq 4.0$  whereas in this study and in the upper and lower bound limit analysis of Salgado et al (2004), the bearing capacity factor  $N_c$  does not reach a limiting value.

For embedment depths of  $D/B < 0.6$ , the modes of failure can best be described as being general shear, as illustrated in Figure 4.22 and Figure 4.23. As can be seen from Figure 4.22 and Figure 4.23, the modes of failure are similar to those of surface footings on undrained soil. The soil elements with a greatest displacement are underneath and along the centre line of the footing. When  $D/B > 0.6$  (Figure 4.23(d)–(i)), the failure mechanism is similar to that of a local shear failure of a surface footing. The failure zone is deeper and is located more in the vicinity of the footing as the ratio  $D/B$  increases. For values of  $D/B > 0.6$ , more soil elements move horizontally away from the footing instead of moving to the surface, see Figure 4.23(h) and Figure 4.23(i). It is likely that when the ratio  $D/B$  rises to a infinite depth, soil displacements will no longer be observed at the surface. In that case, the shear failure mechanism will be contained around the footing toe.

The depth factor  $F_{cd}$  of a strip footing can be calculated using values in Table 4.1 in conjunction with equation (4.1). These depth factors  $F_{cd}$  are shown in Table 4.4.  $F_{cd}$  increases gradually with the ratio of  $D/B$ . In this study, the depth factors  $F_{cd}$  are determined as equations of two variables of  $D/B$  and  $B/L$  and calculated by dividing the bearing capacity factor  $N_c$  at various  $D/B$  values by  $N_c$  for surface footing. For strip footing,  $B/L=0$ , the depth factors  $F_{cd}$  depend on  $D/B$  only. The depth factors  $F_{cd}$  results of Salgado et al (2004) ( $F_{cd} = 1 + 0.27 \sqrt{\frac{D}{B}}$ ), and of Skempton (1951)

$$F_c = \left[ 1 + \sqrt{\left(0.053 \frac{D}{B}\right)} \right], \text{ and of ABAQUS are shown in Figure 4.31.}$$

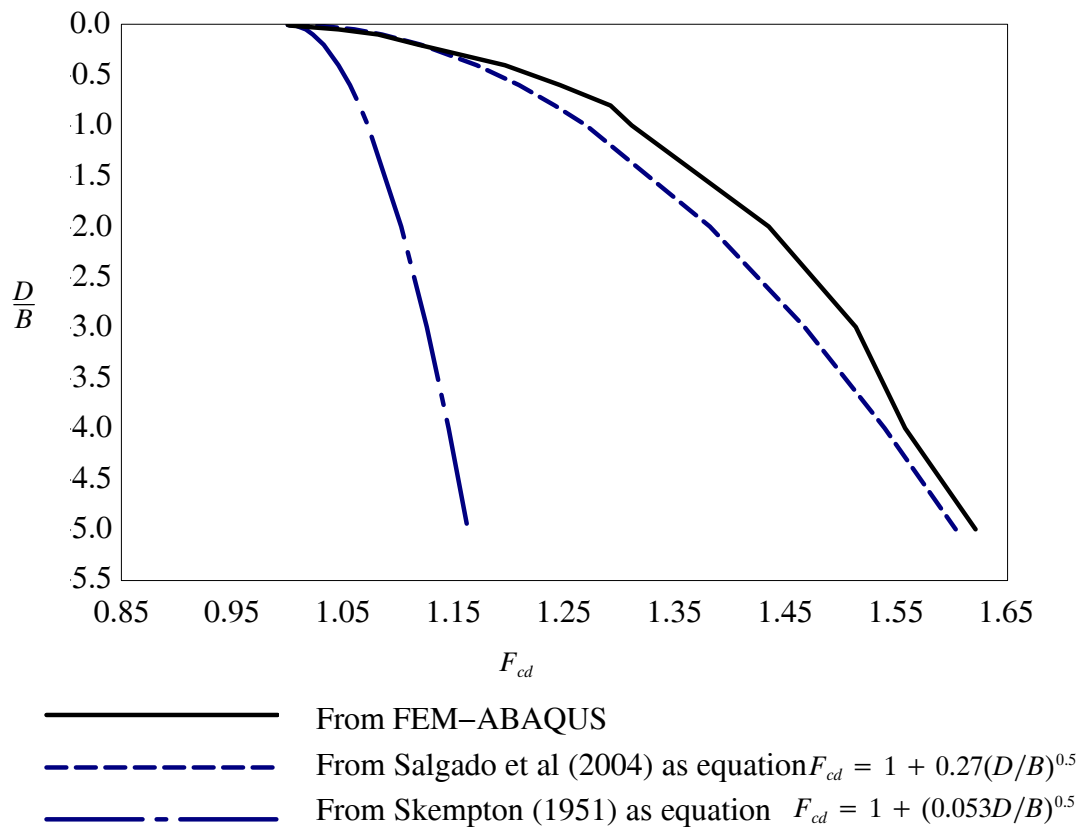


**Figure 4.21** Depth factors for strip footing as calculated by ABAQUS and expressions proposed by Salgado et al (2004), and by Skempton (1951)

As can be seen from Figure 4.21, at the same embedment depths  $D/B$ , depth factor of this study is very close to that of Salgado et al (2004) equation (higher than 1–3%) but much higher than result of Skempton (1951) (maximum at 28%). That differences are larger as footing depths are deeper.

#### 4.4.2 Bearing capacity and depth factor for square footings

Figure 4.13 and Table 4.1 present the undrained bearing capacity factors of embedded square footings. The results of the present study based on the finite element method are very close to those of upper bound limit analysis solutions of Salgado et al. (2004). The numerical solutions differ from each other by only around 0.5% while the empirical solutions of Skempton (1951) are very low relative to both numerical solutions. For example, at  $D/B = 5.0$ , values of  $N_c$  in the present and the previous upper and lower bound limit analysis are 13.848, 13.640 and 11.206 respectively and  $N_c$  is still increasing

with  $D/B$  at this point whereas the Skempton (1951) solution for  $N_c$  reaches a constant value of 9.0 by this  $D/B$  ratio.

The displacement vectors and contours for embedded square footings are shown in Figure 4.24. When the embedment depth of footings is small,  $D/B < 0.5$ , the failure mechanism is very similar to that for surface footings. The passive zones outside the footing have slip surfaces as in general shear failure, but the displacement vectors are at about  $45^\circ$  with respect to the horizontal surface and rise to almost  $90^\circ$  when the ratio  $D/B$  increases to 0.5. When  $0 \leq D/B \leq 0.5$ , the bearing capacity increase rapidly, but when  $0.2 < D/B \leq 5$  there is a more gradual increase in bearing capacity. This can be seen clearly in Figure 4.13. When the ratio  $D/B$  rises above 0.5, the zone of failure underneath the footing becomes more localised near the footing. Some soil goes around to the side of the footing and pushes a large number of soil elements upward.

In this study, for embedded square footings, depth factors  $F_{cd}$  are calculated by dividing the bearing capacity factors  $N_c$  of embedded square footing at the various  $D/B$  by  $N_c$  of surface square footing. The depth factors  $F_{cd}$  for embedment square footing calculated from results of this study are presented in Table 4.4 and shown in Figure 4.27.

For embedment square, circular and rectangular footings, the determination of depth factors  $F_{cd}$  of this study is different from that of results of Skempton (1951) and Salgado et al. (2004). The depth factors  $F_{cd}$  of results of Skempton (1951) and Salgado et al. (2004) are the same for any shape footing, while depth factors  $F_{cd}$  of this study change from footing shape to footing shape.

### 4.4.3 Bearing capacity and depth factor for circular footings

The bearing capacity factor  $N_c$  of this study was found to be almost identical for square and circular footings for all cases. In the cases of  $D/B \leq 3.0$ , the bearing capacity factor for square footings was around 1–2% above that of a circular footing. But in the cases of  $D/B > 3.0$  the bearing capacity factor for circular footings was around 0.5% above that of a square footing. This indicates some level of mesh dependency and is illustrated in Figure 4.19.

The modes of failures and displacement contours can be seen in Figure 4.25, and are similar to embedded square footings as discussed in Section 4.4.2. These results are very close to

the upper bound limit analysis of Salgado et al. (2004), but larger than the results of Skempton (1951), see Figure 4.14. When the ratio  $D/B$  increases from 0 to 0.2, the failure mechanism is similar to that of a footing on the surface of the same soil medium. Within this range of  $D/B$  values, the normalised undrained bearing capacity of embedded circular footings increases rapidly from 6.048 to 7.843 (Table 4.1). However, for  $D/B \geq 0.20$ , the normalised undrained bearing capacity rises gradually to 13.70 when  $D/B = 5$ .

In this study, for embedded circular footings, depth factors  $F_{cd}$  are also calculated by dividing the bearing capacity factors  $N_c$  of embedded circular footings at the various  $D/B$  by  $N_c$  of the surface circular footing. The depth factors  $F_{cd}$  for embedment circular footing calculated from results of this study are presented in Table 4.4 and shown in Figure 4.27.

#### 4.4.4 Bearing capacity and depth factor for rectangular footings

Results of this study on the bearing capacity of embedded rectangular footings are presented in Table 4.2 and graphically in the Figure 4.26.

In general, the results of this study are similar to those obtained from the limit analysis of Salgado et al (2004), tending to be closer to the upper bound than the lower bound results. Bearing capacities of embedded rectangular footing increase as ratios  $D/B$  and  $B/L$  increase.

In the surface footing cases, the normalised bearing capacities of all the rectangular footings from the finite element analysis of this study and from the laboratory investigations of Skempton (1951) are very close to each other (within about 1–2%), Table 4.2. This suggests the shape factor  $F_{cs}$  suggested by Skempton (1951) is similar to the limit analysis results. Again, for embedded footings the bearing capacity factors proposed by Skempton (1951) appear very conservative.

From Figure 4.19, the value of normalised bearing capacity factors  $N_c$  for rectangular footings increase as ratio  $B/L$  rises. For example, at the depth of  $D/B = 3$ , the normalised bearing capacity factor  $N_c$  for rectangular footing of  $B/L=0.2, 0.25, 0.33$  and  $0.50$  are 9.309, 9.545, 9.987 and 10.593 respectively.

The typical displacement vectors and contours for rectangular footing problems in the symmetry planes  $P_1$  and  $P_2$  are presented in Figure 4.26. The failure mechanism in the

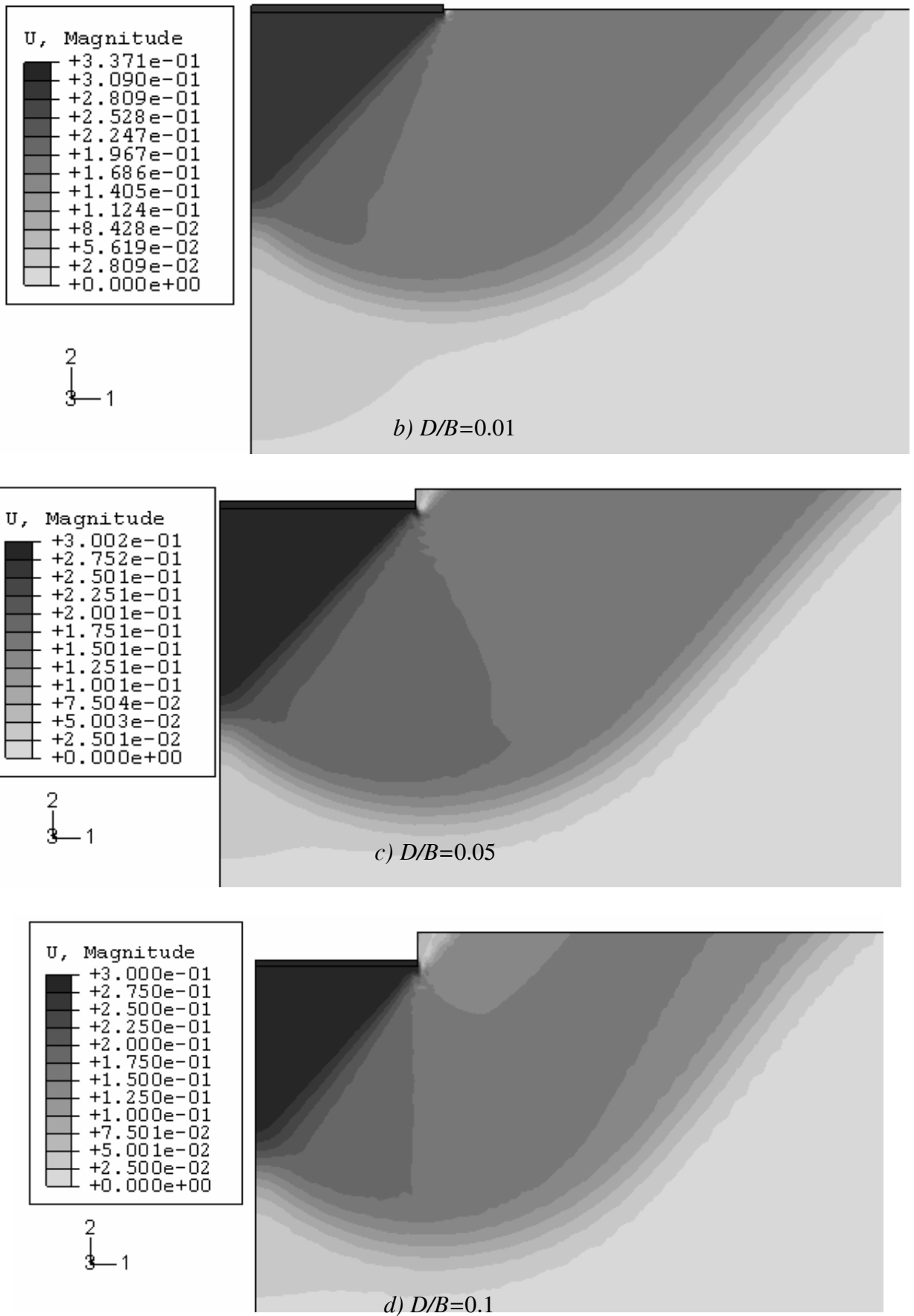
planes  $P_1$  is larger and increasingly happens in the vicinity of the footing as the ratio of  $B/L$  increases from 0.2 to 0.5 for cases where  $D/B \leq 4$ . However, for cases where  $D/B > 4$ , failure tends to be localised around the footing instead of extending to the surface. In the plane  $P_2$ , when  $B/L$  increases from 0.2 to 0.5 the displacement vectors and contours change the active zone from isosceles trapezium to isosceles triangle. This is consistent with the case of strip footings (see Figure 4.23(d) – (i)) which corresponds to a rectangular footing in the case where  $B/L = 0$ .

In this study, for embedded rectangular footings, depth factors  $F_{cd}$  are also calculated by dividing the bearing capacity factors  $N_c$  of embedded rectangular footings at the various  $D/B$  by  $N_c$  of the surface rectangular footing. The depth factors  $F_{cd}$  for embedment rectangular footings calculated from results of this study are presented in Table 4.4 and shown in Figure 4.27.

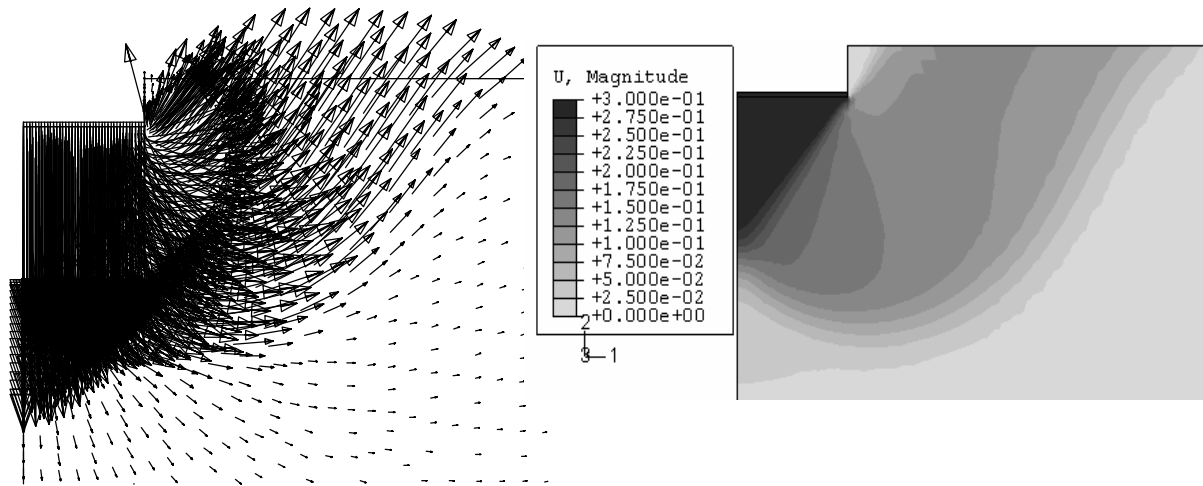
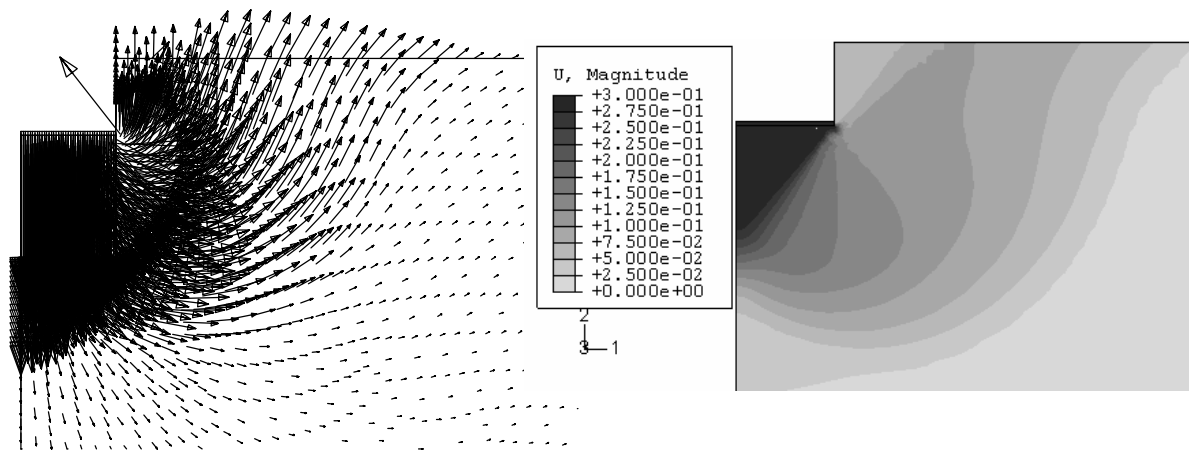
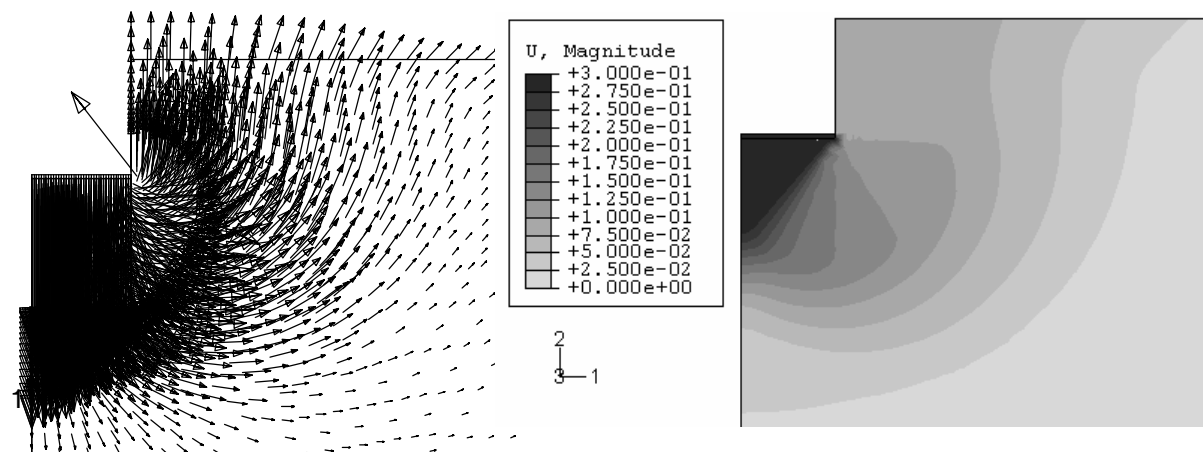
The depth factors  $F_{cd}$  of all footings shapes in this study are determined differently from those of Skempton (1951) and Salgado et al. (2004), which are presented in Table 4.4 and shown in Figure 4.27. The depth factors  $F_{cd}$  contained both parameters  $D/B$  and  $B/L$ . For practical uses, the depth factors  $F_{cd}$  in Table 4.4 and Figure 4.27 can be approximated by following equation of two parameters  $D/B$  and  $B/L$ .

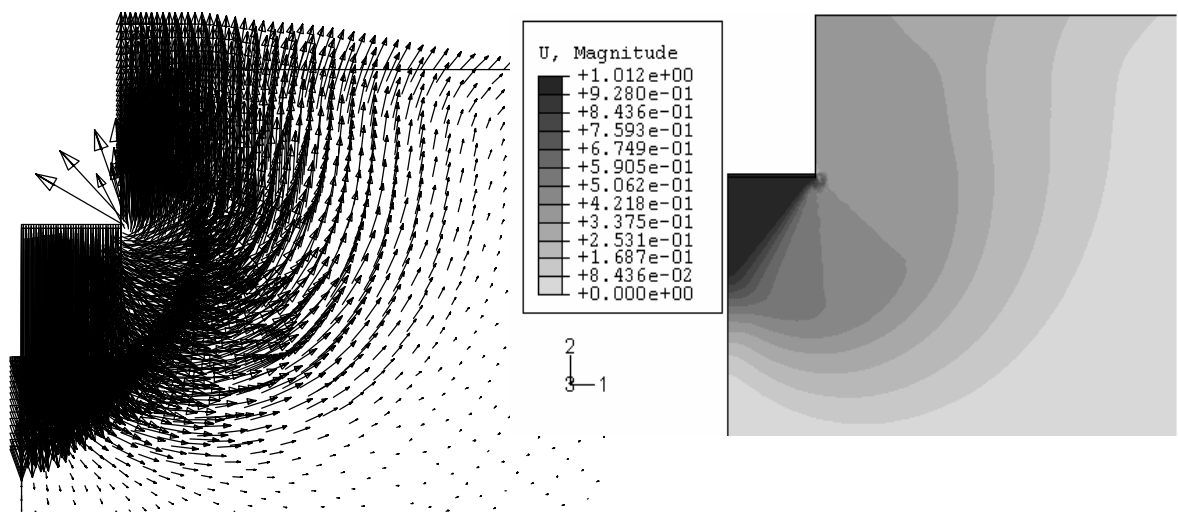
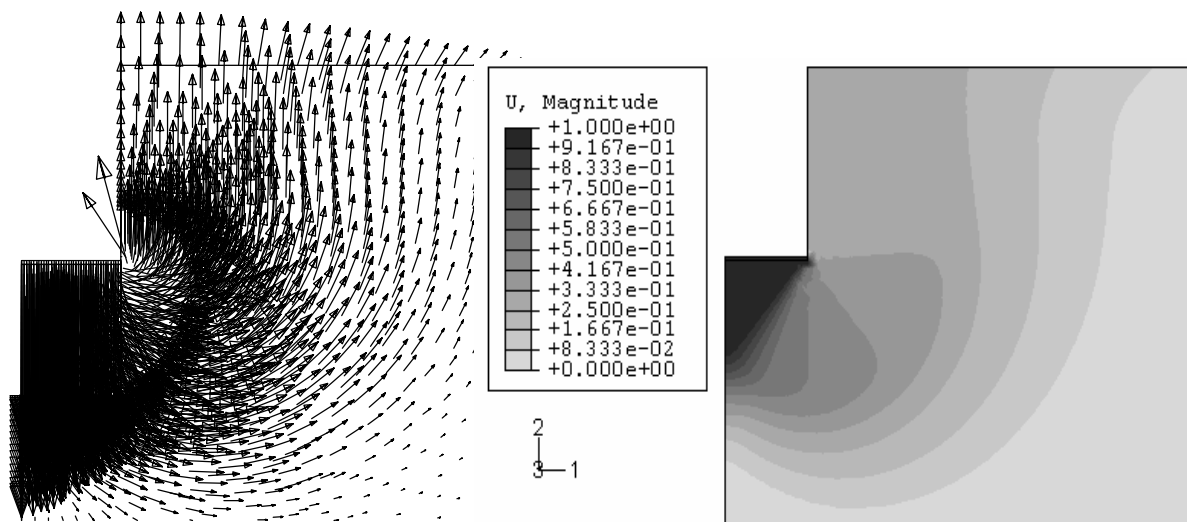
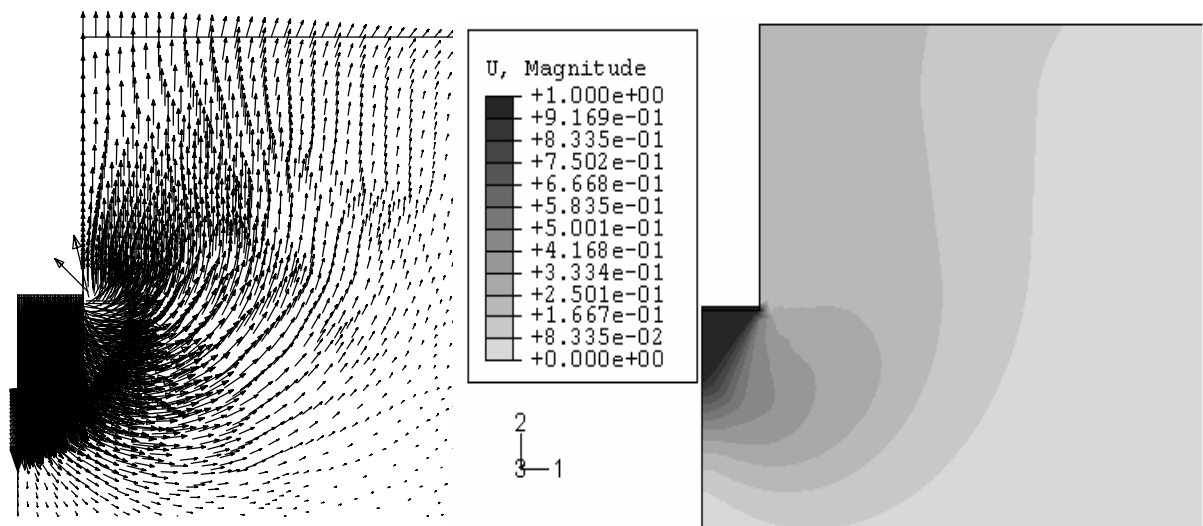
$$F_{cd} = 1 + \sqrt{0.48 - 0.4e^{-B/L}} \sqrt{\frac{D}{B}} \quad (4.6)$$

Equation (4.6) provides estimates of the depth factors to within  $\pm 3.5\%$  of the finite element solutions (ABAQUS) and therefore can be used with confidence to solve practical design problems. Figure 4.28 presents graphically the depth factors from ABAQUS and from the estimated equation (4.6).



**Figure 4.22** Displacement contours for strip footings  $D/B= 0.01, 0.05$  and  $0.1$

a)  $D/B=0.2$ b)  $D/B=0.4$ c)  $D/B=0.6$ **Figure 4.23** Displacement vectors and contours for strip footings  $D/B=0.2$ ,  $0.4$  and  $0.6$

d)  $D/B=0.8$ e)  $D/B=1.0$ f)  $D/B=2.0$ Figure 4.23 (continued) Displacement vectors and contours for strip footings  $D/B=0.8$ ,  $1.0$  &  $2.0$

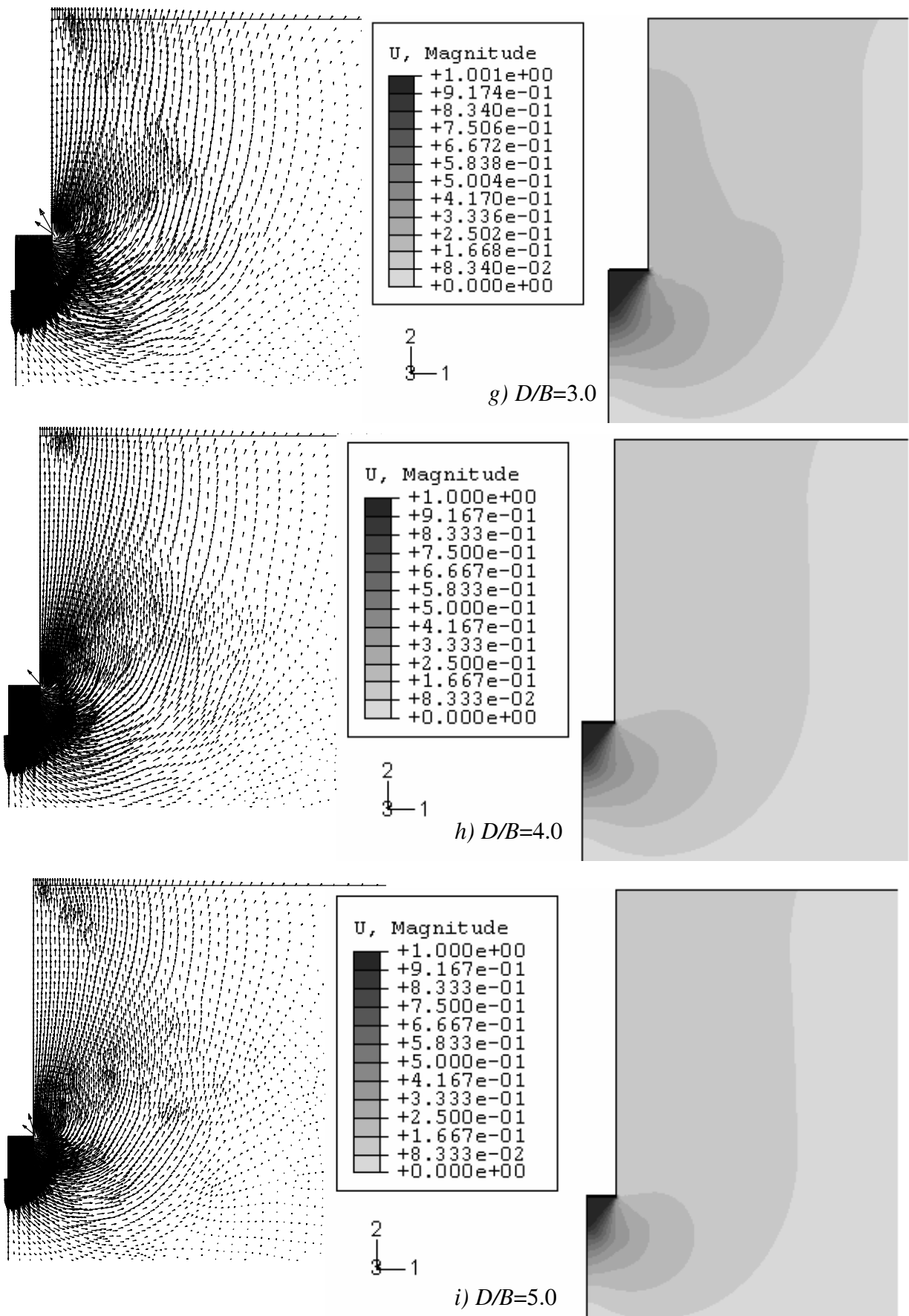
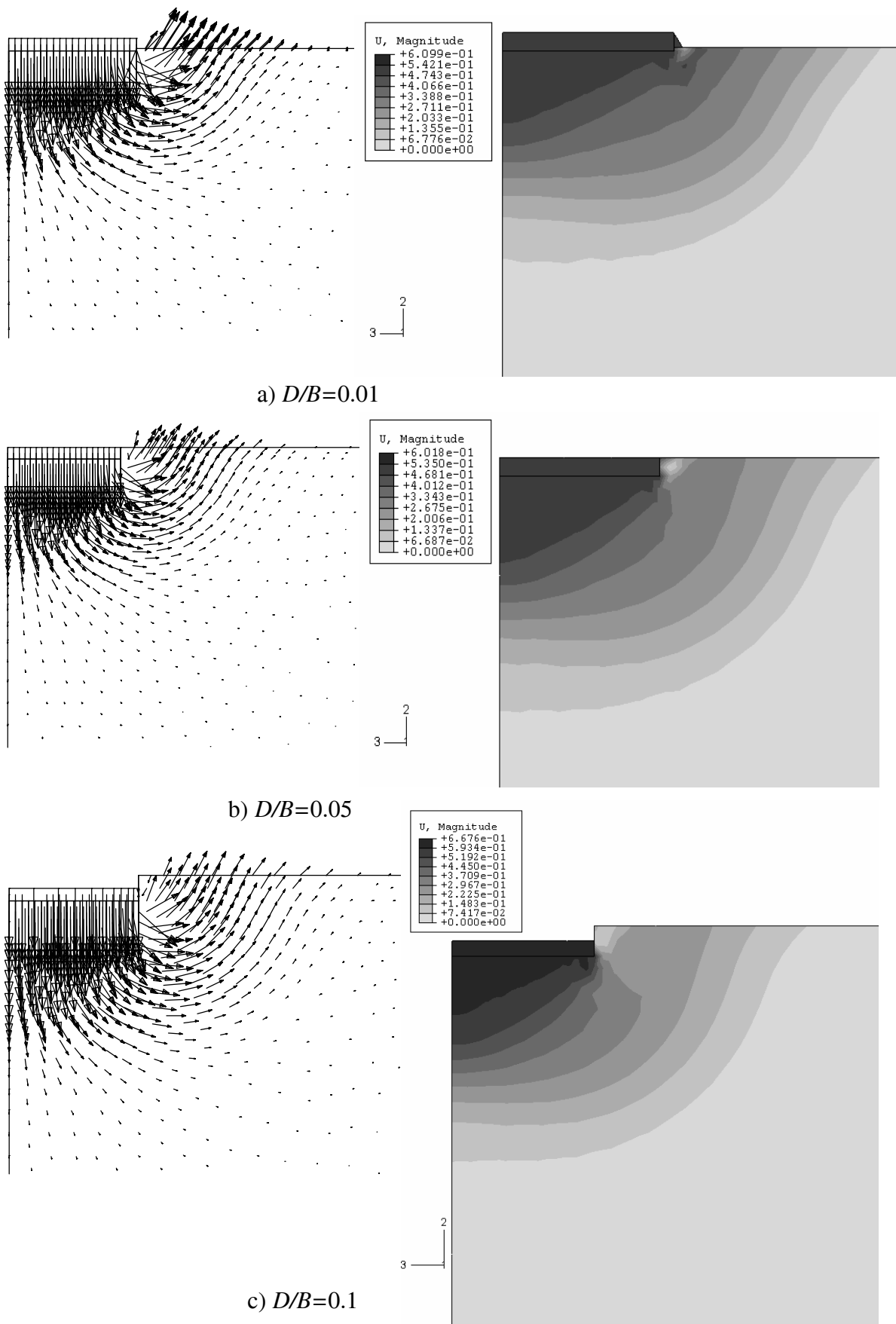
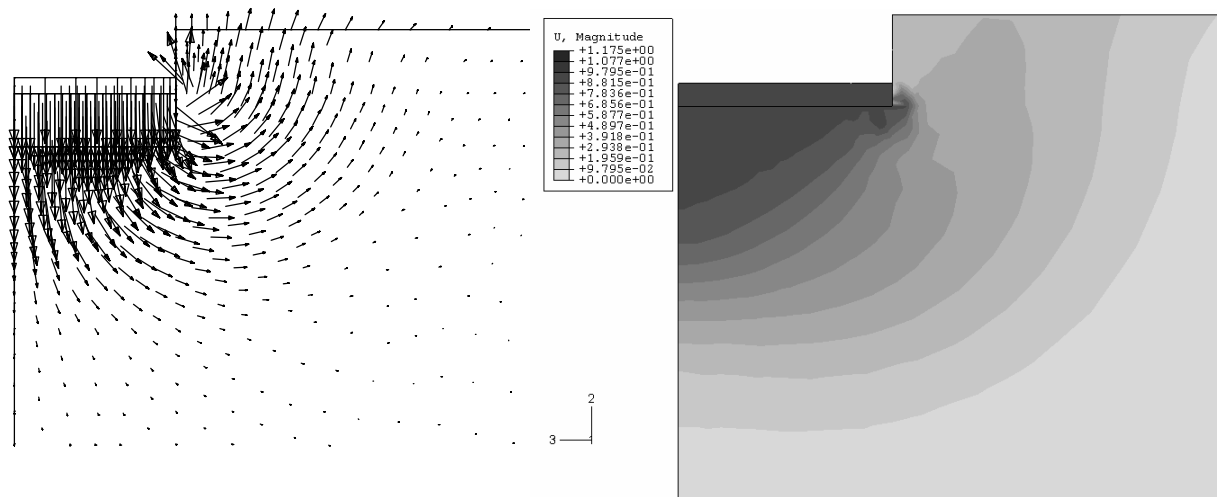
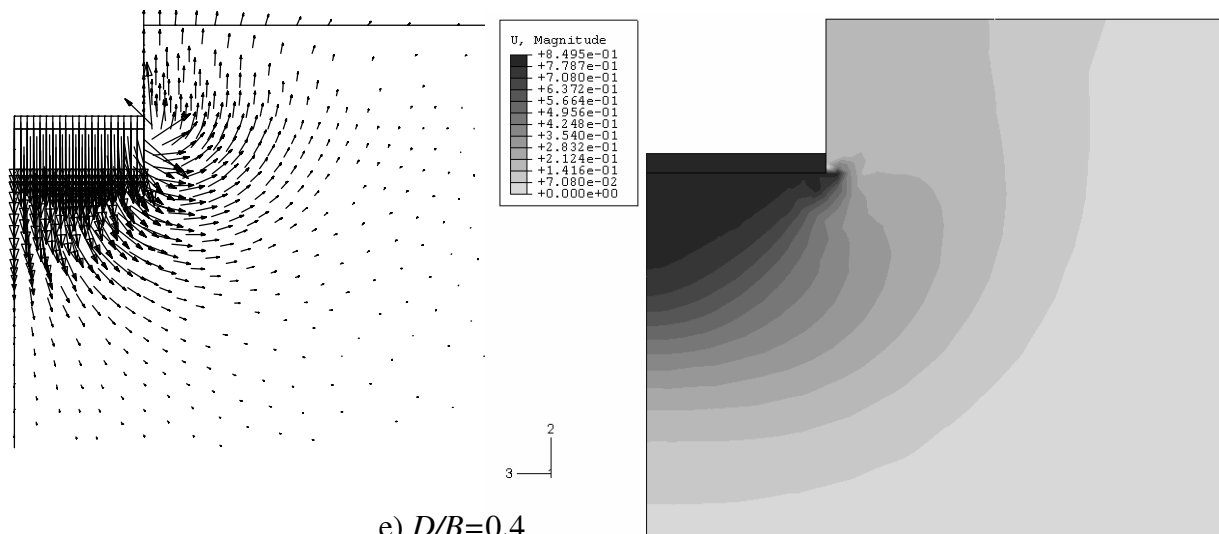
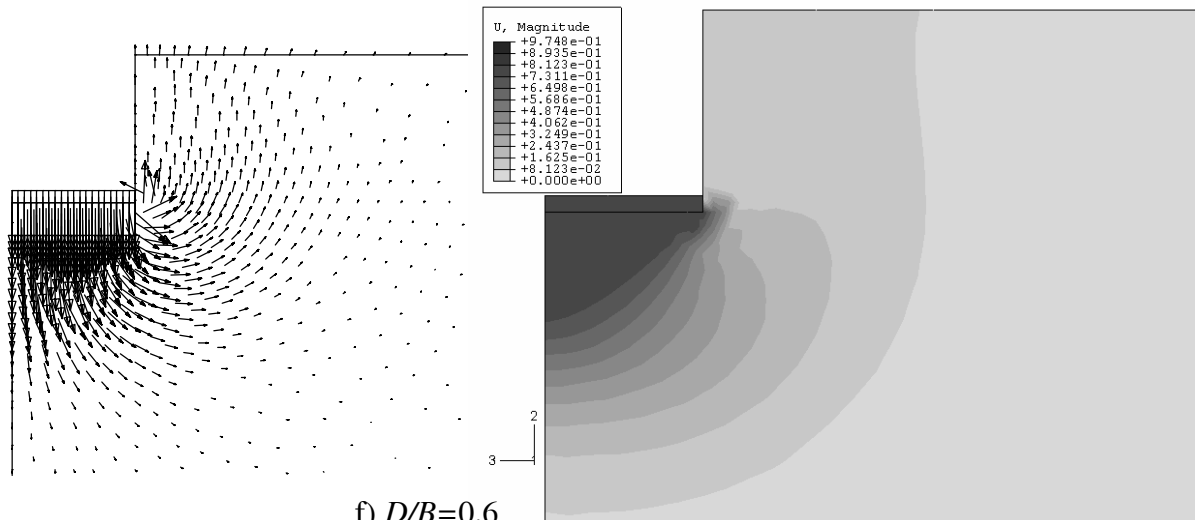


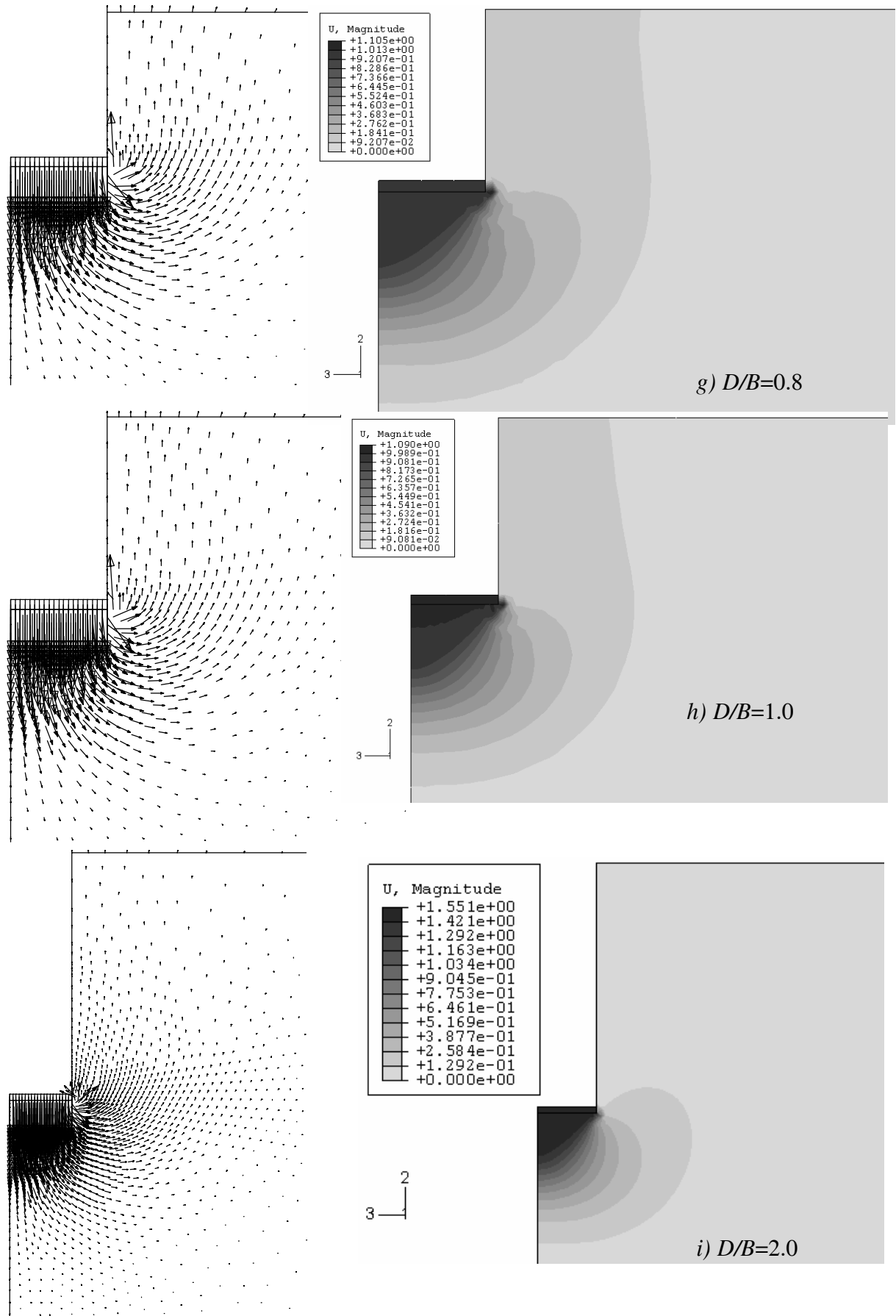
Figure 4.23 (continued) Displacement vectors and contours for strip footings  $D/B=3.0, 4.0$  &  $5.0$



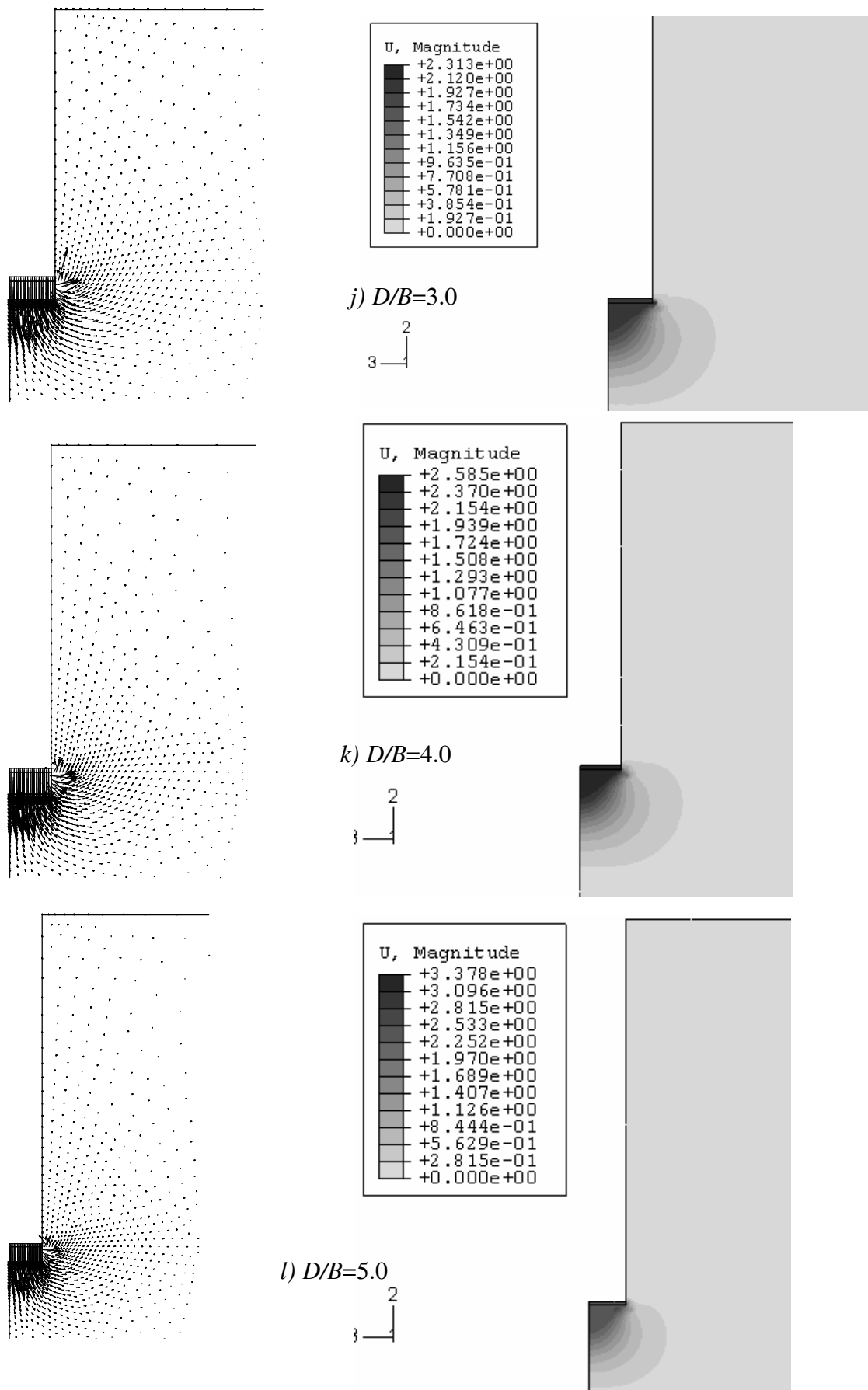
**Figure 4.24** Displacement vectors and contours for square footings  $D/B=0.01, 0.05$  &  $0.1$

d)  $D/B=0.2$ e)  $D/B=0.4$ f)  $D/B=0.6$ 

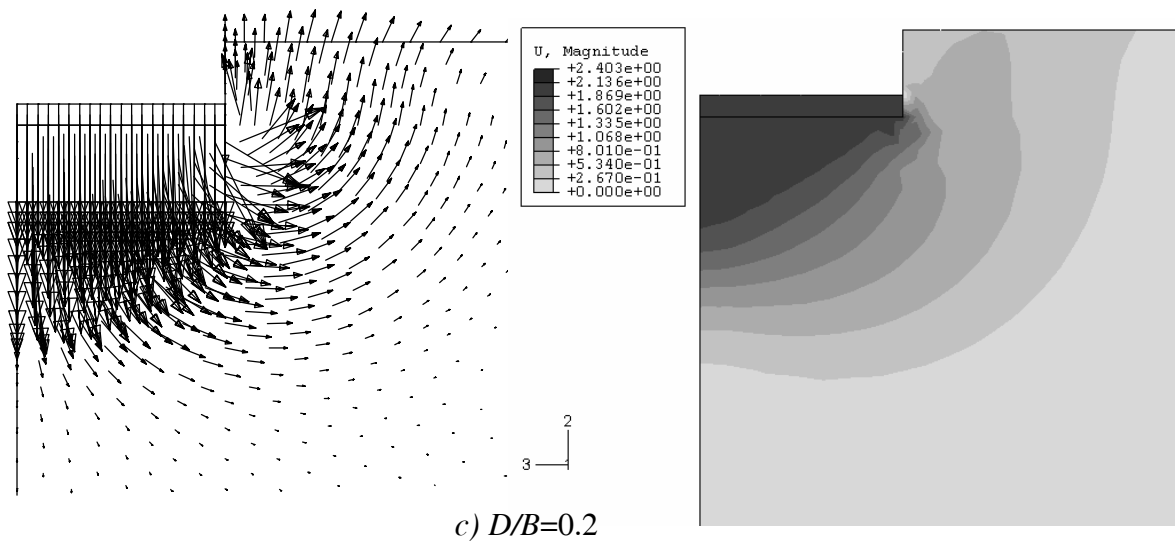
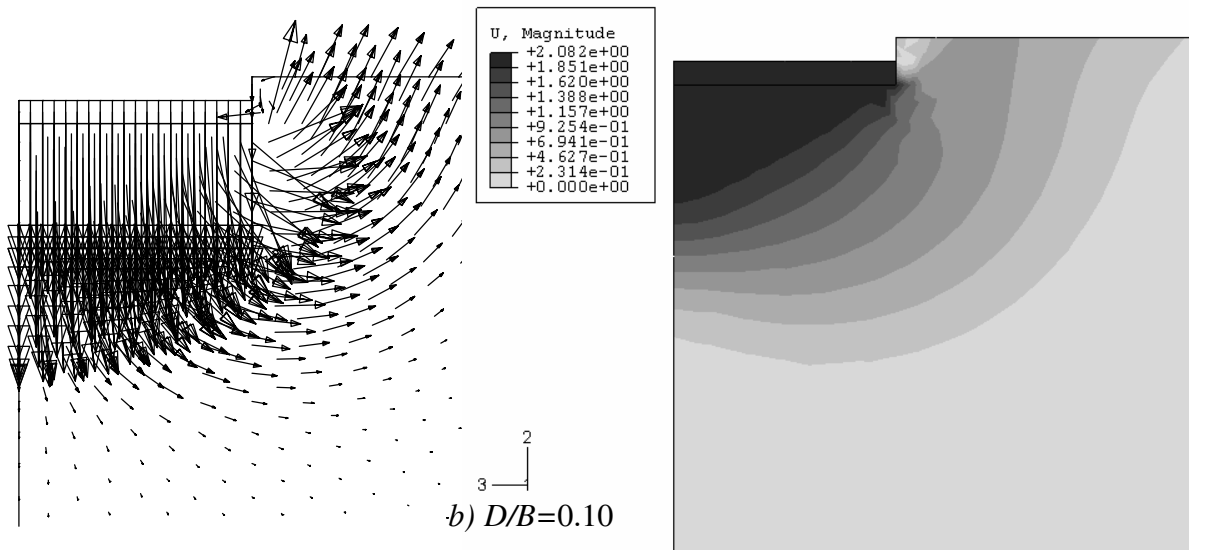
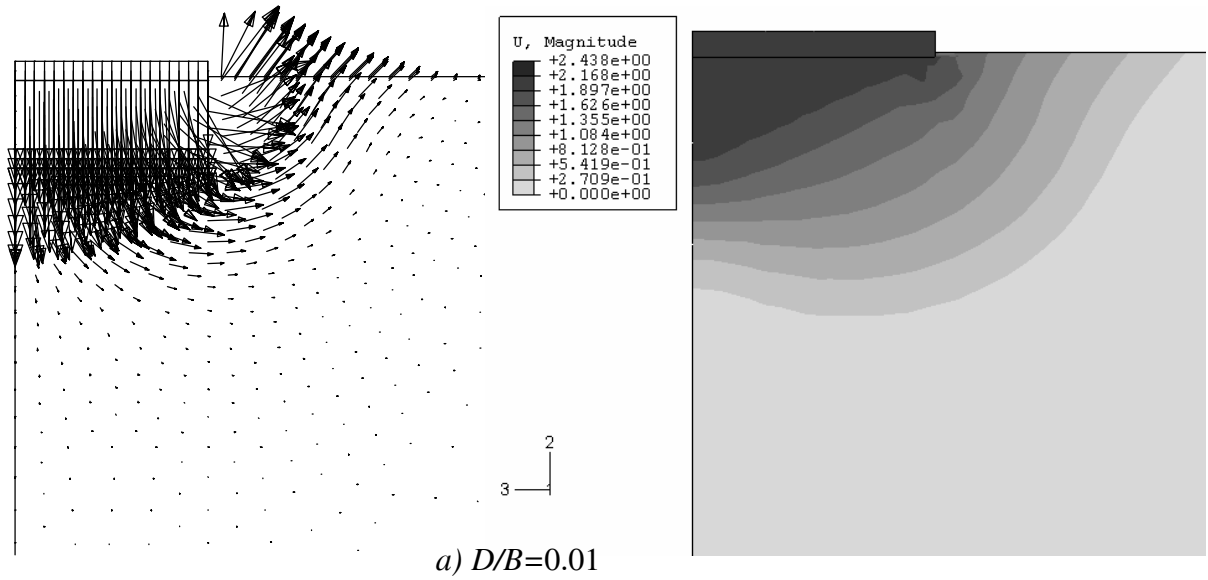
**Figure 4.24 (continued)** Displacement vectors and contours for square footings  $D/B=0.2, 0.4$  &  $0.6$



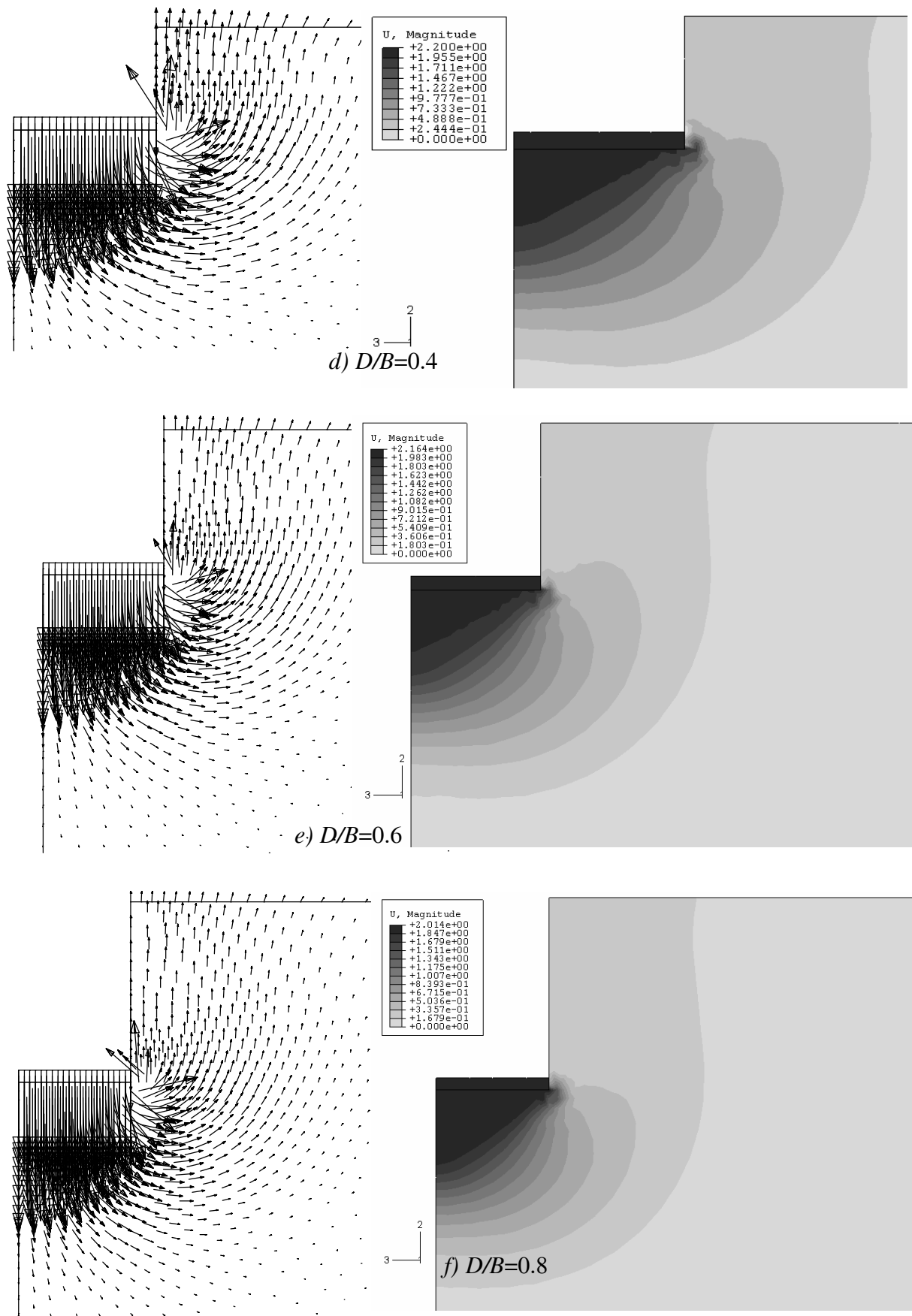
**Figure 4.24 (continued)** Displacement vectors and contours for square footings  $D/B=0.8, 1.0$  &  $2.0$



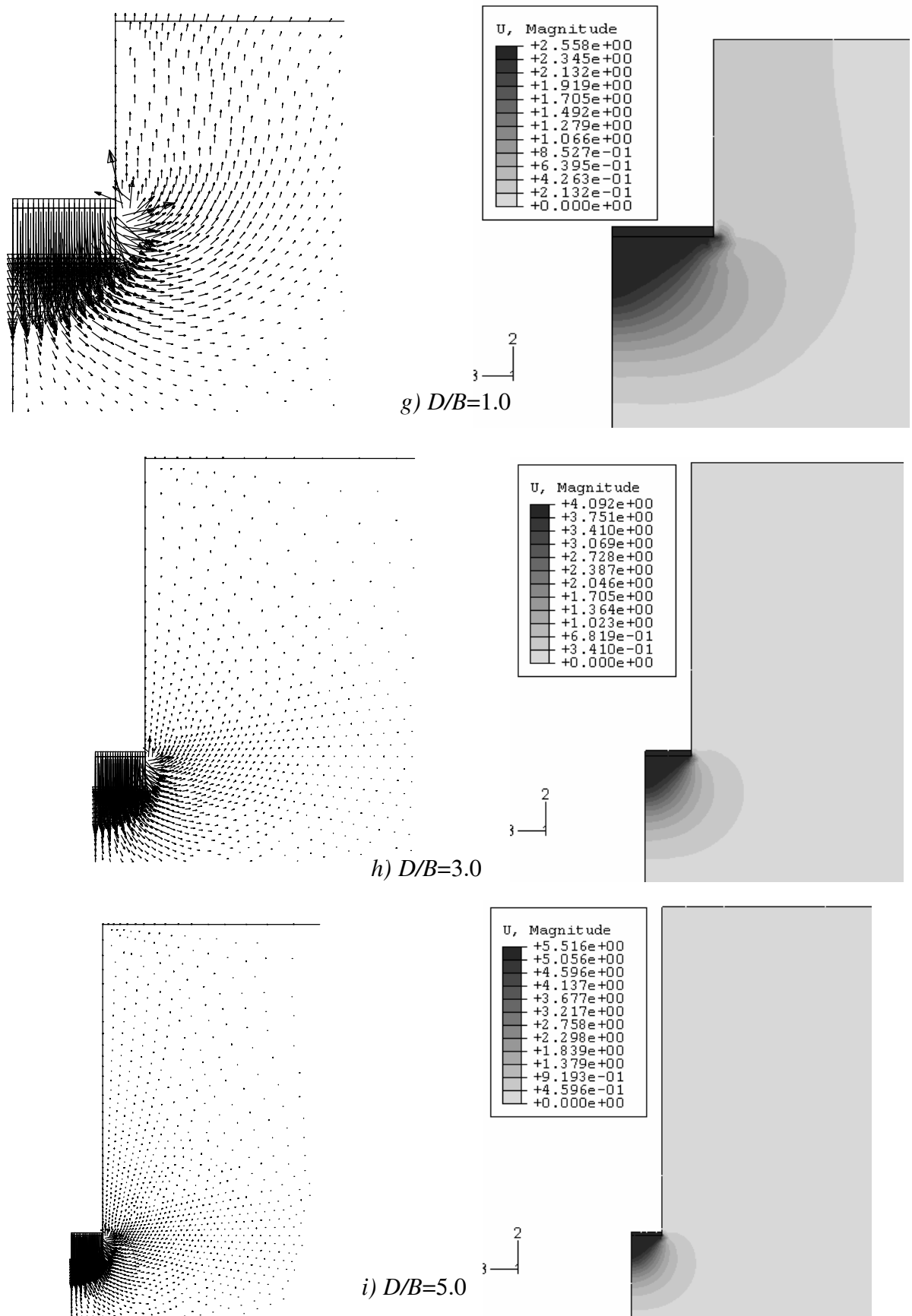
**Figure 4.24 (continued)** Displacement vectors and contours for square footings  $D/B=3.0, 4.0$  and  $5.0$



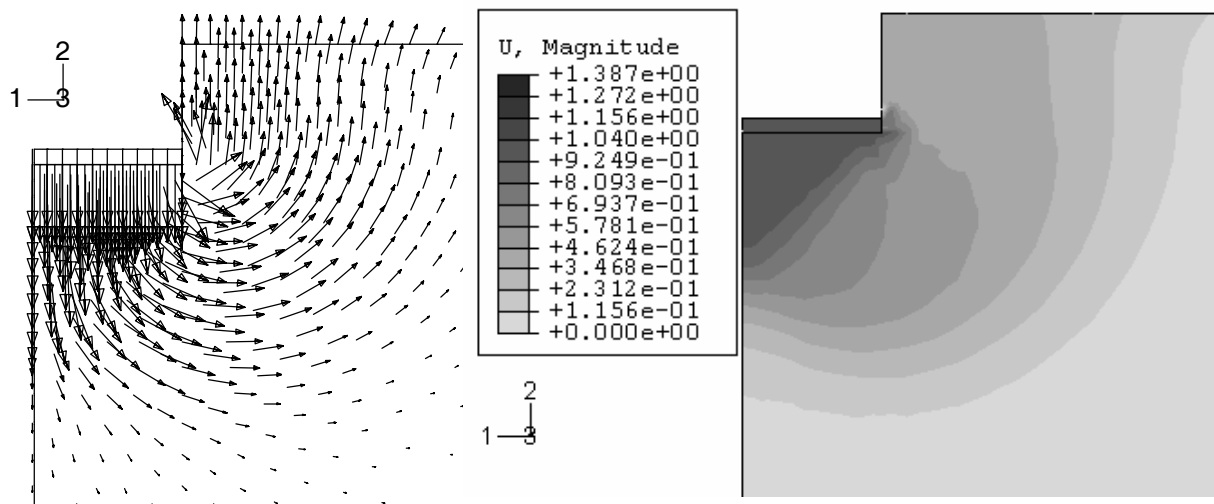
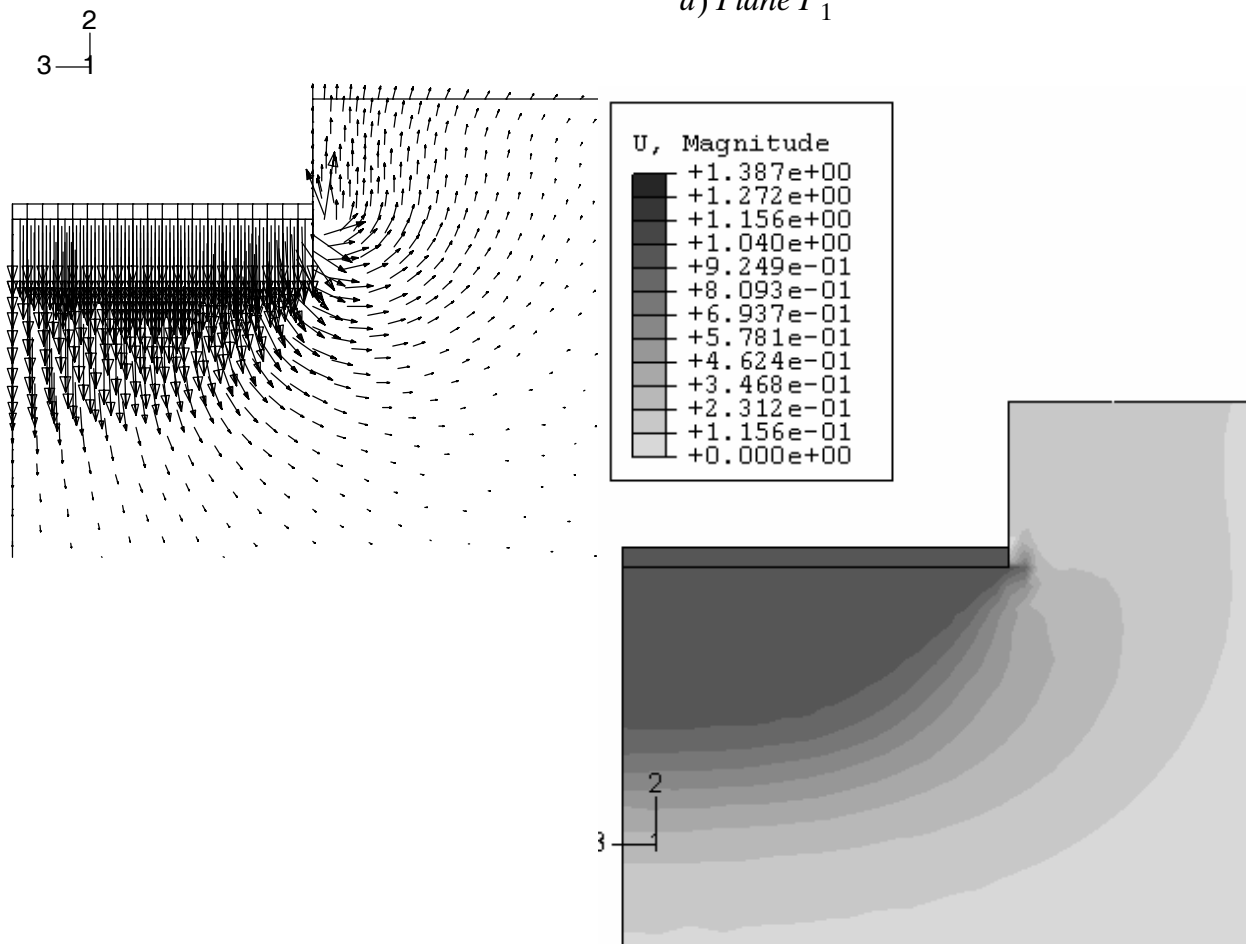
**Figure 4.25** Displacement vectors and contours for circular footings  $D/B=0.01, 0.1$  and  $0.2$



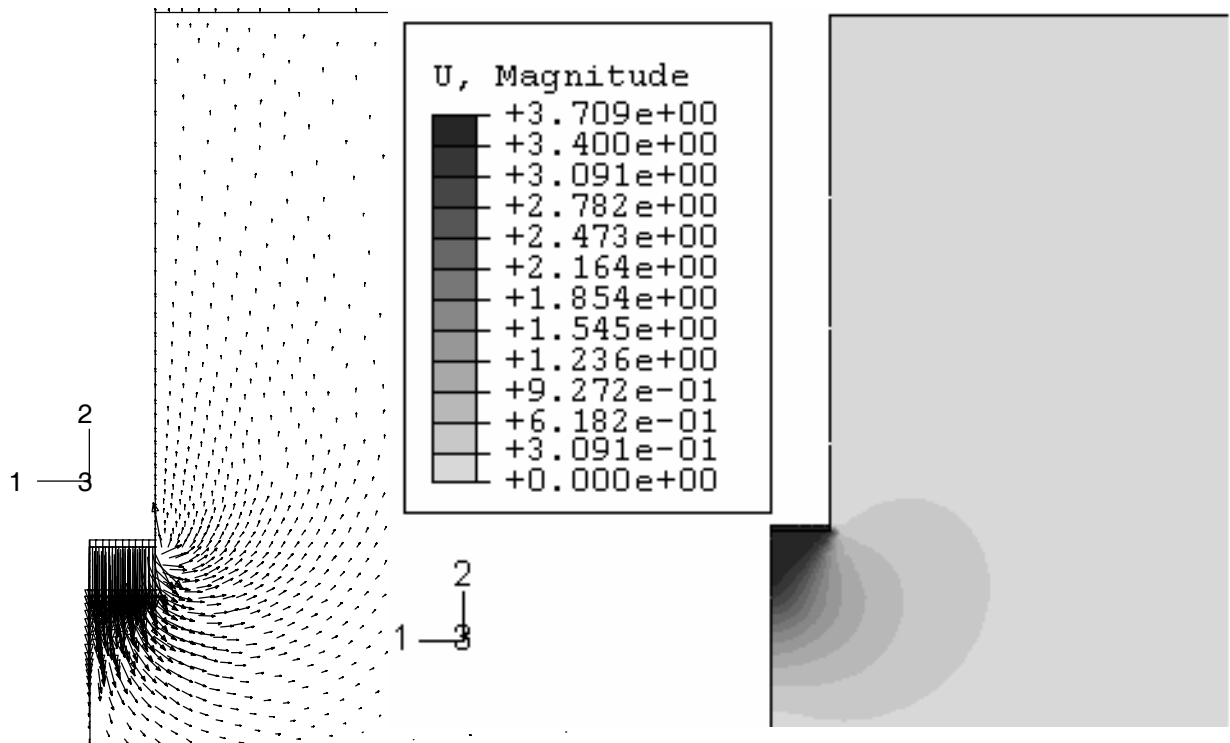
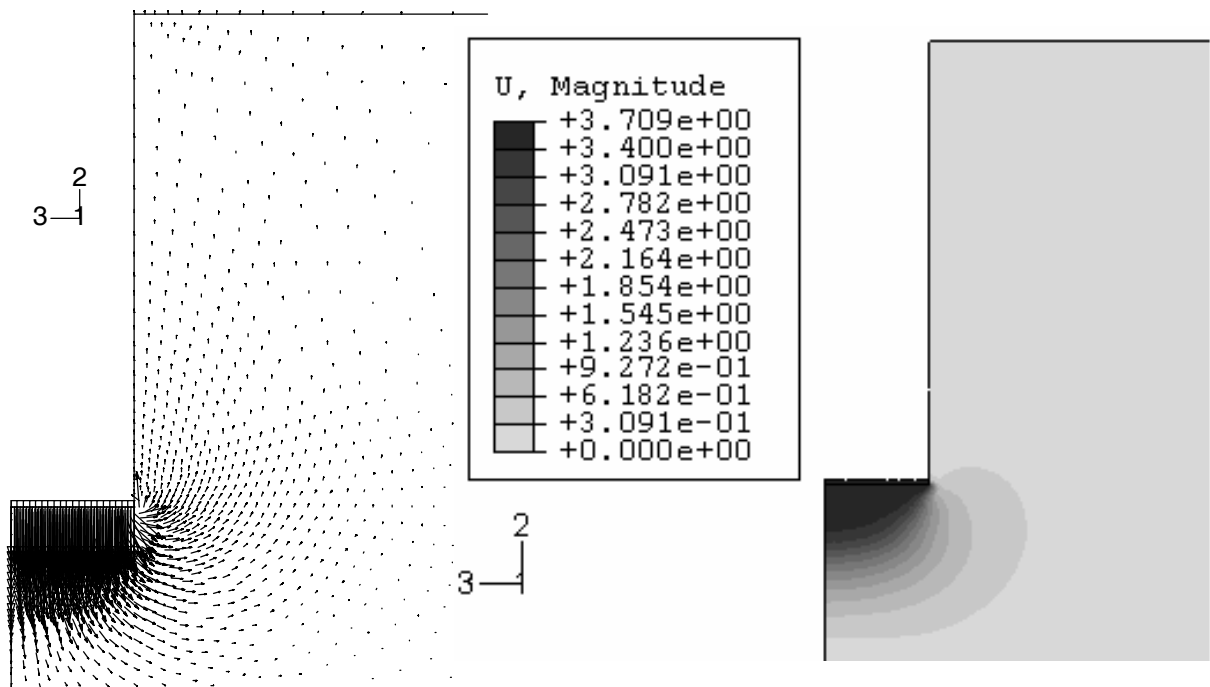
**Figure 4.25 (continued)** Displacement vectors and contours for circular footings  $D/B=0.4, 0.6$  and  $0.8$



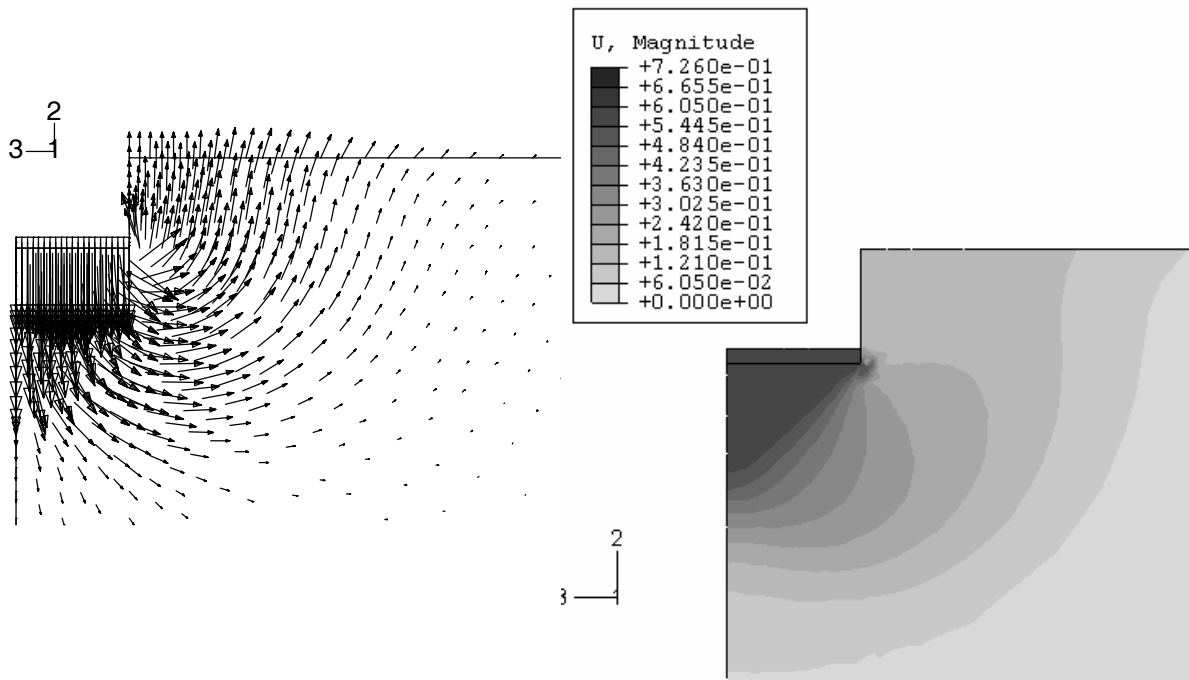
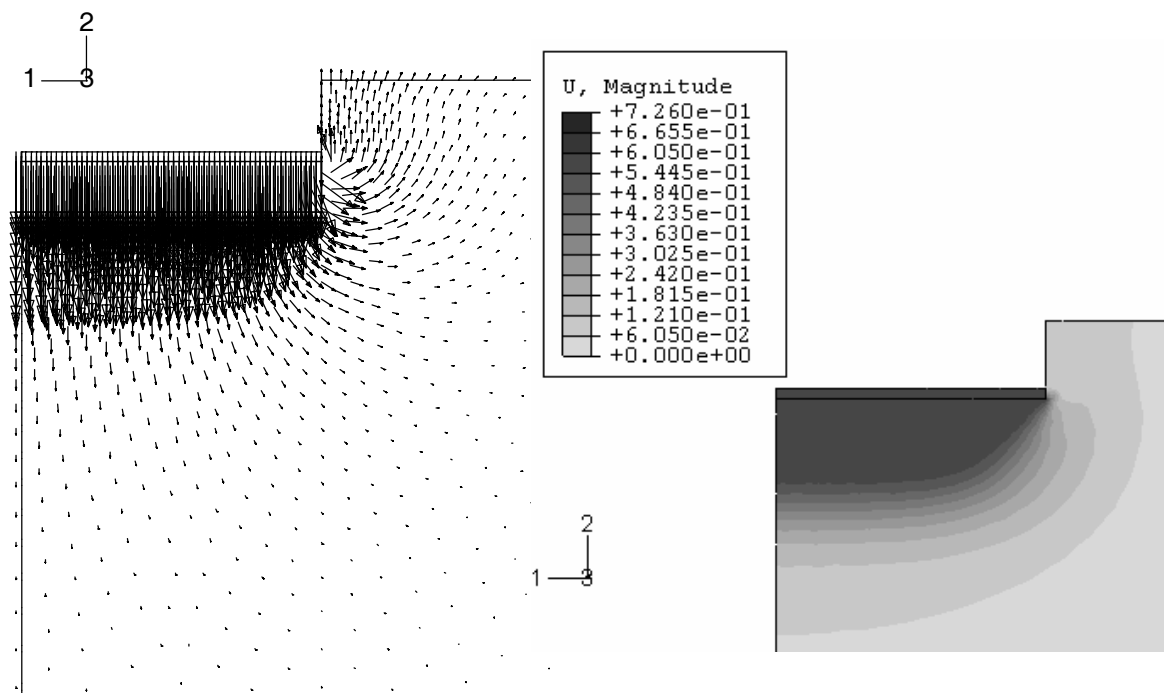
**Figure 4.25 (continued)** Displacement vectors and contours for circular footings  
 $D/B=1.0, 3.0$  &  $5.0$

a) Plane  $P_1$ b) Plane  $P_2$ 

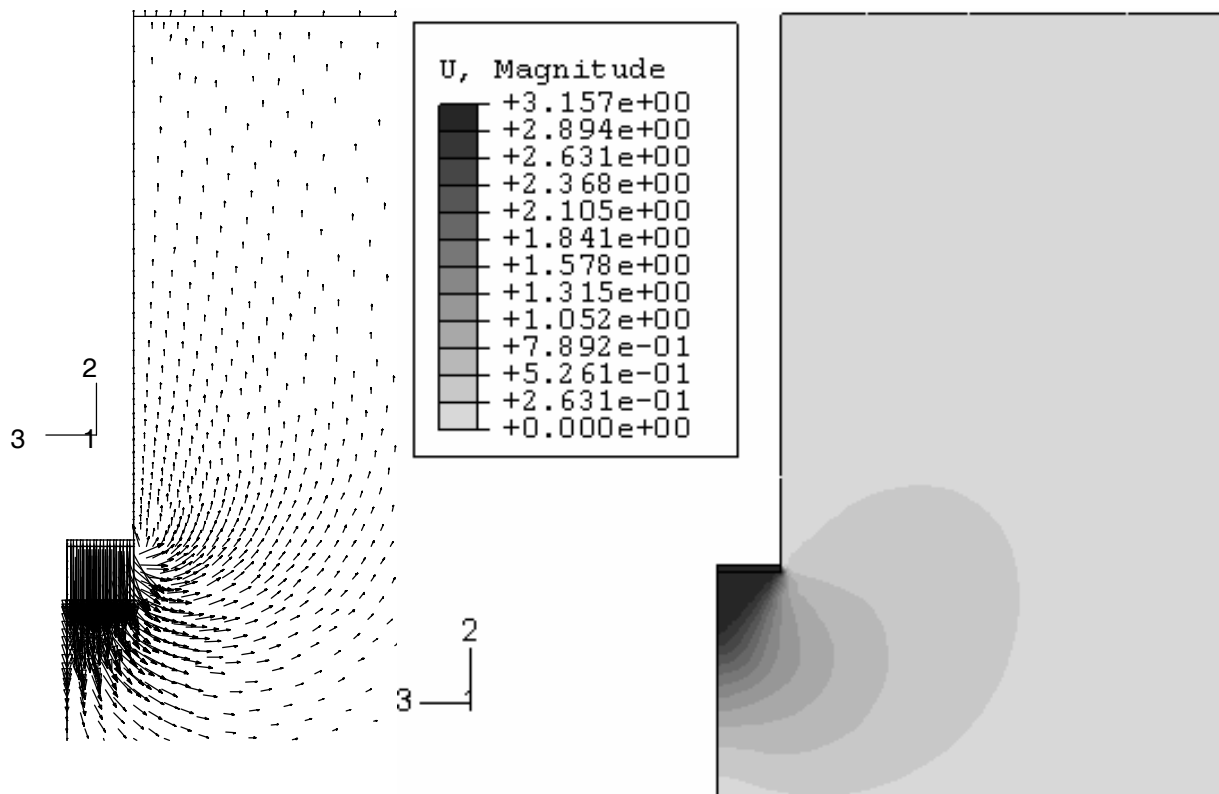
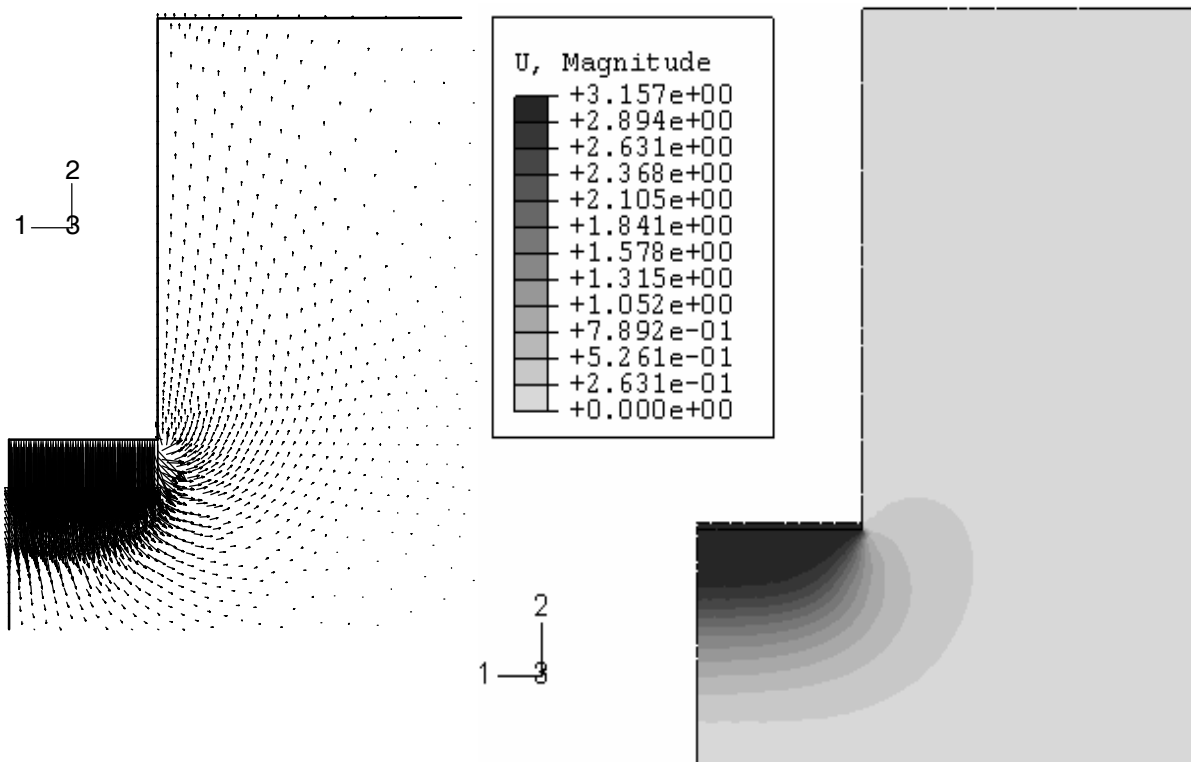
**Figure 4.26** Displacement vectors and contours for rectangular footings  $L/B=0.50$ ,  $D/B=0.4$

c) Plane  $P_1$ d) Plane  $P_2$ 

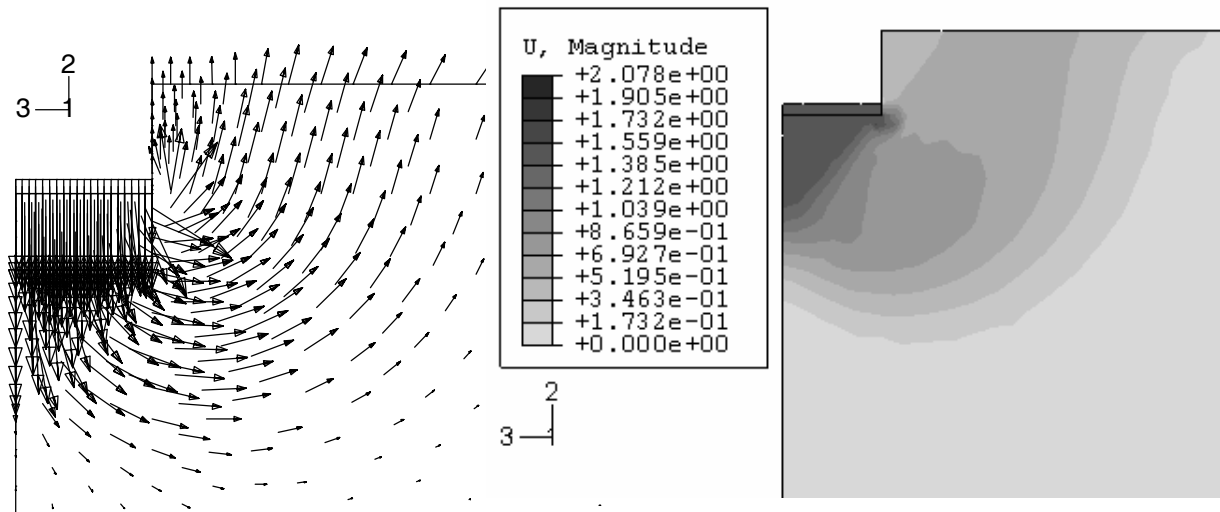
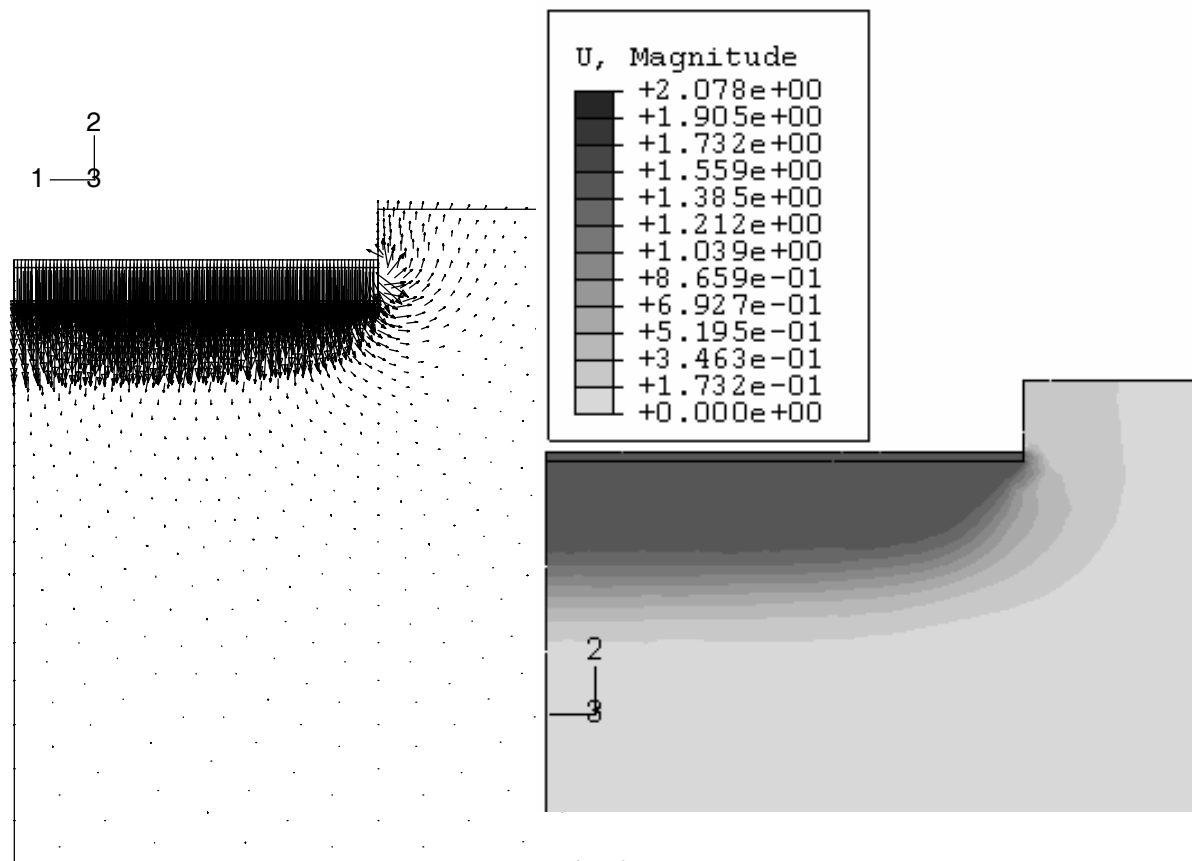
**Figure 4.26 (continued)** Displacement vectors and contours for rectangular footings  
 $L/B=0.50$ ,  $D/B=4.0$

e) Plane  $P_1$ f) Plane  $P_2$ 

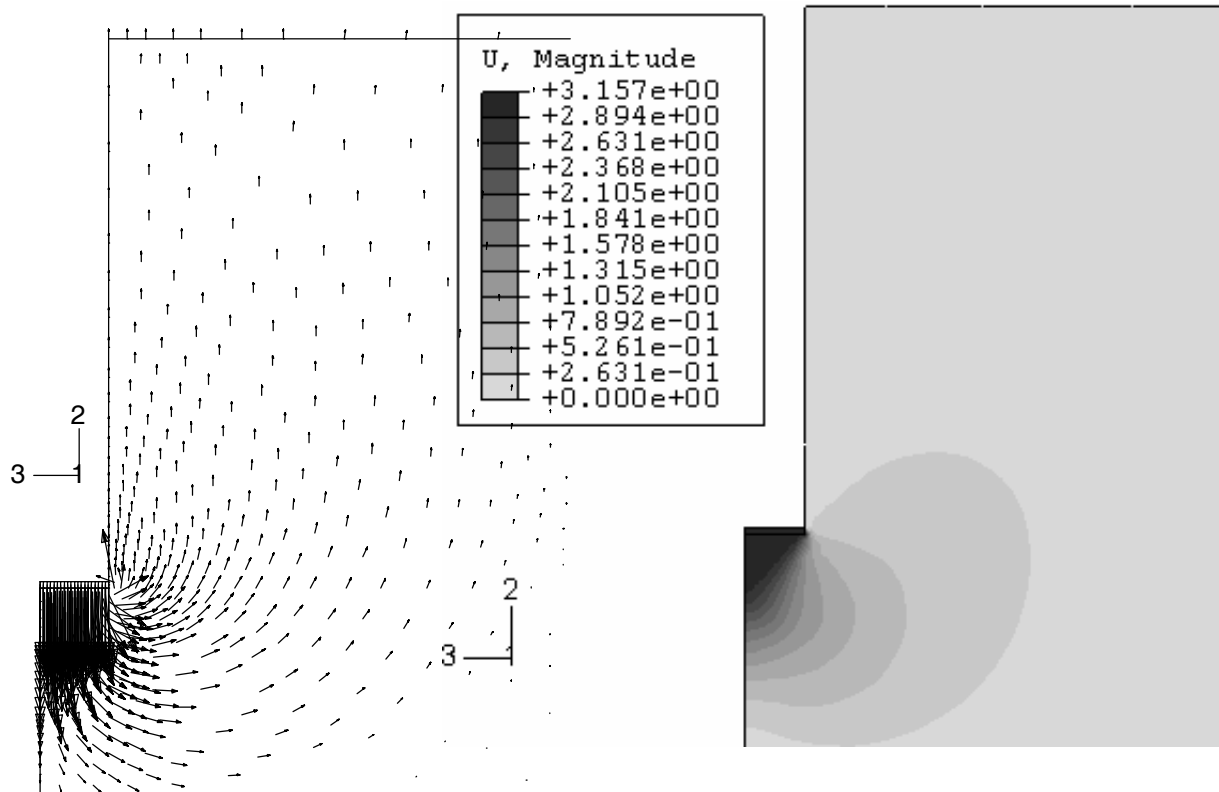
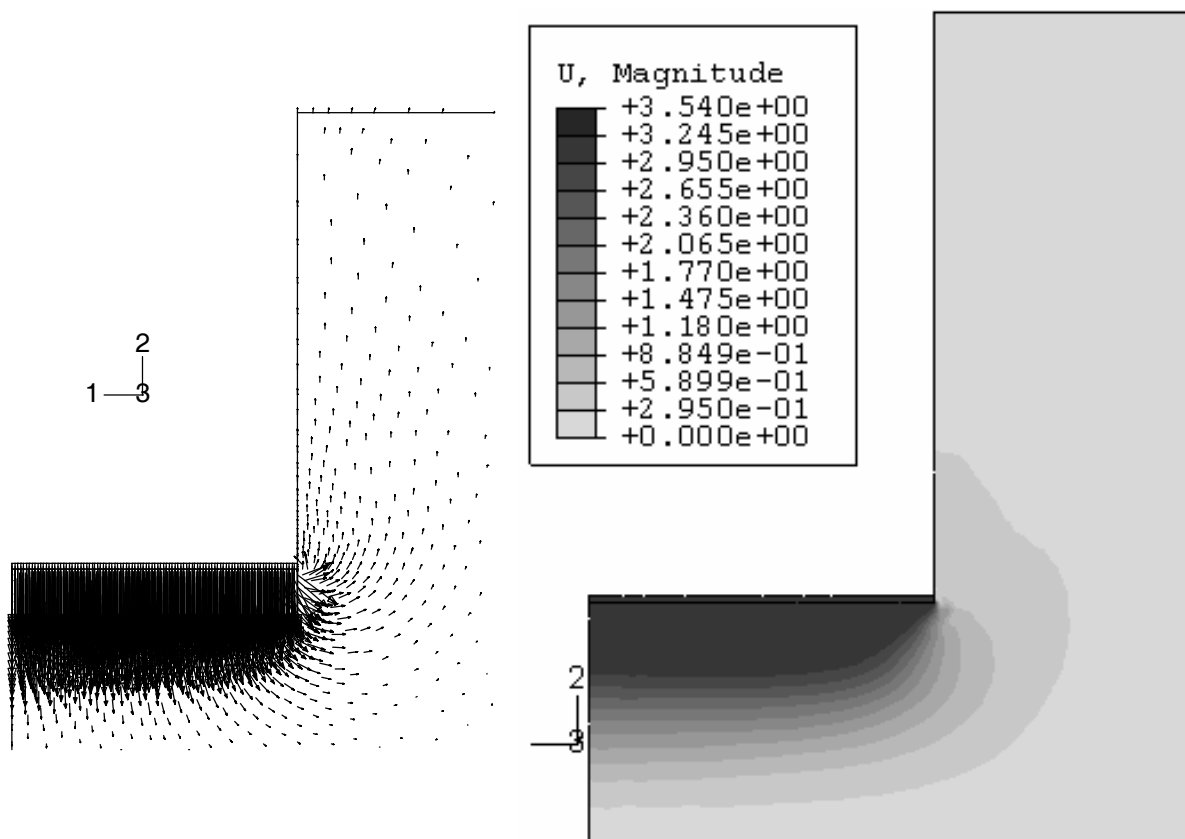
**Figure 4.26 (continued)** Displacement vectors and contours for rectangular footings  
 $L/B=0.33$ ,  $D/B=0.4$

g) Plane  $P_1$ h) Plane  $P_2$ 

**Figure 4.26 (continued)** Displacement vectors and contours for rectangular footings  
 $L/B=0.33$ ,  $D/B=4.0$

i) Plane  $P_1$ j) Plane  $P_2$ 

**Figure 4.26 (continued)** Displacement vectors and contours for rectangular footings  
 $L/B=0.20$ ,  $D/B=0.4$

k) Plane  $P_1$ l) Plane  $P_2$ 

**Figure 4.26 (continued)** Displacement vectors and contours for rectangular footings  
 $L/B=0.2$ ,  $D/B=4.0$

D/B	Strip footing,	Square footing,	Circular footing,	Rectangular footing			
	B/L=0	B/L=1	B/L=2	B/L=0.50	B/L=0.33	B/L=0.25	B/L=0.20
0	1	1	1	1	1	1	1
0.01	1.002	1.044	1.036	1.016	1.01	1.006	1.011
0.05	1.046	1.119	1.133	1.08	1.066	1.069	1.059
0.1	1.082	1.187	1.211	1.151	1.096	1.105	1.113
0.2	1.118	1.267	1.297	1.212	1.181	1.177	1.184
0.4	1.197	1.365	1.378	1.3	1.267	1.257	1.261
0.6	1.246	1.437	1.451	1.367	1.321	1.307	1.308
0.8	1.292	1.499	1.518	1.428	1.373	1.351	1.346
1	1.311	1.558	1.583	1.48	1.424	1.395	1.382
2	1.435	1.783	1.819	1.691	1.627	1.574	1.546
3	1.514	2.035	1.998	1.849	1.779	1.723	1.689
4	1.558	2.197	2.146	1.986	1.906	1.852	1.807
5	1.622	2.327	2.265	2.102	2.022	1.966	1.919

**Table 4.4** Depth factors  $F_{cd}$  for embedded footings from ABAQUS

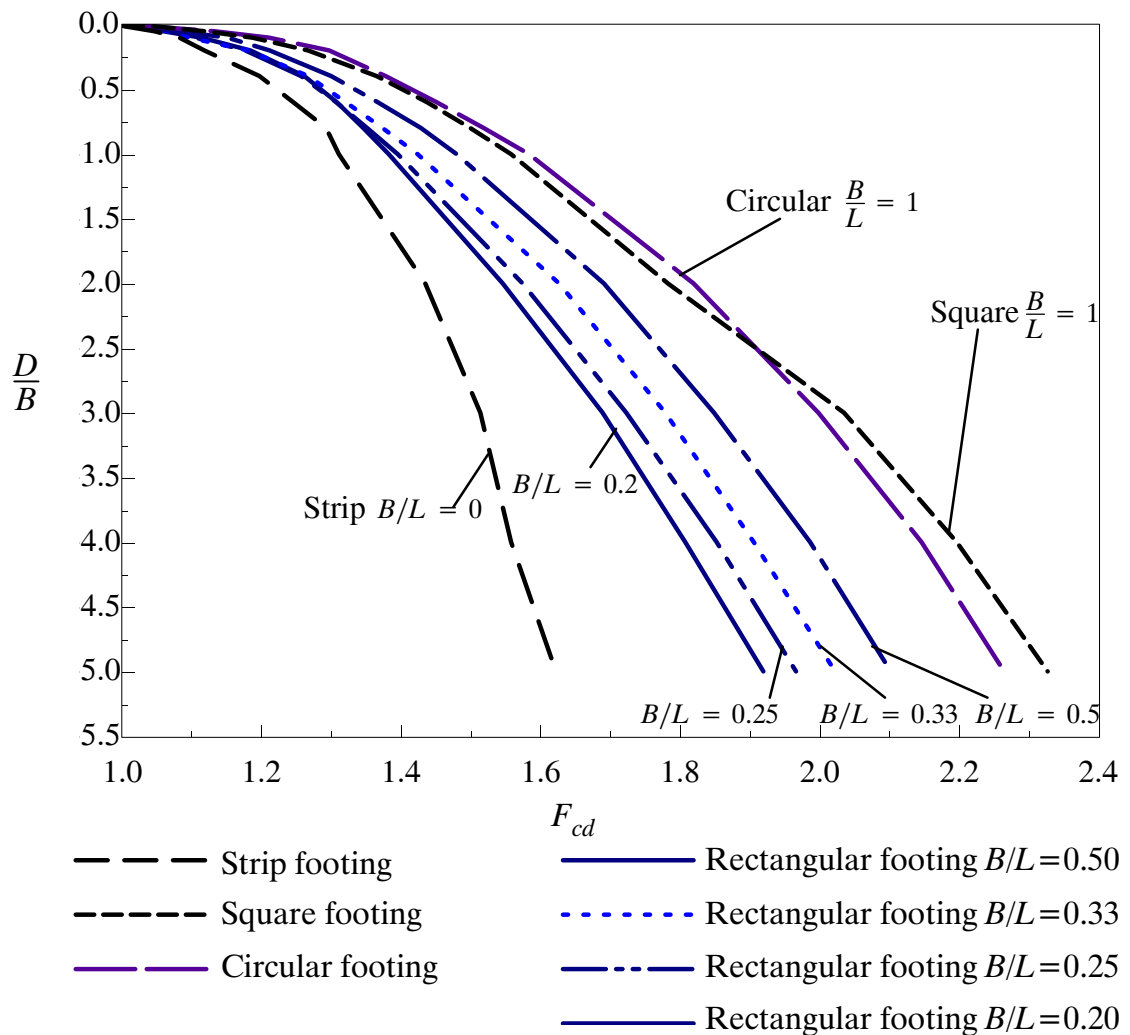
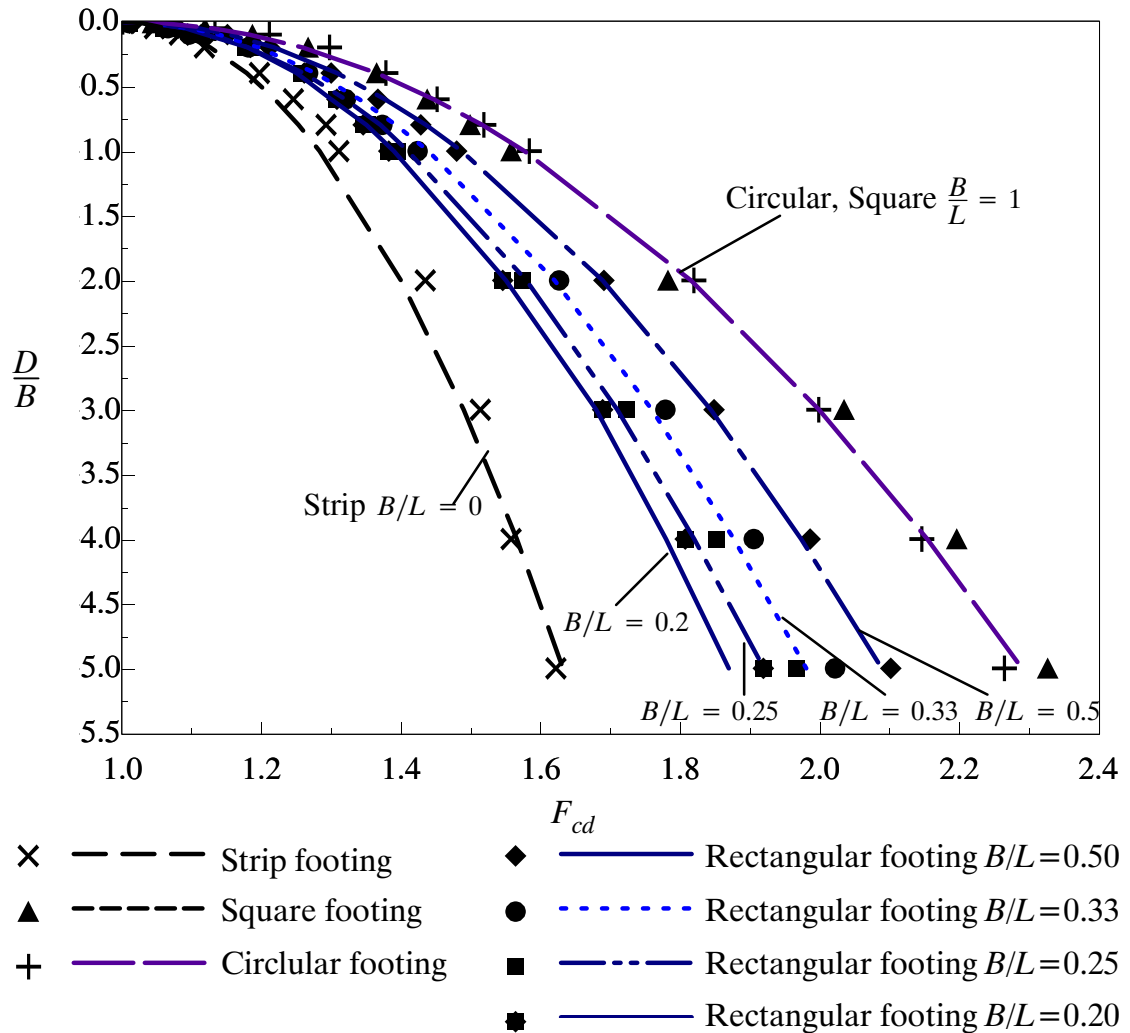


**Figure 4.27** Depth factors for embedded footings from ABAQUS



Note that: The marked points are ABAQUS results,  
the curves are the estimated equation (4.6)

**Figure 4.28** Depth factors for embedded footings from ABAQUS and equation (4.6)

## 4.5 CONCLUSIONS

The ultimate undrained bearing capacity of strip, square, circular and rectangular embedded footings has been investigated by finite element method. The soil is treated as weightless. The interactions between soil and the bottom of the footings are treated as being fully rough. The results obtained have been presented in terms of a normalised bearing capacity factors  $N_c$  in both graphical and tabular form; and the shape factors  $F_{cs}$ ; and the depth factors  $F_{cd}$  to facilitate their use in solving practical design problems.

The following conclusions can be made based on the finite element results:

- 
- In general, the finite element undrained bearing capacity of embedded footing compares well to the previously reported numerical limit analysis solutions. The finite element results are higher than that of Skempton (1951).
  - For strip footings, the bearing capacity factors are higher than that of both the upper and lower bound solutions of Salgado et al (2004). This is somewhat unexpected and may suggest a certain level of mesh dependency in the FE results. For square and circular footing cases, the results are very close to the upper bound limit analysis, while for rectangular footings, the bearing capacity factors lie between upper and lower bound solutions.
  - For cases where  $D/B \leq 0.2$  for strip footing,  $D/B \leq 0.4$  for rectangular footing, and  $D/B \leq 0.1$  for square and rectangular footings the failure mechanism is similar to that of a surface footing. However when the  $D/B$  is larger, the failure mechanism is localised near the footing.
  - Bearing capacity continues to increase for  $D/B \geq 4$ , and this is different from the conclusion of Skempton (1951) where the bearing capacity factor reaches a constant value in the case of  $D/B \geq 4$ . The inclusion of soil weight is likely to limit the growth in bearing capacity indefinitely.
  - The present work also gives the shape and depth factors in the form of an equation and tables to aid in their use.
-



**CHAPTER 5**  
**UNDRAINED BEARING CAPACITY OF**  
**FOOTINGS NEAR SLOPES**

---

## 5.1 INTRODUCTION

Shallow foundations are often placed on slopes, adjacent to slopes or near proposed excavations.

In this chapter, the ultimate undrained bearing capacity of footings near slopes is investigated. Consideration is given to the effect of slope angle, height of slope, the distance from the edge of the slope to the footing, soil properties and the interaction between the soil and footing. Estimates of the bearing capacity of footings on the surface of slopes are obtained using the commercial software package ABAQUS.

There are two possible collapse modes for a footing located near a slope, namely due to overall slope stability or bearing capacity failure. Both of these failure modes are affected not only by the footing load but also by the soil body forces. For these reasons, the problem of footings near slopes is more complex than that of surface footings on flat ground (Chapter 3 and Chapter 4).

This chapter is primarily concerned with estimating the vertical bearing capacity of footings on the surface of the slope in purely cohesive soil. Soil properties and the boundary conditions are able to be modelled using the finite element method. The problem can be solved using a two dimensional analysis because a state of plane strain has been assumed. In this work, soil is homogeneous with unit weight and uniform undrained soil strength.

## 5.2 PROBLEM DEFINITION

A general layout of the problem to be analysed is shown in Figure 5.1. The system includes a rigid footing and a clay soil slope. The bearing force  $Q_u$  of a footing can be expressed as:

$$Q_u = q_u B \quad (5.1)$$

where:  $B$  = footing width;

$q_u$  = the ultimate bearing capacity.

Because the soil unit weight  $\gamma$  influences the overall stability of the slope, it will affect the ultimate bearing capacity. For this problem, the ultimate bearing capacity  $q_u$  can be expressed in an equation (5.2) with dimensionless parameters:

$$\frac{q_u}{\gamma B} = f\left(\beta^\circ, \frac{L}{B}, \frac{c_u}{\gamma B}, \frac{H}{B}\right) \quad (5.2)$$

where:  $\beta^\circ$  = slope angle;

$L$  = distance from footing to the crest of the slope;

$c_u$  = the undrained soil strength;

$\gamma$  = the soil unit weight;

$H$  = the slope height;

$B$  = footing width.

The soil unit weight (i.e. gravity) and footing loads are the forces which cause instability, while resistance to failure is derived from a combination of slope geometry and soil cohesion.

The slope is assumed to be homogeneous clay (internal friction angle  $\phi = 0$ ), isotropic elasto–perfectly plastic with a failure described by the Mohr–Coulomb yield criterion. The elastic behaviour was described by a Poisson’s ratio  $\nu = 0.49$ , shear strength  $c_u$ , Young’s modulus  $E$ , a ratio of Young’s modulus to shear strength of  $E/c_u = 500$ , and soil unit weight  $\gamma$ .

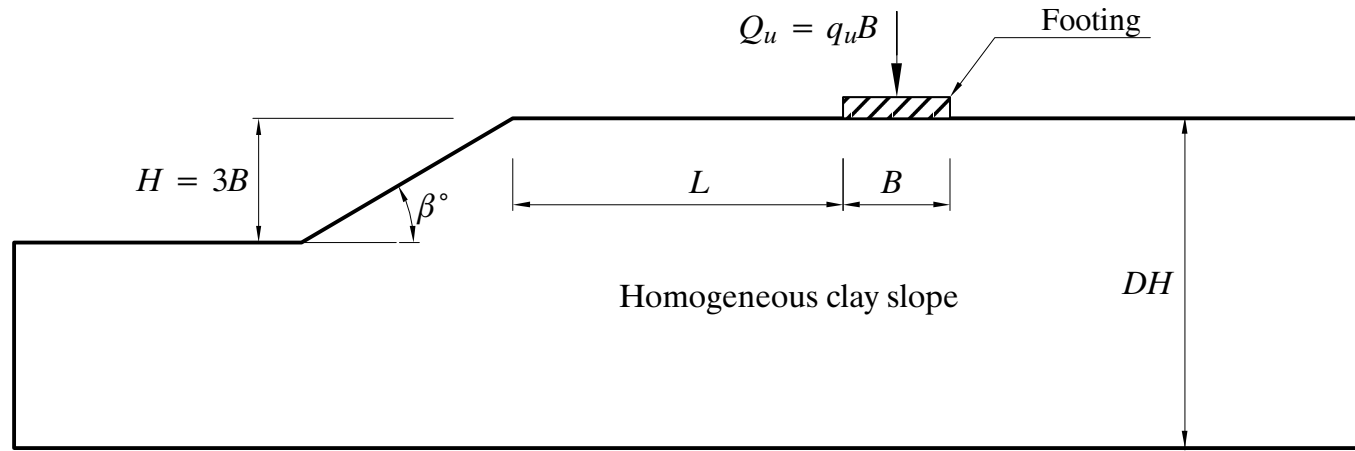
The slope has a slope angle  $\beta^\circ$ , and slope height  $H$  (Figure 5.1).  $H/B = 3$  for the cases of  $\beta^\circ = 15^\circ$  and  $30^\circ$  (Figure 5.1a);  $H/B = 5$  for the cases of  $\beta^\circ = 45^\circ, 60^\circ, 75^\circ$  and  $90^\circ$  (Figure 5.1b). The lower, left, and right limits of the problem domain are considered to be sufficiently far away from the slope so as not to influence the solution. This was achieved by first testing larger models where each side was 10 times the footing width, reductions in dimensions was made while ensuring the results of the bearing capacity changed by less than 2% from the solution obtained in the largest configuration.

In this work, the solutions have been computed for problems where:

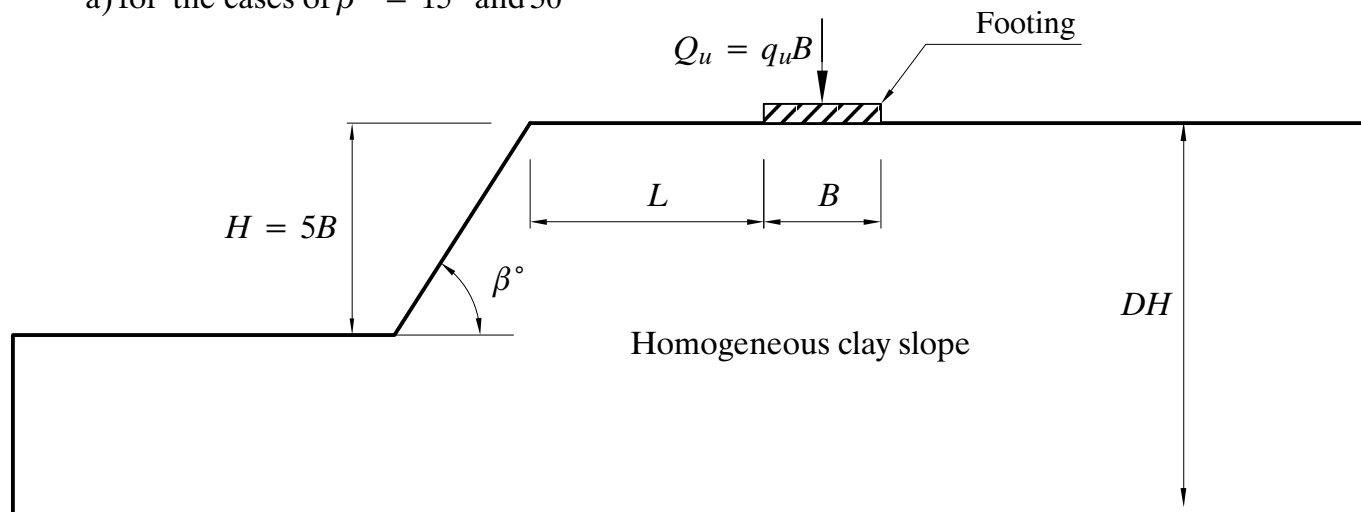
- \* the slope angle  $\beta^\circ$  varies between  $15^\circ$  and  $90^\circ$  in increments of  $15^\circ$ .
- \* the ratio  $c_u/\gamma B$  ranges from 0 to 10.
- \* the ratio  $L/B$  varies between 0 and 9 in increments of 1.

These ranges cover most problems of practical interest.

The output of the computation will be the ultimate bearing capacity  $q_u$  which can be calculated using equation (5.2).



a) for the cases of  $\beta^\circ = 15^\circ$  and  $30^\circ$



b) for the cases of  $\beta^\circ = 45^\circ, 60^\circ, 75^\circ$  and  $90^\circ$

**Figure 5.1** Problem definition for footings near slopes

### 5.3 FINITE ELEMENT MODELLING DETAILS

The finite element software ABAQUS was used for solving this problem. The ABAQUS model consisted of two parts, namely the footing and the homogeneous clay slope. At the interface between the footing and the soil, the elements representing the footing and those representing the soil have the same topology.

Typical meshes for the problem of the two-dimensional strip footings on the surface of the slope, including a magnified zone of meshing, along with the applied displacement boundary conditions, are shown in Figure 5.2 and Figure 5.3. The mesh consisted of 8-node plane strain quadrilateral, hybrid, linear pressure, reduced integration element (CPE8RH) as shown in Figure 5.4 because this element was found to provide the best solution convergence. The mesh averages 7000 quadrilateral elements and 24000 nodes depending on the positions of the footing and the slope angles.

The overall mesh dimensions were selected to ensure that the zones of plastic shearing and the observed displacement fields were contained within the model boundaries at all times. Typically, the lower boundary was fixed as it has no influence on the footing. The left-hand and the right-hand edge of the domain was fixed vertically only, however the domain is large enough so the footing also does not affect the left-hand and right-hand edge.

When a rough footing interaction was simulated, the underside of all footings was modelled as perfectly rough by specifying a “tied” contact constraint at the footing/soil interface. When a smooth footing interaction was simulated, the underside of all footings was modelled as perfectly smooth by specifying a normal contact constraint at the footing/soil interface.

To determine the collapse load of the footing, displacement defined analyses were performed where the footing was considered as being perfectly rigid (i.e. a very large Young’s Modulus was assumed). That is, a uniform vertical prescribed displacement was applied to all those nodes on the footing. The total displacement was applied over a number of sub steps and the nodal contact forces along the footing were summed to compute the equivalent bearing capacity. The number of displacement increments is automatically determined by ABAQUS, within initial, minimum, and maximum values prescribed by users.

---

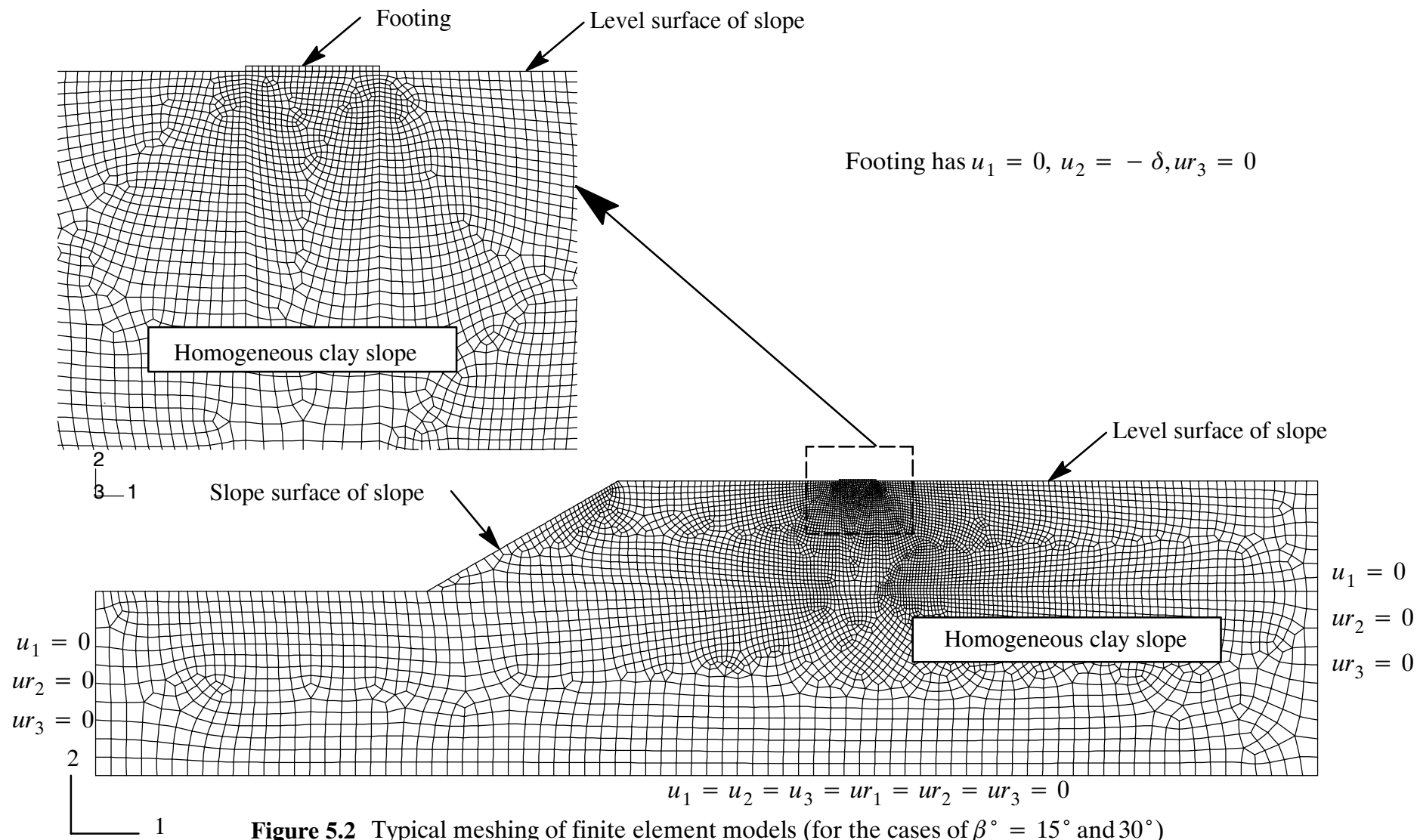


**Figure 5.2** Typical meshing of finite element models (for the cases of  $\beta^\circ = 15^\circ$  and  $30^\circ$ )

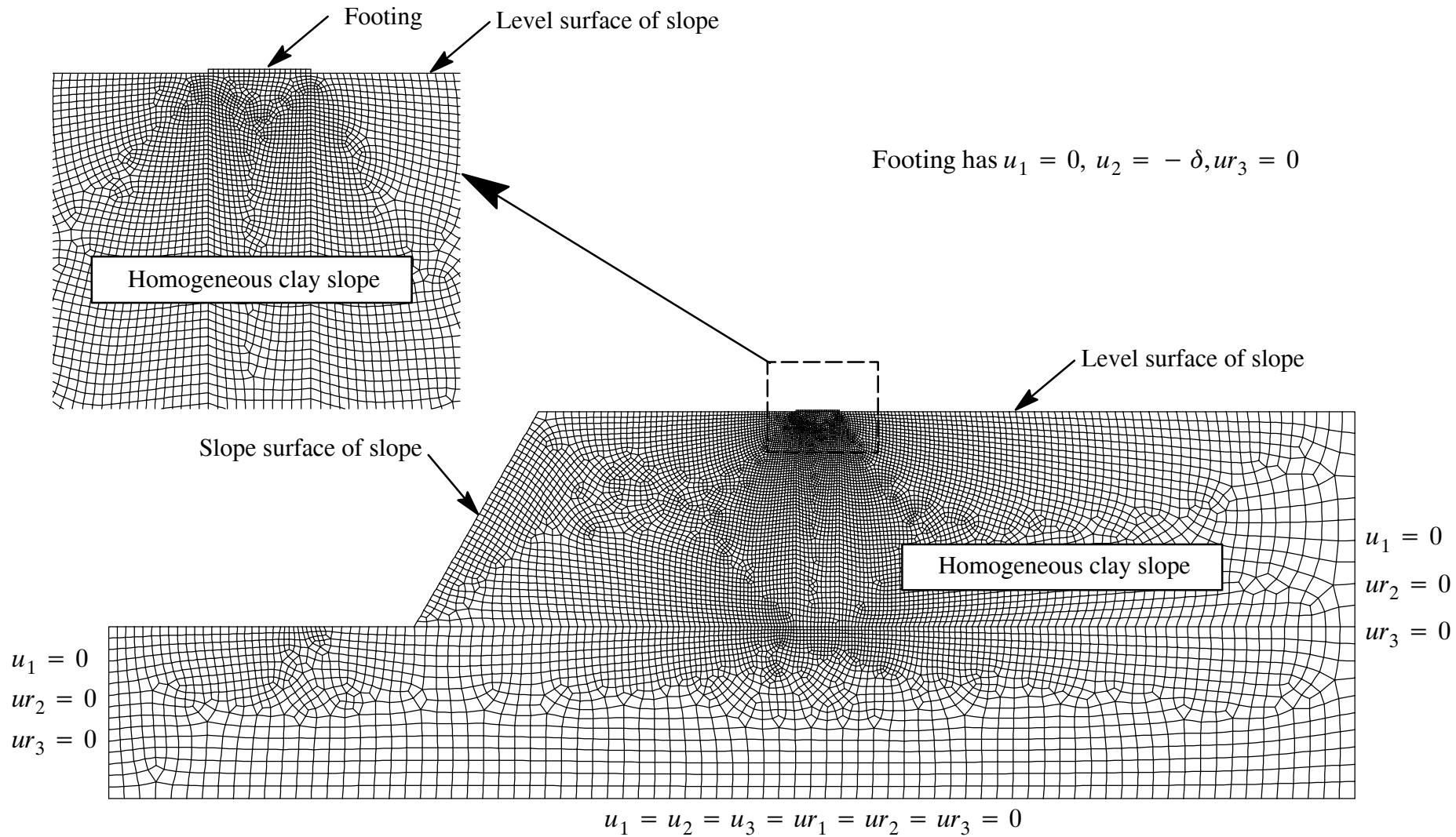
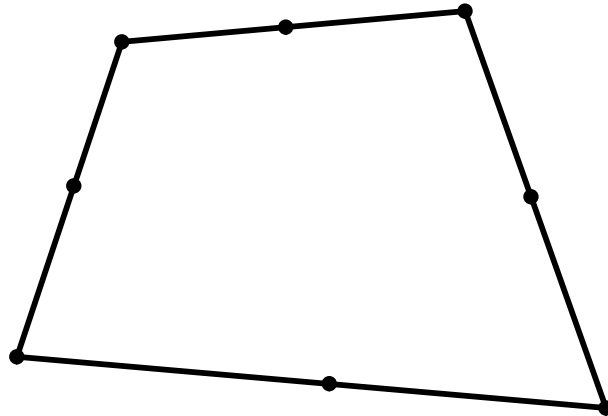


**Figure 5.3** Typical meshing of finite element models (for the cases of  $\beta^\circ = 45^\circ, 60^\circ, 75^\circ$  and  $90^\circ$ )



8–node plane strain quadrilateral, hybrid, linear pressure, reduced integration element for strip footing problems (CPE8RH)

**Figure 5.4** Element type used in ABAQUS modelling

By observing the load displacement response, a check was made to ensure that the ultimate bearing capacity has been reached and that overall collapse has in fact occurred (i.e. the load–displacement plot reaches a plateau, as shown in Figure 3.5).

## 5.4 ABAQUS FINITE ELEMENT ANALYSIS RESULTS

The computed finite element method results of the undrained bearing capacity of strip footings on the surface of slope are presented in Table 5.1 and graphically in Figure 5.5 to Figure 5.14. They express the bearing capacity in the form of the dimensionless parameter  $q_u/\gamma B$  depending on the ratio  $c_u/\gamma B$  for each value of  $L/B$  (from 0 to 9) with smooth or rough footings, where the slope angle  $\beta^\circ$  varies from  $15^\circ$  to  $90^\circ$ .

The results indicate that, in general, the dimensionless bearing capacity  $q_u/\gamma B$  increases with (i) the increase of ratio  $c_u/\gamma B$ , (ii) the increase of the ratio  $L/B$ , and (iii) the decrease of the slope angle  $\beta^\circ$ .

All these curves can be considered to have three main properties, namely (i) a linear section, (ii) a non–linear section and (iii) a point where  $q_u/\gamma B$  approaches zero.

In the linear portions the bearing capacity  $q_u/\gamma B$  increases linearly with the ratio  $c_u/\gamma B$ ; these regions are straight lines in Figure 5.5 to Figure 5.14. The linear portions of the curves shown in Figure 5.5 to Figure 5.14 for  $c_u/\gamma B \gtrsim 0.75, 0.82, 1.35, 1.52, 1.93$ , and

2.11 for the cases of  $\beta^\circ = 15^\circ, 30^\circ, 45^\circ, 60^\circ, 75^\circ$  and  $90^\circ$ , respectively. In these sections, the clay slope is strong enough ( $c_u/\gamma B$  is larger than a certain value) so failure is by bearing capacity failure and occurs either within the slope face or away from the top of the slope. The failure mechanism is that of a general shear failure of a surface footing on a level surface for larger  $L/B$  (Figure 5.17(b) and Figure 5.18(b)). For smaller values of  $L/B$  the failure mechanism occurs within the slope face itself (Figure 5.15 and Figure 5.16).

Referring to Figure 5.15 to Figure 5.20, it can be seen that the slope height  $H$  is sufficiently large for the bearing capacity of these strip footings to be independent of the slope height  $H$ . The results can therefore be used for all geometrically similar slopes with  $H/B$  greater than or equal the value used in the simulations which were 3 for the cases of  $\beta=15^\circ$  and  $30^\circ$ , and were 5 for the cases of  $\beta=45^\circ, 60^\circ, 75^\circ$  and  $90^\circ$ . When the failure is in the linear portion of the curve, the depth of the slope  $DH$  (Figure 5.1) does not affect the bearing capacity.

In the linear section, for both rough and smooth footing cases, the ultimate bearing capacity of the footings is governed by only local foundation failure (without overall stability of the slope) even when the footings stand at the crest of the slope,  $L/B = 0$  (Figure 5.15 to Figure 5.16).

The relation between  $c_u/\gamma B$  and  $q_u/\gamma B$  can be approximated as a straight line function:

$$\frac{q_u}{\gamma B} = C_1 \frac{c_u}{\gamma B} + C_2 \quad (5.3)$$

The values of the two coefficients  $C_1$  and  $C_2$  have been identified by a linear regression to the ABAQUS data and are shown in the Table 5.2 for smooth footing cases and in the Table 5.3 for the rough footing cases. The positive values of coefficient  $C_1$  indicate an increase of bearing capacity  $q_u/\gamma B$  with an increase of  $c_u/\gamma B$ . For cases when  $L/B$  is large enough, and the mode of failure is not affected by the slope, values of  $C_1$  are nearly the same for all values of slope angle  $\beta^\circ$ . In the linear section, generally when  $L/B$  is smaller than 3, the larger the slope angle, the smaller the coefficient  $C_1$ .

	$\beta = 15^\circ$		$\beta = 30^\circ$		$\beta = 45^\circ$		$\beta = 60^\circ$		$\beta = 75^\circ$		$\beta = 90^\circ$	
	$c_u/\gamma B$	$q_u/\gamma B$										
L/B=0 Smooth	10.000	46.959	10.000	41.557	10.000	35.989	10.000	30.606	10.000	25.247	10.000	19.903
	6.000	28.117	6.000	24.832	6.000	21.448	6.000	18.182	6.000	14.938	6.000	11.729
	2.000	9.286	2.000	8.093	2.000	6.884	2.000	5.725	2.000	4.602	2.000	3.527
	1.000	4.570	1.000	3.888	1.500	5.051	1.500	4.150	1.500	3.291	1.500	1.794
	0.700	2.953	0.700	2.400	1.000	2.517	1.200	3.121	1.300	2.272	1.390	1.320
	0.560	1.920	0.620	1.510	0.970	2.360	1.080	2.340	1.230	1.560	1.310	0.000
	0.490	0.000	0.540	0.000	0.925	0.000	0.980	0.000	1.120	0.000	1.310	0.000
L/B=0 Rough	10.000	49.507	10.000	45.674	10.000	41.039	10.000	36.073	10.000	30.890	10.000	25.409
	6.000	29.667	6.000	27.314	6.000	24.447	6.000	21.392	6.000	18.229	6.000	14.935
	2.000	9.822	2.000	8.917	2.000	7.807	2.000	6.635	2.000	5.498	2.000	4.400
	1.000	4.853	1.000	4.265	1.500	5.693	1.500	4.740	1.500	3.859	1.500	2.616
	0.700	3.356	0.700	2.416	1.000	2.615	1.200	3.270	1.300	2.805	1.390	1.320
	0.560	1.920	0.620	1.510	0.970	2.360	1.080	2.340	1.230	1.560	1.310	0.000
	0.490	0.000	0.540	0.000	0.925	0.000	0.980	0.000	1.120	0.000	1.310	0.000
L/B=1 Smooth	10.000	51.232	10.000	49.352	10.000	46.390	10.000	42.667	10.000	38.293	10.000	33.282
	6.000	30.731	6.000	29.559	6.000	27.696	6.000	25.345	6.000	22.560	6.000	19.398
	2.000	10.232	2.000	9.758	2.000	8.935	2.000	7.808	2.000	6.494	2.000	5.156
	1.000	5.103	1.000	4.734	1.500	6.504	1.500	5.032	1.500	3.690	1.500	1.768
	0.700	3.562	0.700	2.440	1.000	2.188	1.200	2.748	1.300	2.325	1.390	1.120
	0.560	1.920	0.620	1.510	0.970	2.060	1.080	1.740	1.230	1.560	1.310	0.000
	0.490	0.000	0.540	0.000	0.925	0.000	0.980	0.000	1.120	0.000	1.310	0.000
L/B=1 Rough	10.000	51.956	10.000	51.080	10.000	48.478	10.000	45.202	10.000	40.974	10.000	35.919
	6.000	31.174	6.000	30.602	6.000	28.956	6.000	26.828	6.000	24.084	6.000	20.871
	2.000	10.382	2.000	10.121	2.000	9.333	2.000	8.117	2.000	6.695	2.000	5.352
	1.000	5.182	1.000	4.800	1.500	6.526	1.500	5.041	1.500	3.756	1.500	2.284
	0.700	3.620	0.700	2.471	1.000	2.559	1.200	3.200	1.300	2.325	1.390	1.320
	0.560	1.920	0.620	1.510	0.970	2.360	1.080	2.340	1.230	1.560	1.310	0.000
	0.490	0.000	0.540	0.000	0.925	0.000	0.980	0.000	1.120	0.000	1.310	0.000

Table 5.1 Bearing capacity results for  $L/B=0$  and 1

	$\beta = 15^\circ$		$\beta = 30^\circ$		$\beta = 45^\circ$		$\beta = 60^\circ$		$\beta = 75^\circ$		$\beta = 90^\circ$	
	$c_u/\gamma B$	$q_u/\gamma B$										
L/B=2 Smooth	10.000	51.966	10.000	52.210	10.000	52.071	10.000	49.389	10.000	45.593	10.000	40.865
	6.000	31.200	6.000	31.324	6.000	31.228	6.000	29.365	6.000	26.821	6.000	23.678
	2.000	10.402	2.000	10.443	2.000	10.140	2.000	8.523	2.000	6.764	2.000	5.156
	1.000	5.201	1.000	5.062	1.500	6.672	1.500	5.024	1.500	3.436	1.500	1.639
	0.700	3.641	0.700	2.579	1.000	1.987	1.200	2.546	1.300	1.888	1.390	1.020
	0.560	1.920	0.620	1.510	0.970	1.360	1.080	1.340	1.230	1.260	1.310	0.000
	0.490	0.000	0.540	0.000	0.925	0.000	0.980	0.000	1.120	0.000	1.310	0.000
L/B=2 Rough	10.000	52.440	10.000	52.991	10.000	52.393	10.000	50.367	10.000	47.097	10.000	42.549
	6.000	31.461	6.000	31.788	6.000	30.700	6.000	29.997	6.000	27.713	6.000	24.573
	2.000	10.489	2.000	10.606	2.000	10.254	2.000	8.594	2.000	6.843	2.000	5.105
	1.000	5.245	1.000	5.108	1.500	6.699	1.500	5.068	1.500	3.537	1.500	2.030
	0.700	3.671	0.700	2.610	1.000	2.092	1.200	2.637	1.300	2.081	1.390	1.020
	0.560	1.920	0.620	1.510	0.970	1.360	1.080	1.340	1.230	1.260	1.310	0.000
	0.490	0.000	0.540	0.000	0.925	0.000	0.980	0.000	1.120	0.000	1.310	0.000
L/B=3 Smooth	10.000	52.077	10.000	52.077	10.000	52.075	10.000	52.081	10.000	50.926	10.000	46.409
	6.000	31.206	6.000	31.247	6.000	31.244	6.000	31.248	6.000	29.925	6.000	26.712
	2.000	10.416	2.000	10.415	2.000	10.415	2.000	9.047	2.000	7.251	2.000	5.175
	1.000	5.208	1.000	5.208	1.500	6.998	1.500	5.305	1.500	3.631	1.500	1.648
	0.700	3.646	0.700	2.771	1.000	1.978	1.200	2.629	1.300	1.983	1.390	1.020
	0.560	1.920	0.620	1.510	0.970	1.360	1.080	1.340	1.230	1.260	1.310	0.000
	0.490	0.000	0.540	0.000	0.925	0.000	0.980	0.000	1.120	0.000	1.310	0.000
L/B=3 Rough	10.000	52.473	10.000	52.495	10.000	52.464	10.000	52.469	10.000	51.785	10.000	47.658
	6.000	31.471	6.000	31.503	6.000	31.500	6.000	31.504	6.000	30.059	6.000	27.378
	2.000	10.489	2.000	10.500	2.000	10.493	2.000	9.127	2.000	7.424	2.000	5.410
	1.000	5.250	1.000	5.250	1.500	7.031	1.500	5.378	1.500	3.857	1.500	2.074
	0.700	3.671	0.700	2.797	1.000	2.092	1.200	2.786	1.300	2.272	1.390	1.020
	0.560	1.920	0.620	1.510	0.970	1.360	1.080	1.340	1.230	1.260	1.310	0.000
	0.490	0.000	0.540	0.000	0.925	0.000	0.980	0.000	1.120	0.000	1.310	0.000

Table 5.1 (continued) Bearing capacity results  $L/B=2$  and 3

		$\beta = 15^\circ$		$\beta = 30^\circ$		$\beta = 45^\circ$		$\beta = 60^\circ$		$\beta = 75^\circ$		$\beta = 90^\circ$	
		$c_u/\gamma B$	$q_u/\gamma B$										
L/B=4 Smooth	10.000	52.146	10.000	52.145	10.000	52.074	10.000	52.068	10.000	52.097	10.000	50.663	
	6.000	31.287	6.000	31.288	6.000	31.450	6.000	31.242	6.000	31.258	6.000	29.051	
	2.000	10.429	2.000	10.429	2.000	10.485	2.000	9.673	2.000	7.880	2.000	5.790	
	1.000	5.215	1.000	5.215	1.500	7.418	1.500	5.783	1.500	4.036	1.500	1.904	
	0.700	3.650	0.700	2.971	1.000	2.092	1.200	2.971	1.300	2.201	1.390	1.020	
	0.560	1.920	0.620	1.510	0.970	1.360	1.080	1.340	1.230	1.260	1.310	0.000	
	0.490	0.000	0.540	0.000	0.925	0.000	0.980	0.000	1.120	0.000	1.310	0.000	
L/B=4 Rough	10.000	52.554	10.000	52.542	10.000	53.256	10.000	52.462	10.000	52.463	10.000	51.355	
	6.000	31.532	6.000	31.539	6.000	31.942	6.000	31.478	6.000	31.493	6.000	29.572	
	2.000	10.511	2.000	10.501	2.000	10.655	2.000	9.759	2.000	8.023	2.000	6.082	
	1.000	5.256	1.000	5.257	1.500	7.478	1.500	5.868	1.500	4.249	1.500	2.443	
	0.700	3.679	0.700	2.989	1.000	2.227	1.200	3.142	1.300	2.550	1.390	1.020	
	0.560	1.920	0.620	1.510	0.970	1.360	1.080	1.340	1.230	1.260	1.310	0.000	
	0.490	0.000	0.540	0.000	0.925	0.000	0.980	0.000	1.120	0.000	1.310	0.000	
L/B=5 Smooth	10.000	52.125	10.000	52.125	10.000	52.070	10.000	52.116	10.000	52.112	10.000	52.129	
	6.000	31.272	6.000	31.277	6.000	31.241	6.000	31.276	6.000	31.252	6.000	31.178	
	2.000	10.422	2.000	10.425	2.000	10.414	2.000	10.356	2.000	8.687	2.000	6.644	
	1.000	5.209	1.000	5.212	1.500	7.798	1.500	6.377	1.500	4.701	1.500	2.479	
	0.700	3.648	0.700	3.156	1.000	2.221	1.200	3.467	1.300	2.779	1.390	1.020	
	0.560	1.920	0.620	1.510	0.970	1.360	1.080	1.340	1.230	1.260	1.310	0.000	
	0.490	0.000	0.540	0.000	0.925	0.000	0.980	0.000	1.120	0.000	1.310	0.000	
L/B=5 Rough	10.000	52.546	10.000	52.541	10.000	52.461	10.000	52.554	10.000	52.510	10.000	52.559	
	6.000	31.526	6.000	31.521	6.000	31.467	6.000	31.228	6.000	31.506	6.000	31.308	
	2.000	10.509	2.000	10.504	2.000	10.489	2.000	10.396	2.000	8.830	2.000	6.913	
	1.000	5.255	1.000	5.251	1.500	7.850	1.500	6.462	1.500	4.903	1.500	2.999	
	0.700	3.678	0.700	3.170	1.000	2.333	1.200	3.623	1.300	3.108	1.390	1.020	
	0.560	1.920	0.620	1.510	0.970	1.360	1.080	1.340	1.230	1.260	1.310	0.000	
	0.490	0.000	0.540	0.000	0.925	0.000	0.980	0.000	1.120	0.000	1.310	0.000	

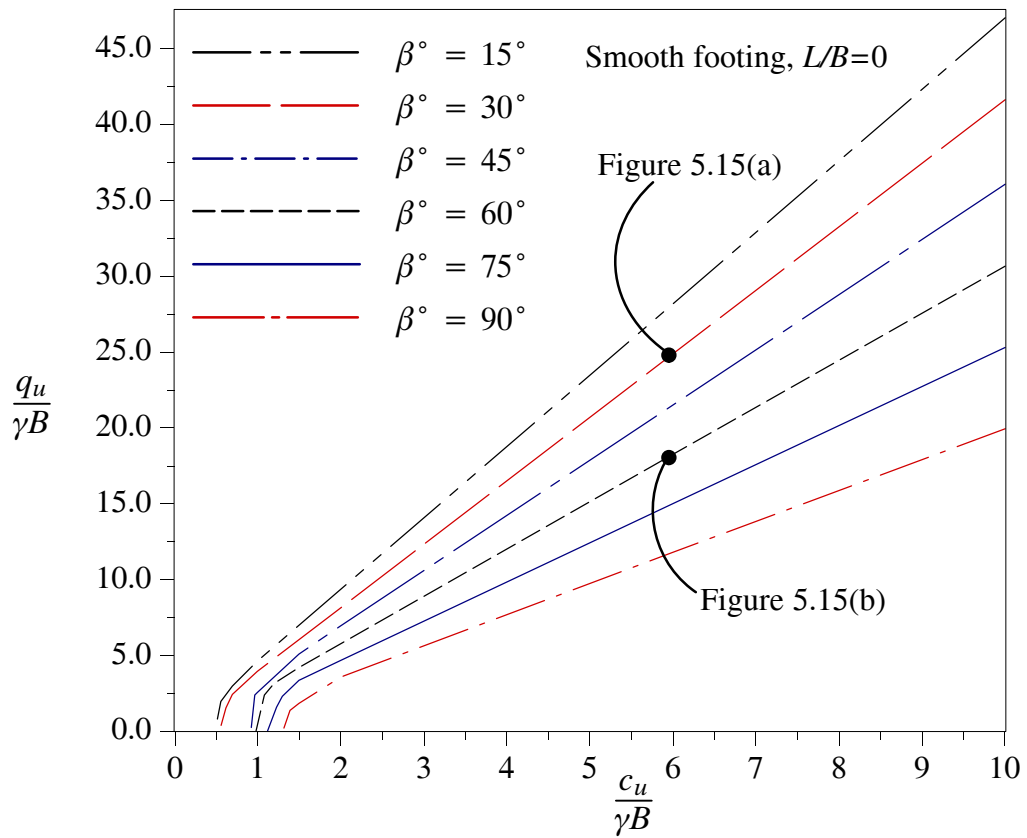
Table 5.1 (continued) Bearing capacity results L/B=4 and 5

	$\beta = 15^\circ$		$\beta = 30^\circ$		$\beta = 45^\circ$		$\beta = 60^\circ$		$\beta = 75^\circ$		$\beta = 90^\circ$	
	$c_u/\gamma B$	$q_u/\gamma B$										
L/B=6 Smooth	10.000	52.121	10.000	52.108	10.000	52.075	10.000	52.073	10.000	52.069	10.000	52.070
	6.000	31.271	6.000	31.269	6.000	31.245	6.000	31.238	6.000	31.241	6.000	31.243
	2.000	10.424	2.000	10.423	2.000	10.415	2.000	10.414	2.000	9.504	2.000	7.612
	1.000	5.211	1.000	5.208	1.500	7.811	1.500	6.948	1.500	5.455	1.500	3.363
	0.700	3.648	0.700	3.327	1.000	2.344	1.200	3.977	1.300	3.497	1.390	1.020
	0.560	1.920	0.620	1.510	0.970	1.360	1.080	1.340	1.230	1.260	1.310	0.000
	0.490	0.000	0.540	0.000	0.925	0.000	0.980	0.000	1.120	0.000	1.310	0.000
L/B=6 Rough	10.000	52.510	10.000	52.537	10.000	52.484	10.000	52.477	10.000	52.456	10.000	52.461
	6.000	31.521	6.000	31.523	6.000	31.492	6.000	31.485	6.000	31.470	6.000	31.477
	2.000	10.508	2.000	10.507	2.000	10.497	2.000	10.496	2.000	9.631	2.000	7.858
	1.000	5.254	1.000	5.253	1.500	7.873	1.500	7.030	1.500	5.633	1.500	3.811
	0.700	3.676	0.700	3.339	1.000	2.442	1.200	4.110	1.300	3.768	1.390	1.020
	0.560	1.920	0.620	1.510	0.970	1.360	1.080	1.340	1.230	1.260	1.310	0.000
	0.490	0.000	0.540	0.000	0.925	0.000	0.980	0.000	1.120	0.000	1.310	0.000
L/B=7 Smooth	10.000	52.115	10.000	52.113	10.000	52.192	10.000	52.163	10.000	52.195	10.000	52.193
	6.000	31.270	6.000	31.269	6.000	31.316	6.000	31.316	6.000	31.315	6.000	31.317
	2.000	10.423	2.000	10.423	2.000	10.439	2.000	10.438	2.000	10.300	2.000	8.645
	1.000	5.211	1.000	5.212	1.500	7.829	1.500	7.544	1.500	6.210	1.500	4.370
	0.700	3.648	0.700	3.485	1.000	2.467	1.200	4.498	1.300	4.230	1.390	1.020
	0.560	1.920	0.620	1.510	0.970	1.360	1.080	1.340	1.230	1.260	1.310	0.000
	0.490	0.000	0.540	0.000	0.925	0.000	0.980	0.000	1.120	0.000	1.310	0.000
L/B=7 Rough	10.000	52.532	10.000	52.527	10.000	52.629	10.000	52.635	10.000	52.637	10.000	52.620
	6.000	31.520	6.000	31.517	6.000	31.582	6.000	31.576	6.000	31.580	6.000	31.582
	2.000	10.500	2.000	10.498	2.000	10.528	2.000	10.473	2.000	10.361	2.000	8.870
	1.000	5.257	1.000	5.254	1.500	7.890	1.500	7.603	1.500	6.371	1.500	4.734
	0.700	3.677	0.700	3.496	1.000	2.565	1.200	4.598	1.300	4.452	1.390	1.020
	0.560	1.920	0.620	1.510	0.970	1.360	1.080	1.340	1.230	1.260	1.310	0.000
	0.490	0.000	0.540	0.000	0.925	0.000	0.980	0.000	1.120	0.000	1.310	0.000

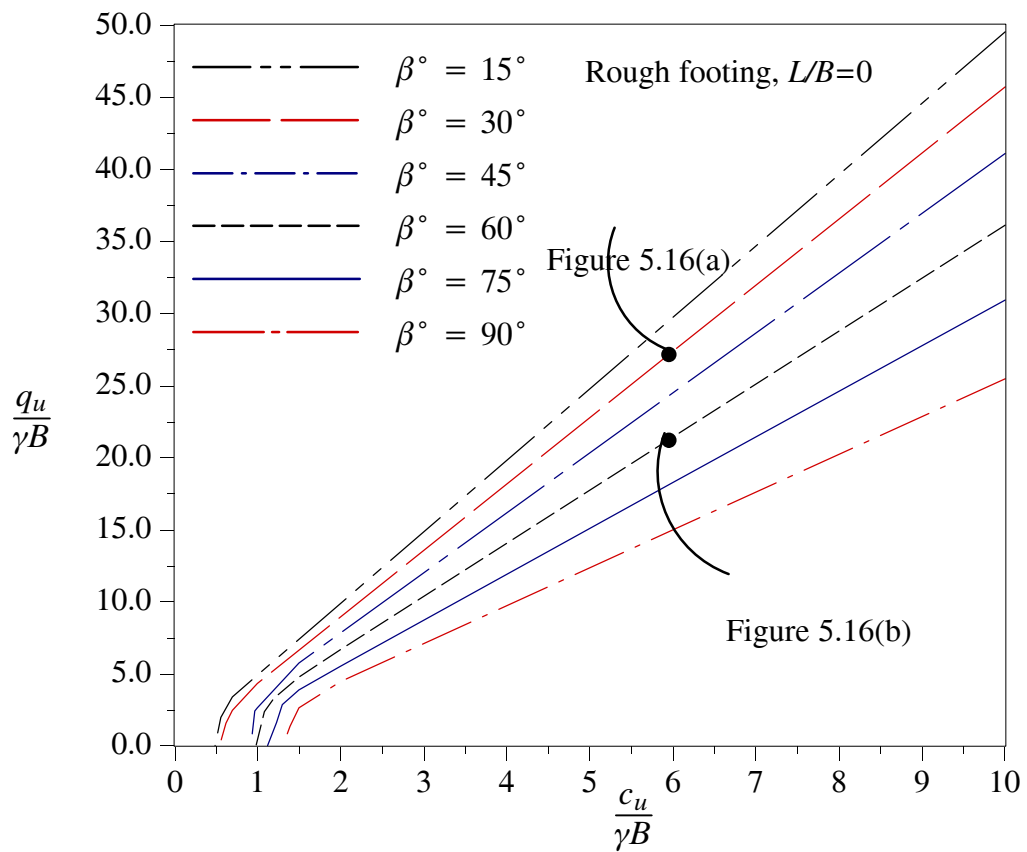
Table 5.1 (continued) Bearing capacity results  $L/B=6$  and  $7$

	$\beta = 15^\circ$		$\beta = 30^\circ$		$\beta = 45^\circ$		$\beta = 60^\circ$		$\beta = 75^\circ$		$\beta = 90^\circ$	
	$c_u/\gamma B$	$q_u/\gamma B$										
L/B=8 Smooth	10.000	52.167	10.000	52.181	10.000	52.204	10.000	52.205	10.000	52.206	10.000	52.202
	6.000	31.280	6.000	31.280	6.000	31.340	6.000	31.323	6.000	31.324	6.000	31.324
	2.000	10.434	2.000	10.437	2.000	10.441	2.000	10.441	2.000	10.441	2.000	9.562
	1.000	5.211	1.000	5.210	1.500	7.831	1.500	7.831	1.500	6.914	1.500	5.295
	0.700	3.651	0.700	3.633	1.000	2.650	1.200	4.938	1.300	4.912	1.390	1.020
	0.560	1.920	0.620	1.510	0.970	1.360	1.080	1.340	1.230	1.260	1.310	0.000
	0.490	0.000	0.540	0.000	0.925	0.000	0.980	0.000	1.120	0.000	1.310	0.000
L/B=8 Rough	10.000	52.582	10.000	52.617	10.000	52.648	10.000	52.641	10.000	52.646	10.000	52.640
	6.000	31.511	6.000	31.555	6.000	31.587	6.000	31.585	6.000	31.564	6.000	31.614
	2.000	10.522	2.000	10.510	2.000	10.530	2.000	10.530	2.000	10.528	2.000	9.725
	1.000	5.261	1.000	5.262	1.500	7.898	1.500	7.897	1.500	7.042	1.500	5.580
	0.700	3.683	0.700	3.643	1.000	2.751	1.200	5.012	1.300	5.077	1.390	1.020
	0.560	1.920	0.620	1.510	0.970	1.360	1.080	1.340	1.230	1.260	1.310	0.000
	0.490	0.000	0.540	0.000	0.925	0.000	0.980	0.000	1.120	0.000	1.310	0.000
L/B=9 Smooth	10.000	52.138	10.000	52.137	10.000	52.266	10.000	52.269	10.000	52.231	10.000	52.221
	6.000	31.282	6.000	31.281	6.000	31.360	6.000	31.358	6.000	31.341	6.000	31.335
	2.000	10.428	2.000	10.427	2.000	10.453	2.000	10.452	2.000	10.447	2.000	10.422
	1.000	5.211	1.000	5.214	1.500	7.840	1.500	7.841	1.500	7.547	1.500	6.186
	0.700	3.650	0.700	3.649	1.000	3.034	1.200	4.925	1.300	5.504	1.390	1.020
	0.560	1.920	0.620	1.510	0.970	1.360	1.080	1.340	1.230	1.260	1.310	0.000
	0.490	0.000	0.540	0.000	0.925	0.000	0.980	0.000	1.120	0.000	1.310	0.000
L/B=9 Rough	10.000	52.567	10.000	52.523	10.000	52.767	10.000	52.773	10.000	52.736	10.000	52.739
	6.000	31.543	6.000	31.537	6.000	31.655	6.000	31.648	6.000	31.642	6.000	31.645
	2.000	10.515	2.000	10.512	2.000	10.555	2.000	10.555	2.000	10.542	2.000	10.471
	1.000	5.253	1.000	5.257	1.500	7.916	1.500	7.916	1.500	7.618	1.500	6.186
	0.700	3.680	0.700	3.680	1.000	2.938	1.200	5.384	1.300	5.627	1.390	1.020
	0.560	1.920	0.620	1.510	0.970	1.360	1.080	1.340	1.230	1.260	1.310	0.000
	0.490	0.000	0.540	0.000	0.925	0.000	0.980	0.000	1.120	0.000	1.310	0.000

Table 5.1 (continued) Bearing capacity results  $L/B=8$  and  $9$

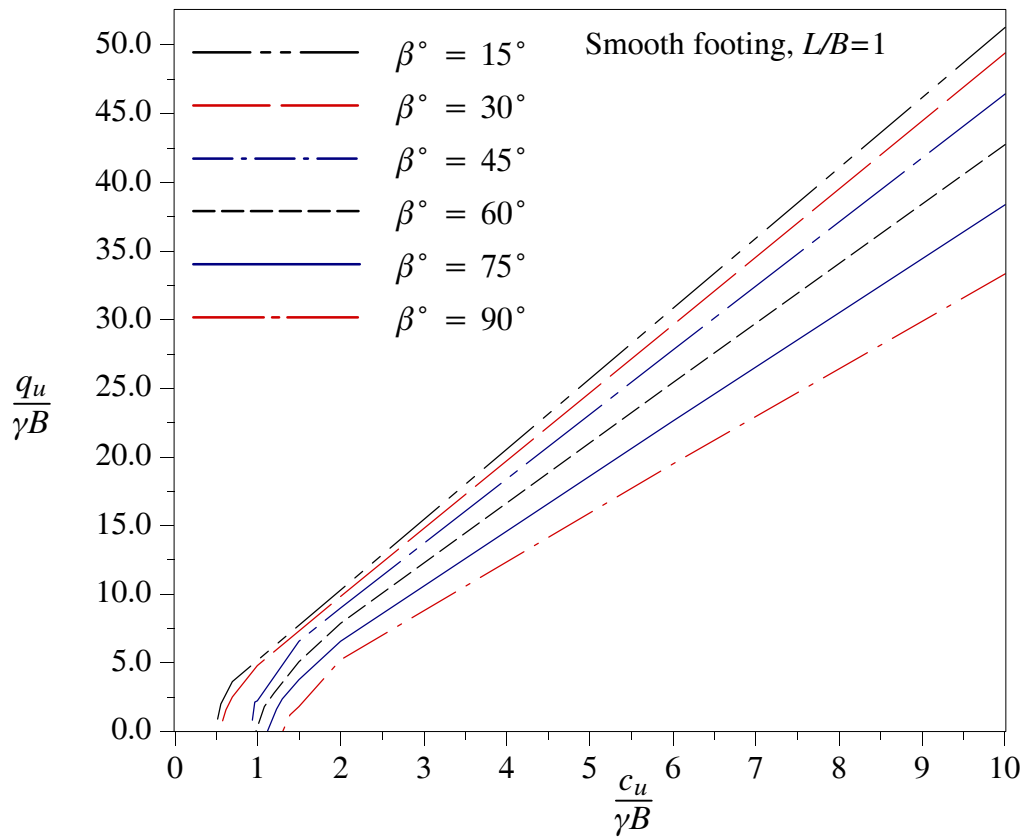


(a)

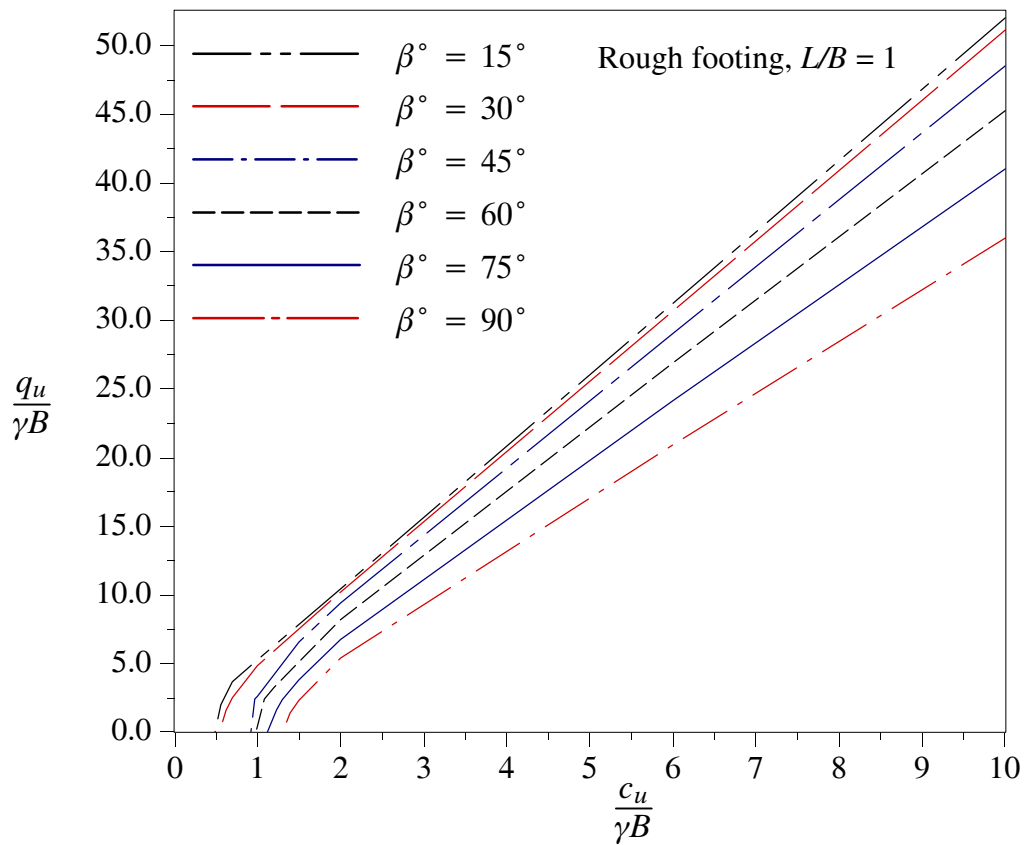


(b)

**Figure 5.5** Bearing capacity of (a) smooth & (b) rough footings, ( $L/B=0$ )



(a)



(b)

**Figure 5.6** Bearing capacity of (a) smooth & (b) rough footings, ( $L/B=1$ )

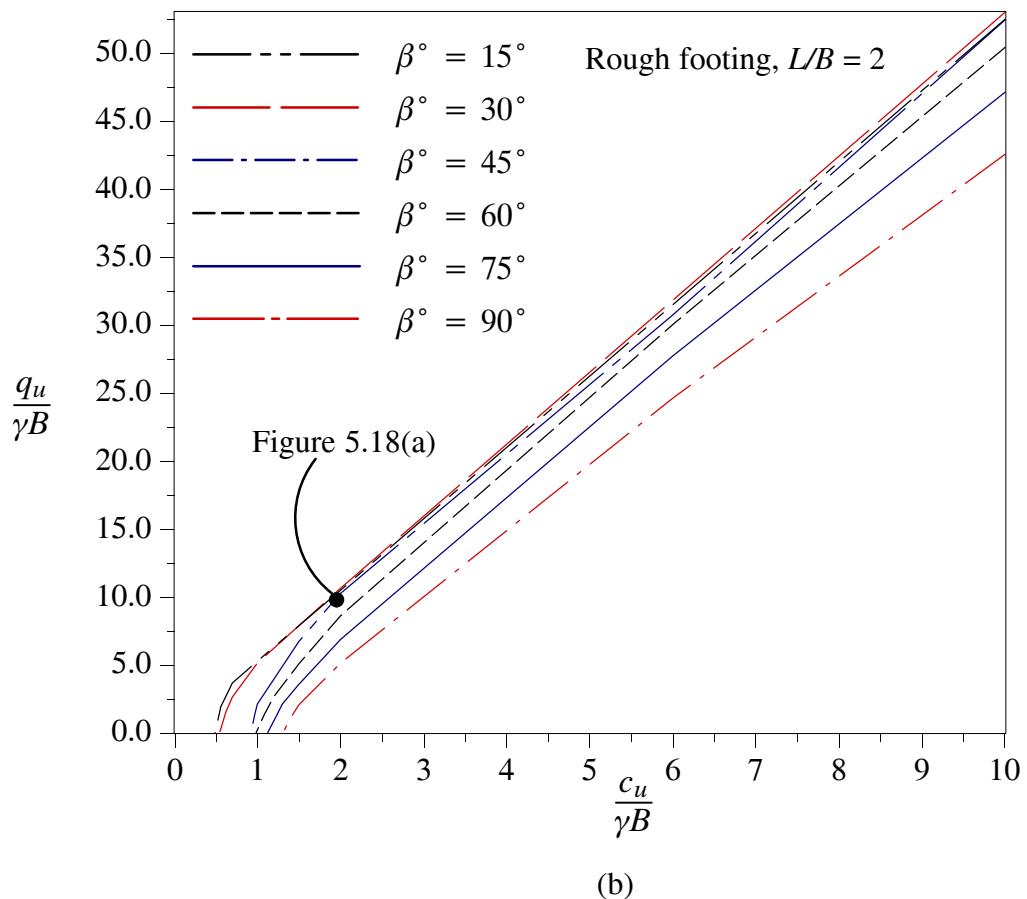
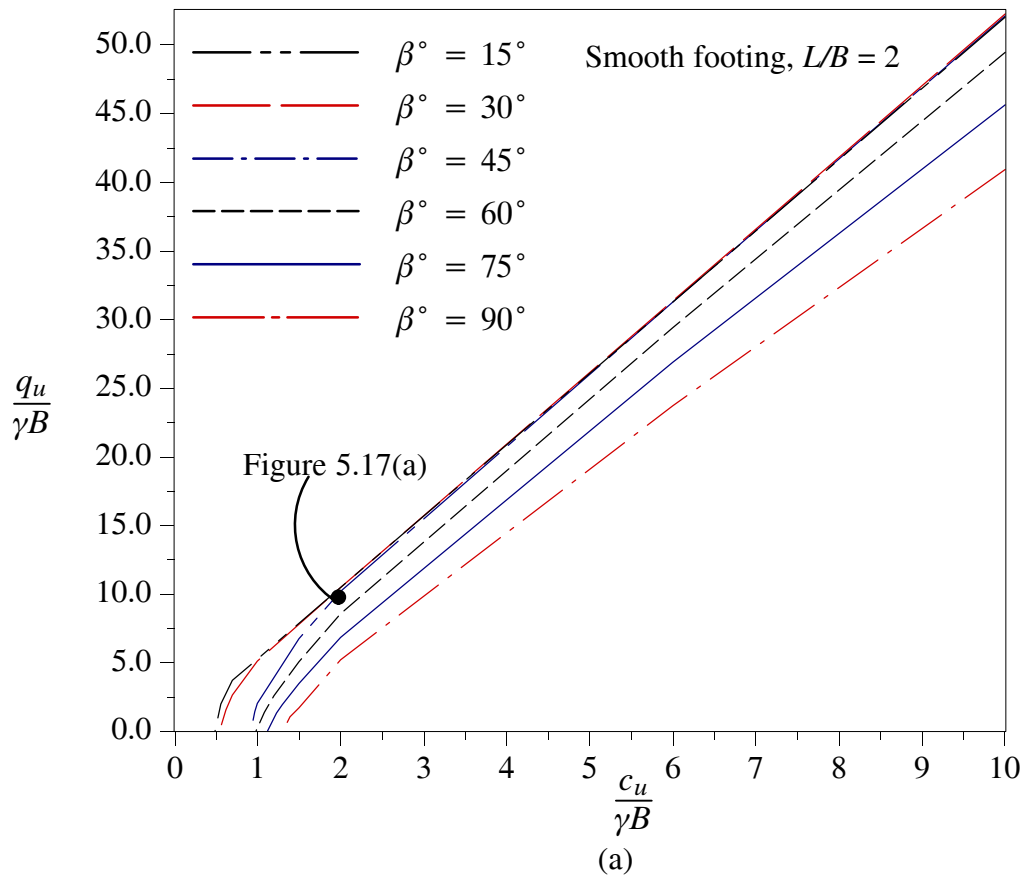


**Figure 5.7** Bearing capacity of (a) smooth & (b) rough footings, ( $L/B=2$ )

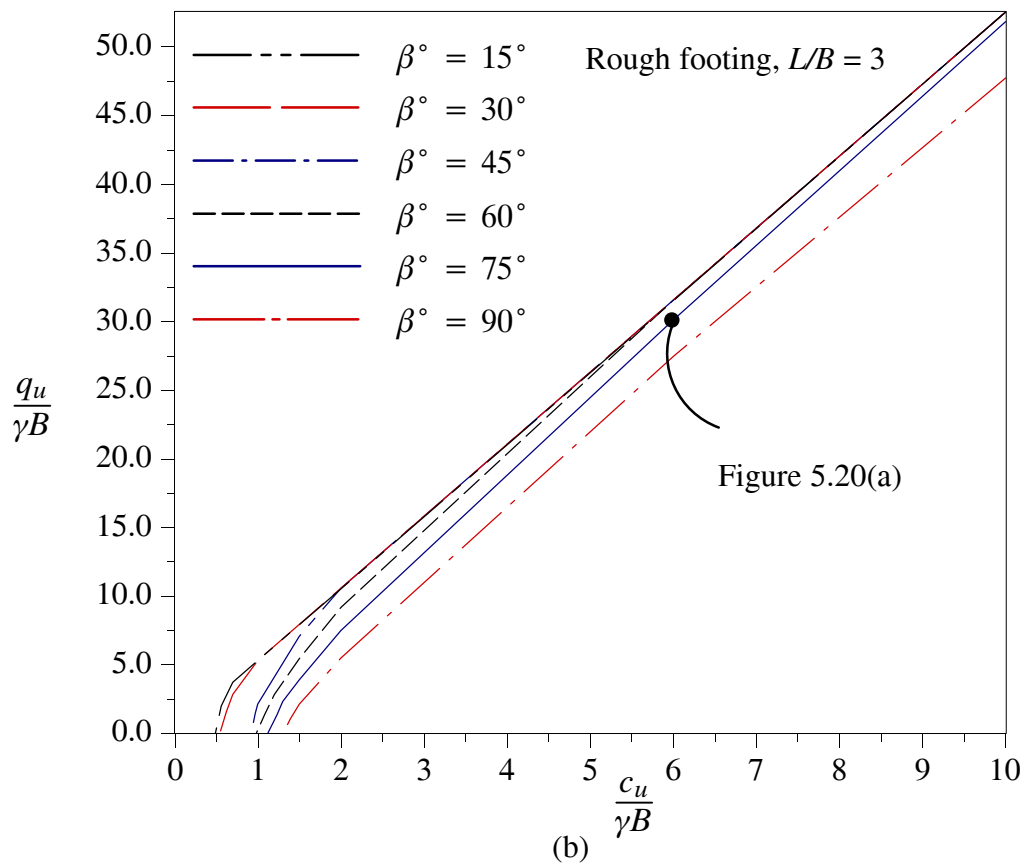
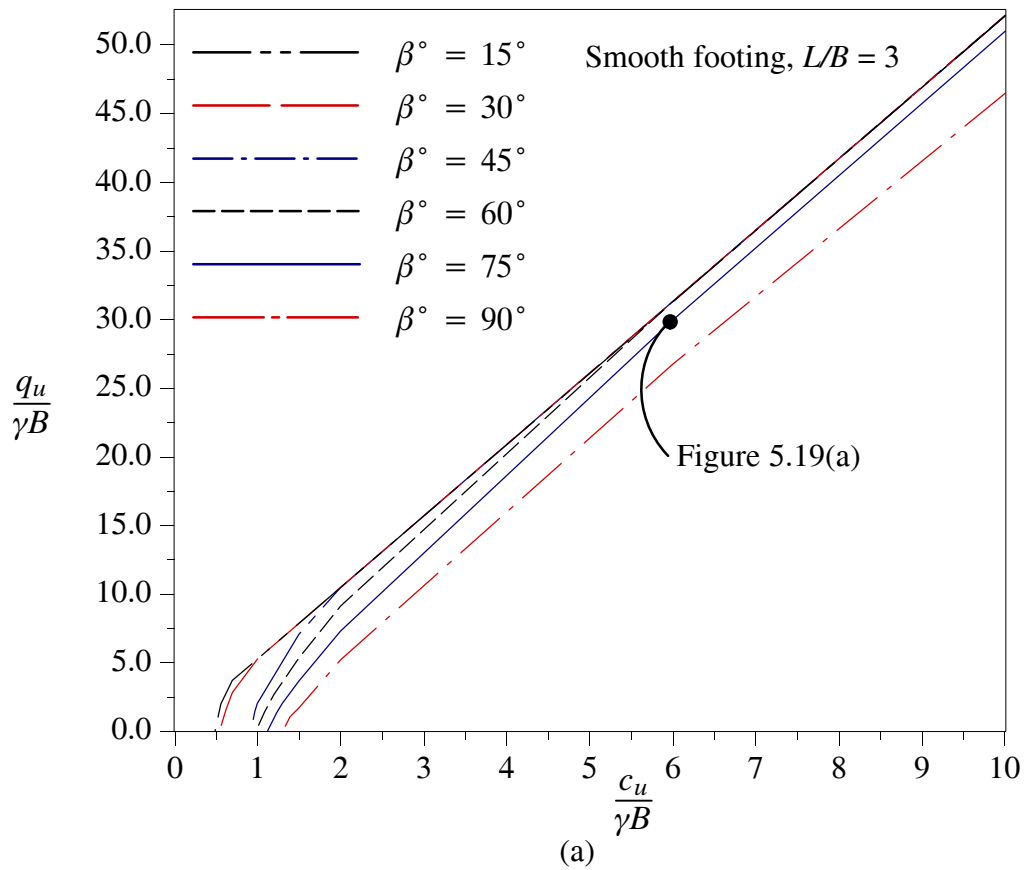


**Figure 5.8** Bearing capacity of (a) smooth & (b) rough footings, ( $L/B=3$ )

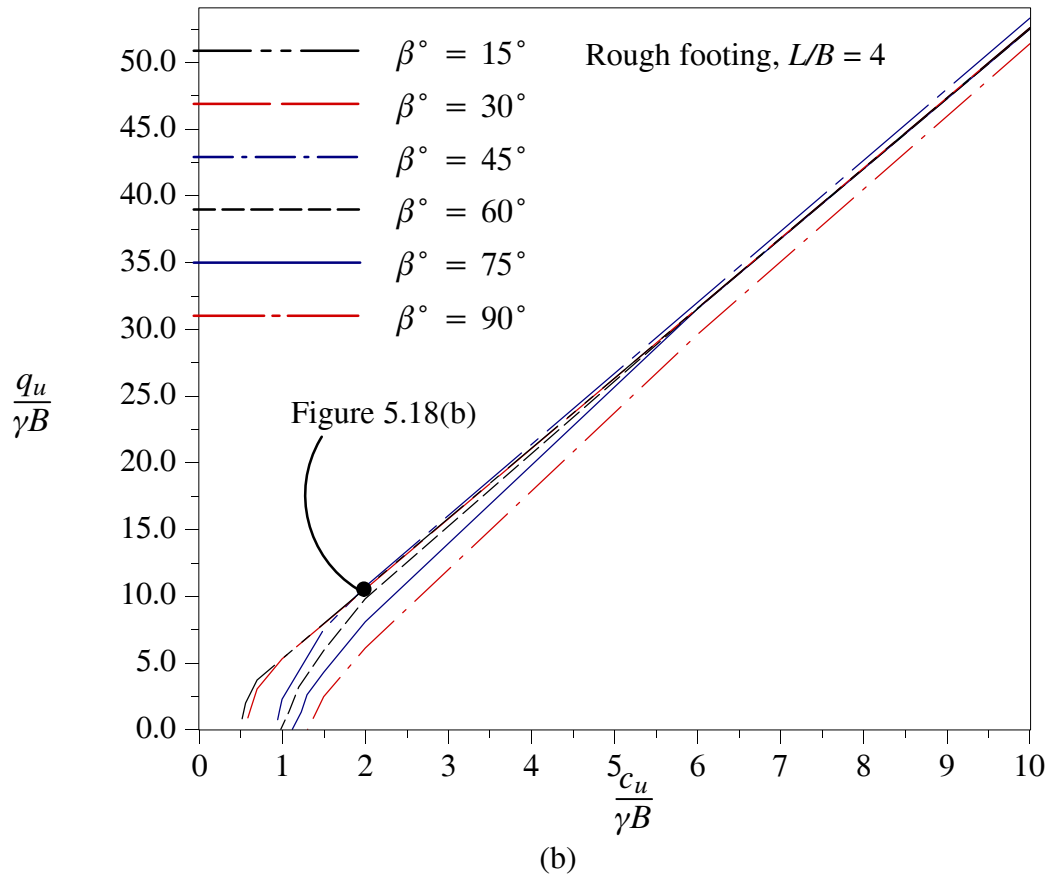
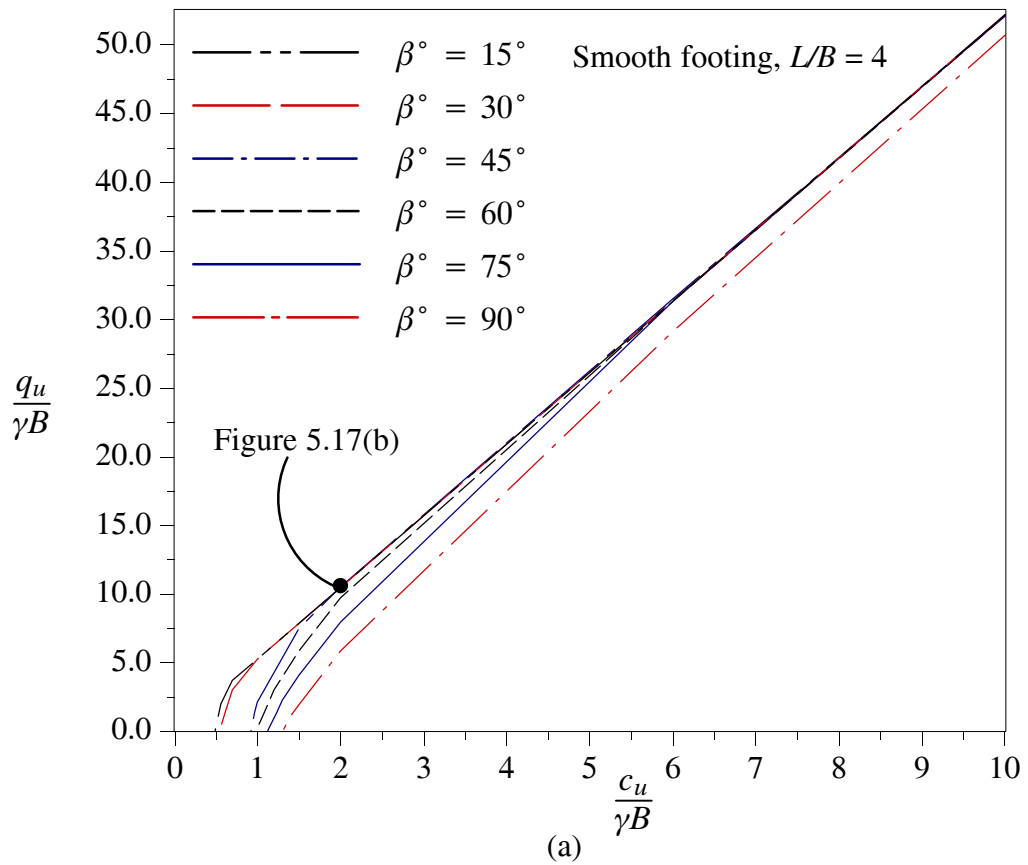


**Figure 5.9** Bearing capacity of (a) smooth & (b) rough footings, ( $L/B=4$ )

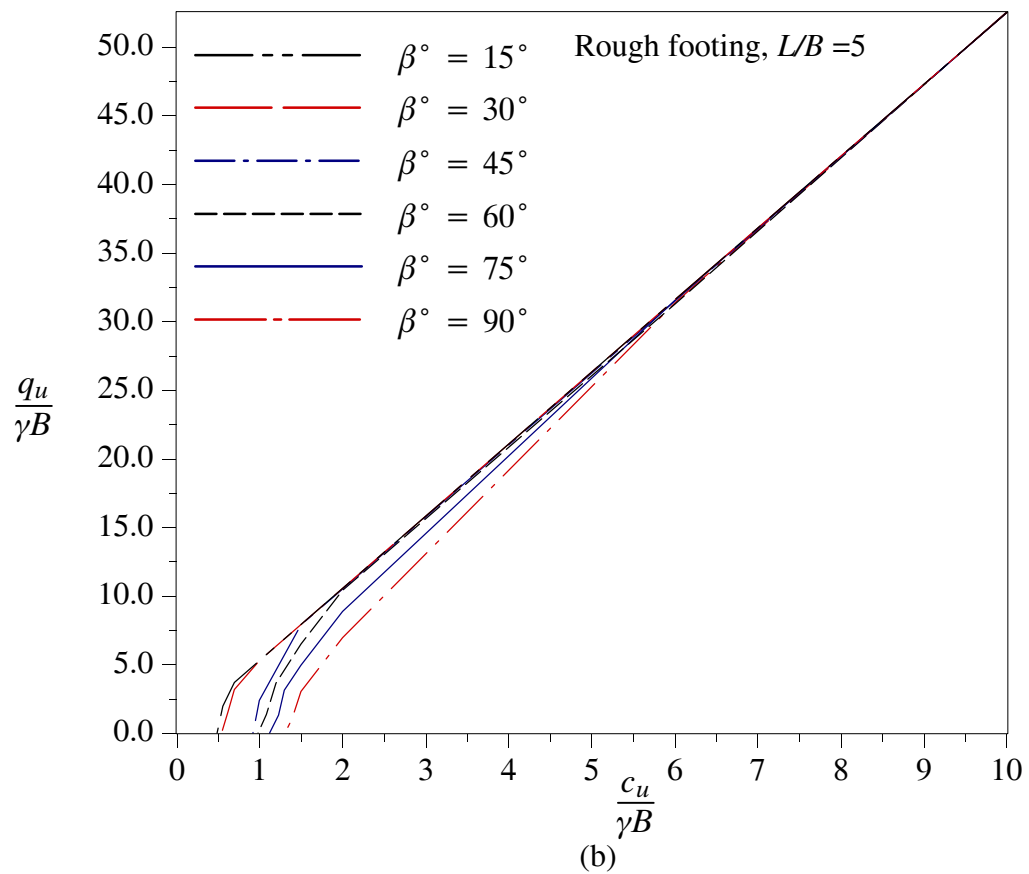
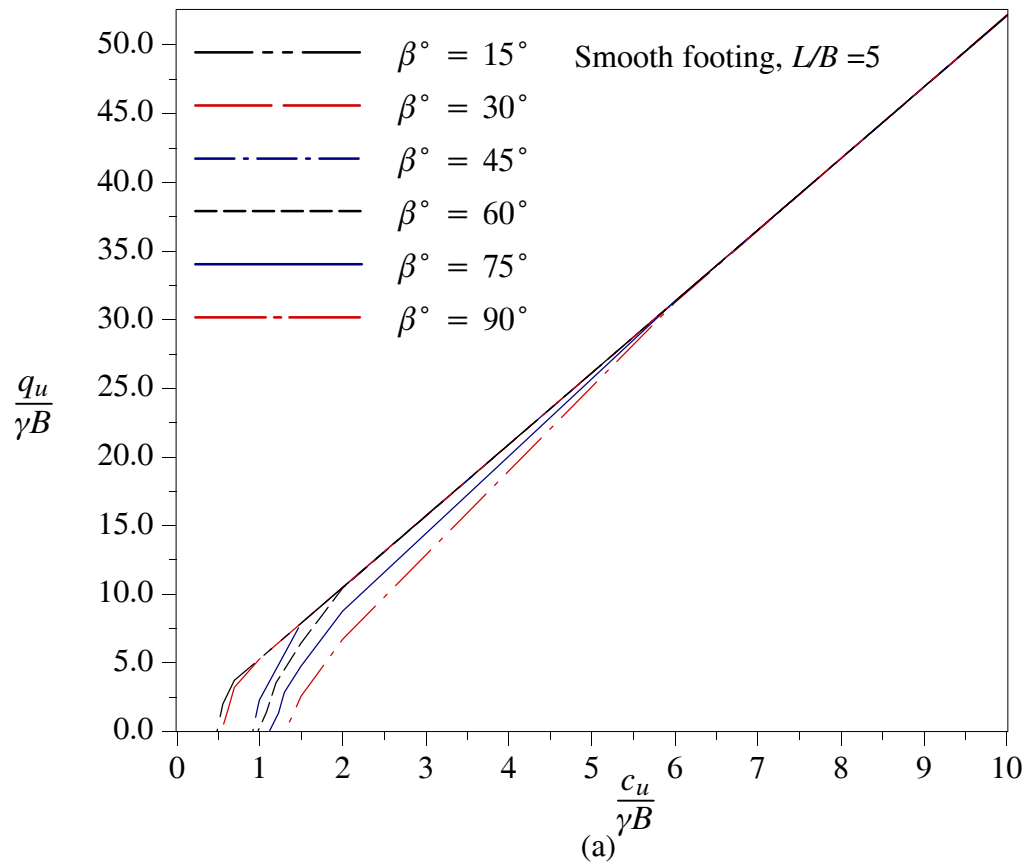


**Figure 5.10** Bearing capacity of (a) smooth & (b) rough footings, ( $L/B=5$ )

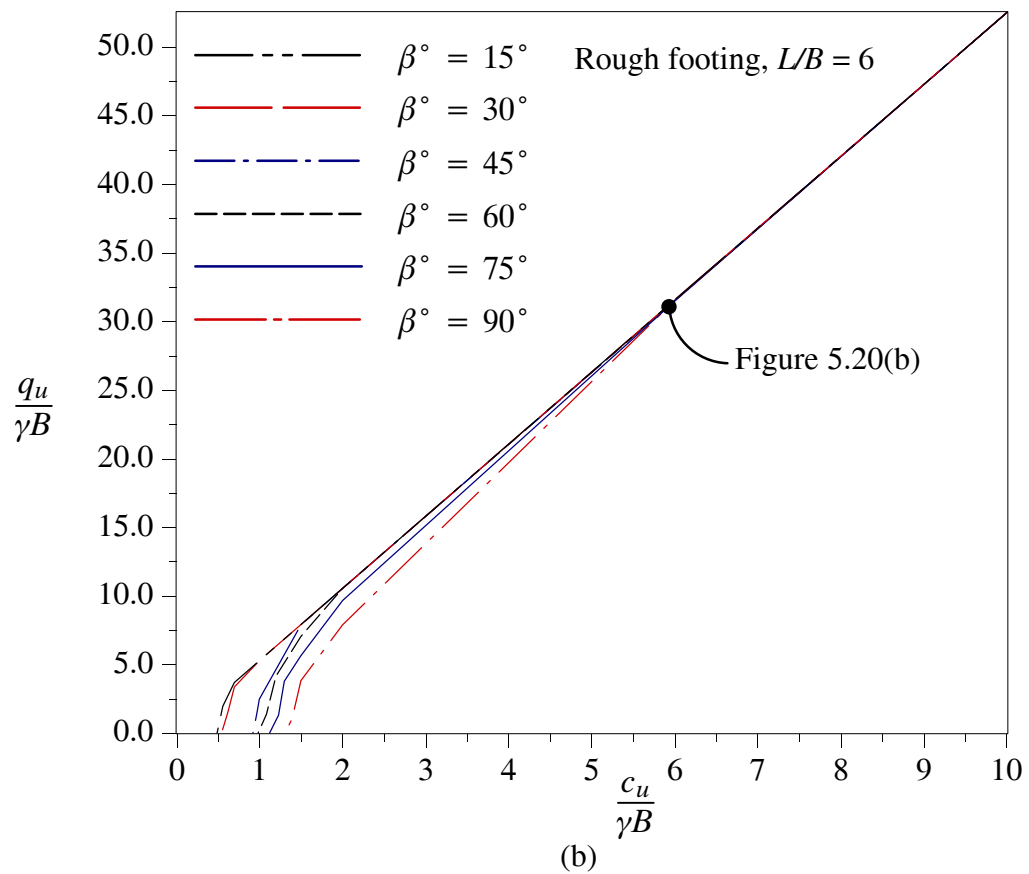
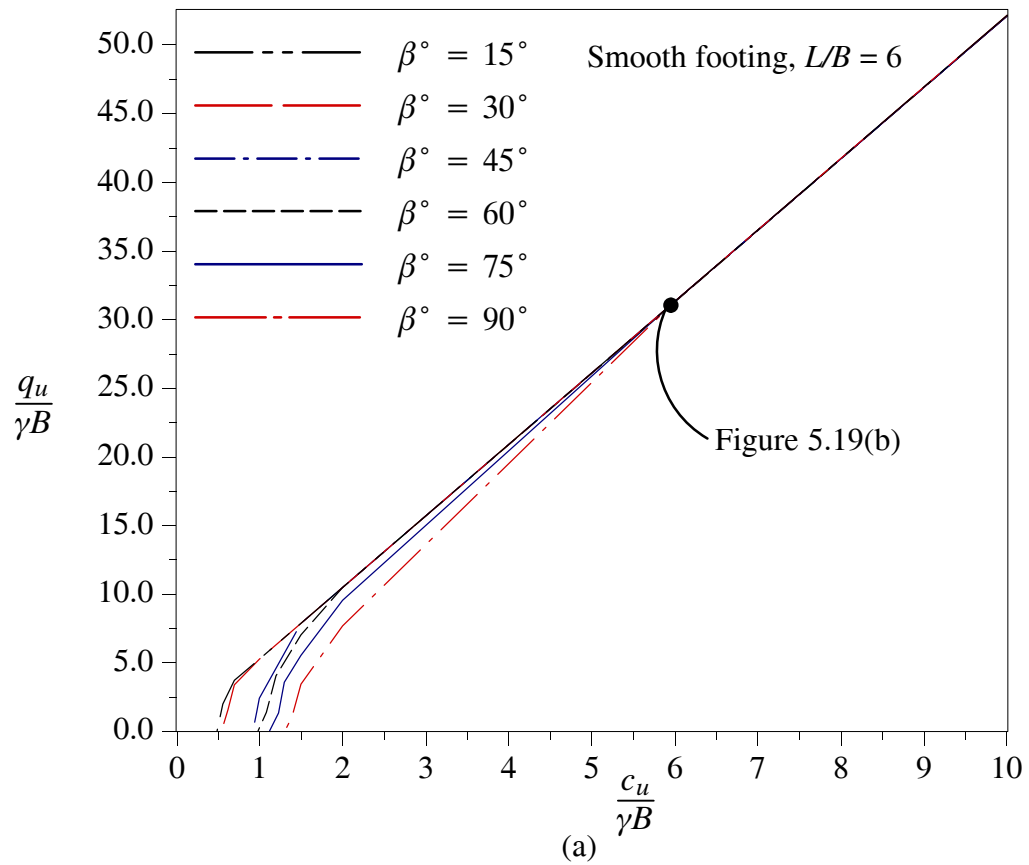


**Figure 5.11** Bearing capacity of (a) smooth & (b) rough footings, ( $L/B=6$ )

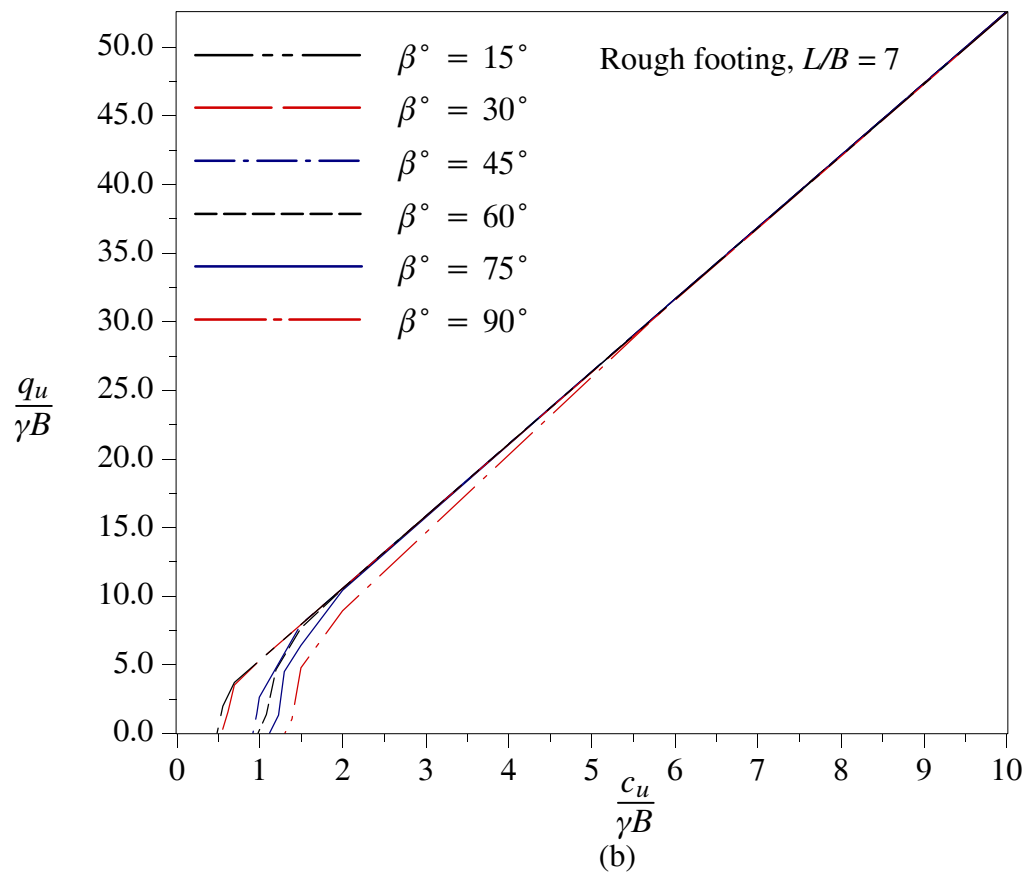
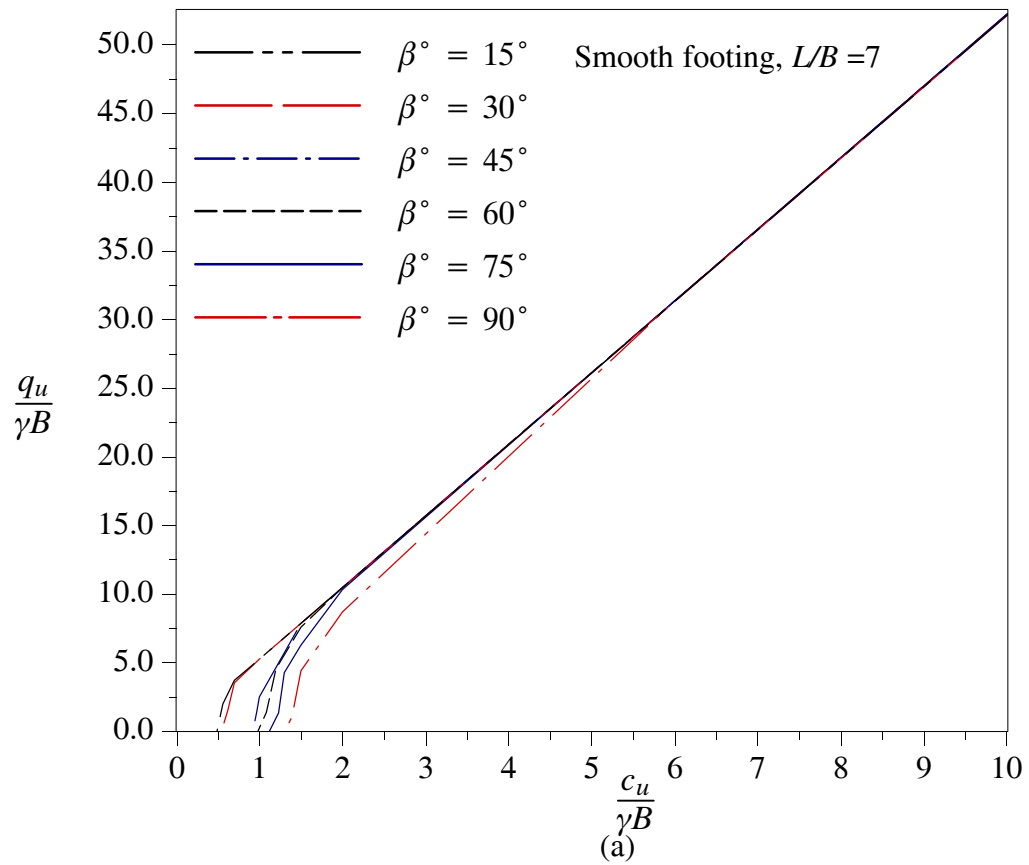


**Figure 5.12** Bearing capacity of (a) smooth & (b) rough footings, ( $L/B=7$ )

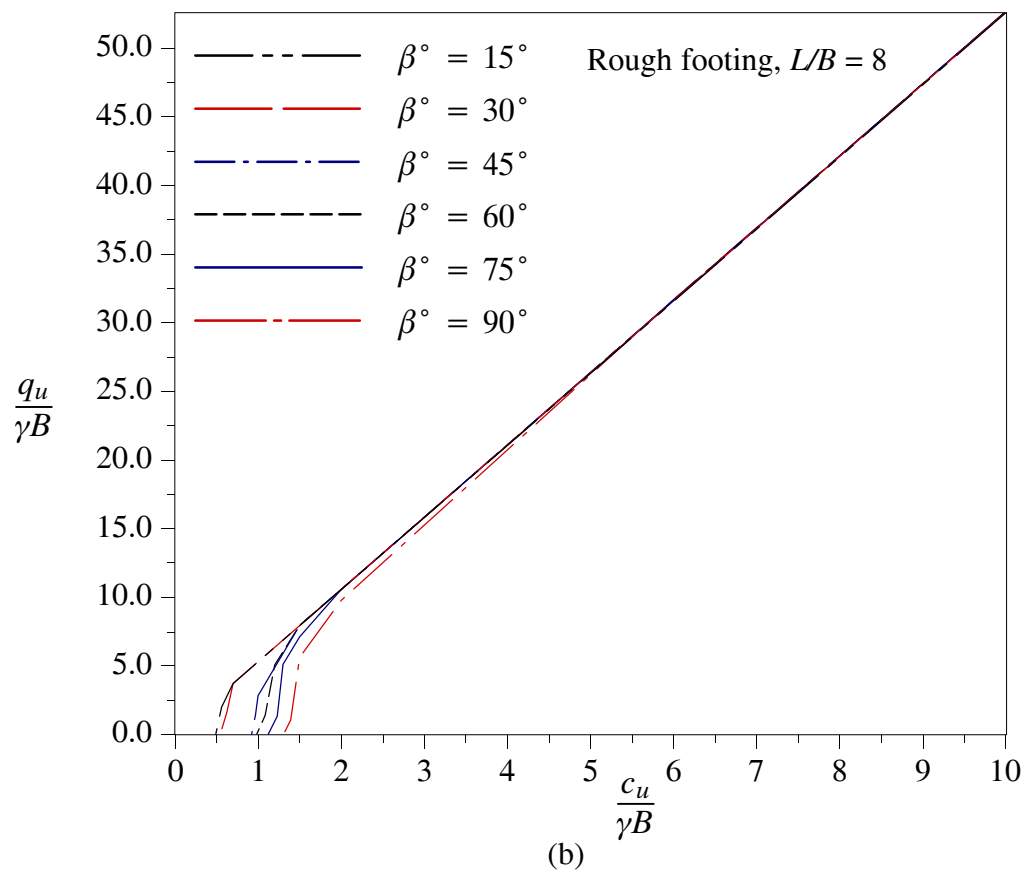
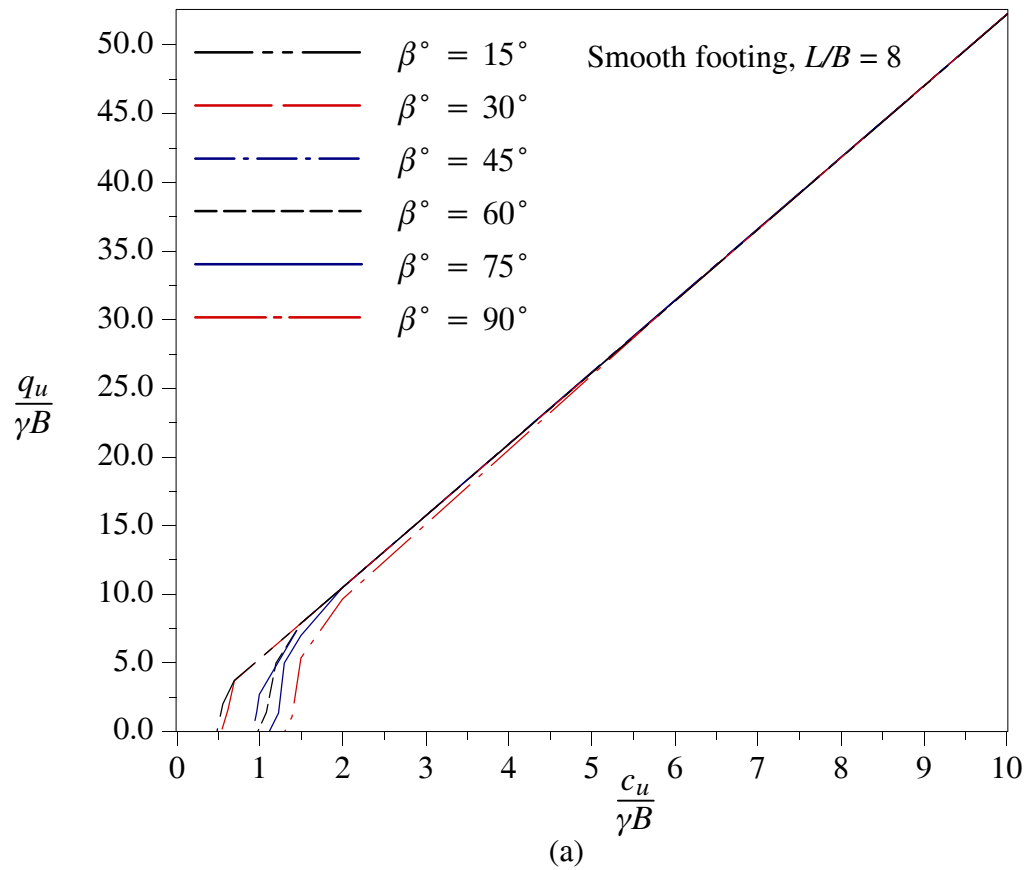


**Figure 5.13** Bearing capacity of (a) smooth & (b) rough footings, ( $L/B=8$ )

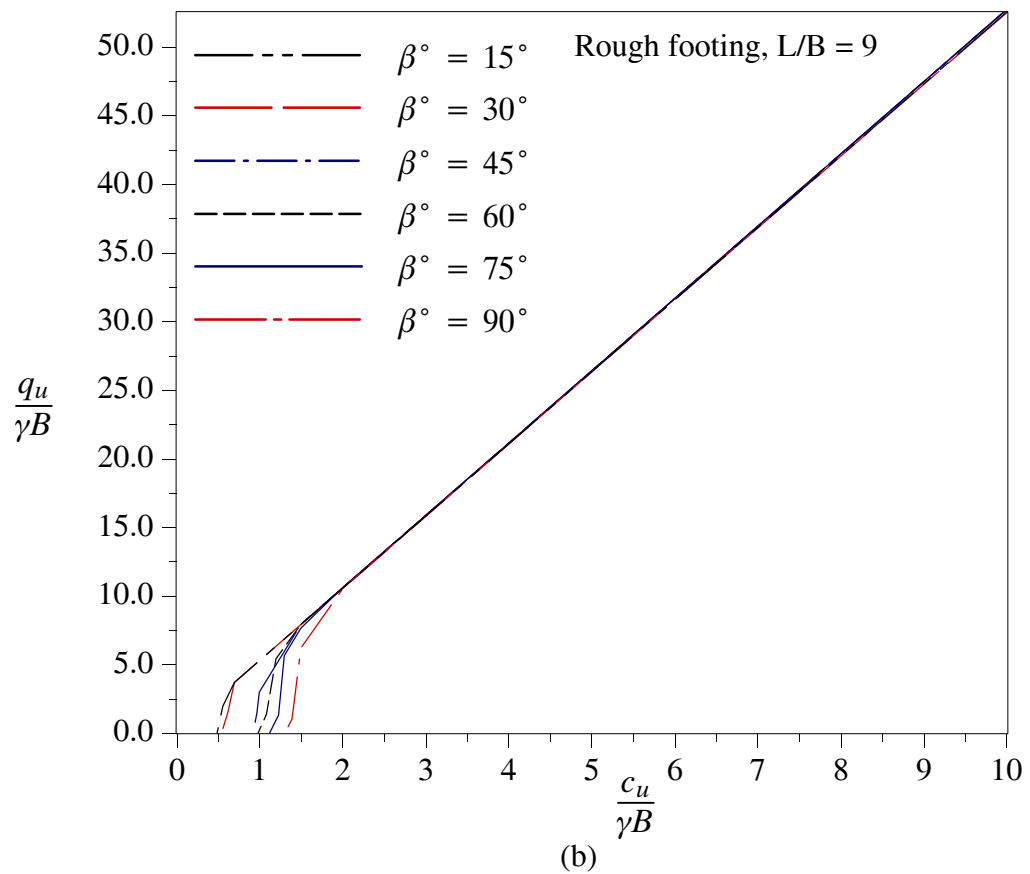
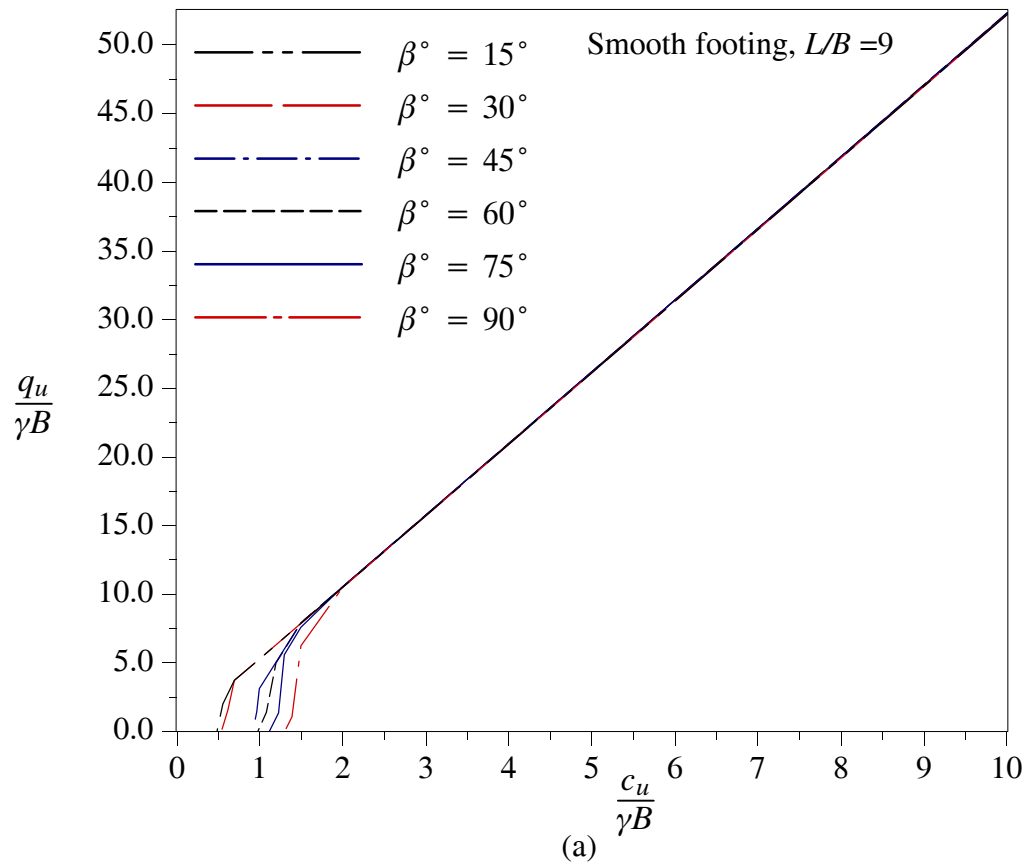
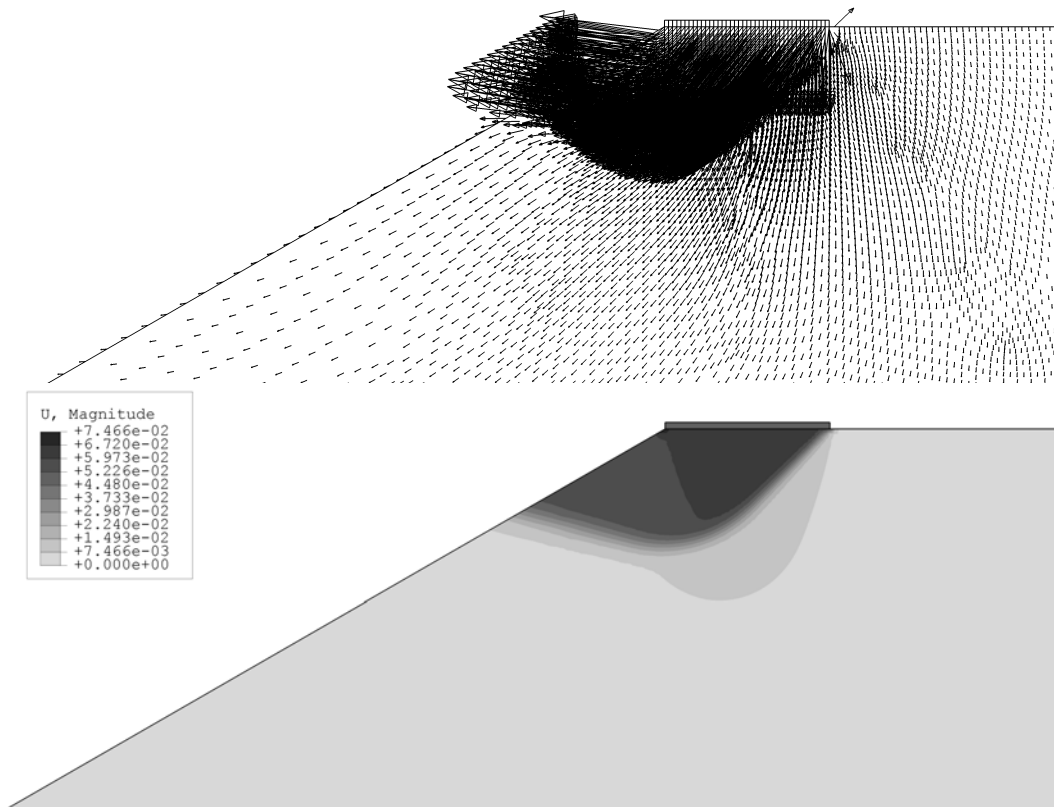
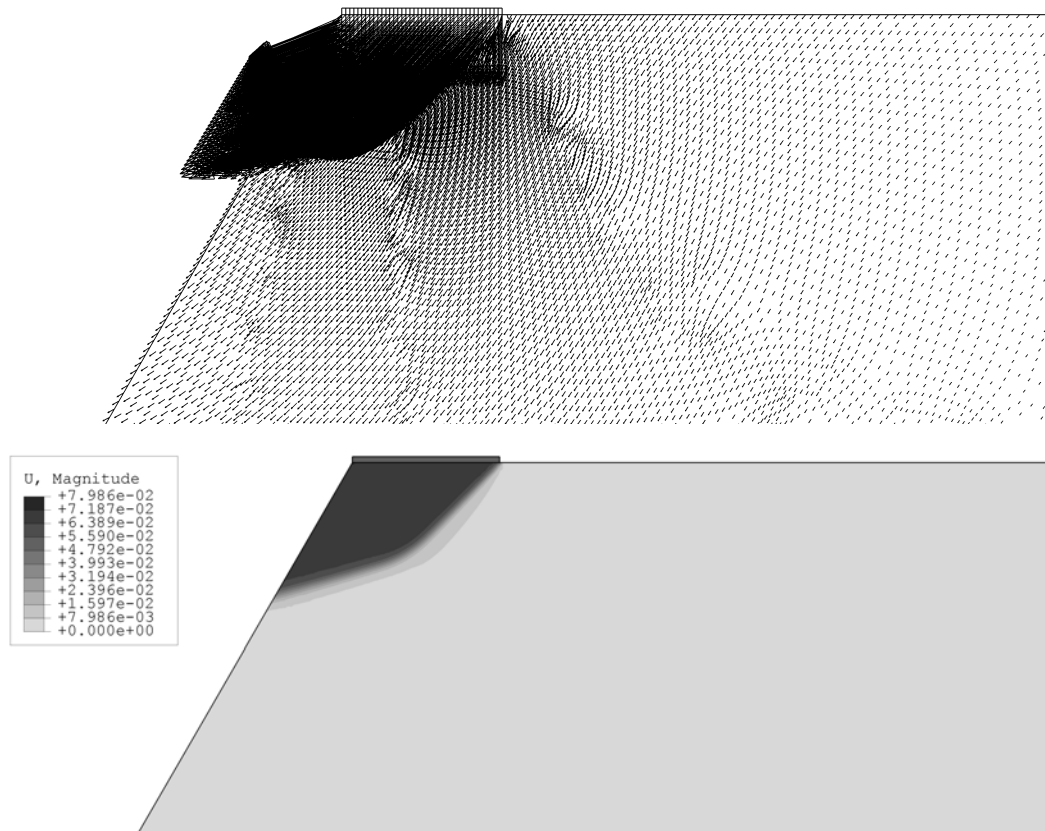


**Figure 5.14** Bearing capacity of (a) smooth & (b) rough footings, ( $L/B=9$ )

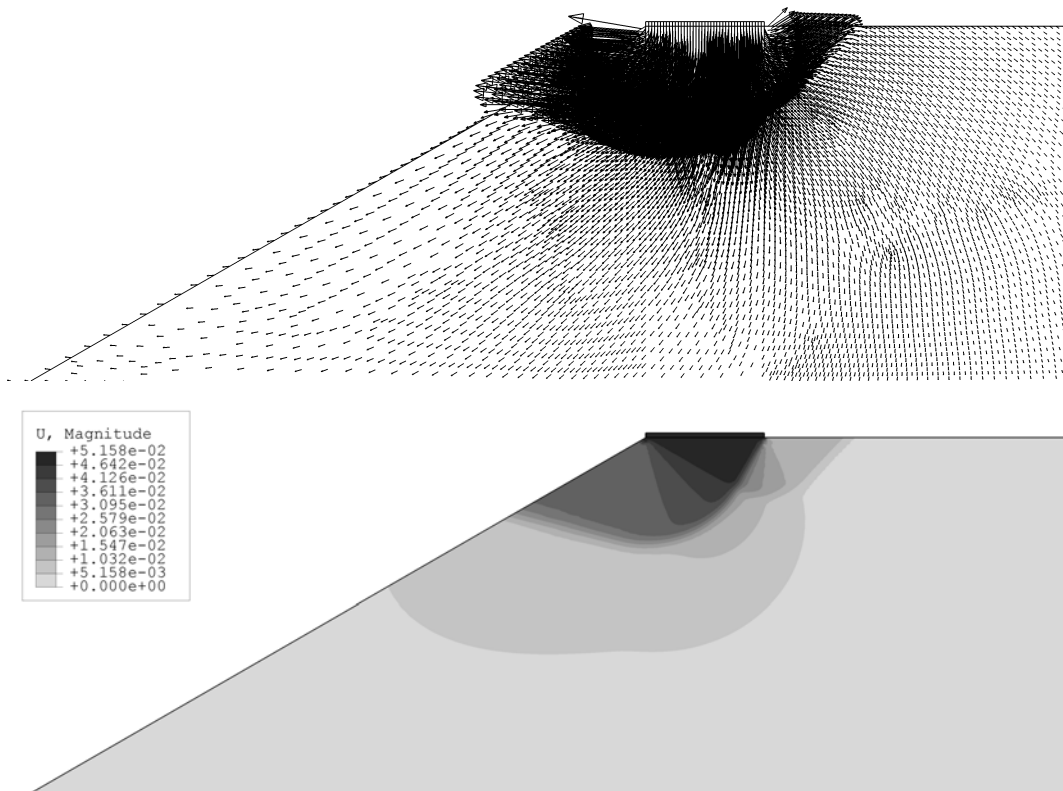


a)  $\beta^\circ = 30^\circ, c_u/\gamma B = 6, L/B = 0$

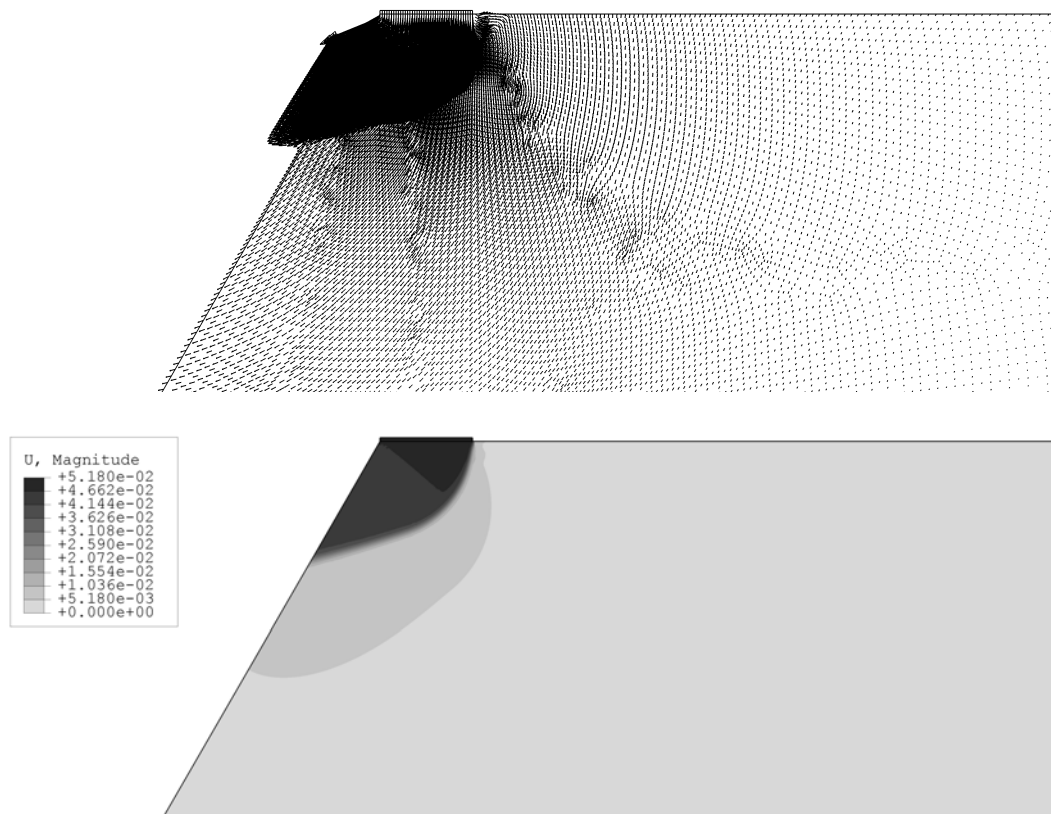


b)  $\beta^\circ = 60^\circ, c_u/\gamma B = 6, L/B = 0$

**Figure 5.15** Typical displacement vectors and contours for smooth footings

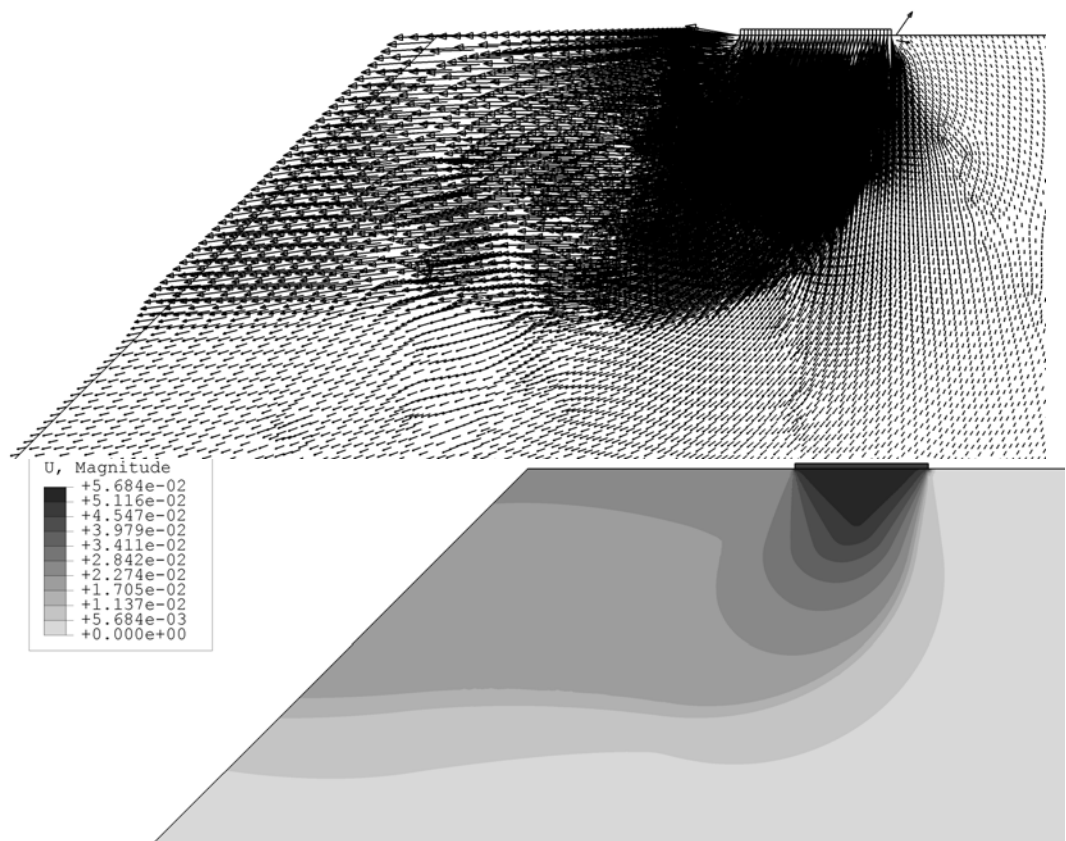


a)  $\beta^\circ = 30^\circ, c_u/\gamma B = 6, L/B = 0$

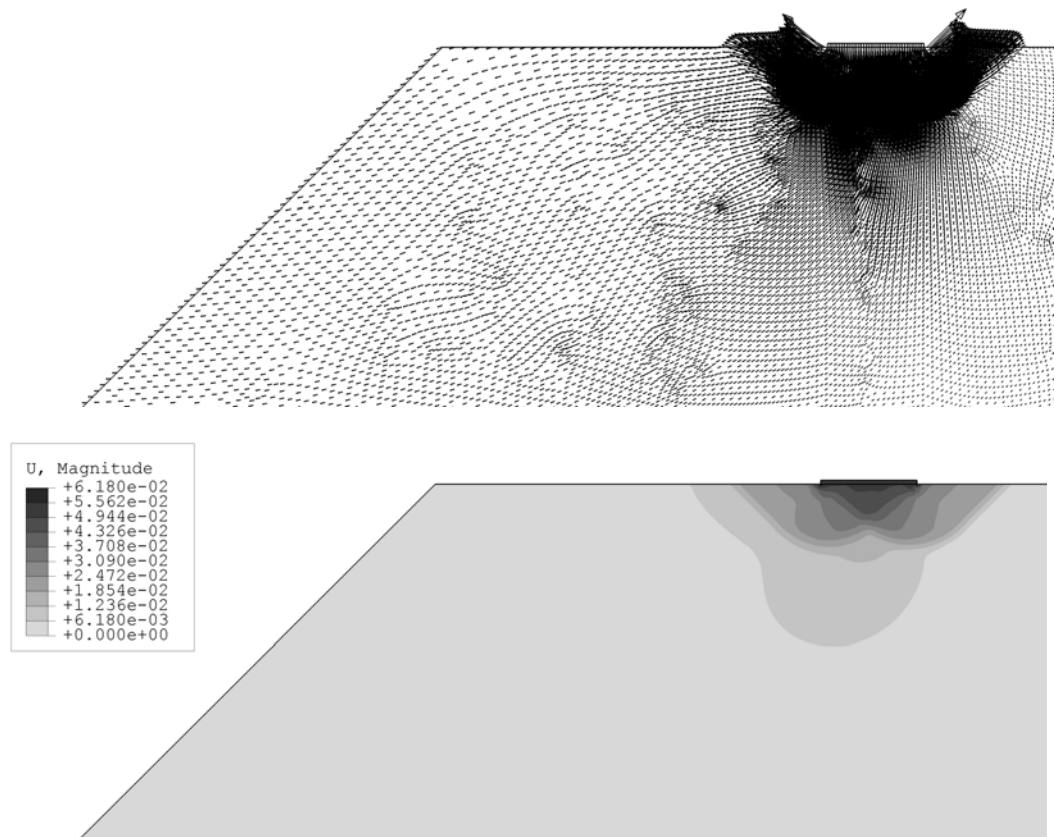


b)  $\beta^\circ = 60^\circ, c_u/\gamma B = 6, L/B = 0$

**Figure 5.16** Typical displacement vectors and contours for rough footings

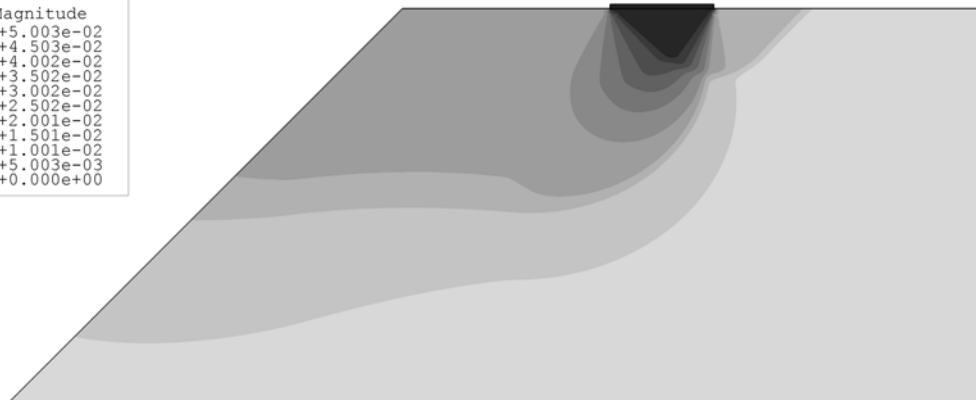
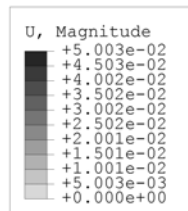
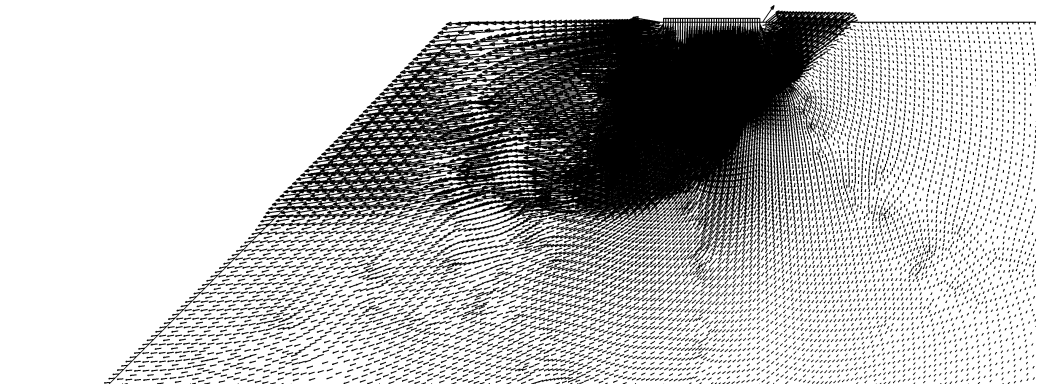


a)  $\beta^\circ = 45^\circ, c_u/\gamma B = 2, L/B = 2$

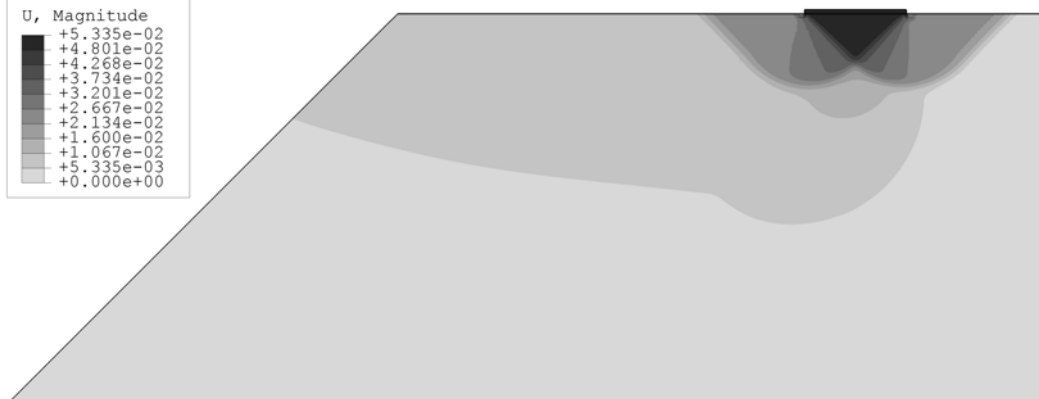
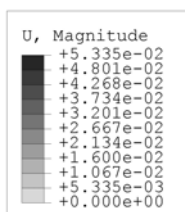
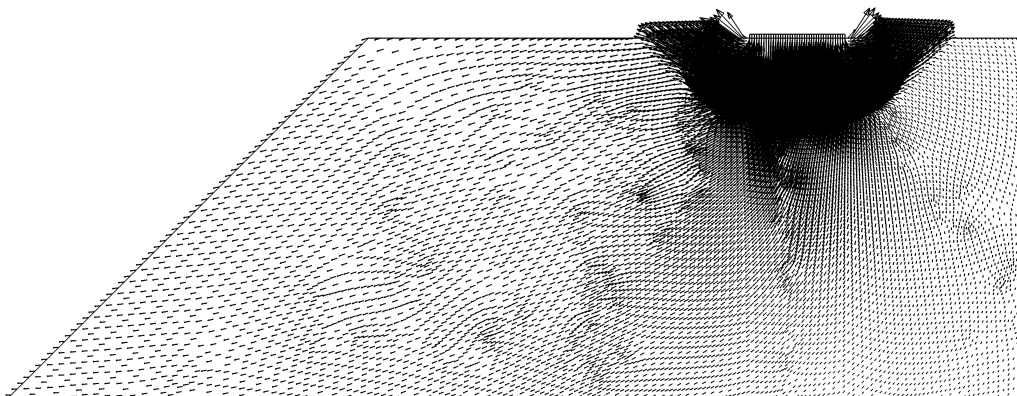


b)  $\beta^\circ = 45^\circ, c_u/\gamma B = 2, L/B = 4$

**Figure 5.17** Typical displacement vectors and contours for smooth footings



a)  $\beta^\circ = 45^\circ, c_u/\gamma B = 2, L/B = 2$



b)  $\beta^\circ = 45^\circ, c_u/\gamma B = 2, L/B = 4$

**Figure 5.18** Typical displacement vectors and contours for rough footings

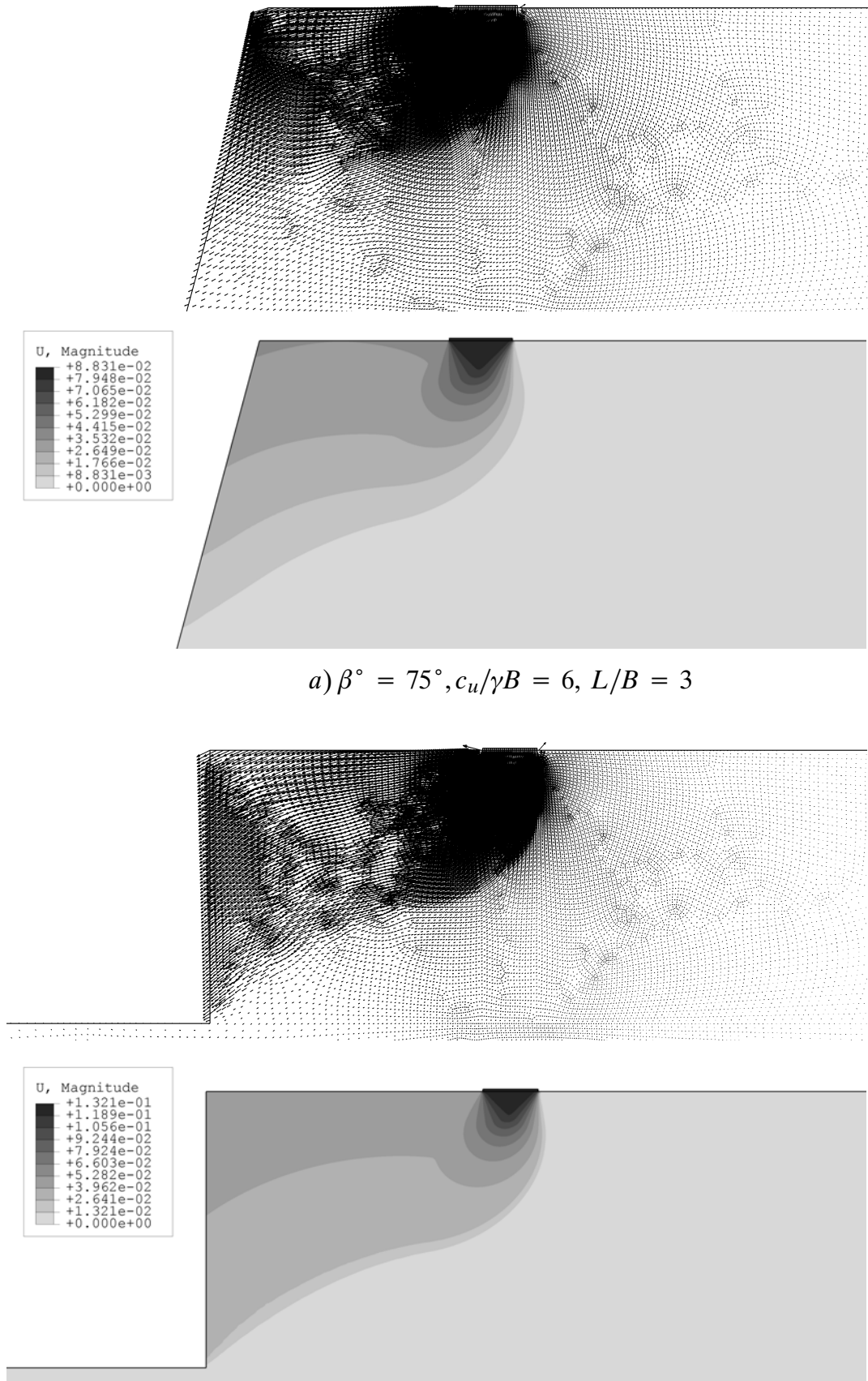
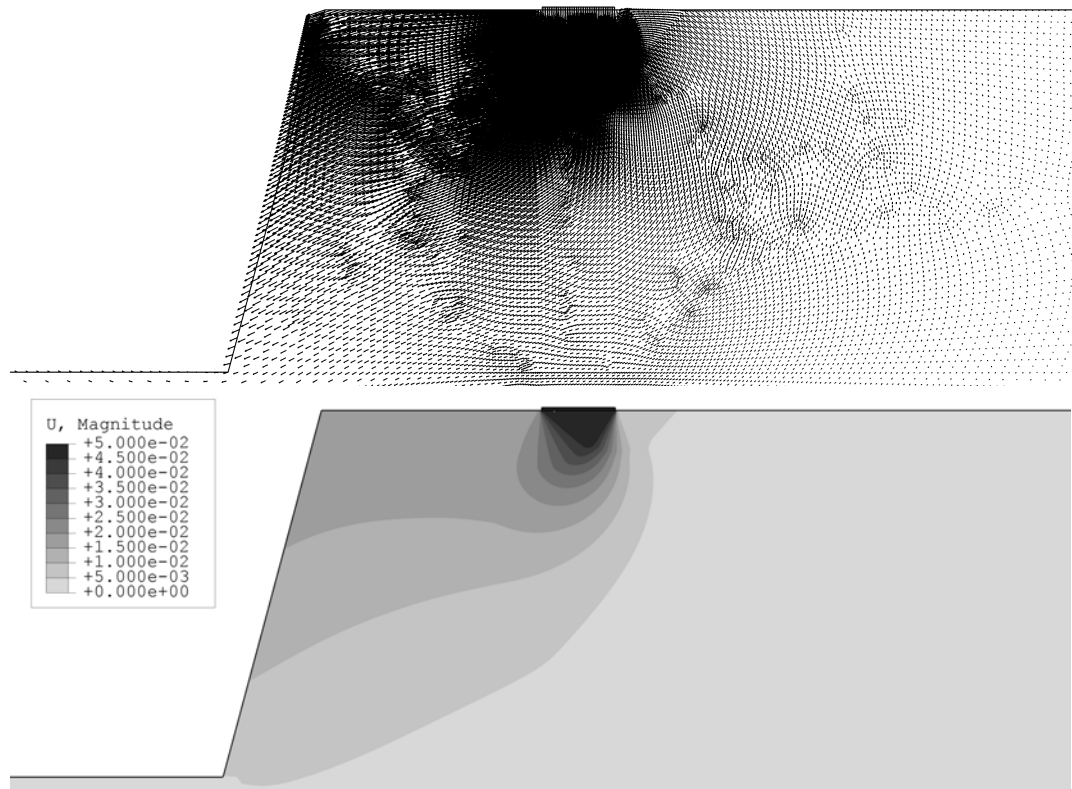
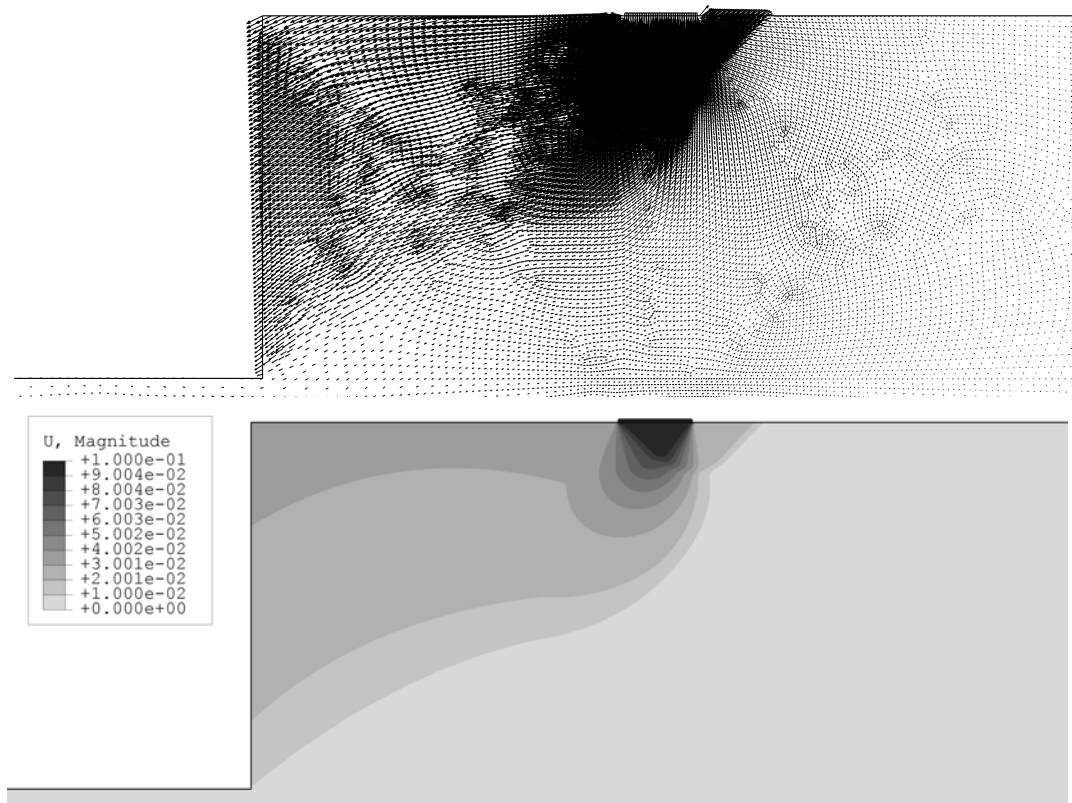


**Figure 5.19** Typical displacement vectors and contours for smooth footings



a)  $\beta^\circ = 75^\circ, c_u/\gamma B = 6, L/B = 3$



b)  $\beta^\circ = 90^\circ, c_u/\gamma B = 6, L/B = 6$

**Figure 5.20** Typical displacement vectors and contours for rough footings

Slope angle	$\beta = 15^\circ$		$\beta = 30^\circ$		$\beta = 45^\circ$		$\beta = 60^\circ$		$\beta = 75^\circ$		$\beta = 90^\circ$	
Linear section	$\frac{c_u}{\gamma B} \geq 0.75$		$\frac{c_u}{\gamma B} \geq 0.82$		$\frac{c_u}{\gamma B} \geq 1.35$		$\frac{c_u}{\gamma B} \geq 1.52$		$\frac{c_u}{\gamma B} \geq 1.93$		$\frac{c_u}{\gamma B} \geq 2.11$	
Coefficients	$C_1$	$C_2$	$C_1$	$C_2$	$C_1$	$C_2$	$C_1$	$C_2$	$C_1$	$C_2$	$C_1$	$C_2$
$L/B=0$	4.709	-0.132	4.183	-0.273	3.638	-0.393	3.110	-0.495	2.581	-0.559	2.047	-0.567
$L/B=1$	5.125	-0.019	4.949	-0.141	4.682	-0.429	4.357	-0.907	3.975	-1.455	3.516	-1.876
$L/B=2$	5.196	0.010	5.221	0.001	5.241	-0.3435	-5.108	-1.693	-4.854	-2.943	4.464	-3.772
$L/B=3$	5.208	0.000	5.208	-0.000	5.207	0.001	5.379	-1.712	5.459	-3.667	5.154	-5.133
$L/B=4$	5.215	0.000	5.215	0.000	5.199	0.088	5.299	-0.925	5.527	-3.174	5.609	-5.428
$L/B=5$	5.213	-0.003	5.213	0.000	5.207	0.000	5.220	-0.084	5.428	-2.169	5.686	-4.727
$L/B=6$	5.212	-0.001	5.211	0.002	5.208	-0.001	5.207	0.000	5.321	-1.137	5.557	-3.503
$L/B=7$	5.212	-0.001	5.211	0.001	5.219	0.001	5.216	0.006	5.237	-0.174	5.443	-2.241
$L/B=8$	5.217	0.001	5.218	0.001	5.220	0.000	5.220	0.001	5.221	0.000	5.330	-1.098
$L/B=9$	5.214	0.000	5.214	-0.001	5.227	0.000	5.227	-0.002	5.223	0.001	5.225	-0.028

**Table 5.2** Bearing capacity coefficients  $C_1$  and  $C_2$  for smooth footings

Slope angle	$\beta = 15^\circ$		$\beta = 30^\circ$		$\beta = 45^\circ$		$\beta = 60^\circ$		$\beta = 75^\circ$		$\beta = 90^\circ$	
Linear section	$\frac{c_u}{\gamma B} \geq 0.75$		$\frac{c_u}{\gamma B} \geq 0.82$		$\frac{c_u}{\gamma B} \geq 1.35$		$\frac{c_u}{\gamma B} \geq 1.52$		$\frac{c_u}{\gamma B} \geq 1.93$		$\frac{c_u}{\gamma B} \geq 2.11$	
Coefficients	$C_1$	$C_2$										
$L/B=0$	4.961	-0.099	4.595	-0.273	4.154	-0.501	3.680	-0.725	3.174	-0.850	1.626	-0.852
$L/B=1$	5.197	-0.012	5.120	-0.119	4.893	-0.454	4.893	-1.154	4.285	-1.875	3.821	-2.290
$L/B=2$	5.244	0.001	5.298	0.010	5.267	-0.281	5.222	-1.849	5.032	-3.220	4.681	-4.256
$L/B=3$	5.248	-0.007	5.249	0.001	5.246	0.000	5.418	1.708	5.545	-3.666	5.281	-5.153
$L/B=4$	5.255	0.000	5.255	-0.010	5.325	0.005	5.338	-0.917	5.555	-3.086	5.659	-5.273
$L/B=5$	5.255	-0.001	5.255	-0.005	5.247	-0.004	5.270	-0.143	5.460	-2.090	5.706	-4.498
$L/B=6$	5.250	0.008	5.254	0.000	5.248	0.000	5.248	0.000	5.353	-1.075	5.575	-3.292
$L/B=7$	5.254	-0.008	5.254	-0.010	5.263	0.003	5.270	-0.067	5.285	-0.208	5.469	-2.067
$L/B=8$	5.258	0.007	5.263	-0.017	5.265	0.001	5.264	0.002	5.265	-0.001	5.364	-1.004
$L/B=9$	5.257	0.002	5.251	0.010	5.277	0.001	5.277	0.000	5.274	-0.007	5.284	-0.096

**Table 5.3** Bearing capacity coefficients  $C_1$  and  $C_2$  for rough footings

The non-linear portions of the curves in Figure 5.5 to Figure 5.14 appear when  $c_u/\gamma B < 0.75, 0.82, 1.35, 1.52, 1.93,$  and  $2.11$  for the cases of  $\beta^\circ = 15^\circ, 30^\circ, 45^\circ, 60^\circ, 75^\circ$  and  $90^\circ$ , respectively (Figure 5.21). The non-linear portions shown graphically on plots in Figure 5.5 to Figure 5.14 reflects the complex interactions between the footing bearing capacity and the overall slope stability and can be best explained by referring to the magnified zone shown in Figure 5.21. The non-linear portion of the curves in Figure 5.5 to Figure 5.14 occurs due to relatively weak soil and the failure types are mixed between local bearing capacity failure and global slope stability failure depending on the distance  $L$ , the slope height  $H$ , and  $c_u/\gamma B$ . The finite element method results show that, in the non-linear sections, when  $c_u/\gamma B$  is small, the type of failure tends to be global slope failure and the bearing capacity is small. Conversely, when  $c_u/\gamma B$  is large, the type of failure tends to be local bearing capacity failure and the bearing capacity of the footing is large. Note that in these cases, if the footing is absent from the slope, the slope remains stable without any failure.

These transition points were identified by testing the domains with changes of the parameters and watching results following these steps: (i) If the footing is absent from the slope, the slope remains stable, this case belongs to the linear or non-linear sections. (ii) When applying a certain value of displacement increments until the slope failure occurs. If the model has global slope failure, it belongs to non-linear sections. Whereas, if the model has local bearing capacity failure, it belongs to linear sections. (iii) change the value  $c_u/\gamma B$  until a point, at which the model sometimes has local bearing capacity failure and sometimes has global slope failure, this point is transition points.

The non-linear sections end at points where bearing capacity is equal to zero (overall slope failure).

The values of  $q_u/\gamma B$  in Table 5.1 show that in the non-linear section the bearing capacity  $q_u/\gamma B$  is almost independent from position of footing on the slope  $L/B$ . This can be best explained that in the non-linear portions, the model is governed by global slope failure.

---

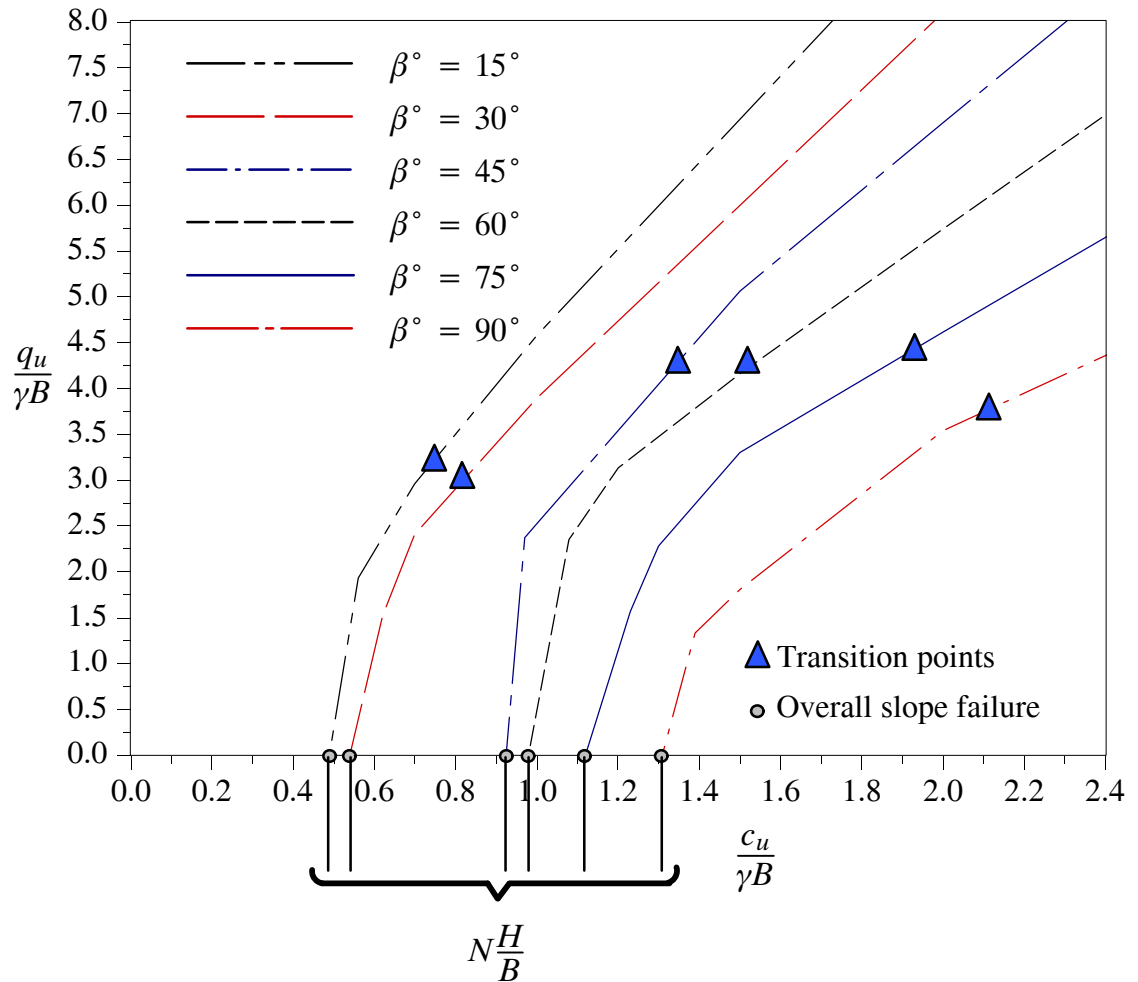


**Figure 5.21** Bearing capacity of footing for various slope angles

The overall slope failure points are the points when the curves  $(c_u/\gamma B, q_u/\gamma B)$  reach the horizontal axis (i.e.  $q_u/\gamma B = 0$ ), as shown in Figure 5.21. The finite element results show that  $q_u/\gamma B$  will be zero at  $c_u/\gamma B = 0.49, 0.54, 0.925, 0.98, 1.12$  and  $1.31$  for  $\beta = 15^\circ, 30^\circ, 45^\circ, 60^\circ, 75^\circ$  and  $90^\circ$ , respectively. In order to determine these values, the footing is removed from the slope, so gravity is the only force applied to the slope. When  $c_u/\gamma B$  is less than value of the overall slope failure point, overall slope failure occurs (Figure 5.22). While  $c_u/\gamma B$  is greater than value of the overall slope failure point, the slope is stable and only fails at a certain load after the footing is applied,  $q_u/\gamma B > 0$ .

According to the Shiau et al. (2008), the overall slope failure points have a relation to stability number of Taylor (1937). Shiau et al. (2008) found:

$$N \frac{H}{B} = \frac{c_u}{\gamma H F_s} \frac{H}{B} = \frac{c_u}{\gamma B} \text{ for factor of safety } F_s = 1 \quad (5.4)$$

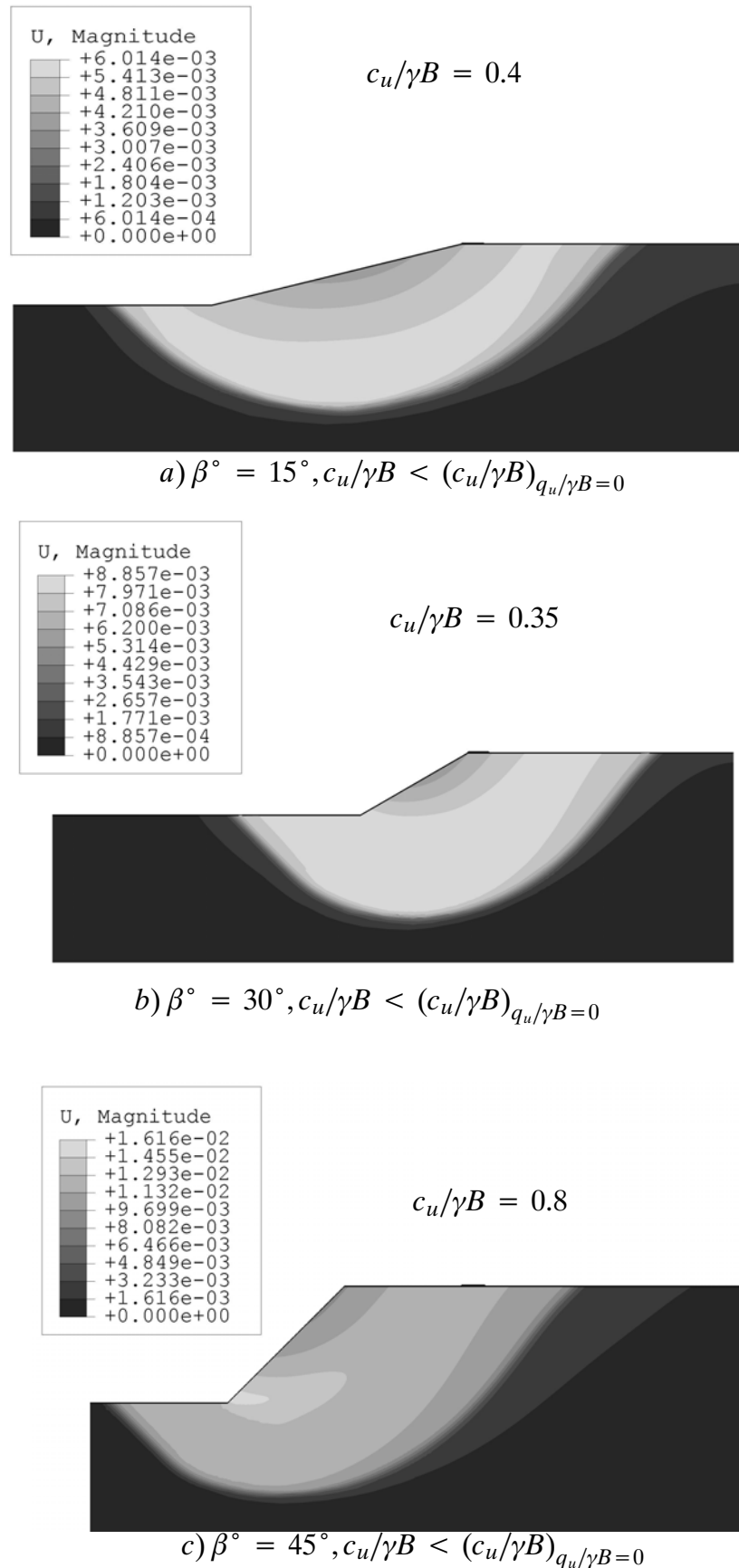


**Figure 5.22** Typical displacement contours for overall failure without footings

$\beta^\circ$	$N$	$H/B$	$N\frac{H}{B}$	$\frac{c_u}{\gamma B}$	$(N\frac{H}{B} - \frac{c_u}{\gamma B}) / \frac{c_u}{\gamma B}$
15°	0.181	3	0.543	0.49	-10.816%
30°	0.181	3	0.543	0.54	-0.556%
45°	0.181	5	0.905	0.925	2.162%
60°	0.192	5	0.96	0.98	2.041%
75°	0.22	5	1.1	1.12	1.786%
90°	0.25	5	1.25	1.31	4.580%

**Table 5.4** The relation between overall slope failure points and stability numbers

Table 5.4 shows the comparison values of overall slope failure points found from the finite element method (using ABAQUS) with stability numbers  $N$  of Taylor chart (1937) for  $HD = \infty$ .

The values of  $N\frac{H}{B}$  and  $\frac{c_u}{\gamma B}$  of finite element analysis in Table 5.4 are within 10.8% of each other.

### 5.4.1 Effect of ratio $L/B$

In Figure 5.5 to Figure 5.10 when  $L/B \leq 5$ , the curves representing the relations  $(c_u/\gamma B, q_u/\gamma B)$  for many cases of the slope angle  $\beta^\circ$ , are far apart. When the ratio  $L/B$  becomes larger, the curves converge together. For example, for a smooth footing, when:

$L/B=2, c_u/\gamma B=10, \beta = 15^\circ, q_u/\gamma B = 51.966$  and  $L/B=2, c_u/\gamma B=10, \beta = 90^\circ, q_u/\gamma B = 40.865$ , while

$L/B=5, c_u/\gamma B=10, \beta = 15^\circ, q_u/\gamma B = 52.125$  and  $L/B=2, c_u/\gamma B=10, \beta = 90^\circ, q_u/\gamma B = 52.129$ .

This can be explained by observing failure mechanism when the distance from the footing to the crest of the slope  $L/B \leq 5$ , the failure occurs toward the slope and level surface (Figure 5.15 and Figure 5.16) while for  $L/B > 5$ , failure occurs within the level surface only, and hence the slope does not influence bearing capacity  $q_u/\gamma B$  (i.e. bearing capacity remains constant), (Figure 5.19(b) and Figure 5.20(b)).

However, for soft soil slope, (i.e. in the non-linear section) the failure zone depends on the position of the footing  $L/B$  and the height of the slope  $H/B$ , but the bearing capacity

$q_u/\gamma B$  is nearly the same when  $L/B$  changed in each case of slope angle  $\beta^\circ$  and strength ratio  $c_u/\gamma B$  (Table 5.1).

### 5.4.2 Effect of the footing roughness

In general, the bearing capacity of rough footings was found to be larger than that of smooth footings (Figure 5.5 to Figure 5.14, and Table 5.1). However, these values are closer to each other for the smaller slope angles  $\beta^\circ$  and for larger distance ratios  $L/B$ . In the linear portion, for otherwise identical problems with slope angle  $\beta \leq 45^\circ$  and  $L/B \geq 5$ , the bearing capacity  $q_u/\gamma B$  of rough footings is higher than that of smooth footing by around only 0.5 to 1%, and the domain of influence of rough footings is larger than of smooth footings.

However, when the slope angle  $\beta > 45^\circ$ , and the distance ratio  $L/B < 5$ , in the linear section, the footing roughness contributes significantly to bearing capacity of footing. In this region,  $q_u/\gamma B$  for a perfect rough footing is larger than that for a smooth footing by around 20% to 28%. This influence is reflected in the shape of the failure mechanism as shown in Figure 5.15 and Figure 5.16.

In the non-linear section the roughness of the footing does not influence bearing capacity very much. The reasons for this can be seen from many tests in non-linear section and explained by the fact that the overall slope stability failure tends to occur rather than local bearing capacity failure. Normally, in the linear section, instead of starting from footing edge, the failure zone starts from a point in the level surface and ends at a point near the base of the slope. After a certain increment of displacement, the overall footing failure occurs and the bearing capacity approaches the same value with any type of footing/soil interaction.

### 5.4.3 Effect of slope angle $\beta^\circ$

In general, the bearing capacity  $q_u/\gamma B$  decreases as the slope angle  $\beta^\circ$  increases. The finite element method results show that the bearing capacity of a strip footing on the level surface of a slope is a strong function of the slope angle  $\beta^\circ$  for  $L/B < 5$ . For distances  $L/B < 5$ , in the linear section, the bearing capacity  $q_u/\gamma B$  is larger if the slope angle  $\beta^\circ$  is smaller. However, for distances  $L/B \geq 5$ , in the linear section, bearing capacity  $q_u/\gamma B$  is the same even when the slope angle  $\beta^\circ$  changes from  $15^\circ$  to  $90^\circ$ .

---

#### 5.4.4 Comparison of this study with Narita and Yamaguchi (1990) & Kusakabe (1981)

Narita and Yamaguchi (1990) investigated the bearing capacity of foundations on slopes using log–spiral sliding surfaces as mentioned in the section 2.3.3 of Chapter 2. Results from previous studies in this area are limited so cases of clay slope with  $\beta = 30^\circ$  are considered. ABAQUS results are compared with those of Narita and Yamaguchi (1990), the simplified Bishop method, and the upper bound solutions of Kusakabe (1981). Note that in these previous studies, the authors did not indicate what the footing/soil roughness was. However, comparisons show that their studies are assumed to be for smooth footing.

$c_u/\gamma B$	$q/\gamma B$			
	ABAQUS	Narita & Yamaguchi (1990) Log–spiral	Bishop	Kusakabe (1981) Upper bound
25	104.30	107	104.4	102
5	20.64	21.1	20.8	20.2
1	3.91	3.94	4.03	3.84
0.5	0	–	1.92	1.78

**Table 5.5** Comparison of F.E. results with analytical solutions ( $\phi = 0$ ,  $L/B = 0$ ,  $\beta = 30^\circ$ ,  $L/B=0$ )

The results from finite element method (ABAQUS) presented in Table 5.5 are close to the results of the log–spiral and Bishop methods. However, bearing capacity from the finite element method solution is higher than that from upper bound solution of Kusakabe (1981) by around 1%.

## 5.5 CONCLUSION

The bearing capacity of strip footings on clay slopes has been investigated using the finite element method. The results obtained have been presented in terms of a ratio of bearing capacity  $q_u/\gamma B$  in both graphical and tabular form to facilitate their use in solving practical design problems. The following conclusions can be made based on the finite element results:

- In general, the dimensionless bearing capacity  $q_u/\gamma B$  increases with the increase of the ratio  $c_u/\gamma B$ , the increase of  $L/B$ , and decrease of the slope angle  $\beta$ . A wide range

---

of these parameters has been investigated: the strength ratio  $c_u/\gamma B$  ranges from 0 to 10, the ratio of distance from footing edge to the crest of the footing  $L/B$  ranges from 0 to 9 and the slope angle  $\beta$  varies from  $15^\circ$  to  $90^\circ$  in increments of  $15^\circ$ .

- The curves describing the relationship between  $c_u/\gamma B$  and  $q_u/\gamma B$  can be characterised using three main properties, namely a linear section, a non-linear section, and zero bearing capacity point of the curves (overall slope failure).
  - In the linear section, the bearing capacity  $q_u/\gamma B$  is proportional to the strength ratio of soil  $c_u/\gamma B$ , and can be determined by Equation (5.3) with the two coefficients  $C_1$  and  $C_2$ , described in the Table 5.2 for smooth footings, and in the Table 5.3 for rough footings. Within the linear section, local bearing capacity failure contained to within the face of the slope. The failure occurs in the region above the toe of the slope; the height of the slope does not influence the bearing capacity, meaning the bearing capacity  $q_u/\gamma B$  obtained from these simulations can be applied in other configurations with larger heights. If  $L/B$  increases, the lines describing the relation  $(c_u/\gamma B, q_u/\gamma B)$  are closer to each other, and when  $L/B \geq 5$ , the lines are nearly the same for all slope angles. In the linear section, rough footings have higher bearing capacity than that of smooth footings.
  - In the non-linear section, the curves of the relation  $(c_u/\gamma B, q_u/\gamma B)$  stay far apart as the failure mechanism is governed by overall slope failure. Slope angles do influence the bearing capacity while footing/soil interaction does not.
  - Some of the results of this study compare well to the results of the previous investigations by log-spiral, Bishop and upper bound method.
-

**CHAPTER 6**  
**CONCLUDING REMARKS**

---

## 6.1 INTRODUCTION

Predicting the bearing capacity of foundations plays a central role in the design of many civil engineering works. The current theoretical understanding of the bearing capacity of the foundations is unsatisfactory in some respects. This work addresses this deficiency through numerical simulation.

This work aims to provide a more rigorous set of numerical solutions to three common bearing capacity problems: (i) the undrained bearing capacity of surface footings on layered soils; (ii) the undrained bearing capacity of embedded footings; and (iii) the undrained bearing capacity of footings near slopes. This work also aims to verify the application of numerical software using finite element method in particular problems.

The majority of past research on bearing capacity of foundation has been experimentally based and, as a result, current design practices are largely based on empiricism. Very few rigorous numerical analyses have been performed to determine the ultimate bearing capacity of foundations. This fact was clearly highlighted in the historical review in Chapter 2. Furthermore, the majority of existing numerical studies are not considered rigorous as they are based on approximate methods such as limiting equilibrium or the method of characteristics (without extension of the stress field). A comparison of the results obtained from previous studies provides an opportunity to validate the findings and provides a truly comprehensive evaluation of the bearing capacity of a foundation.

## 6.2 UNDRAINED BEARING CAPACITY OF SURFACE FOOTINGS ON LAYERED SOILS

The undrained bearing capacity of surface footings on layered soils has been presented in the Chapter 3. The bearing capacity of strip, square and circular footings on two-layered clays using the finite element method has been investigated. The results obtained have been presented in terms of a modified bearing capacity factor  $N_c^*$  in both graphical and tabular form to facilitate their use in solving practical design problems. The results showed that two-layered clay problems can be effectively solved by the finite element method. In the same system of  $H/B$  the ultimate bearing capacity increases as the relative ratio of  $c_{u1}/c_{u2}$  decreases. In the same system of  $H/B$  and  $c_{u1}/c_{u2}$ , the ultimate bearing capacity of circular footing is around 2% larger than that of a square footing, and that of strip footing is the

---

smallest. The ultimate bearing capacity of circular footings and square footings could not be related to that of strip footing by a constant coefficient.

This work could be extended to include multi-layered soil, deep penetration, arbitrary footing shapes, inclined footings, or finite footings spacing.

### **6.3 UNDRAINED BEARING CAPACITY OF EMBEDDED FOOTINGS**

The bearing capacity of embedded footings in clay has been investigated and is presented in Chapter 4. The bearing capacity of embedded strip, circular, square and rectangular footings in purely cohesive soil was studied. Results presented contribute to the understanding of undrained bearing capacity of embedded footings.

The results obtained have been presented in terms of a normalised bearing capacity factors  $N_c$  in both graphical and tabular form; and the shape factors  $F_{cs}$ ; and the depth factors  $F_{cd}$  to facilitate their use in solving practical design problems.

The range of footings parameters considered in this work covers most problems of interest. However, only cohesive soil has been considered. In future work, cohesionless and cohesion–frictional soil should be studied in a similar manner. The soil in this study is homogeneous clay with constant cohesion. The finite element method provides an opportunity to solve a more complex problems with increasing cohesion clay in depth or layered soil.

### **6.4 UNDRAINED BEARING CAPACITY OF FOOTINGS NEAR SLOPES**

In Chapters 5 the undrained bearing capacity of strip footings on slopes with a wide range of soil types and positions of footing on level surface was investigated.

To cover most problems of practical interest, solutions for strip footings on undrained soil slopes with variety of slope angles were presented. For design purposes, parametric equations have been provided that enable the bearing capacity of footings to be estimated reliably. Such equations can be used to solve practical design problems.

The finite element package ABAQUS provides an ability to solve three–dimensional problems of footing on level surface of the slope such as square, circular or rectangular

---

footing. The soil can be investigated not only for cohesive but also for cohesionless, and cohesion–frictional soil. The depth of slope in this investigation is infinite, however, in practical design, the depth can be limited and not a level base. The water table can be modelled in the finite element problems to examine the effect of a position of the water table to bearing capacity of footing on slope. These problems can be solved in future work by the finite element method.

---

---

## REFERENCES

- ABAQUS, Standard User's Manual: Version 6.5.4, 2005, Pawtucket, RI: Hibbitt, Karlsson & Sorensen Inc.
- Askari, F. & Farzaneh, O. (2003), "Upper-bound solution for seismic bearing capacity of shallow foundations near slopes". *Géotechnique* 53, No. 8, 697–702.
- Beer, E. E., (1967) "Experimental determination of the shape factors and the bearing capacity factors of sand", *Géotechnique*, 1970, 20: 387–411.
- Bishop, A. W. (1955). "The use of the slip circle in the stability analysis of slope". *Geotechnique*, 5, 7–17.
- Brown, J. D., and Meyerhof, G.G. (1969 ). "Experimental study of bearing capacity in layered clays", *Proceedings, 7th International Conference on Soil Mechanics and Foundation Engineering, Mexico*, 2: 45–51.
- Button, S.J. (1963). "The bearing capacity of footings on a two-layer cohesive subsoil". *Proceedings, 7th International Conference on Soil Mechanics and Foundation Engineering, Zurich*, 1: 332–335.
- Carter, J.P., Balaam, N.P., (1990). Program AFENA, A general finite element algorithm. Centre for Geotechnical Research, University of Sydney, New South Wales, Australia.
- Chen, W. F. (1975). *Limit Analysis and Soil Plasticity*, 1975, Elsevier, Amsterdam.
- Coduto, D.P., (2001) *Foundation Design, Principles and Practices* (2nd ed), Prentice–Hall, Inc., New Jersey.
- Das Braja M. and Dallo Karim F. (1984). "Bearing capacity of shallow foundations on a strong sand layer underlain by soft clay", *Civil engineering fro practicing and design engineers*, Vo1. 3, pp. 417–438.
- Davis E. H. and Booker J. R. (1973). "The effect of increasing strength with depth on the bearing capacity of clays", *Géotechnique*, 23(4), 551–563.
- Day, R. W. (2001). "Soil Mechanics and Foundations." Section 6 of *Building Design and Construction Handbook*, 6th ed. Frederick S. Merritt and Jonathan T. Ricketts, eds. McGraw–Hill, New York, pp. 6.1 to 6.121.
-

- 
- De Beer, E. E. (1970). "Experimental determination of the shape factors and the bearing capacity factors of sand." *Geotechnique*, 20(4), 387–411.
- Drucker, D. C., Greenberg, H. J. & Prager, W. (1951) The safety factor of an elastic–plastic body in plane strain. *J. Appl. Mech. Trans. ASME* 73, 371–378.
- Drucker, D. C. and W. Prager (1952). "Soil mechanics and plastic analysis or limit design." *Quarterly of Applied Mathematics* 10(2): 157–165.
- Eason, G. & Shield, R. T. (1960). "The plastic indentation of a semiinfinite solid by a perfectly rough circular punch". *J. Appl. Math. Phys. (ZAMP)* 11, No. ...
- Edwards, D. H., Zdravkovic, L. & Potts, D. M. (2005). "Depth factors for undrained bearing capacity". *Géotechnique* 55, No. 10, 755–758.
- FLAC3D , Fast Lagrangian analysis of continua in 3 dimensions, user's manual, Itasca Consulting Group 1997, Minneapolis.
- Griffiths, D.V. (1982). "Computation of bearing capacity on layered soils". *Proc. 4th Int. Conf. Num. Meths. Geomech.*, Edmonton, Canada, (ed.Z. Eisenstein), Pub. Balkema pp.163–170.
- Griffiths, D.V., Fenton, G.A. and Manoharan, N. (2002). "Bearing capacity of a rough rigid strip footing on cohesive soil – a probabilistic study", *ASCE Journal of Geotechnical and Geoenvironmental Engineering*, 128(9).
- Hansen, B., (1969). "Bearing Capacity of Shallow Strip Footings in Clay". *Proceedings of the 7th International Conference on Soil Mechanics and Foundation Engineering*, Vol. 3, pp. 107–113.
- Hill, R., (1951)., *The Mathematical Theory of Plasticity*, Oxford University Press.
- Houlsby, G. T. and C. M. Martin (2003). "Undrained bearing capacity factors for conical footings on clay." *Geotechnique* 53(5): 513–520.
- Hu, Y. and Randolph, M. F. (1998), "Deep penetration of shallow foundations on non–homogeneous soil", *Soil and Foundation*, Vol. 38, No. 1, pp. 241–246.
- Hu, Y., Randolph, M. F. and Watson, P. G. (1999), "Bearing response of skirted foundation on nonhomogeneous soil". *Journal of Geotechnical and Geoenvironmental Engineering*, ASCE, Vol. 125, No. 11, pp. 924–935.
-

- 
- Kumar, J. & Kumar, N. (2003). "Seismic bearing capacity of rough footings on slopes using limit equilibrium". *Géotechnique*, 53(3), 363–369.
- Kumar, J. & Mohan Rao, V. B. K. (2003). "Seismic bearing capacity of foundations on slopes. *Géotechnique*, 53(3), 347–361.
- Kusakabe, O., Kimura, T., Yamaguchi, H., 1981. "Bearing capacity of slopes under strip loads on the top. surfaces". *Soils and Foundations* 21 (4), 29– 40
- Liu C. and Evett. B. J. (1998), "Soils and Foundations", 4th –ed, pp. 265–317.
- Lundgren, H. and Mortensen, K. (1953). Determination by the Theory of Plasticity of the Bearing Capacity of Continuous Footings on Sand. *Proceedings of the 3rd International Conference on Soil Mechanics and Foundation Engineering*, Vol. 1, pp. 409–412.
- Martin, C. M. and G. T. Hously (2001). "Combined loading of spudcan foundations on clay: Numerical modelling." *Geotechnique* 51(8): 687–699.
- Merifield R. S. (2005). "Geotechnical engineering" University of Southern Queensland.
- Merifield R. S. , Sloan S. W. and Yu H. S. (1999). "Rigorous plasticity solutions for the bearing capacity of two-layered clays". *Géotechnique*, 49(4), 471–490. Awarded 2000 Telford Medal, Institution of Civil Engineers, London.
- Merifield R. S. and Nguyen V. Q. (2006). "Two and three-dimensional bearing capacity solutions for footings on two-layered clays". *Geomechanics and Geoengineering*, Taylor and Francis, 1(2) , pp.151–162.
- Meyerhof, G. G. (1974). "Ultimate Bearing Capacity of Footings on Sand Overlying Clay", *Canadian Geotechnical Journal*, Vol 11, pp 223–229. Available from National Research Council of Canada, Research Journals, Ottawa, ON K1A OR6, Canada.
- Meyerhof, G. G. (1963). "Some recent research on the bearing capacity of foundations". *Can. Geotech. J.*, 1: 16–26.
- Meyerhof, G.G, and Hanna, A.M. (1978). "Ultimate bearing capacity of foundations on layered soils under inclined load". *Canadian Geotechnical Journal*, 15(4): 565–572.
- Meyerhof, G.G. (1951), "The ultimate bearing capacity of foundations", *Géotechnique*, 2: 301–332.
- Michalowski, R. L. and Lei Shi, (1995), "Bearing Capacity of Footings over Two-Layer Foundation Soils". *J. Geotech. Engrg.*, Volume 121, Issue 5, pp. 421–428.
-

- 
- Michalowski, R. L. (2001). "Upper-bound load estimates on square and rectangular footings". *Géotechnique*, 51(9): 787–798.
- Narita, K. and Yamaguchi, H. (1990). "Bearing capacity analysis of foundation on slopes by use of log-spiral sliding surfaces". *Soil and foundation*, 30(3), 144–152.
- Poulos, H.G., Carter, J.P. and Small, J.C., "Foundations and Retaining Structures – Research and Practice". State of the Art Lecture, 14 Int. Cong. Soil Mechs. Geot. Eng., 2001, Istanbul.
- Potts, D. M. & Zdravkovic, L. (1999). *Finite element analysis in geotechnical engineering: Theory*. London: Thomas Telford.
- Prandtl L. (1921) "Über die eindringungsfestigkeit plastischer baustoffe und die festigkeit von schneiden", *Z. Ang. Math. Mech.*, Basel, Switzerland, 1, No. 1, 15.
- Prandtl L. (1920). "Über die Härte plastischer Körper", *Nachr. Königl. Ges. Wissensch., Göttingen, Mathematisch-physikalische Klasse*, 74–85.
- Reddy, A.S. and Srinivasan, R.J. (1967). "Bearing capacity of footings on layered clays". *Journal of the Soil Mechanics and Foundations Division, ASCE*, 93(2): 83–99.
- Salgado, R., Lyamin, A. V., Sloan, S. W. & Yu, H. S. (2004). "Two- and three-dimensional bearing capacity of foundations in clay". *Géotechnique*, 54(5): 297–306.
- Saran, S., Sud, V.K. and Handa, S.C., (1989). *Bearing Capacity of Footings Adjacent to Slopes*. *Journal of Geotechnical Engineering, ASCE*, Vol. 115, No. GT4, pp. 553–573.
- Saran, S. (1969). "Bearing capacity of footing subject to moments", thesis presented to the University of Roorkee, India, at Roorkee, in partial fulfillment of the requirements for the degree of Doctor of Philosophy.
- Shiau J, Merifield R. S. , Lyamin A. V. , and Sloan, S. W. (2008). "Undrained stability of footings on slopes". *Computers and Geotechnics*, (Submitted).
- Skempton, A. W. (1951). "The bearing capacity of clays". *Proc. Building Research Cong. London*, 1, 180–189.
- Taylor, D. W. (1937). "Stability of earth slopes." *Boston Society of Civil Engineers Journal* 24(3): 197–246.
- Tani, K. & Craig, W.H. (1995). "Bearing capacity of circular foundations on soft clay of strength increasing with depth", *Soils and Foundations*, 35(4): 21–35.
-

Terzaghi, K. (1943). *Theoretical soil mechanics*. John Wiley, New York.

Vesiv, A.S. (1973). Analysis of Ultimate Loads of Shallow Foundations. *Journal of the Soil Mechanics and Foundation Division, ASCE*, Vol. 99, No. SM1, pp. 45–73.

Wang C.X. & Carter J.P. (2000). “Penetration of strip and circular footings into layered clays”. *Advances in Theoretical Geomechanics – Proceedings of the John Booker Memorial Symposium*; Sydney. Rotterdam: Balkema. 193–210.

Whitlow, R. (1995). “Basic soil mechanics”, Edition 3rd ed., Harlow, Essex, England : Longman Scientific & Technical ; New York : Wiley.

Zhu, M., and Michalowski, R. L. (2005). “Shape Factors for Limit Loads on Square and Rectangular Footings”. *Journal of Geotechnical and Geoenvironmental Engineering, ASCE*, 131(2): 223–231.

---